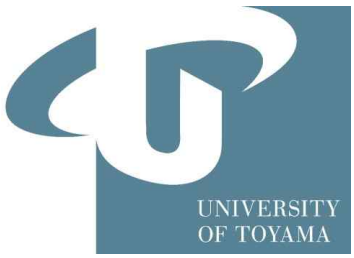
Melanogenesis Regulatory Constituents from *Premna serratifolia*, *Jatropha multifida* and *Clathria prolifera* Collected in Myanmar



SOYEUN WOO

DIVISION OF NATURAL PRODUCTS CHEMISTRY

INSTITUTE OF NATURAL MEDICINE

UNIVERSITY OF TOYAMA

2019

Table of Contents

Abbreviations 1
Chapter 1 Introduction 3
Chapter 2 Constituents of the *Premna serratifolia* wood collected in Myanmar and their melanogenesis regulatory activities 13
2.1 Introduction 14
2.2 Extraction and isolation 15
2.3 Structure elucidation of new compounds 18
2.3.1 Premnan A (**1**) 18
2.3.2 Premnan B (**2**) 24
2.3.3 Taungtangyiol C (**3**) 29
2.3.4 7,9-Dihydroxydolichanthin B (**4**) 33
2.3.5 Premnan C (**5**) 38
2.4 Anti-melanin deposition activity of isolated compounds against a mouse melanoma cell line (B16-F10) 43
2.5 Tyrosinase inhibition activity of compounds **4** and **11** 46
2.6 mRNA expression of compounds **4** and **11** 47
2.7 Summary of chapter 2 48
Chapter 3 Constituents of the *Jatropha multifida* stems collected in Myanmar and their anti-melanin deposition activities 49
3.1 Introduction 50
3.2 Extraction and isolation 53
3.3 Anti-melanin deposition activity of isolated compounds against a mouse melanoma cell line (B16-F10) 56
3.4 Tyrosinase inhibition activity of compounds **15** and **20** 57
3.5 mRNA expression of compounds **15** and **20** 58
3.6 Summary of chapter 3 59
Chapter 4 Constituents of the Myanmar marine sponge of *Clathria prolifera* and their anti-melanin and antifungal activities 60
4.1 Introduction 61
4.2 Extraction and isolation of active constituents 62
4.3 Structure elucidation of new compounds 64
4.3.1 Clathrirole A (**21**) 64
4.3.2 Clathrirole B (**22**) 69

4.4 Anti-melanin deposition activities of clathrirole A (**21**) and clathrirole B (**22**) 72
4.5 Antifungal activities of compounds clathrirole A (**21**) and clathrirole B (**22**) 73
4.6 Summary of chapter 4 74
Conclusions 75
Experimental 76
I. General experimental procedures 77
II. Experimental detail of chapter 2 80
III. Experimental detail of chapter 3 88
IV. Experimental detail of chapter 4 93
References 96
List of publications 108
Acknowledgements 109
Supplementary data 111

Abbreviations

µg/mL	Microgram per milliliter
µL	Micro liter
µM	Micro molar
^{13}C NMR	Carbon Nuclear Magnetic Resonance
^{1}H NMR	Proton Nuclear Magnetic Resonance
calcd	Calculated
CD	Circula Dichroism
$CDCl_3$	Deuterated chloroform
CH_2Cl_2	Dichloromethane
CH_3	Methyl
CH_3CN	Acetonitrile
$CHCl_3$	Chloroform
CO_2	Carbondioxide
COSY	Correlation Spectroscopy
DMEM	Dulbecco's Modified Eagle's Medium
DMSO	Dimethylsulfoxide
EtOAc	Ethyl acetate
g	Gram
H_2O	Water
HCl	Hydrochloric acid
HeLa	Human cervical cancer cell line
HMBC	Heteronuclear Multiple Bond Correlation
HMQC	Heteronuclear Multiple Quantum Correlation
HPLC	High Performance Liquid Chromatography
HREIMS	High Resolution Electron Impact Mass Spectrometry
HRESIMS	High Resolution Electron Spray Ionization Mass Spectrometry
IC_{50}	Concentration of inhibitory causing 50% reduction in activity relative to the control
IR	Infrared

KBr	Potassium bromide
J	Coupling constant
m/z	Mass-to-charge ratio
MeOH	Methanol
mg	Milligram
MHz	Megahertz
MIC	Minimum inhibitory concentration
min	Minute
mM	Millimolar
MPLC	Medium Pressure Liquid Chromatography
MS	Mass Spectroscopy
m	Multiplicity
nm	Nanometer
NMR	Nuclear Magnetic Resonance
NOESY	Nuclear Overhauser Effect Spectroscopy
OH	Hydroxy
OCH_3	Methoxy
pTLC	Preparative Thin Layer Chromatography
PBS	Phosphate buffered saline
RP	Reversed Phase
TLC	Thin Layer Chromatography
TMS	Tetramethylsilane
UV	Ultra Violet
YP	Yeast extract Peptone

Chapter 1 Introduction

Melanin is a mixture of pigmented biopolymers synthesized by the basal layer of the epidermal melanocytes. The important role of melanin is to prevent skin damage by harmful ultraviolet (UV) radiation, stress from the different sources of environmental pollutants, toxic drugs, and chemicals. However, excessive synthesis of melanin in human body from overexposure to UV radiation causes hyperpigmentation and our skin becomes darker. Hyperpigmentation led to dermatological problems, which include age spots, melasma, melanoderma, lentigo, and freckles. On the other hand, decrease of the melanin synthesis led to hypopigmentation, such as vitiligo and albinism.[1–6] Therefore, melanin synthesis (melanogeneis) has an important role in skin pigmentation.

Melanin is distinguished into two different types, eumelanin (dark brown/black insoluble pigments found in dark skin and dark hair) and pheomelanin (lighter red/yellow). Melanin is formed by melanogenesis through the complex enzymatic and biochemical-catalyzed reactions. Enzymatically, three key enzymes, tyrosinase (TYR), tyrosinase-related protein-1 (TRP-1), and tyrosinase-related protein-2 (TRP-2, also known as dopachrome tautomerase), regulate the melanogenesis. Tyrosinase catalyzes hydroxylation of tyrosine to form L-β-3,4-dihydroxyphenylalanine (L-DOPA) and oxidation of L-DOPA to produce DOPA quinone. TRP-2 converts DOPA chrome to 5,6-dihydroxyindole-2-carboxylic acid (DHICA), and then TRP-1 catalyzes the oxidation of DHICA to form indole-5,6-dihydroxyindole-2-carboxylic acid (Figure 1.1).[7–14]

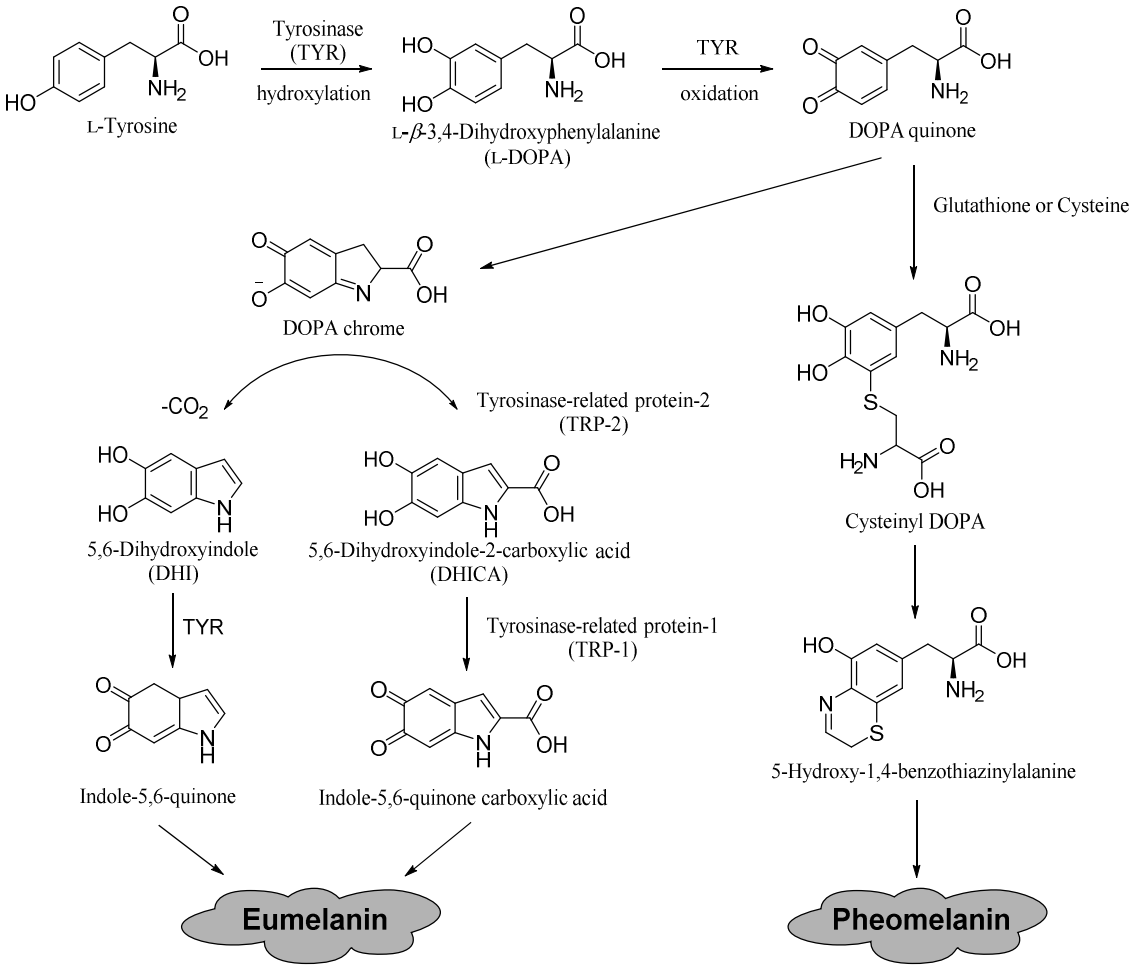


Figure 1.1 Biosynthesis of eumelanin and pheomelanin

The expression of three melanogenic enzymes (TYR, TRP-1, and TRP-2) is stimulated through the intracellular pathways. The major pathway of melanogenesis is supposed to be the cAMP dependent pathway. UV exposure causes the production of alpha melanocyte-stimulating hormone (α-MSH). When α-MSH binds to its receptor, melanocortin receptor 1 (MC1R) located on the membrane of melanocytes activates cyclic adenosine monophosphate (cAMP) pathway. Protein kinase A (PKA) and other proteins were activated by cAMP. The cAMP response element binding protein (CREB) is phosphorylated by PKA and activates the gene expression of microphthalmia-

associated transcription factor (MITF) (Figure 1.2).[15–17] The activation of MITF leads to the expression of the melanogenesis-related enzymes, thus up-regulating melanogenesis. However, inhibition of the MITF activity results in down-regulation of the melanogenesis-related enzymes and thereby inhibites melanogenesis. Hence, MITF and the melanogenesis related enzymes are known as the target to regulate melanogenesis. Secondary metabolites derived from natural products have been shown to inhibit the process of melanogenesis with down regulation of cAMP pathway (Figure 1.3).

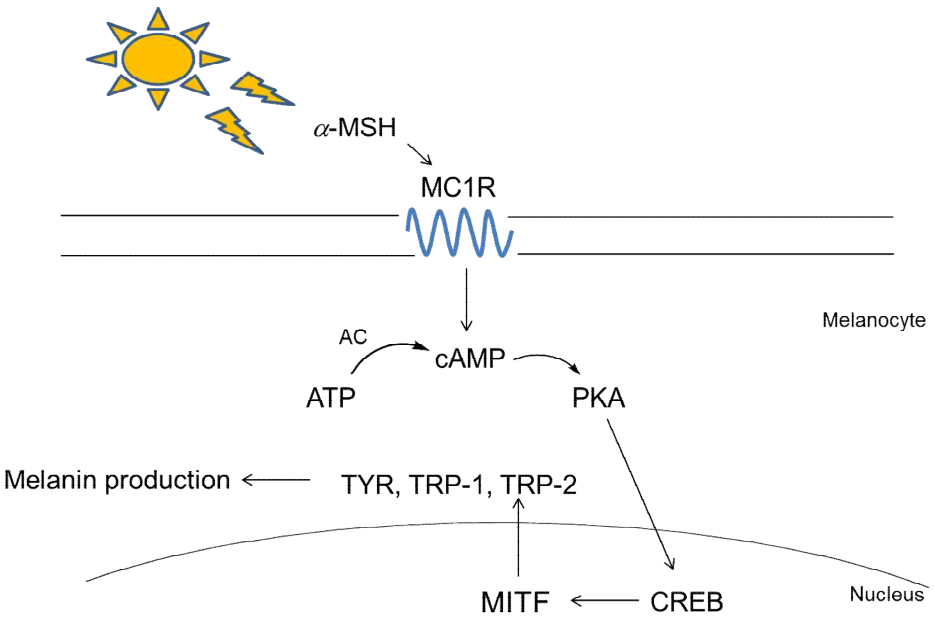


Figure 1.2 cAMP pathway of melanogenesis

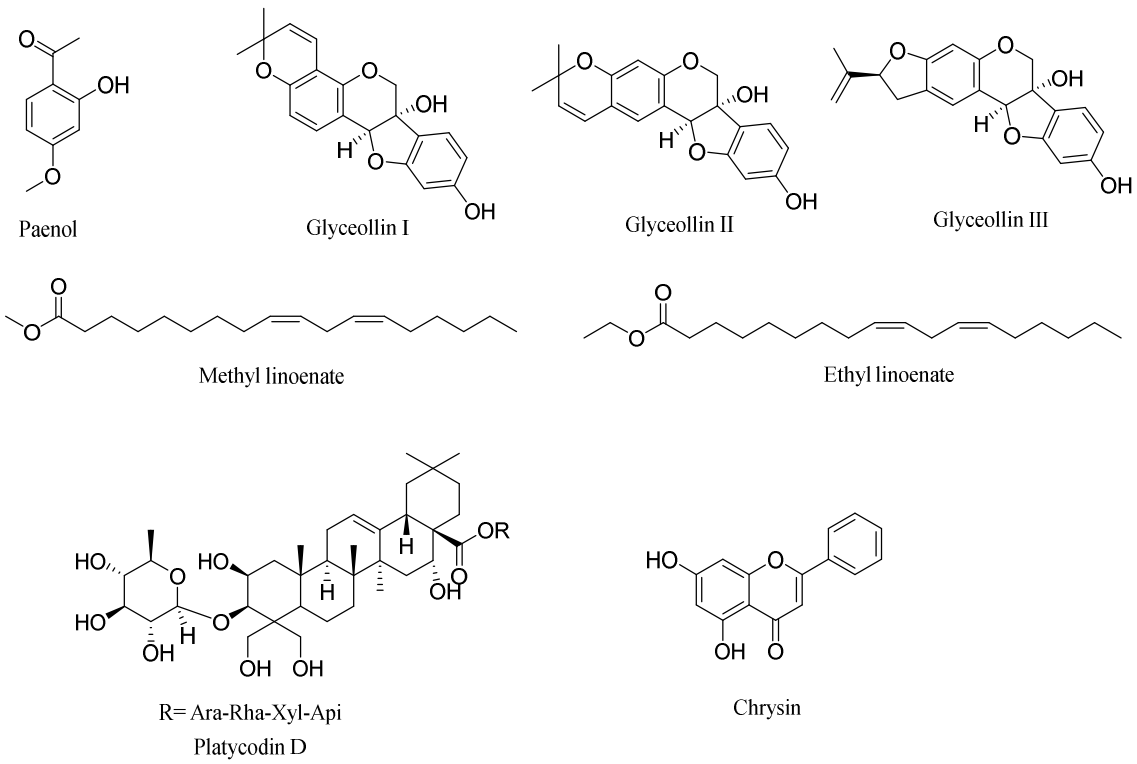


Figure 1.3 Chemical structures of cAMP pathway melanogenesis inhibitiors

Myanmar is located in South-East Asia bordered by India and Bangladesh, Thailand, Laos, and China (Figure 1.4). More than 40% of Myanmar is covered by mountains. Myanmar is characterized by three seasons, wet, cold, and dry. According to International Union for Conservation of Nature (IUCN), more than 18,000 species of plants have been recorded in Myanmar. Many of them have been used as traditional cosmetics or folk medicine. However, scientific evidence for using them is not fully reported.[18] Furthermore, Myanmar is well known as a rich source of not only medicinal plants, but also marine sponges.

Sponges are spineless animals that belong to phylum, Porifera, and considered as the most primitive multicellular animals existing for million years before. Marine

sponges have soft or hard bodies with many particles, and take nutrients such as organic particle and microorganism with filter feeding of see water.[19–21] In the last decades, approximately 200 new compounds have been isolated from marine sponges for every year. Most of the compounds isolated from marine sponges exhibited antitumor, antiviral, anti-inflammatory, antimalarial, immunosuppressive, or antibiotic activities,[22–35] and clinical trials were conducted for some of the compounds to develop new drugs, as exampled by salinosporamide A, bryostatin 1, tetrodotoxin (TTX), and anthramycin for cancer, Alzheimer, pain, and bacterial infections.[36] However, to the best of our knowledge, none of the Myanmar marine sponges has been studied for their chemical constituents. These facts encouraged us to discover bioactive secondary metabolites from Myanmar natural resources (plants and sponges).

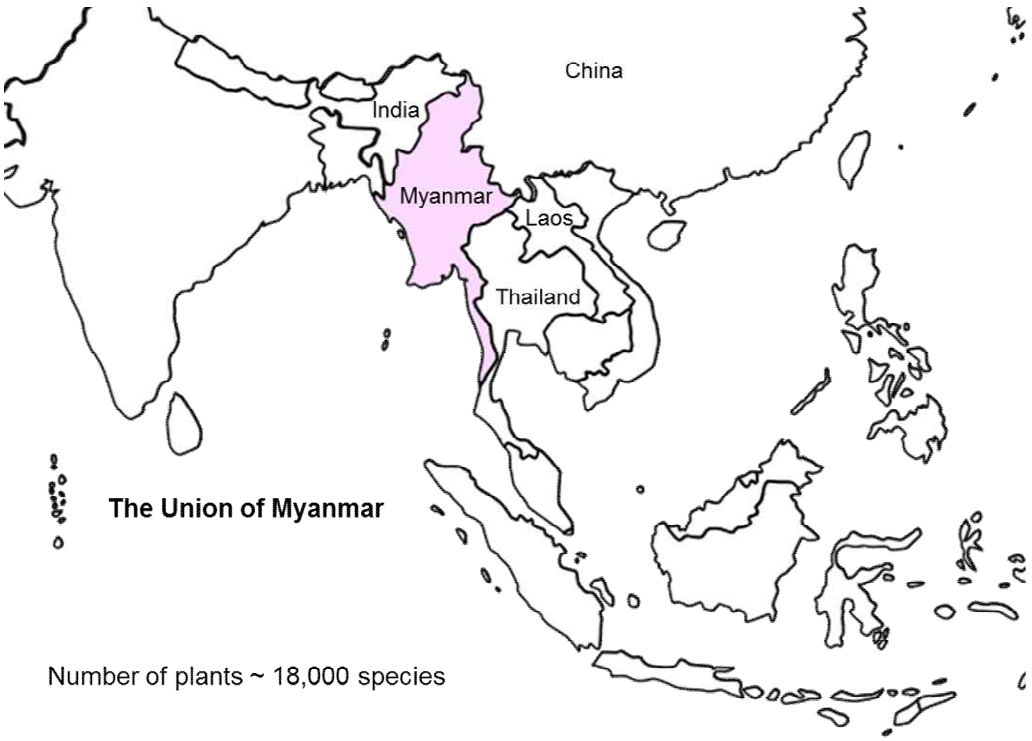


Figure 1.4 The union of Myanmar

In order to find new candidates with significant anti-melanin deposition activity, five plants, *Premna serratifolia* (syn: *P. integrifolia*), *Naringi crenulata*, *Hesperethusa crenulata*, *Gentiana kurroo*, and *Jatropha multifida*, were collected in Myanmar. All these plants were extracted with $CHCl_3$ and MeOH to obtain crude extracts. Anti-melanin deposition activity against a mouse melanoma cell line (B16-F10) supplied with α-melanocyte-stimulating hormone (α-MSH) and a potent cyclic nucleotide phosphodiesterase inhibitor, 3-isobutyl-1-methylxanthine (IBMX) to produce melanin revealed that the $CHCl_3$ extracts of the *Premna serratifolia* wood and the *Jatropha multifida* stems showed moderate anti-melanin deposition activities with IC_{50} values of 81.3 and 22.7 μg/mL, respectively, as compared with that of the positive control, arbutin (Figure 1.5).

On the other hand, a 50% MeOH fraction obtained from a MeOH-acetone mixture (2:1) crude extract of a *Clathria prolifera* sponge also exhibited moderate anti-melanin deposition activity against B16-F10 with an IC_{50} value of 76.9 μg/mL, as compared to the positive control, arbutin (Figure 1.6). The cell viability was evaluated with the total protein contents by using Bio-rad Bradford assay.

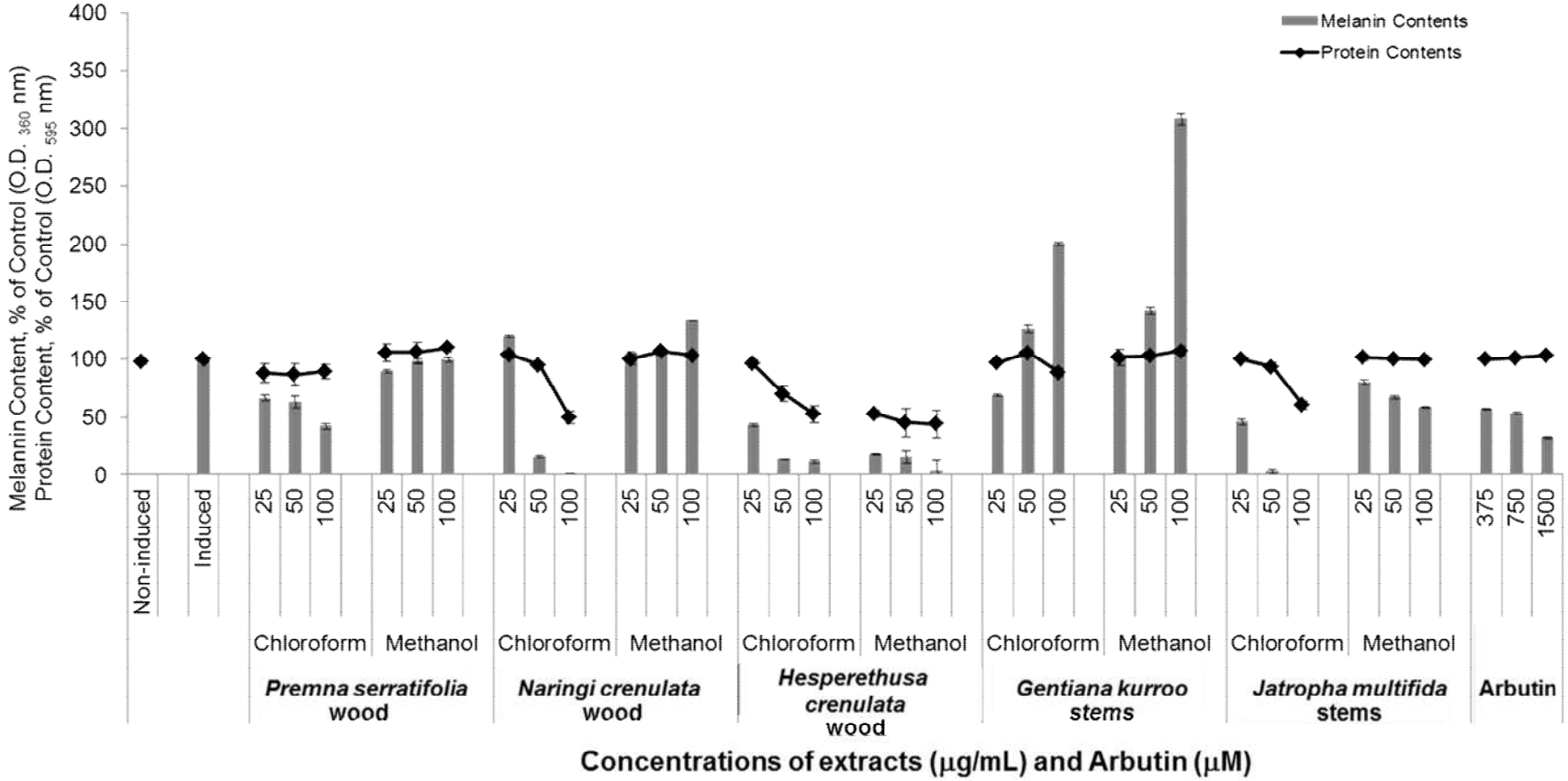


Figure 1.5 Anti-melanin deposition activities of crude extracts ($CHCl_3$ and MeOH) in a mouse melanoma cell line B16-F10

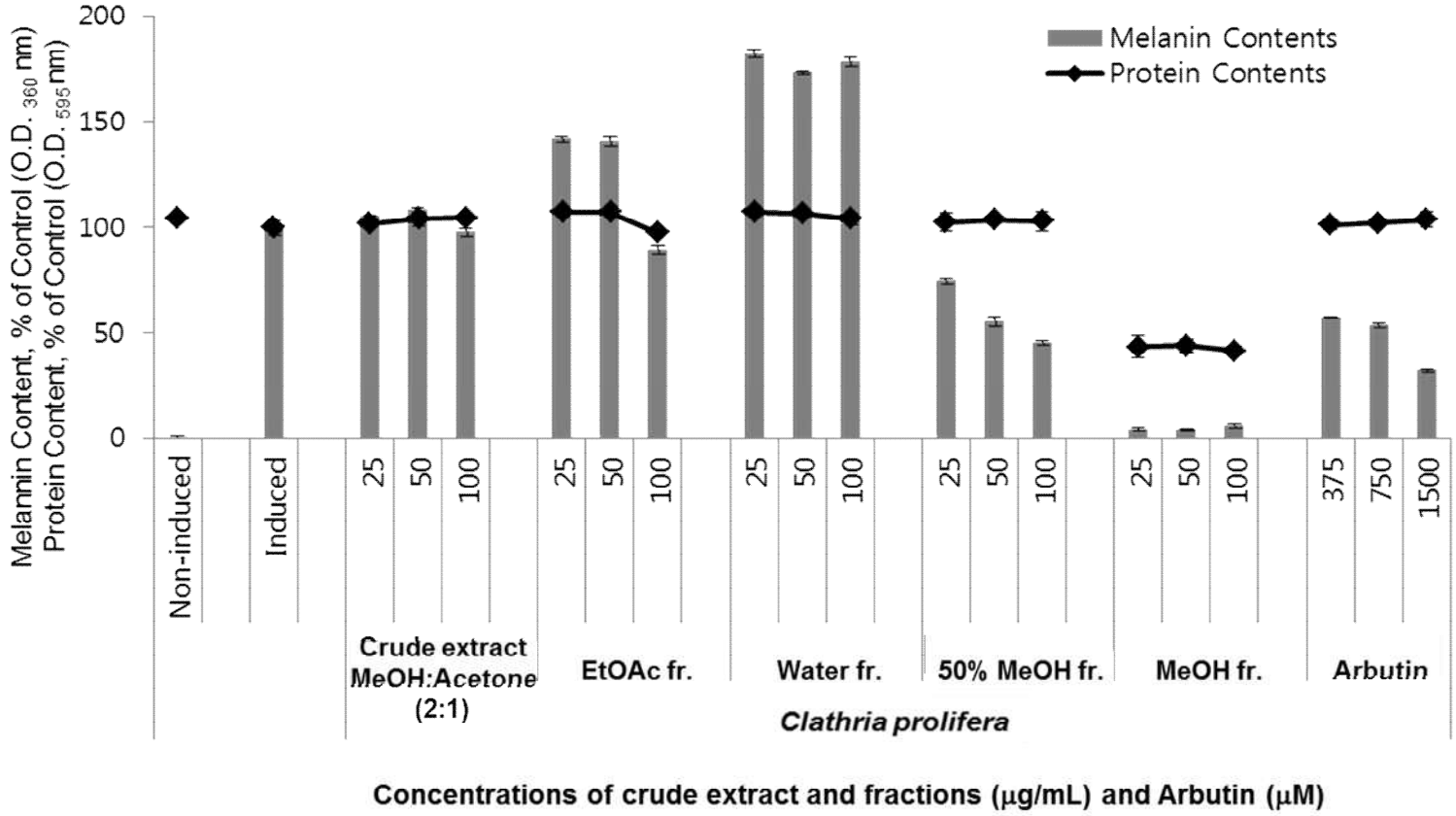


Figure 1.6 Anti-melanin deposition activities of crude extract of *C. prolifera* and each fraction of *C. prolifera* in a mouse melanoma cell line B16-F10

Thus, this study aimed to isolate new compounds from two plants, the *P. serratifolia* wood and the *J. multifida* stems, and a marine sponge *C. prolifera* by focusing on anti-melanin deposition activity.

Chapter 2 will discuss about the isolation and structure elucidation of new compounds from the *P. serratifolia* wood as well as the anti-melanin deposition activities of all isolated compounds from this plant. Chapter 3 will mainly discuss about the anti-melanin deposition activities of isolated compounds from the *J. multifida* stems. Finally, isolation and structure elucidation of new compounds from the marine sponge *C. prolifera* collected in Myanmar and their anti-melanin deposition activities will be discussed in Chapter 4.

Chapter 2 Constituents of the *Premna serratifolia* wood collected in Myanmar and their melanogenesis regulatory activities

2.1 Introduction

P. serratifolia (syn: *P. integrifolia*) (Verbenaceae) (Figure 2.1) is widely distributed in near western sea coast from South Asia to South East Asia, which include India, Malaysia, Vietnam, Cambodia, and Sri Lanka. A part of this plant such as leaves and roots are used for treatment of various diseases, including indigestion, dysuria, dysentery, stomachache, fever, diabetes, inflammation, headache, and bronchitis, as well as kidney and liver problems.[37–40] The leaves of this plant have been reported for anti-coagulant, anti-inflammatory, anti-microbial, cytotoxicity, antioxidant, and gastroprotective activities. In addition, the roots of *P. serratifolia* exhibited cytotoxicity, antioxidant, and anti-microbial activities. Furthermore, the flowers, bark, and wood of this plant showed anti-inflammatory and antioxidant activities.[41–50] *P. serratifolia* is usually called as "*Taung-tangyi*" in Myamar, and people in Tanintharyi region located in the southern part of Myanmar have utilized the bark and wood of *P. serratifolia* as ingredient to make the traditional cosmetics "Thanaka" for many centuries. Thanaka is applied in the form of paste onto face, arms, and legs to make smooth and clear skin as well as to prevent wrinkles, skin aging, excessive facial oil, pimples, blackheads, and whiteheads.[51] Several phytochemical studies reported the isolation of alkaloids, iridoid glycosides, steroids, acteoside, diterpenes, and polyisoprenoid as well as pharmaceutical properties of those compounds such as anti-coagulant, anti-arthritic, anti-hyperglycemic, cytotoxicity, antioxidant, antinociceptive, gastroprotective, anti-inflammatory, and anti-microbial activities.[37, 52–54] However, its cosmetic properties have not yet been investigated.

2.2 Extraction and isolation

The dried powder of the *P. serratifolia* wood (4.8 kg) was sonicated in $CHCl_3$ (8 L, 90 min, ×4) at room temperature and after removing the solvent under reduced pressure, the $CHCl_3$ extract (31.5 g) was obtained. The $CHCl_3$ extract (31.5 g) was applied to silica gel column chromatography eluted with *n*-hexane–EtOAc (10:1, 8:2, 7:3, 5:5, 3:7, 2:8, 0:10, v/v) as a gradient solvent system to give ten fractions (Fr. 1–10). These fractions were further subjected to series of chromatographic separation, which led to isolation of eleven compounds including four new lignoids, premnan A (**1**, 1.7 mg), premnan B (**2**, 1.6 mg), taungtangyiol C (**3**, 3.0 mg),[55] and 7,9-dihydroxydolichanthin B (**4**, 8.1 mg),[56] together with premnan C (**5**, 2.1 mg)[55] assumed to be an artifact, one natural new lignoid (3*R*,4*S*)-4-(1,3-benzodioxol-5-ylcarbonyl)-3-[(*R*)-1-(1,3-benzodioxol-5-yl)-1-hydroxymethyl]tetrahydro-2-furanone (**6**, 1.6 mg),[57] and five known compounds (-)-aptosimon (**7**, 3.4 mg), (-)-diasesamin-di-γ-lactone (**8**, 17.1 mg),[58] and (+)-epi-sesaminone (**9**, 4.0 mg),[59] oleanonic acid (**10**, 4.2 mg),[60] and (2α, 3α)-dihydroxyolean-12-en-28-oic acid (**11**, 3.3 mg)[61]] (Figures 2.2, 2.3 and 2.4). All new compounds were elucidated based on 1D and 2D NMR, IR spectroscopy, and HRESIMS. The absolute configurations of **1**–**3** and **5** were also determined by optical rotation and circular dichroism (CD) data analysis, and the known compounds **6**–**11** were identified by comparisons of their spectroscopic data and the reported literatures.



Figure 2.1. *Premna serratifolia* wood

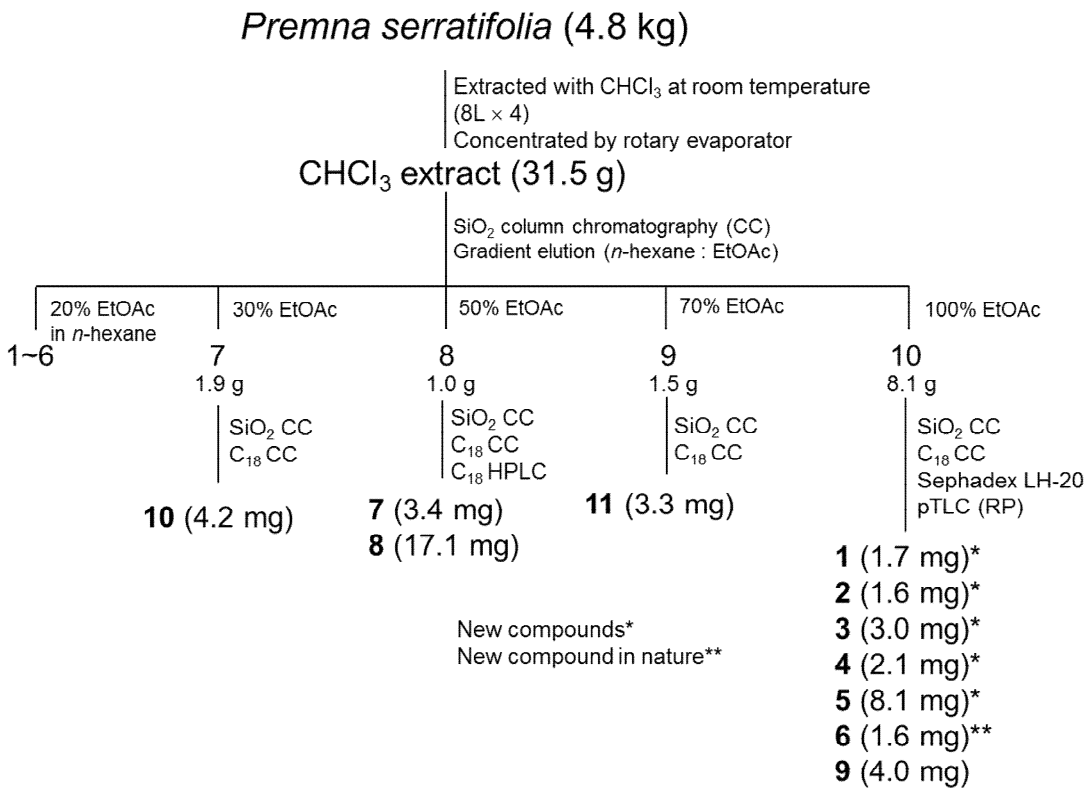


Figure 2.2 Extraction and isolation of compounds from $CHCl_3$ extract of *P. serratifolia* wood

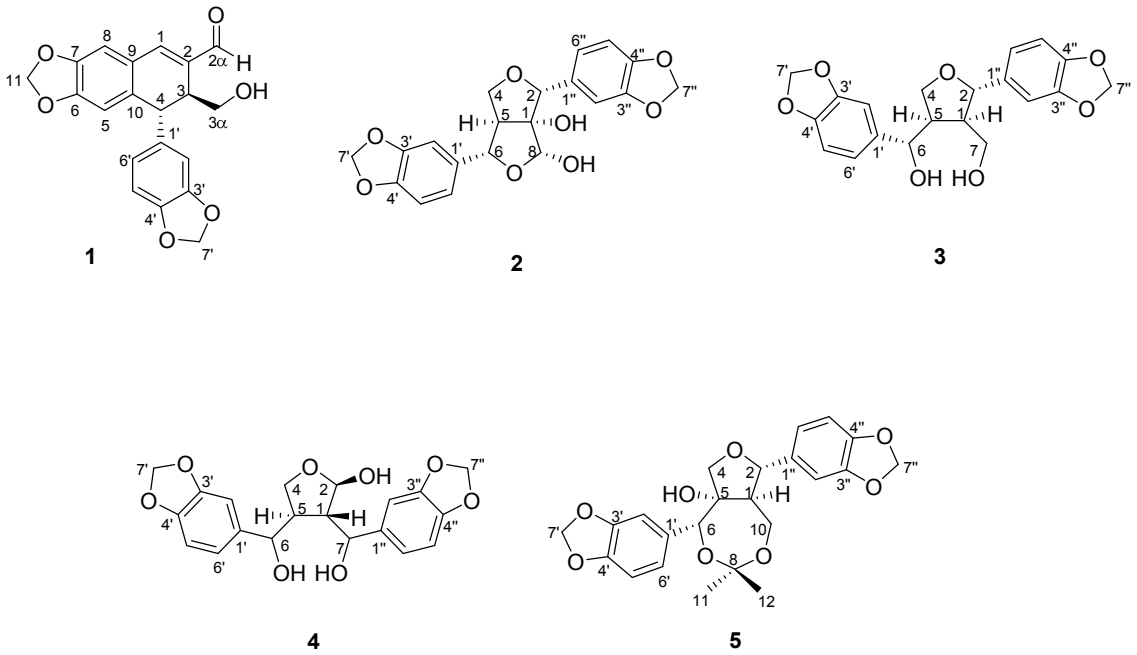


Figure 2.3 Structures of new compounds isolated from $CHCl_3$ extract of *P. serratifolia* wood

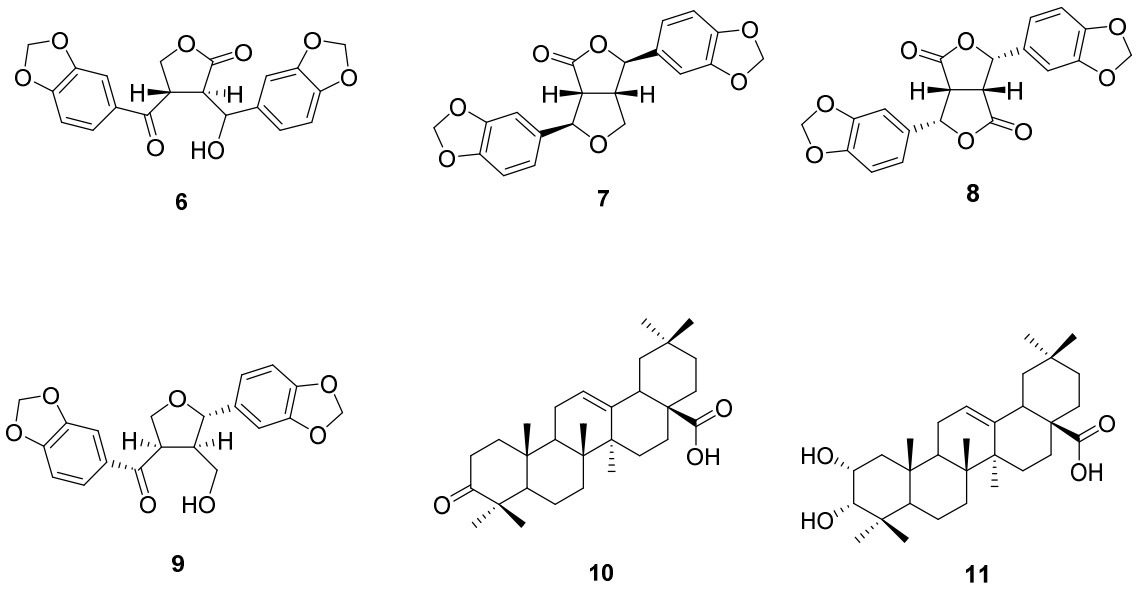


Figure 2.4 Structures of known compounds isolated from $CHCl_3$ extract of *P. serratifolia* wood

2.3 Structure elucidation of new compounds

2.3.1 Premnan A (1)

Compound **1** was obtained as a pale yellowish amorphous solid with positive optical rotation ($[\alpha]_D^{25}$ +83.2° (*c* 0.1, MeOH)). The HRESIMS of **1** indicated molecular ion clusters $[M+Na]^+$ (*m/z* 375.0869) and its molecular formula was deduced as $C_{20}H_{16}O_6$ in conjugation with NMR data. The IR spectrum showed characteristic absorption bands corresponding to the hydroxy functional group (3463 cm^{-1}) and the aromatic ring (1640, 1592, and 1485 cm^{-1}). The UV spectrum of **1** showed absorption maxima at 247 and 360 nm. The ^1H NMR spectrum (Figure 2.5, Table 2.1) showed signals of an aldehyde group [δ_H 9.54, (s, H-2α)], three aromatic/olefinic methines [δ_H 7.27 (s, H-1), 6.86 (s, H-8), 6.68 (s, H-5)], a 1,3,4-trisubstituted phenyl group [δ_H 6.42 (d, *J* = 1.8 Hz, H-2′), 6.63 (d, *J* = 8.1 Hz, H-5′), 6.44 (dd, *J* = 1.8, 8.1 Hz, H-6′)], two dioxymethylenes [δ_H 5.87 (d, *J* = 1.5 Hz, H-7′a), 5.86 (d, *J* = 1.5 Hz, H-7′b), 6.01 (d, *J* = 1.5 Hz, H-11a), 6.00 (d, *J* = 1.5 Hz, H-11b)], an oxymethylene [δ_H 3.63 (dd, *J* = 5.7, 10.7 Hz, H-3αa), 3.40 (dd, *J* = 8.6, 10.7 Hz, H-3αb)], and two methines [δ_H 4.28, (s, H-4), 3.20 (m, H-3)]. The ^{13}C NMR (Figure 2.6, Table 2.1) and HMQC data revealed the presence of 20 carbon signals, including an aldehyde carbonyl [δ_C 193.1 (C-2α)], four oxygenated aromatic quaternary carbons [(δ_C 150.6 (C-6), 147.8 (C-3′), 147.4 (C-7), 146.3 (C-4′)], an olefinic methine [δ_C 146.8 (C-1)], four aromatic/olefinic non-protonated carbons [(δ_C 137.7 (C-1′), 135.3 (C-2), 134.4 (C-10), 125.1 (C-9)], five aromatic methines [(δ_C 120.5 (C-6′), 110.9 (C-5), 109.0 (C-8), 108.3 (C-5′), 108.0 (C-2′)], two dioxymethylenes [δ_C 101.9 (C-11), 101.1 (C-7′)], an oxymethylene [δ_C 63.6 (C-3α)], and two sp^3 methines [δ_C 44.5 (C-4), 42.8 (C-3)]. According to the HMBC correlations from H-1 to C-2/C-3/C-8/C-10, from H_2-3α to C-2/C-4, from H-4 to

C-2/C-5/C-9/C-10, from H-5 to C-6/C-7/C-9, and from H-8 to C-6/C-7/C-10 (Figure 2.7a), a 3-hydroxymethyl-3,4-dihydronapthalene ring (numbering according to **1**) was established in the structure of **1**. ^{1}H-^{1}H COSY correlations of H-3/H-4 and H-3/H-3α allowed us to attach the hydroxymethyl group at C-3 (Figure 2.7a). Furthermore, the downfield shifts of the C-1 methine proton (δ_H 7.27) and the carbon (δ_C 146.8), and the HMBC correlations from H-1 to C-2α and from H-2α to C-2/C-3 suggested that the aldehyde group was attached to C-2. The HMBC correlations from H-1 to C-2α/C-3/C-8/C-10, from H-4 to C-2/C-5/C-9/C-10, from H-5 to C-6/C-7/C-9, and from H-8 to C-6/C-7/C-10 suggested the presence of a 1,2-dihydronaphthalene in **1**. Based on the observation of HMBC correlation from H_2-11 to the downfield-shifted aromatic quaternary carbons at C-6 and C-7, a methylenedioxy group was directly attached to the 1,2-dihydronaphthalene at C-6 and C-7. In contrast, the COSY correlation of H-5′/H-6′ and the HMBC correlations from H-2′/H-6′ to C-4′, from H-5′ to C-1′/C-3′, and from H_2-7′ to C-3′/C-4′ revealed the presence of the methylenedioxyphenyl group as a partial structure of **1**. The HMBC correlations from H-4 to C-1′/C-2′/C-6′ confirmed the attachment of the methylenedioxyphenyl group at C-4. Thus, compound **1** was determined to be a phenylnaphthalene-type lignan containing two piperonyl rings as the partial structure, and the planar structure of **1** was elucidated as shown in Figure 2.3.

The planner structure of **1** was close resemblance to vitexdoin A,[62] containing the 3,4-dihydroxybenzene and 4-hydroxy-3-methoxybenzene rings, instead of the piperonyl rings of **1**. The singlet methine signal at H-4 in **1**, associated with a small coupling constant close to zero due to the dihedral angle of ca. 90° between H-3 and H-4, and the cross peak of H-4/H_2-3α in the NOESY spectrum suggested the *trans*

relationship between H-3 and H-4 (Figure 2.7b), as observed in the relationships of the corresponding protons in vitexdoin A.[62,63] However, comparisons of ECD curves (242 and 348 nm were positive, while 213, 260, and 316 nm were negative for **1**; 242 and 348 nm were negative, while 213, 260, and 316 nm were positive for vitexdoin A) (Figure 2.8) and optical rotation ($[\alpha]_D^{25}$ +83.2° for **1**; $[\alpha]_D^{15}$ -156.0° for vitexdoin A)[62–64] between **1** and vitexdoin A with the 3*R*, 4*S* absolute configuration revealed that they are totally opposite. Thus, the absolute configurations of **1** were determined as 3*S* and 4*R*, and **1** was named premnan A.

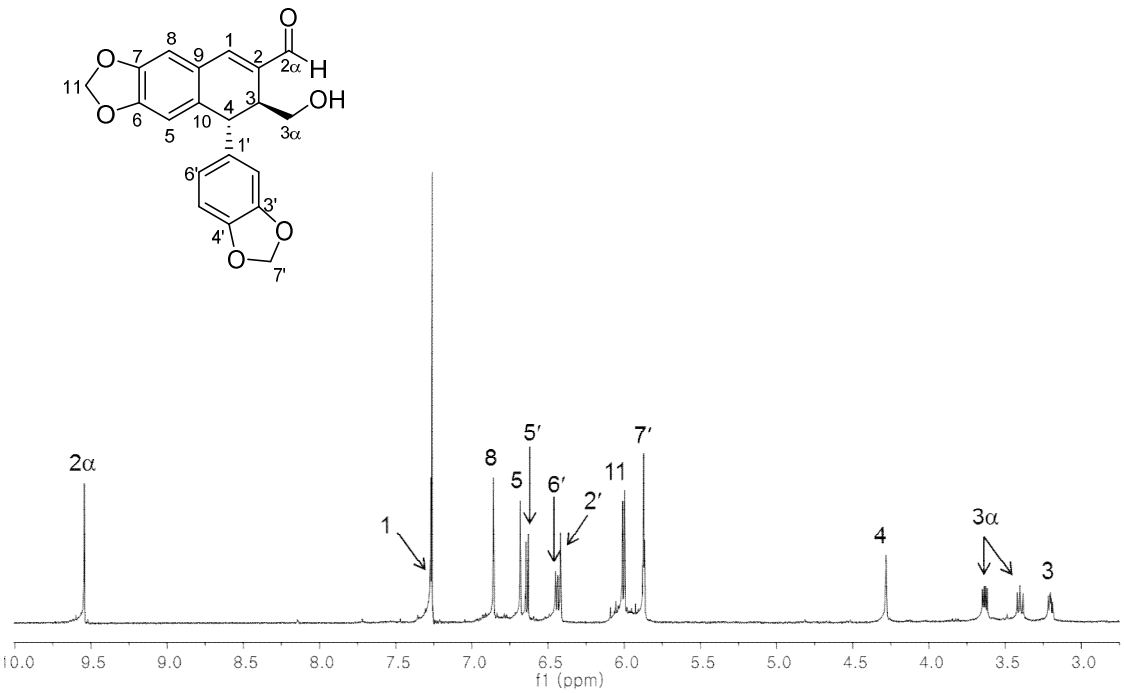


Figure 2.5 ^{1}H NMR spectrum (500 MHz) of **1** in $CDCl_3$

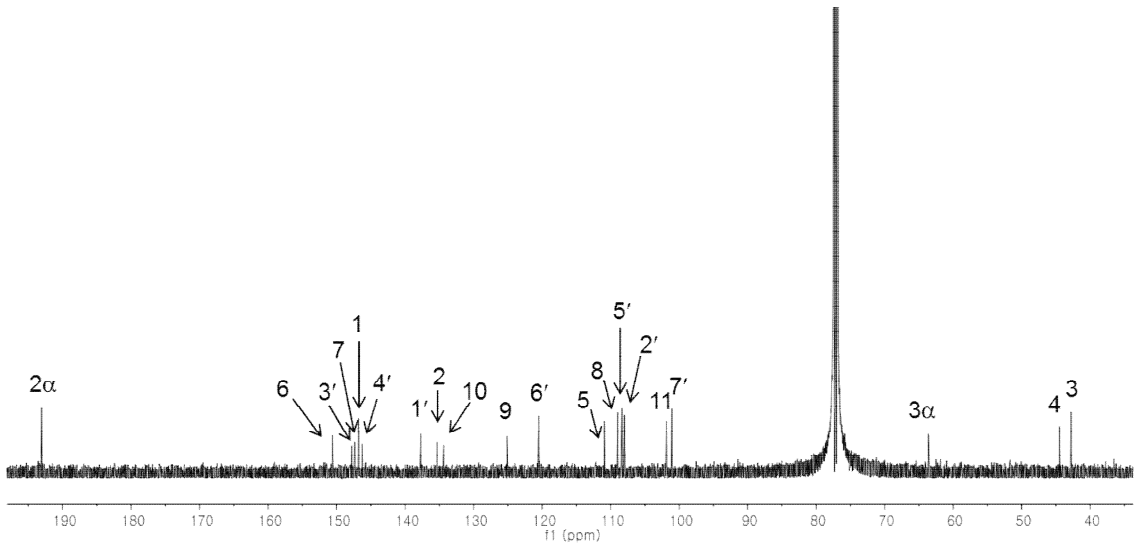


Figure 2.6 ^{13}C NMR spectrum (125 MHz) of **1** in $CDCl_3$

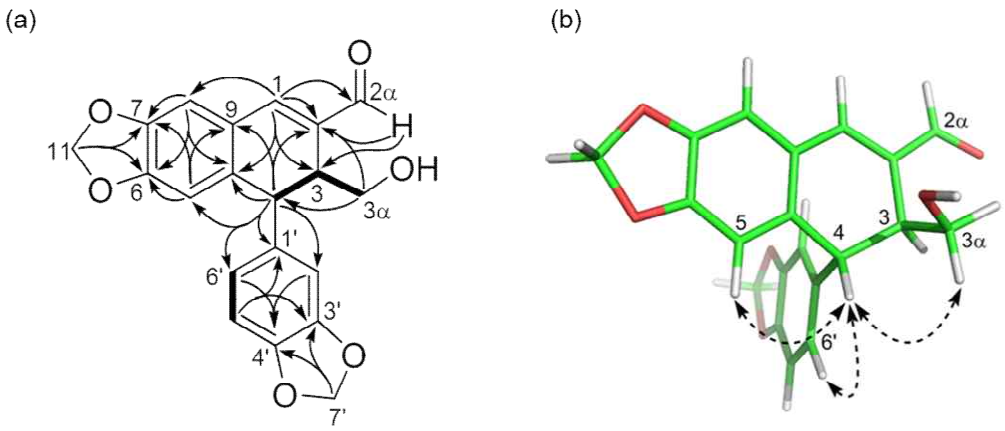


Figure 2.7 ^{1}H-^{1}H COSY correlations (bold lines) and key HMBC correlations (arrows) (a) and key NOESY correlations (dashed arrows) of **1** (b)

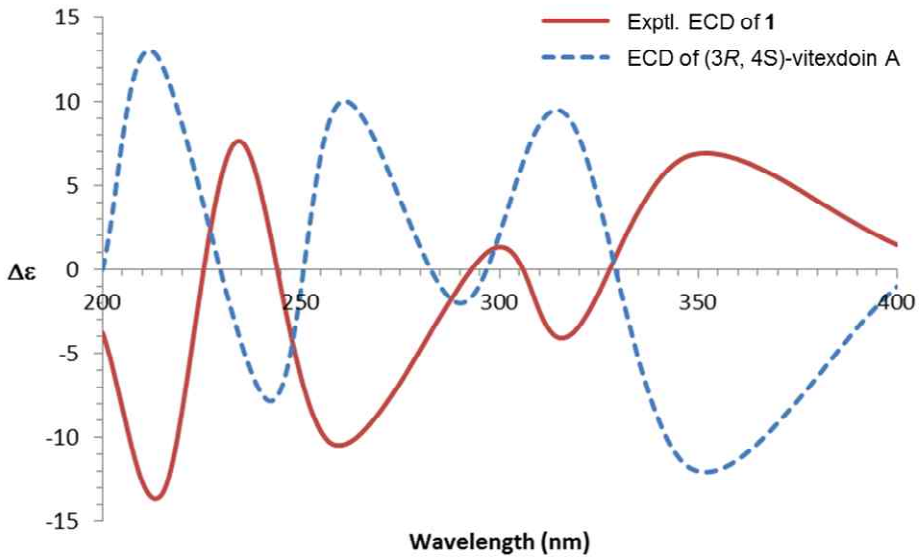


Figure 2.8 Experimental ECD spectra of **1** and vitexdoin A

Table 2.1

^{1}H (500 MHz) and ^{13}C NMR (125 MHz) spectroscopic data for **1** in $CDCl_3$ (δ in ppm and *J* values in (Hz) in parentheses)

	1	
position	δ_H	δ_C
1	7.27, s	146.8, CH
2		135.3, C
2α	9.54, s	193.1, CH
3	3.20, m	42.8, CH
3αa	3.63, dd (5.7, 10.7)	63.6, CH_2
3αb	3.40, dd (8.6, 10.7)	
4	4.28, brs	44.5, CH
5	6.68, s	110.9, CH
6		150.6, C
7		147.4, C
8	6.86, s	109.0, CH
9		125.1, C
10		134.4, C
11a	6.01, d (1.5)	101.9, CH_2
11b	6.00, d (1.5)	
12		
1′		137.7, C
2′	6.42, d (1.8)	108.0, CH
3′		147.8, C
4′		146.3, C
5′	6.63, d (8.1)	108.3, CH
6′	6.44, d (1.8, 8.1)	120.5, CH
7′a	5.87, d (1.5)	101.1, CH_2
7′b	5.86, d (1.5)	

2.3.2 Premnan B (2)

Compound **2** was isolated as a white amorphous solid. The optical rotation of **2** exhibited $[\alpha]_D^{25}$ +1.6° (*c* 0.1, MeOH). The HRESIMS analysis of **2** showed molecular ion peak at *m/z* 409.0868 $[M+Na]^+$ corresponding to molecular formula $C_{20}H_{18}O_8$. The IR spectrum of **2** showed absorption bands of the hydroxy group at 3470 cm^{-1} and the aromatic ring at 1638 and 1498 cm^{-1}, respectively. The UV spectrum showed absorption maxima at 245 and 288 nm. The ^{1}H NMR spectrum of **2** (Figure 2.9, Table 2.2) revealed resonances characteristic of a 1,3,4-trisubstituted phenyl group [δ_H 7.03 (d, *J* = 1.3 Hz, H-2″), 6.86 (dd, *J* = 1.3, 7.9 Hz, H-6″), 6.77 (d, *J* = 7.9 Hz, H-5″)], three aromatic methines [δ_H 6.92 (brs, H-2′), 6.83 (m each, H-5′, H-6′)], two dioxymethylenes [δ_H 5.98 (s, H_2-7″), 5.96 (s, H_2-7′)], three oxymethines [δ_H 5.34 (s, H-8), 4.97 (s, H-2), 4.88 (d, *J* = 7.4 Hz, H-6)], an oxymethylene [δ_H 4.41 (dd, *J* = 6.2, 9.1 Hz, H-4a), 4.08 (dd, *J* = 2.6, 9.1 Hz, H-4b)], an aliphatic methine [δ_H 2.91 (m, H-5)], and a hydroxy group [δ_H 2.30 (s, 1-OH)]. The ^{13}C-NMR spectrum (Figure 2.10, Table 2.2) showed four oxygenated aromatic quaternary carbons [(δ_C 148.3 (C-3″), 148.2 (C-3′), 148.1 (C-4′), 147.6 (C-4″)], two aromatic non-protonated carbons [(δ_C 135.4 (C-1″), 129.6 (C-1′)], six aromatic methines [(δ_C 120.4 (C-6′), 120.0 (C-6″), 108.5 (C-5′), 108.2 (C-5″), 107.8 (C-2′), 107.0 (C-2″)], two dioxymethylenes [δ_C 101.4 (C-7″), 101.3 (C-7′)], four sp^3 oxymethines [δ_C 97.6 (C-8), 85.8 (C-2), 85.3 (C-6)], an oxygenated sp^3 quaternary carbon [δ_C 90.5 (C-1)], an sp^3 oxymethylene [δ_C 70.9 (C-4)], and an sp^3 methine [δ_C 58.6 (C-5)]. The above NMR data of **2** and the HMBC experiment (Figure 2.11a) revealed a close structural resemblance to (+)-paulownin, the furoruran lignan isolated from *Cycas vespertilio*.[65] Significant difference was the presence of a hydroxy group at C-8 in **2**. The HMBC correlations from 1-OH/H-2/H-6 to C-8, as well as downfield-shifted sp^3 methine signal

at C-8 in **2**, instead of the sp^3 methylene signal at this position in paulownin also supported this assignment. A *cis* relationship of H-5 and the hydroxyl group at C-1, as well as the α-orientations of H-5, the two methylenedioxyphenyl groups at C-2 and C-6, and the C-1 and C-8 hydroxyl groups were revealed by the NOESY correlations of H-2/H-6, H-2/H-8, H-4a/H-6, 1-OH/H-5, and 1-OH/H-6′ (Figure 2.11b). Furthermore, the absolute configurations of **2** were determined as 1*R*, 2*R*, *5R*, 6*S*, and 8*R* from the ECD spectra analysis (Figure 2.12) and **2** was named premnan B.

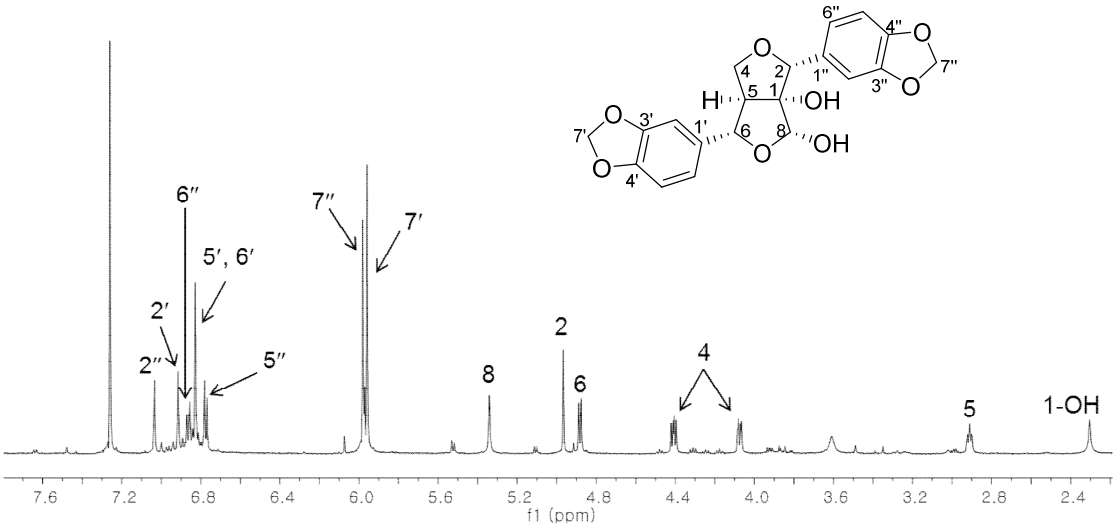


Figure 2.9 ^{1}H NMR spectrum (500 MHz) of **2** in $CDCl_3$

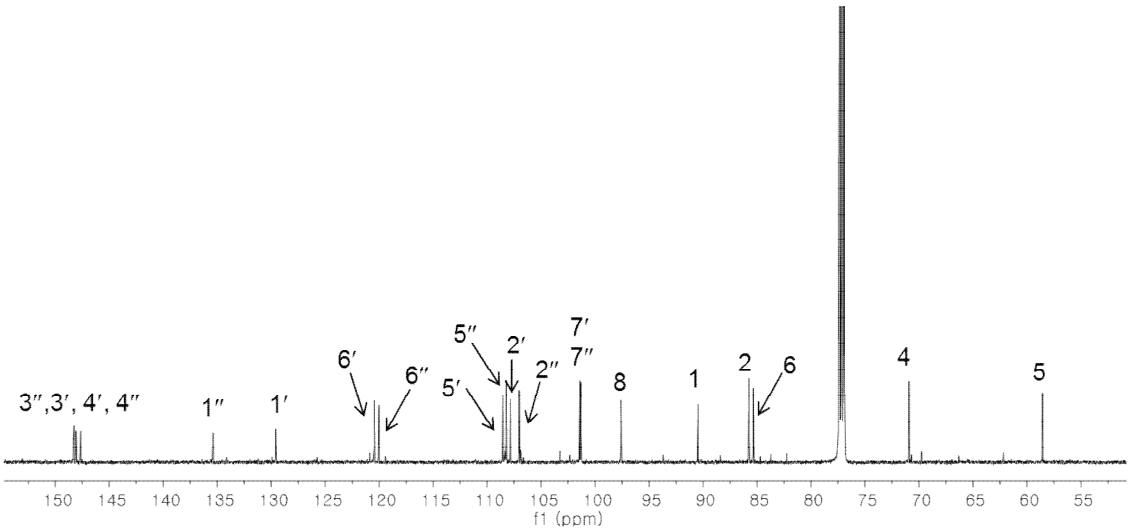


Figure 2.10 ^{13}C NMR spectrum (125 MHz) of **2** in $CDCl_3$

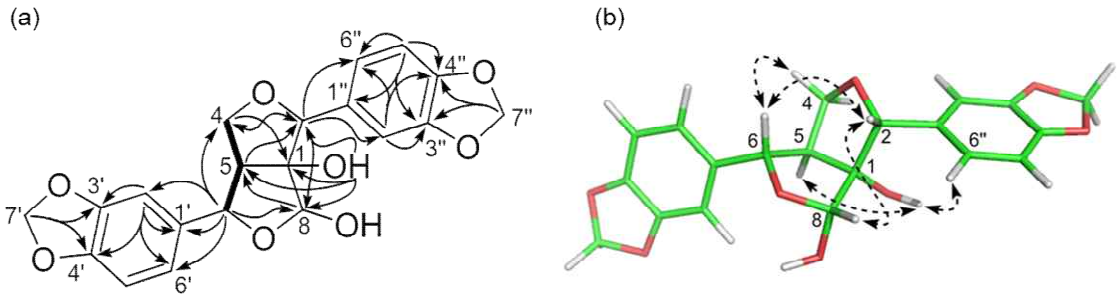


Figure 2.11 ^{1}H-^{1}H COSY correlations (bold lines) and key HMBC correlations (arrows) (a) and key NOESY correlations (dashed arrows) of **2** (b)

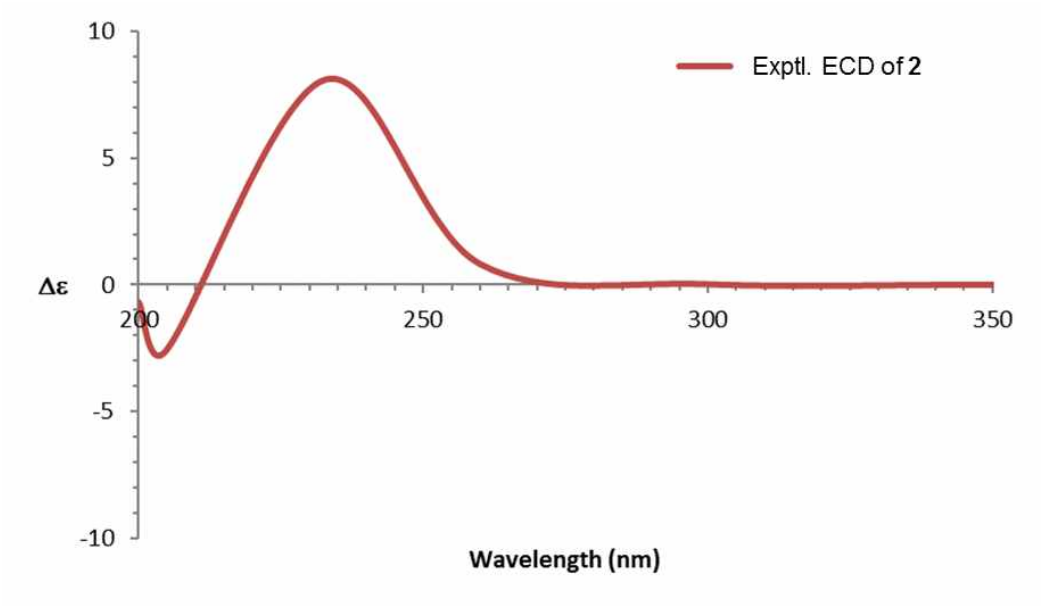


Figure 2.12 ECD spectra of **2**

Table 2.2

^{1}H (600 MHz) and ^{13}C NMR (150 MHz) spectroscopic data for **2** in $CDCl_3$ (δ in ppm and *J* values in (Hz) in parentheses)

	2	
position	δ_H	δ_C
1		90.5, C
2	4.97, s, 1H	85.8, CH
4a	4.41, dd (6.2, 9.1),	70.9, CH_2
4b	4.08, dd (2.6, 9.1)	
5	2.91, m	58.6, CH
6	4.88, d (7.4)	85.3, CH
8	5.34, s	97.6, CH
1′		129.6, C
2′	6.92, brs	107.8, CH
3′		148.2, C
4′		148.1, C
5′	6.83[c], m	108.5, CH
6′	6.83[c], m	120.4, CH
7′	5.96, 2H, s	101.3, CH_2
1″		135.4, C
2″	7.03, d (1.3)	107.0, CH
3″		148.3, C
4″		147.6, C
5″	6.77, d (7.9)	108.2, CH
6″	6.86, dd (1.3, 7.9)	120.0, CH
7″	5.98, 2H, s	101.4, CH_2
1-OH	2.30, s	

2.3.3 Taungtangyiol C (3)

Compound **3** was found as a white amorphous solid with a negative optical rotation ($[\alpha]_D^{25}$ −55.5°(*c* 0.1, MeOH)). Its molecular formula was elucidated as $C_{20}H_{20}O_7$ from molecular ion peak at *m/z* 395.1101 $[M+Na]^+$ in the HRESIMS (calcd. for $C_{20}H_{20}O_7Na$: 395.1101) and NMR data. The IR spectrum of **3** showed a characteristic absorption band of the hydroxy group at 3436 cm^{-1}. The UV spectrum showed absorption maxima at 247 and 285 nm. The ^1H and ^{13}C NMR spectra (Figures 2.13 and 2.14, Table 2.3), in combination with the HMQC spectroscopic data of **3** recorded in $CDCl_3$, were quite similar to those of taungtangyiol A,[41] previously reported by our group recorded in $CDCl_3$ (see experimental section). The significant difference between **3** and taungtangyiol A was the absence of the hydroxy group at C-5 in **3**. This assignment was supported by the COSY correlations of H-1 (δ_H 2.56)/H-2 (δ_H 4.52), H-1/H-5 (δ_H 2.82), H-1/H_2-7 (δ_H 4.01, 3.74), H-5/H_2-4 (δ_H 3.72, 3.39), and H-5/H-6 (δ_H 4.77) and the HMBC correlations of H_2-7 to C-5 (Figure 2.15a). The relative configuration of the tetrahydrofuran ring moiety of **3** (C-1, C-2, and C-5) was determined by a NOESY experiment (Figure 2.15b). The cross peaks of H-4b (δ_H 3.39)/H-6, H-4b/H-7a (δ_H 4.01), H-6/H-7a, H-2/H-7b (δ_H 3.74), and H-1/H-2″ in the NOESY spectrum suggested β-orientations of H-2, C-6, and C-7, and α-orientations of H-5 and the methylenedioxyphenyl group at C-2. Based on the observations of the NOESY correlations of H-2′ (δ_H 6.88)/H_2-4 and H-4b/H-6 as well as comparison with the experimental ECD spectra and calculated ECD spectra (Figure 2.16), the absolute configurations of **3** were determined 1*R*, 2*S*, *5R*, and 6*S* and **3** was named taungtangyiol C.

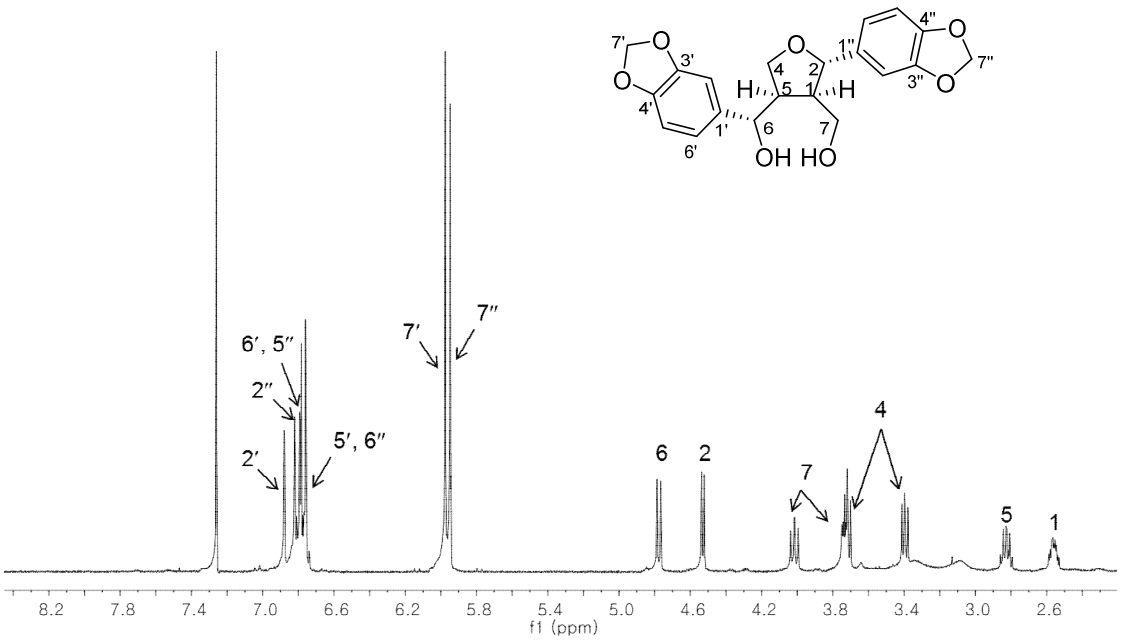


Figure 2.13 ^{1}H NMR spectrum (500 MHz) of **3** in $CDCl_3$

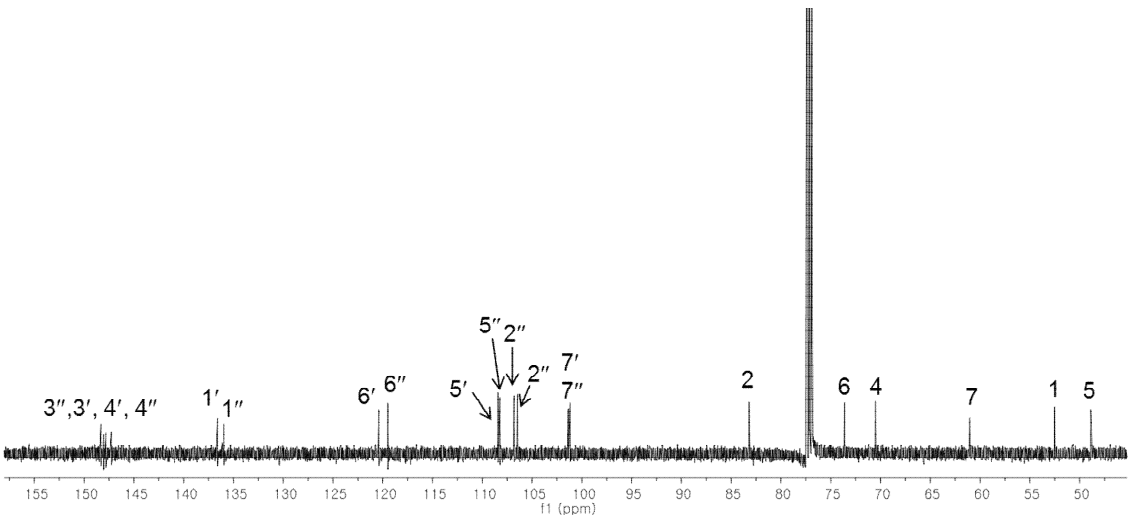


Figure 2.14 ^{13}C NMR spectrum (125 MHz) of **3** in $CDCl_3$

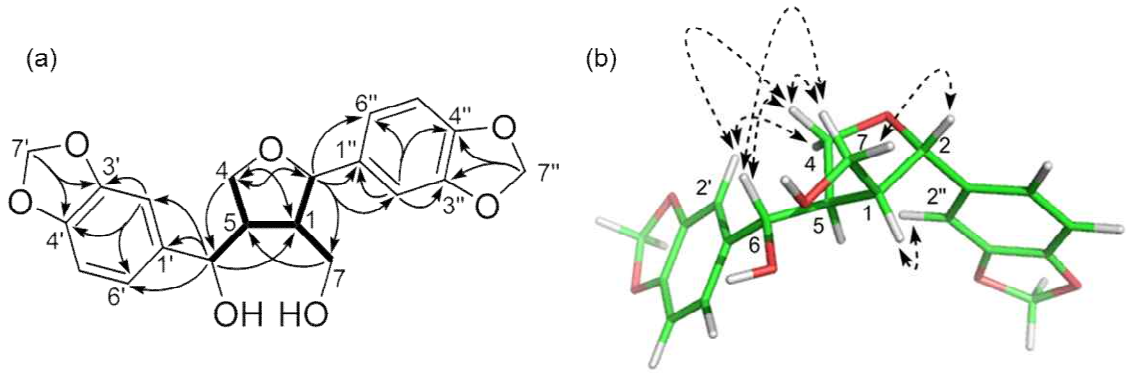


Figure 2.15 ^{1}H-^{1}H COSY correlations (bold lines) and key HMBC correlations (arrows) (a) and key NOESY correlations (dashed arrows) of **3** (b)

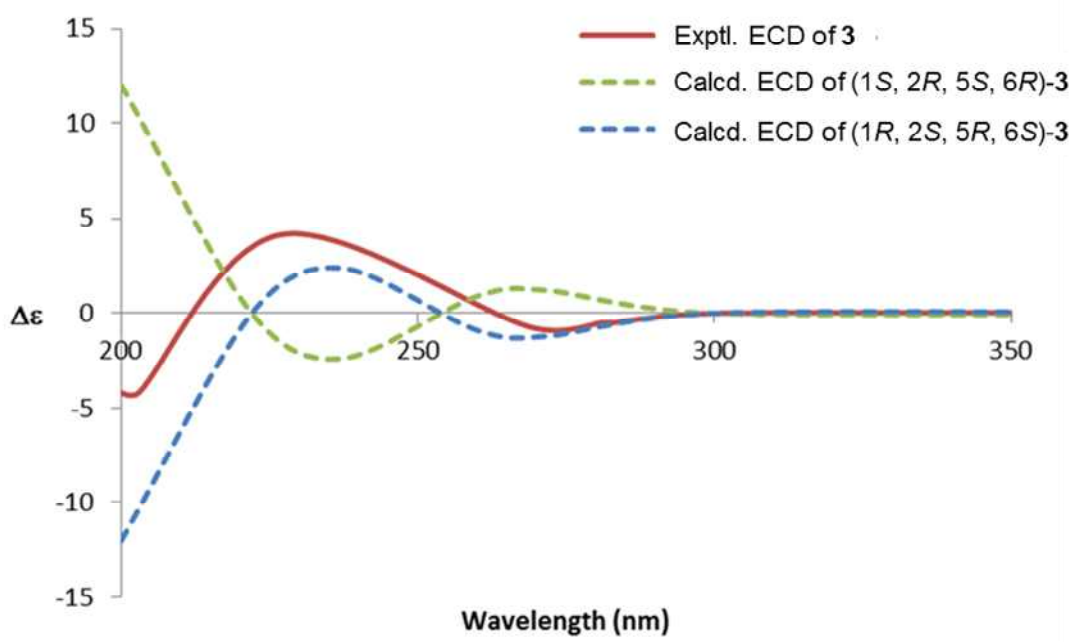


Figure 2.16 Experimental and calculated ECD spectra of **3**

Table 2.3

^{1}H (500 MHz) and ^{13}C NMR (125 MHz) spectroscopic data for **3** in $CDCl_3$ (δ in ppm and *J* values in (Hz) in parentheses)

	3	
position	δ_H	δ_C
1	2.56, m	52.5, CH
2	4.52, d (7.1)	83.2, CH
4a	3.72, dd (7.4, 9.3)	70.5, CH_2
4b	3.39, dd (5.9, 7.4)	
5	2.82, m	48.9, CH
6	4.77, d (10.0)	73.6, CH
7a	4.01, dd (9.8, 11.3)	61.0, CH_2
7b	3.74, m	
1′		136.6, C
2′	6.88, d (1.5)	106.8, CH
3′		148.0, C
4′		147.8, C
5′	6.75 [a], m	108.4, CH
6′	6.78 [a], m	120.4, CH
7′	5.98, 2H, s	101.4, CH_2
1″		136.0, C
2″	6.81, brs	106.5, CH
3″		148.3, C
4″		147.3, C
5″	6.78 [a], m	108.2, CH
6″	6.75 [a], m	119.5, CH
7″	5.95, 2H, s	101.2, CH_2

[a] Overlapping resonances assigned by HMQC spectrum.

2.3.4 7,9-Dihydroxydolichanthin B (4)

Compound **4** was purified as a white amorphous solid, and displayed a molecular formula of $C_{20}H_{20}O_8$ as deduced from the molecular ion adduct peak at *m/z* 411.1049 $[M+Na]^+$ (calcd. for $C_{20}H_{20}O_8Na$: 411.1050) in the HRESIMS. The IR spectrum indicated the absorbance bands at 3405 cm^{-1} for hydroxyl group and 1646, 1613 and 1490 cm^{-1} for aromatic rings. The UV spectrum showed absorption maxima at 245 and 288 nm. The ^1H NMR spectrum of **4** (Figure 2.17, Table 2.4) showed the resonances of two sets of 1,3,4-trisubstituted phenyl groups [δ_H 6.84 (d, J = 1.5 Hz, 1H, H-2″), 6.83 (brs, 1H, H-2′), 6.82 (d, J = 8.0 Hz, 1H, H-5′), 6.81 (d, J = 8.0 Hz, 1H, H-5″), 6.77 (dd, J = 1.5, 8.0 Hz, 1H, H-6′), 6.74 (dd, J = 1.5, 8.0 Hz, 1H, H-6″)], two methylene dioxy groups [δ_H 5.99 (d, J = 1.0 Hz, 2H, H-7″), 5.98 (d, J = 1.0 Hz, 2H, H-7′)], a dioxymethine [δ_H 4.89 (dd, J = 1.5, 5.5 Hz, 1H, H-2)], two oxygenated methines [δ_H 4.44 (dd, J = 3.2, 8.3 Hz, 1H, H-6), 4.33 (dd, J = 3.2, 8.6 Hz, 1H, H-7)], an oxygenated methylene [δ_H 3.53 (t, J = 8.6 Hz, 1H, H-4a), 3.39 (t, J = 8.3 Hz, 1H, H-4b)], two methine protons [δ_H 2.41 (m, 1H, H-5), 2.25 (ddd, J = 1.5, 5.4, 8.6 Hz, 1H, H-1)], and three hydroxy groups [δ_H 6.01 (d, J = 3.2 Hz, HO-6), 5.85 (d, J = 5.5 Hz, HO-2), 5.84 (d, J = 3.2 Hz, HO-7)]. The ^{13}C NMR (Figure 2.18, Table 2.4) and HMQC spectra confirmed the presence of six sp^2 quaternary carbons [δ_C 147.1 (C-3″), 147.0 (C-3′/C-4″), 146.2 (C-4′), 138.3 (C-1′), 138.1 (C-1″)], six sp^2 methine carbons [δ_C 120.4 (C-6″), 119.6 (C-6′), 107.7 (C-5″), 107.6 (C-2″), 107.2 (C-5′), 106.6 (C-2′)], two methylenedioxy carbons [δ_C 100.8 (C-7′/C-7″)], one sp^3 dioxymethine carbon [δ_C 100.4 (C-2)], two sp^3 oxymethine carbons [δ_C 74.3 (C-6), 73.9 (C-7)], an oxymethylene carbon [δ_C 68.2 (C-4)], and two sp^3 methine carbons [δ_C 58.2 (C-1), 50.1 (C-5)]. The ^1H NMR and ^{13}C NMR spectroscopic data of **4** were quite similar to those of dolichanthin

B isolated from *Wikstroemia dolichantha*,[66] except for the presence of a hydroxy group at C-2 instead of the methoxy group in dolichanthin B and an additional hydroxy group at C-7 in **4**. This was also confirmed by deshielded C-1 (δ_C 58.2) and C-7 (δ_C 73.9) in **4**, as compared with those of dolichanthin B (δ_C 49.8 and 38.9), respectively, as well as the COSY correlations of HO-2/H-2 and HO-7/H-7 and the HMBC correlations from HO-2 to C-1, from H_2-4 to C-2, from H-2 to C-1/C-5, from HO-7 to C-1/C-7/ C-1″, from H-7 to C-2/C-2″/C-6″, and from H-6″/C-7 (Figure 2.19a). Furthermore, the NOESY correlations of H-1 with H-4a/H-6, of H-4a with H-6, of H-2 with H-5/H-7, and of H-5 with H-7 indicated that **4** adopts the same relative configurations at H-1, H-2, H-5, C-6, and C-7 with those of corresponding H-8, H-9, H-8′, C-7 and C-7′ in dolichanthin B.[66] Based on these observations, H-1, the hydroxy group at C-2, and C-6 were assumed to be β-orientations, while H-2, H-5, and C-7 were assigned to be α-orientations. The large $J_{5,6}$ values of 8.3 Hz and $J_{1,7}$ values of 8.6 Hz, as observed at H-8′ and H-7′ in dolichanthin A (7.7 Hz) with a *anti* configuration,[66] also supported each relationship to be the *anti*-configuration in **4**, respectively. In addition, the NOESY spectrum (Figure 2.19b) showed the correlations of H-4a/H-2′, HO-6/H-1, HO-6/H-5, HO-7/H-1, HO-7/H-5, and H-2/H-2″ suggested the hydroxy groups at C-6 and C-7 faced each other. Considering the NOESY correlations observed in **4** comprehensively, the relative structure of **4** was assigned as shown in Figure 2.19b. Hence, compound **4** was deduced to be a new dolichanthin B analog and was named 7,9-dihydroxydolichanthin B (numbering according to dolichanthin B).

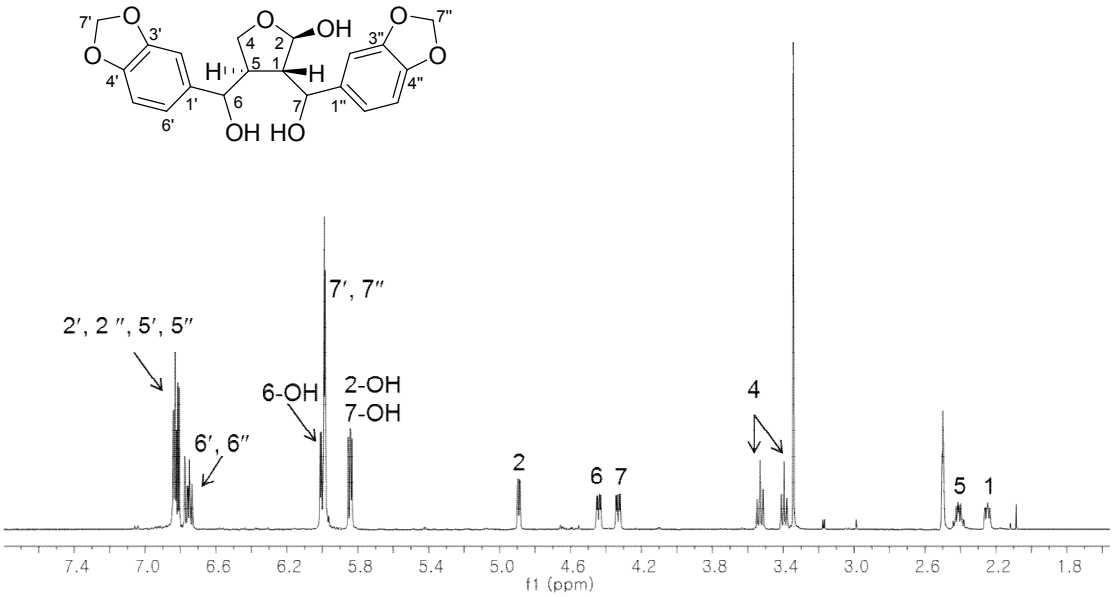


Figure 2.17 ^{1}H NMR spectrum (500 MHz) of **4** in $CDCl_3$

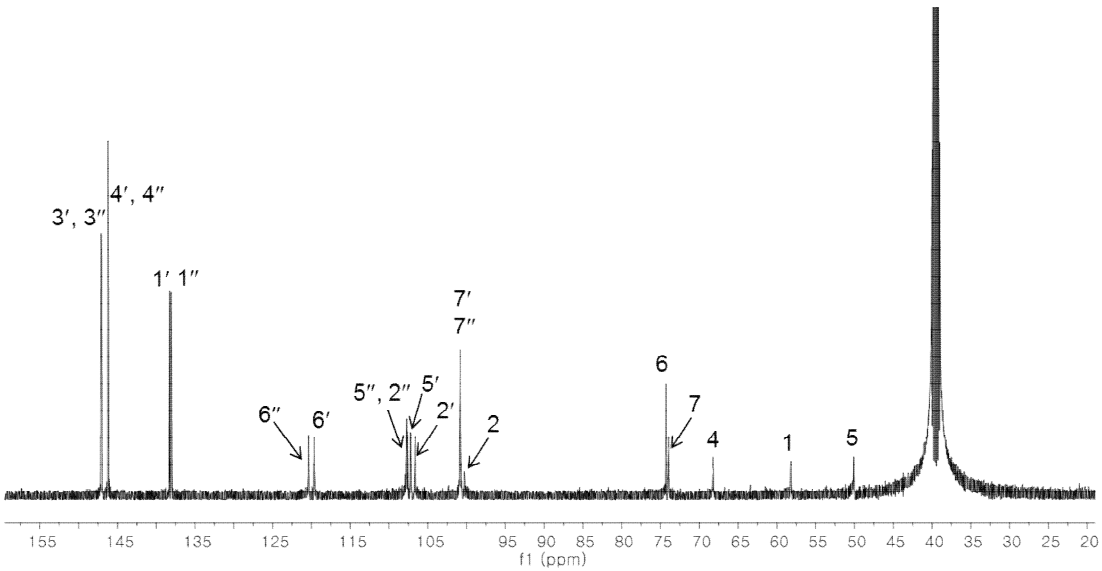


Figure 2.18 ^{13}C NMR spectrum (125 MHz) of **4** in $CDCl_3$

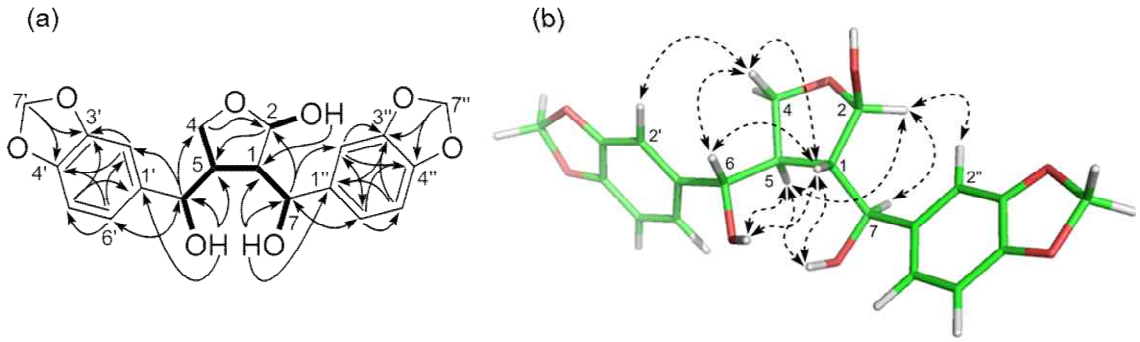


Figure 2.19 ^{1}H-^{1}H COSY correlations (bold lines) and key HMBC correlations (arrows) (a) and key NOESY correlations (dashed arrows) of **4** (b)

Table 2.4 ^{1}H (500 MHz) and ^{13}C (125 MHz) NMR data of **4** in DMSO-d_6 (δ in ppm and J values in (Hz) in parentheses)

	4	
position	δ_H	δ_C
1	2.25, ddd (1.5, 5.4, 8.6)	58.2, CH
2	4.89, dd (1.5, 5.5)	100.4, CH
4a	3.53, t (8.6)	68.2, CH_2
4b	3.39, t (8.3)	
5	2.41, m	50.1, CH
6	4.44, dd (3.2, 8.3)	74.3, CH
7	4.33, dd (3.2, 8.6)	73.9, CH
1′		138.3, C
2′	6.83, brs	106.6, CH
3′		147.0 [a], C
4′		146.2, C
5′	6.82, d (8.0)	107.2, CH
6′	6.77, dd (1.5, 8.0)	119.6, CH
7′	5.98, d (1.0)	100.8 [a], CH_2
1″		138.1, C
2″	6.84, d (1.5)	107.6, CH
3″		147.1, C
4″		147.0 [a], C
5″	6.81, d (8.0)	107.7, CH
6″	6.74, dd (1.5, 8.0)	120.4, CH
7″	5.99, d (1.0)	100.8 [a], CH_2
HO-2	5.85, d (5.5)	
HO-6	6.01, d (3.2)	
HO-7	5.84, d (3.2)	

[a] Overlapping resonances within the same column.

2.3.5 Premnan C (5)

Compound **5** was obtained as a white amorphous solid with a positive optical rotation ($[\alpha]_D^{25}$ +4.7° (*c* 0.1, MeOH)). HRESIMS suggested its molecular formula of $C_{23}H_{24}O_8$ based on *m/z* 451.1368 $[M+Na]^+$ (calcd. for $C_{23}H_{24}O_8Na$: 451.1363), accounting for 12 indices of hydrogen deficiency. Absorption bands of the hydroxy group (3458 cm^{-1}) and the aromatic ring (1547 and 1465 cm^{-1}) were observed in the IR spectrum. The UV spectrum showed absorption maxima at 245 and 285 nm. The assignment of all protons and carbons of **5** was confirmed by 1D and 2D NMR spectroscopic data. The ^1H and ^{13}C NMR spectroscopic data recorded in $CDCl_3$ (Figures 2.20 and 2.21, Table 2.5) and the observation of the cross peaks in the HMBC spectra (Figure 2.22a) of **5** showed a close structural resemblance to taungtangyiol A.[41] However, the HMBC correlations from the two methyl groups at H_3-11 (δ_H 1.44)/H_3-12 (δ_H 1.40) to C-8 (δ_C 102.0) indicated the presence of a 1,1-dimethylmethylenedioxy group in **5**. Taking the indices of hydrogen deficiency into account, one more ring system should be included in the structure of **5** to fulfill the remaining degree of unsaturation. Thus, the presence of a 8,8-dimethyl-7,9-dioxepane ring (numbering according to **5**) was supported by the HMBC correlations from H-6 (δ_H 4.92)/H_2-10 (δ_H 3.99, 3.47)/H_3-11/H_3-12 to C-8. The NOESY correlation (Figure 2.22b) between the 5-OH (δ_H 2.85) and H-1 (δ_H 2.04) suggested that H-1 and the hydroxy group at C-5 existed in a *cis* relationship, while the NOESY correlation of H-2/H-10b (δ_H 3.47) and the lack of NOESY correlation between 5-OH and H-2 (δ_H 5.04) indicated that H-1 and H-2 was *trans* relationship. Furthermore, the *trans* relationship between 5-OH and H-6, as well as H-2 and H-6 adopted β-orientations as verified from the NOESY correlations of 5-OH (δ_H 2.85)/H-2′ (δ_H 7.00) and H-6 (δ_H 4.92)/H-6′ (δ_H 6.86), and the lack of a

correlation between 5-OH/H-6. The absolute configurations of **5** were defined 1*R*, 2*S*, 5*S*, and 6*R* by comparing the experimental ECD spectra with calculated ECD spectra and **5** was named premnan C. However, the existence of **5** in the $CHCl_3$ extract was not proved by LC-HRESIMS analysis, suggesting that **5** may be an artifact produced during the purification process.

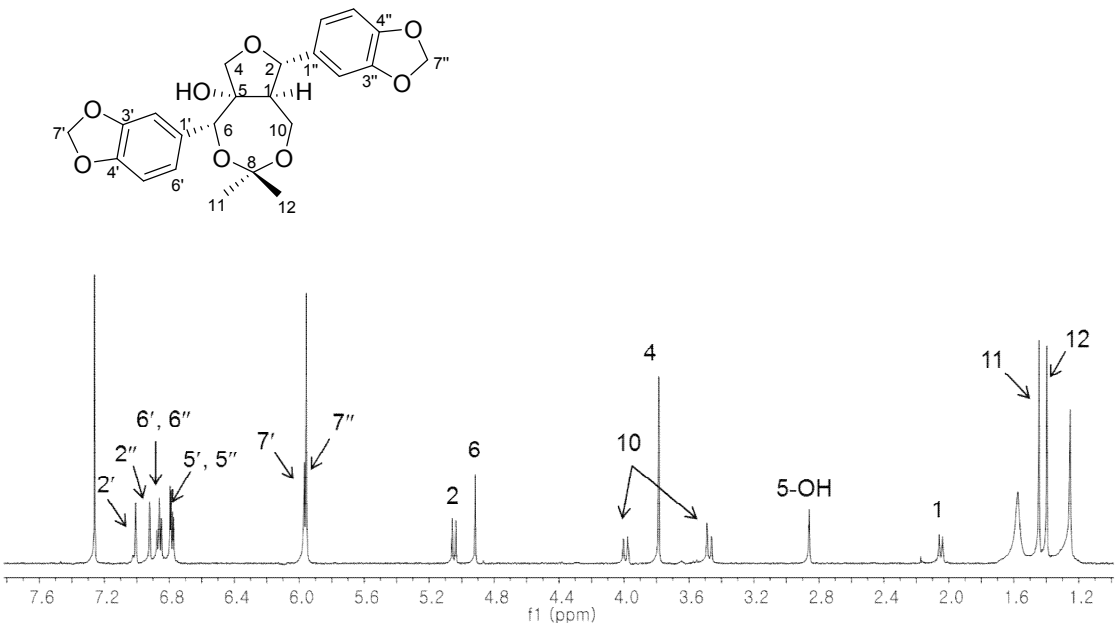


Figure 2.20 ^{1}H NMR spectrum (500 MHz) of **5** in $CDCl_3$

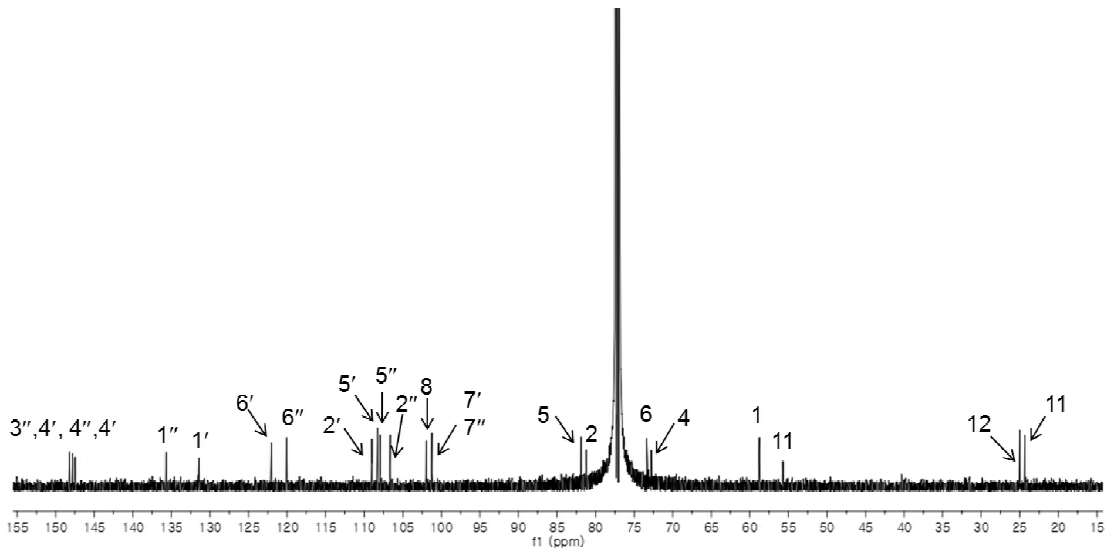


Figure 2.21 ^{13}C NMR spectrum (125 MHz) of **5** in $CDCl_3$

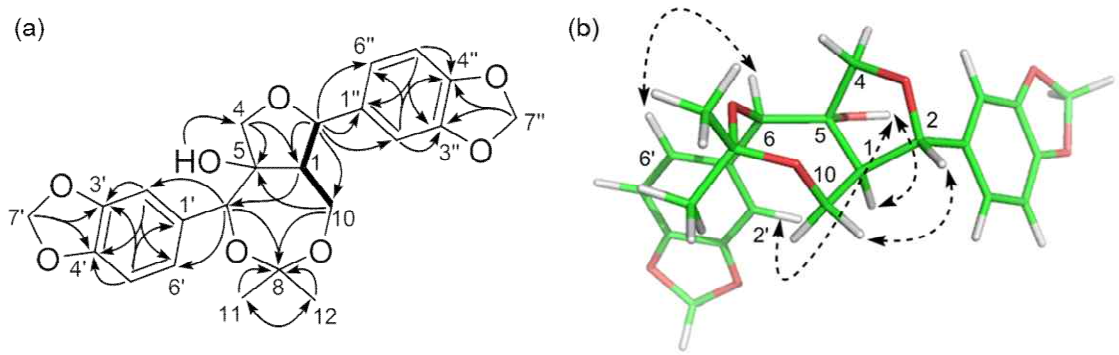


Figure 2.22 ^{1}H-^{1}H COSY correlations (bold lines) and key HMBC correlations (arrows) (a) and key NOESY correlations (dashed arrows) of **5** (b)

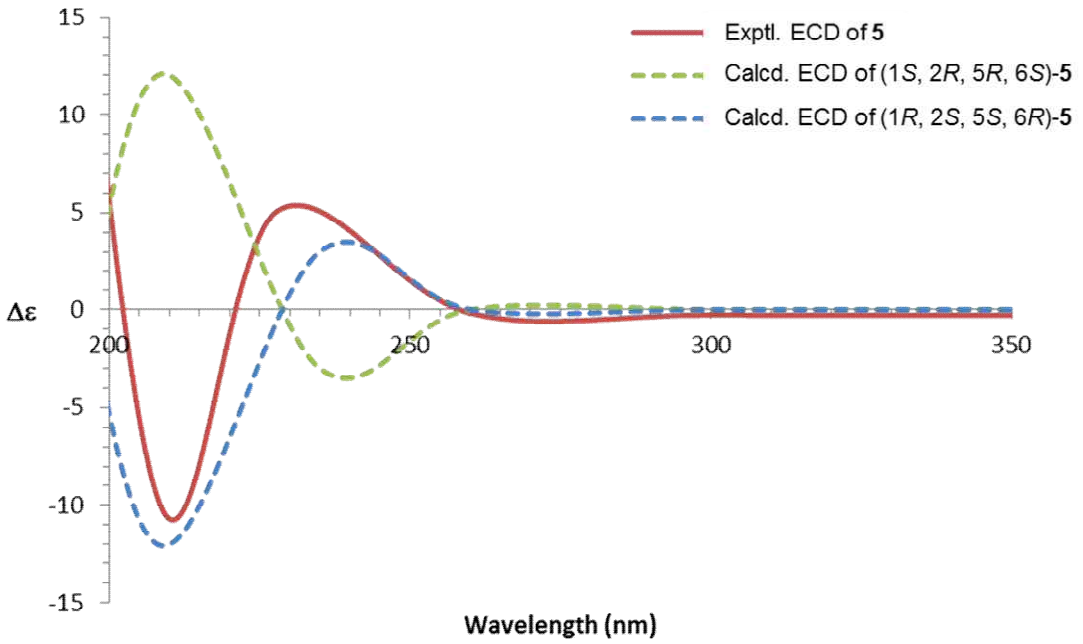


Figure 2.23 Experimental and calculated ECD spectra of **5**

Table 2.5

^{1}H (500 MHz) and ^{13}C NMR (125 MHz) spectroscopic data for **5** in $CDCl_3$ (δ in ppm and J values in (Hz) in parentheses)

	5	
position	δ_H	δ_C
1	2.04, m	58.7, CH
2	5.04, d (10.8)	81.2, CH
4	3.79, 2H, s	72.8, CH_2
5		81.9, C
6	4.92, s	73.4, CH_2
8		102.0, C
10a	3.99, dd (2.3, 13.7)	
10b	3.47, dd (2.0, 13.7)	55.7, CH_2
11	1.44, 3H, s	24.3, CH_3
12	1.40, 3H, s	25.0, CH_3
1′		131.4, C
2′	7.00, d (1.7)	109.0, CH
3′		147.4, C
4′		147.8, C
5′	6.78, d (8.0)	108.3, CH
6′	6.86, dd (1.7, 8.0)	122.0, CH
7′	5.97, 2H, d (1.5)	101.2, CH_2
1″		135.7, C
2″	6.92, d (1.7)	106.6, CH
3″		148.2, C
4″		147.5, C
5″	6.77, d (8.0)	107.9, CH
6″	6.85, dd (1.7, 8.0)	120.1, CH
7″	5.96, 2H, d (1.5)	101.2, CH_2
5-OH	2.85, s	

2.4 Melanogenesis regulatory activity of isolated compounds in a mouse melanoma cell line (B16-F10)

All the isolated compounds (**1**–**11**) were evaluated their anti-melanin deposition activities against a mouse melanoma cell line (B16-F10) at the concentration of 10, 50, and 100 μM. The cell viability was evaluated with the total protein contents by using Bio-rad Bradford assay. The positive control, arbutin, showed an IC_{50} value of 698 μM (Figure 2.24). Among these compounds, 7,9-dihydroxydolichanthin B (**4**) and (2α,3α)-olean-12-en-28-oic acid (**11**) showed anti-melanin deposition activities with IC_{50} values of 18.4 and 11.2 μM, respectively, without any cytotoxicity. Oleanonic acid (**10**) showed dose-dependent of anti-melanin deposition activities with IC_{50} values of 17.7 μM (Figures 2.24 and 2.25).[56] However, at concentration above 50 μM, **10** showed slight cytotoxicity against B16-F10 cell line. It is in agreement with previous report on cytotoxic activity of oleanonic acid against B16-BL6 cell line.[67] On the other hand, compounds **1**–**3**, **5**, and **7** showed melanogenesis enhancing activities. Compounds **1** and **5** increased melanin production by 31% and 50% at a 50 μM concentration, respectively, while **1** and **5** showed slight cytotoxicity at the concentration of 100 μM, which would account for the reduction of the melanin production. Compounds **2**, **3**, and **7** exhibited dose-dependent enhancement of melanin production by 67%, 30%, and 45%, respectively, at the concentration of 100 μM as compared to the cells treated only with IBMX and α-MSH (Figure 2.24).[55]

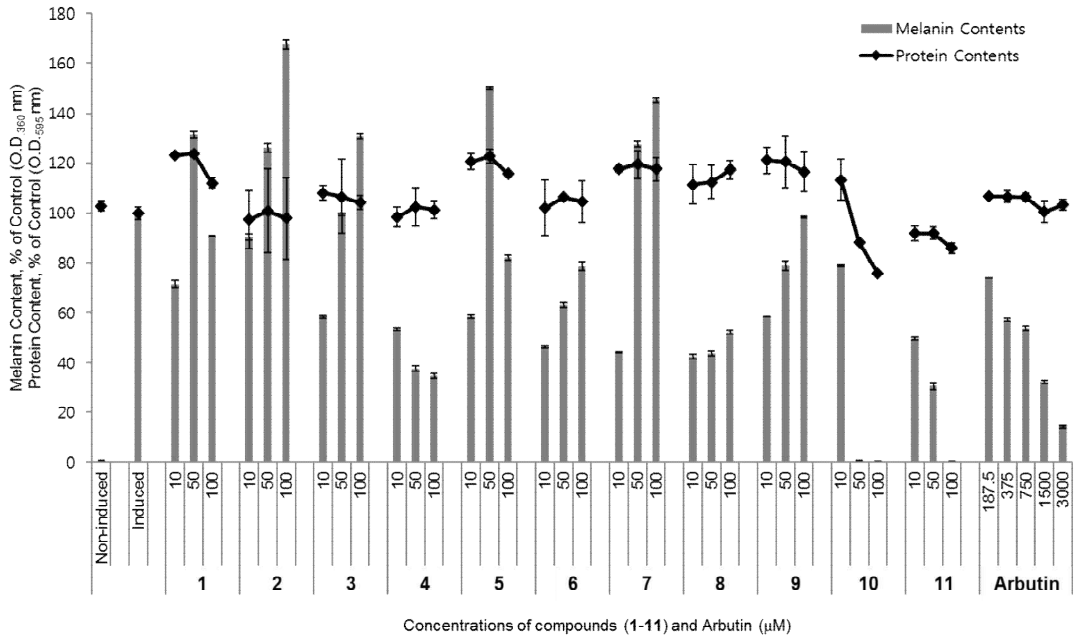


Figure 2.24 Melanogenesis regulatory activities of **1**–**11** against α-MSH and IBMX-induced melanogenesis, as well as protein contents in B16-F10 cell line. Cells were seeded on a 24-well plate at 5.0×10^4 cells/well and cultured in 500 μL of medium (DMEM at 37 °C, under a 5% CO_2 and 95% air atmosphere). After culture of 24 h, 500 μL of medium containing different doses of the tested samples (final conc. 10, 50, and 100 μM), α-MSH (final conc. 0.25 μM), and IBMX (final conc. 100 μM) were added to each well. After a 48 h incubation, 500 μL of the medium was discarded, and 500 μL of medium containing different doses of the tested samples (final conc. 10, 50, and 100 μM), α-MSH (final conc. 0.25 μM), and IBMX (final conc. 100 μM) were added to each well and the cells were further incubated for 48 h. The cells were then lysed by incubation in 1 M NaOH (150 μL) at 95 °C for 15 min, and the melanin contents were observed at 360 nm with a micro plate reader. The effect of cell viability (protein contents) was evaluated by measuring at 595 nm.

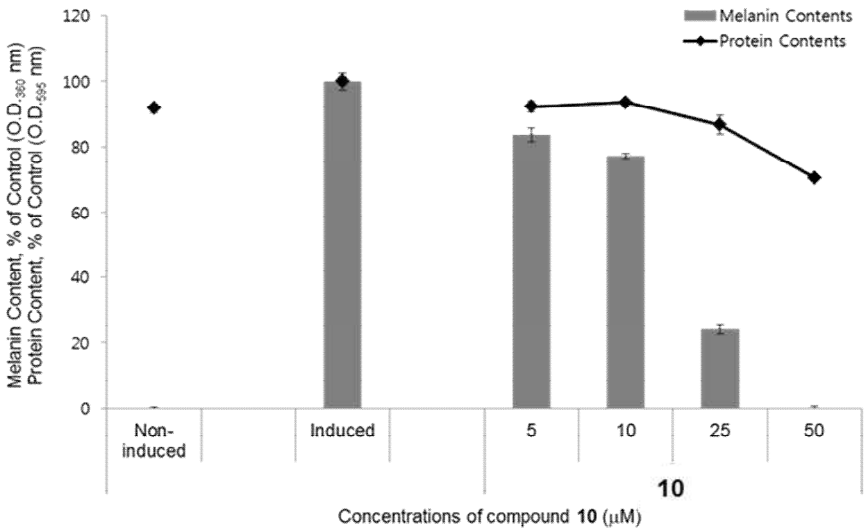


Figure 2.25 Anti-melanin deposition activities of **10** at lower concentration against α-MSH and IBMX-induced melanogenesis, as well as protein contents in B16-F10 cell line. The assay was performed as the same procedure as those shown in Figure 2.24, except for final concentrations of samples (5, 10, 25, and 50 μM).

2.5 Tyrosinase inhibition activity of compounds 4 and 11

To better understand anti-melanin deposition mechanism, the effects of **4** and **11** on tyrosinase activities were investigated. Tyrosinase is the key enzyme catalyzing the hydrolation of tyrosine for the formation of L-DOPA and oxidation of L-DOPA for the DOPA quinone formation in the melanin biosynthesis (Figure 1.1).[68] Tyrosinase inhibition activity was measured intermittently every 3 minutes for a total of 30 minute, in different concentrations (6.25, 12.5, 25, 50, 100, and 200 μM) (Figure 2.26). Kojic acid was used as a positive control. However, **4** and **11** did not inhibit tyrosinase activities.

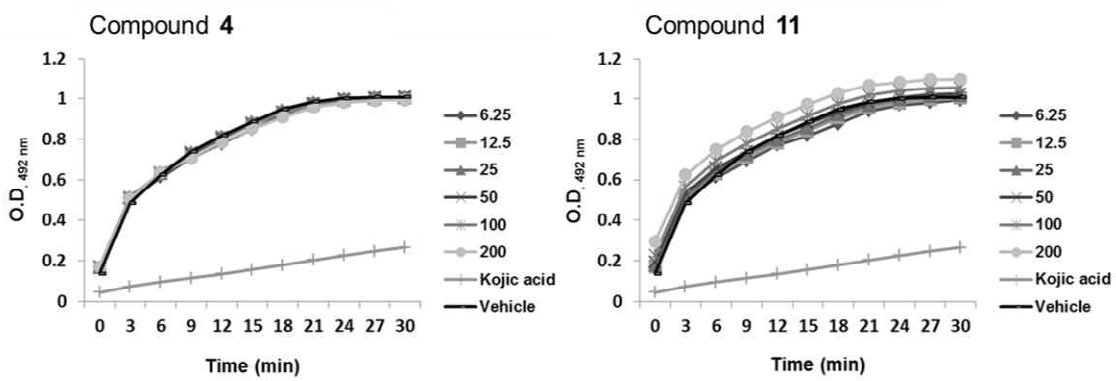


Figure 2.26 Effects of **4** and **11** on tyrosinase inhibition activity. The assay was performed on 96-well plate (final concentrations of **4** and **11** at 6.25, 12.5, 25, 50, 100, and 200 μM). The assay mixture containing 2.5 mM of L-DOPA as a substrate, 80 units/mL of mushroom tyrosinase, and **4** or **11** at final concentration of 6.25, 12.5, 25, 50, 100, or 200 μM was incubated at 37 °C for 10 min. The absorbance of DOPA quinone at 492 nm was measured intermittently for 30 min. Kojic acid (250 μM) was used as positive control.

2.6 mRNA expression of compounds 4 and 11

Compounds **4** and **11** did not inhibit tyrosinase activities. Therefore, it is assumed that **4** and **11** showed the melanin deposition activity by inhibiting the cAMP pathway of melanogenesis. To further characterize the anti-melanin deposition activity, I examined the expression of mRNA using the specific primers for MITF, TYR, TRP-1, and TRP-2. The assay revealed that glyceraldehyde 3-phosphate dehydrogenase (GAPDH) was used as the internal control. As a result, compound **4** down-regulated the *Tyr* mRNA expression. On the other hand, **11** showed down-regulation of the *Mitf* mRNA expression, together with those of *Tyr*, *Trp-1*, and *Trp-2* (Figure 2.27). Considering these observations, anti-melanin deposition activity of **4** could be resulted from the *Tyr* mRNA expression, while that of **11** was caused from the down-regulation of the *Mitf* mRNA expression located upstream of *Tyr*, *Trp-1*, and *Trp-2* in the cAMP pathway (Figure 1.2).

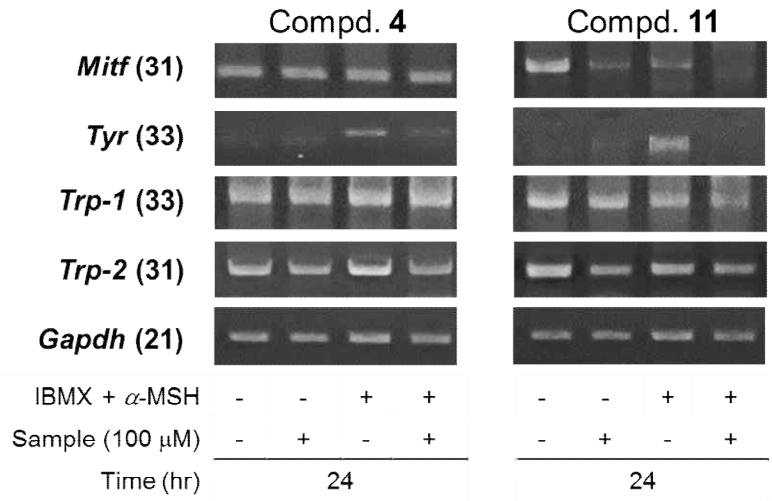


Figure 2.27 Effects of **4** and **11** on mRNA expression. B16-F10 cells were seeded at 6.0 × 10^5 cells/dish on 6-cm dish, and mRNAs were induced by IBMX (100 μM) and α-MSH (0.25 μM) in the presence or absence of 100 μM of **4** and **11** for 24 h. *Gapdh* was used as an internal control. Numbers within parentheses indicate the number of PCR cycles.

2.7 Summary of chapter 2

Four new lignoids, premnan A (**1**), premnan B (**2**), taungtangyiol C (**3**), and 7,9- dihydroxydolichanthin B (**4**), together with premnan C (**5**) assumed to be an artifact, one natural new lignoid (3*R*,4*S*)-4-(1,3-benzodioxol-5-ylcarbonyl)-3-[(*R*)-1-(1,3-benzodioxol-5-yl)-1-hydroxymethyl]tetrahydro-2-furanone (**6**), and five known compounds (**7**–**11**) were isolated from the $CHCl_3$ extract of the *P. serratifolia* wood. 7,9-Dihydroxydolichanthin B (**4**) and (2α,3α)-olean-12-en-28-oic acid (**11**) displayed anti-melanin deposition activity against B16-F10 cell line with the IC_{50} values of 18.4 and 11.2 μM, respectively. Furthermore, compounds **4** and **11** showed down-regulations of the *Tyr* and *Mitf* mRNA expressions, respectively. In contrast, **1**−**3**, **5** and **7** showed melanogenesis enhancing activities. The anti-melanin deposition activity observed in the $CHCl_3$ extract supported its effectiveness as natural cosmetics. Investigation of the chemical constituents and anti-melanin deposition activity of the *P. serratifolia* wood thus provided insight into the effectiveness of the *P. serratifolia* wood as a cosmetic agent. However, the present results also suggest that the cosmetic anti-melanin deposition efficacy of the *P. serratifolia* wood should be discussed with consideration of the melanogenesis enhancing activities of the chemical constituents in this plant.

Chapter 3 Constituents of the *Jatropha multifida* stems collected in Myanmar and their anti-melanin deposition activities

3.1 Introduction

The genus, *Jatropha*, belongs to the Euphorbiaceae family and consists of 175 species.[69,70] Among them, *J. multifida* (Figures 3.1) is a shrub of 2-3 m in height and is grown as an ornamental plant in North Australia, South east Africa, Philippines, Srilanka, Indonesia, and India.[71–73] In India and Africa, the whole parts of this plant likewise leaves, stem, bark, and roots have been used as ethno-medicines for a long time, to treat fever, pain, infection, wounds, ulcer, and various inflammatory skin conditions.[74–76] Furthermore, several kinds of secondary metabolites such as acylfloroglucinols (multifidol and multifidol glucoside),[77] diterpenoids (multifolone, (4*E*)-jatrogrossidenta-dione acetate, jatrophone, citlalitrione, 3β-acetoxy-12-metoxy-13 -methyl-podocarpa-8,11,13-trien-7-one, (4*E*)-jatrogrossident adione, 15-*epi*-(4*E*)-jatrogrossidentadione,[73] jatromulone A, 3β,12-dihydroxy-13-methylpodocarpane-8,10,13-trien,(2*S*,3*R*,5*S*,10*R*)-2,3-dihydroxy-15,16-dinor-ent-pimar-8,11,13-trien, (2*S*, 3*R*,5*S*,10*R*)-2-acetoxy-3-hydroxy-15,16-dinor-ent-pimar-8,11,13-trien, gossweilone, jatrointeline A, jatrophodione A, heudelotinone[78]) and coumarino-lignan (cleomiscosin A)[79] were isolated from this plant (Figure 3.2). Previous studied have indicated antibacterial activities against *Bacillus subtilis* and *Staphylococus aureus*,[80] anti-influenza virus activity,[81] anti-inflammatory, antioxidant activities,[82] cytotoxicity,[83] antifungal activity against *Candida albicans,*[84] and antimalarial activities.[85] However, there are no report for anti-melanin deposition activity and a few scientific reports have been described for the stems of *J. multifida*.



Figure 3.1 Stems of *Jatropha multifida*

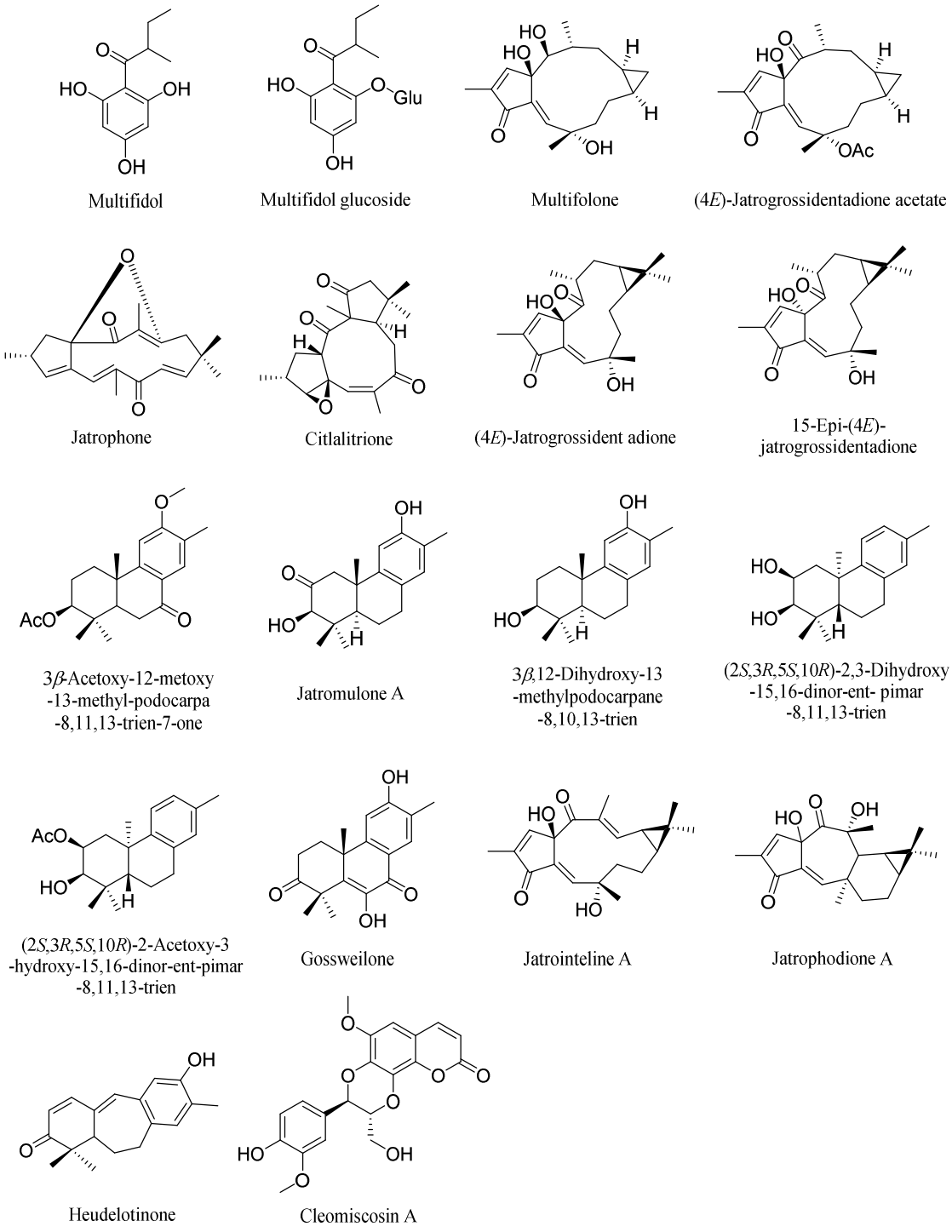


Figure 3.2 Chemical structures of acylfloroglucinols, diterpenoids, and coumarino-lignan from *J. multifida.*

3.2 Extraction and isolation

The dried *J. multifida* stems (3.0 kg) were pulverized and extracted with $CHCl_3$ at room temperature four times. After filtration of the suspension, the resulting solution was evaporated under reduced pressure to yield a $CHCl_3$ extract (11.0 g). The $CHCl_3$ extract (11.0 g) was chromatographed with silica gel column using a gradient system of increasing polarity with $CHCl_3$ and EtOAc (10:1–0:10) to obtain five fractions (Fr. 1–Fr. 5). These fractions were further separated by repeated column chromatography (Figure 2.3), which furnished nine known compounds including two coumarins, scoparone (**12**)[86] and scopoletin (**13**),[87] and seven lignoids, salicifoliol (**14**),[88] glaberide I (**15**),[89] pinoresinol (**16**), medioresinol (**17**), syringaresinol (**18**),[90] matairesinol (**19**),[87] and shonanin (**20**)[91] (Figures 3.3 and 3.4). The chemical structures of all compounds were determined by NMR spectroscopic data, and by comparison with reported data. All of these compounds have been isolated for the first time from this plant.

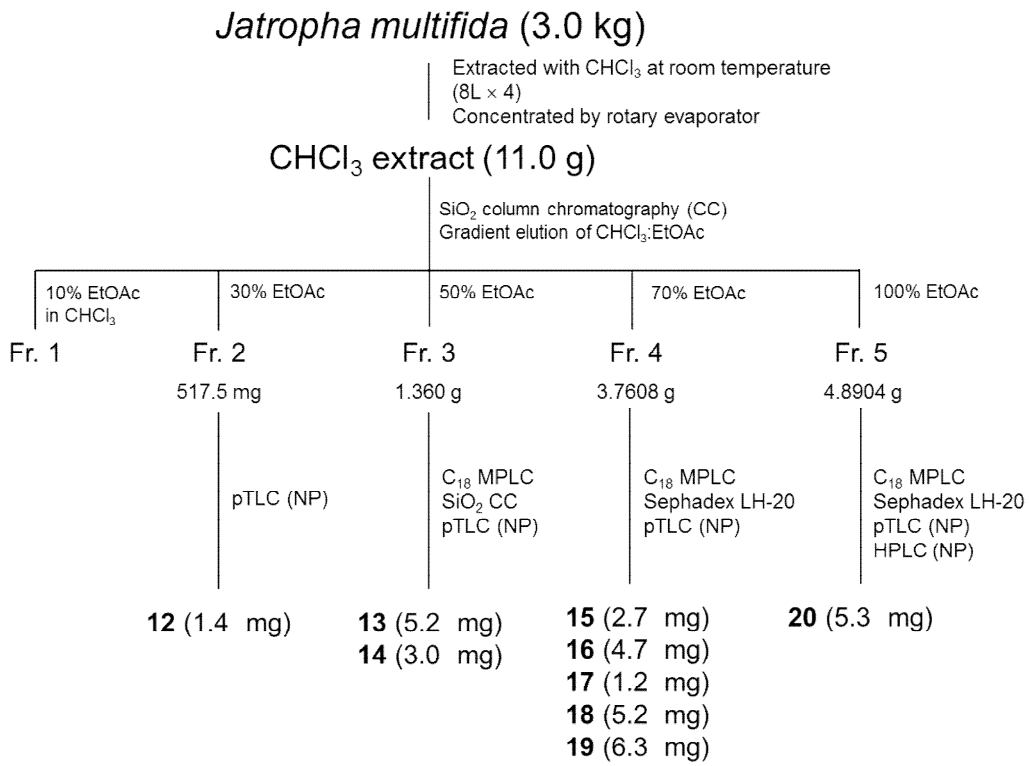


Figure 3.3 Extraction and isolation of compounds from $CHCl_3$ extract of stems of *J. multifida*

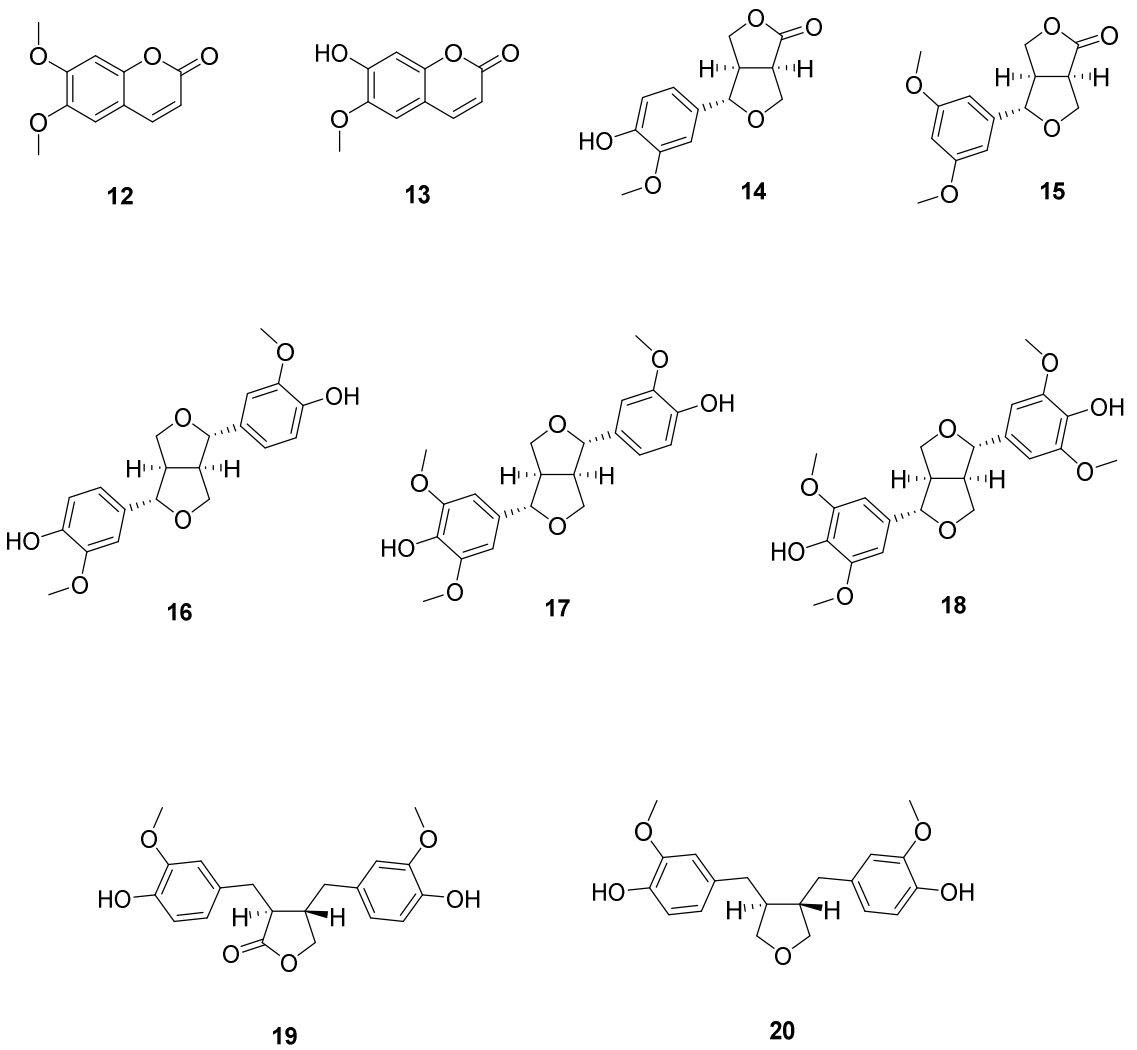


Figure 3.4 Structures of compounds isolated from $CHCl_3$ extract of *J. multifida* stems

3.3 Anti-melanin deposition activity of isolated compounds against a mouse melanoma cell line (B16-F10)

The anti-melanin deposition activities of the isolated compounds **12**–**20** in a mouse melanoma cell line (B16-F10) were evaluated. Among the tested compounds, glaberide I (**15**) and shonanin (**20**) had anti-melanin deposition activities with IC_{50} values of 49.9 and 37.5 μM, respectively, without any cytotoxicity (Figure 3.5).

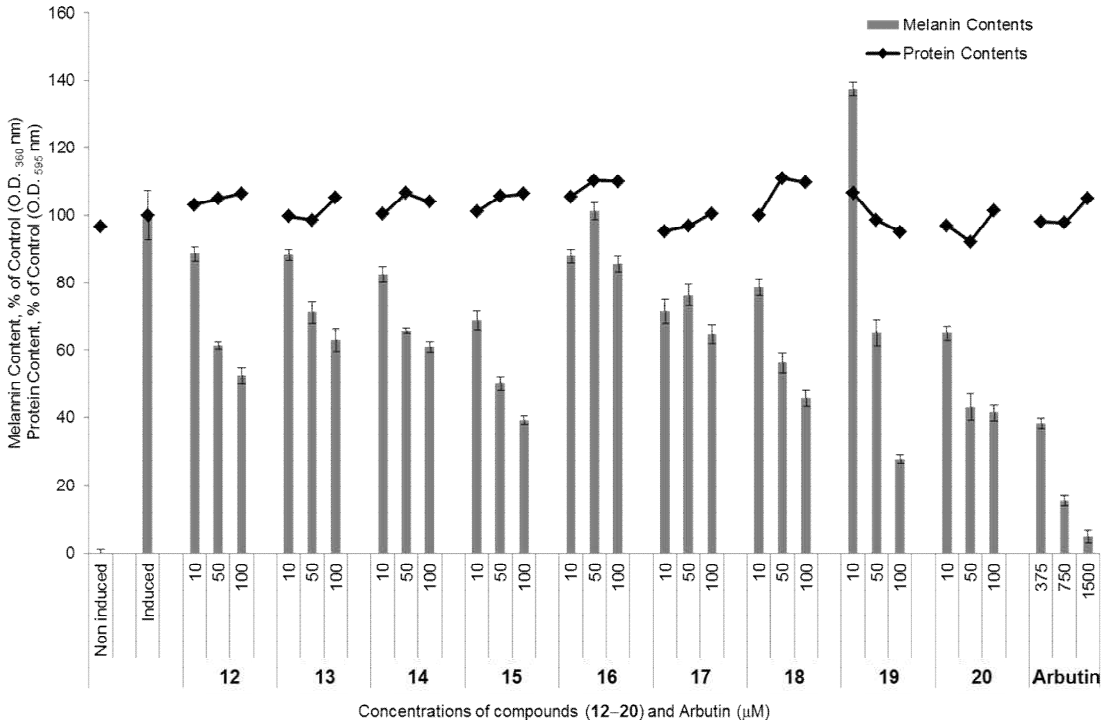


Figure 3.5 Anti-melanin deposition activities of **12**–**20** against α-MSH and IBMX-induced melanogenesis and protein contents in B16-F10 cell line. The assay was performed with the same procedures as those described in chapter 2.

3.4 Tyrosinase inhibition activity of compounds 15 and 20

Since compounds **15** and **20** possessed the anti-melanin deposition activity, I examined the tyrosinase inhibition activity of **15** and **20**. Tyrosinase inhibition activity was evaluated as same as chapter 2. However, **15** and **20** did not show the activity (Figure 3.6).

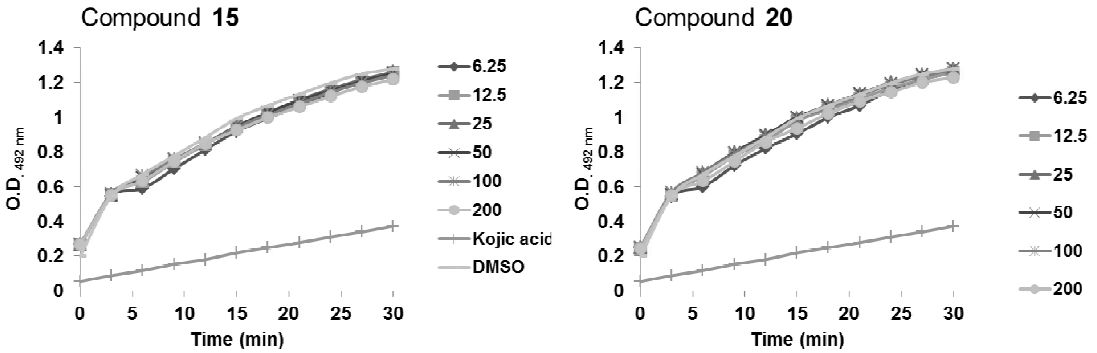


Figure 3.6 Effects of **15** and **20** on tyrosinase inhibition activity. The assay was performed with the same procedures as those described in chapter 2.

3.5 mRNA expression of compounds 15 and 20

In order to further clarify the inhibitory mechanism, I investigated the effects of **15** and **20** on the mRNA expression of MITF, TYR, TRP-1, and TRP-2 and found that only **20** down-regulated the *Tyr* mRNA expression. However, **15** did not affect any mRNA expression (Figure 3.26). These results suggested that anti-melanin deposition activity of **20** could be resulted from the down-regulation of the *Tyr* mRNA expression, while anti-melanin deposition activity of **15** is caused from inhibition of other melanogenesis pathway.

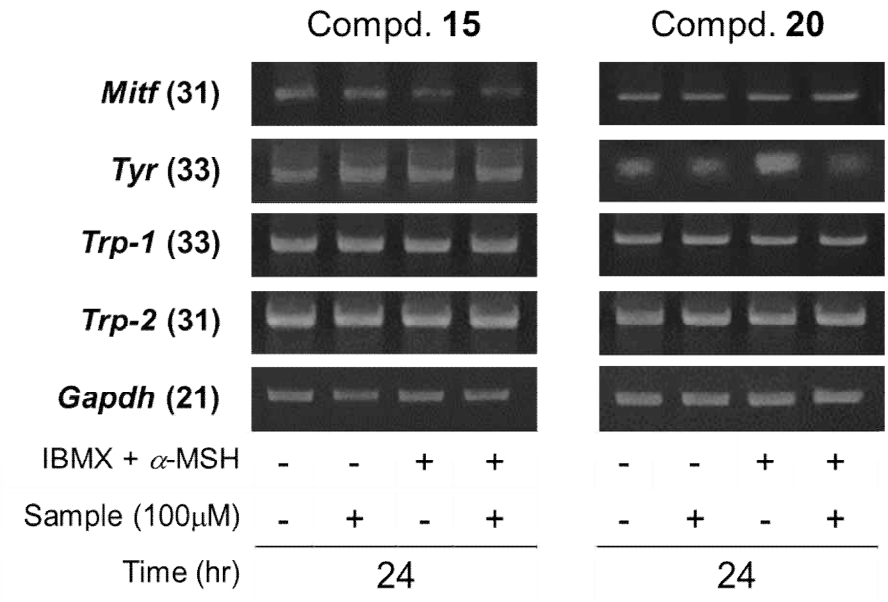


Figure 3.26 Effects of **15** and **20** on mRNA expression. The assay was performed with the same procedures as those described in chapter 2.

3.6 Summary of chapter 3

Two coumarins, scoparone (**12**), scopoletin (**13**), and seven lignoids, salicifoliol (**14**), glaberide I (**15**), pinoresinol (**16**), medioresinol (**17**), syringaresinol (**18**), matairesinol (**19**), and shonanin (**20**) were isolated from the $CHCl_3$ extract of the *J. multifida* stems. To the best of our knowledge, this is the first report of the isolation of the compounds **12**–**20** from *J. multifida*. Glaberide I (**15**) and shonanin (**20**) showed anti-melanin deposition activities with IC_{50} values of 49.9 and 37.5 μM, respectively. Further mechanistic investigation suggested that anti-melanin deposition activity of **20** was caused by down-regulation of the *Tyr* mRNA expression. On the other hand, **15** did not show any effects on the expression of melanogenesis associated mRNA and tyrosinase inhibition activity, suggesting that the other inhibitory mechanism was occurred by **15** to decrease the melanin production. *J. multifida* was not used as traditional cosmetics. The results of this study may suggest that this plant is potentially used as a cosmetic ingredient.

Chapter 4 Constituents of the Myanmar marine sponge of *Clathria prolifera* and their anti-melanin and antifungal activities

4.1 Introduction

Marine sponges from the genus *Clathria* are brightly orange or red colored encrustations with miniscule pores covered by finger-like branches or spikes.[92,93] Previous studies revealed that *Clathria* species harbor alkaloids, polyketide alkaloids, and steroids.[94–98] Among the reported metabolites, clathsterol, a steroid from *Clathria* sp., reportedly possesses anti-HIV activity.[96] The genus *Clathria* have provided some pharmacologically interesting compounds. Despite high possibility of this genus, the constituents of *Clathria prolifera* (Figure 4.1), which has been previously known as *Microciona prolifera*, have not been fully elucidated. Only previous chemical studies of *C. prolifera* revealed the presence of steroids. However, no biological activity has been reported.

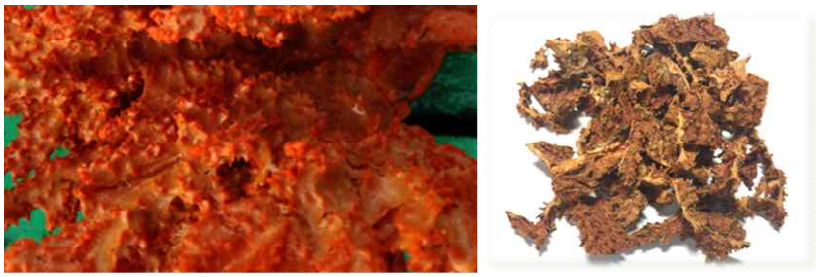


Figure 4.1 *Clathria prolifera*

4.2 Extraction and isolation of active constituents

Dried pieces of *C. prolifera* (79.5 g) were extracted in a MeOH-acetone mixture (2:1) with sonication (600 mL, 90 min× 6) at room temperature, and the solvent was evaporated under reduced pressure to obtain the crude extract (11.9 g). The crude extract (11.9 g) was then suspended in water and successively partitioned with EtOAc (8 × 0.6 L), to obtain the EtOAc- (1.8 g) and water-soluble portions (9.6 g). The water-soluble portion (9.6 g) was fractionated on a DIAION HP-20 column, which was eluted stepwise with 2 L each of 100% H_2O (Fr. 1), 50% MeOH (Fr. 2), and 100% MeOH (Fr. 3) to give three fractions. Fr. 2 (1.0 g) was further separated by sephadex LH-20 column chromatography and reverse-phase pTLC to furnish clathriroles A (**21**, 1.0 mg) and B (**22**, 2.3 mg) (Figures 4.2 and 4.3). Two new compounds were elucidated based on 1D and 2D NMR, IR spectroscopy, HRESIMS, and comparisons of the reported literatures. Furthermore, the absolute configuration of **21** was determined by optical rotation and CD data analysis.

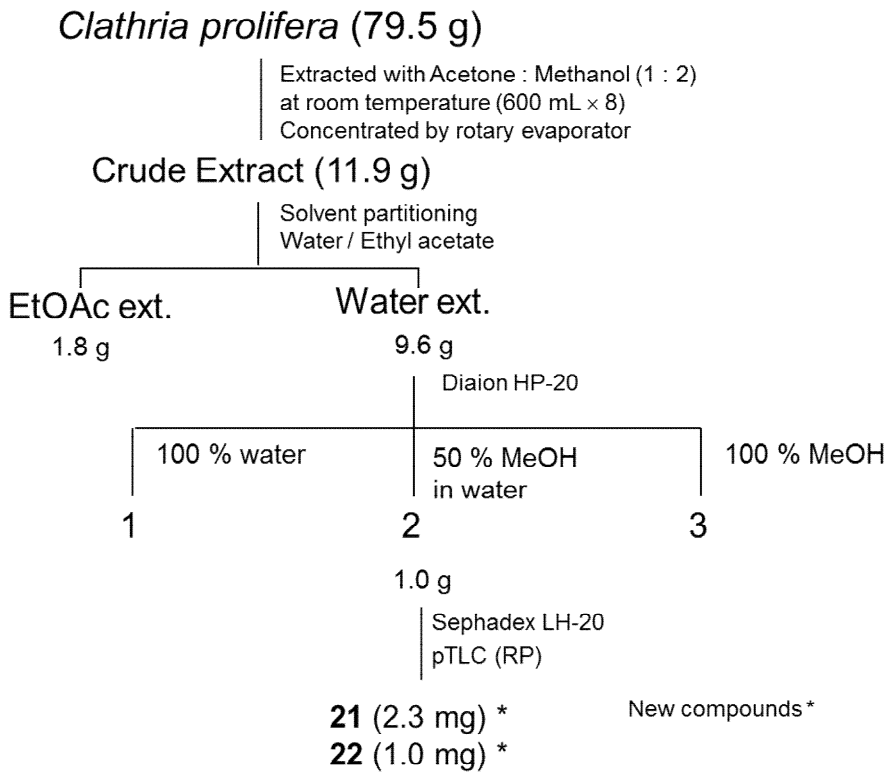


Figure 4.2 Extraction and isolation of compounds from *C. prolifera.*

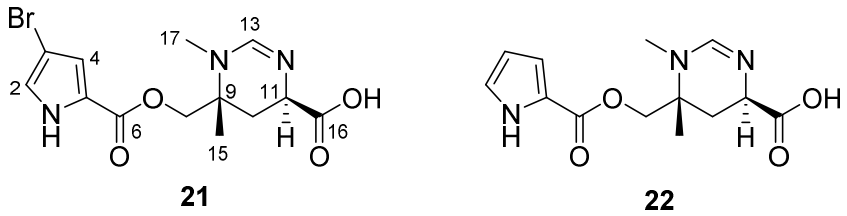


Figure 4.3 Structure of compounds isolated from *C. prolifera.*

4.3 Structure elucidation of new compounds

4.3.1 Clathrirole A (21)

Compound **21** was isolated as a white amorphous solid, with $[\alpha]_D^{25}$ –27.7° (*c* 0.1, $CHCl_3$). The HRESIMS exhibited a 1:1 ion cluster at *m/z* 358.0398 $[M+H]^+$ and 360.0390, $[M+2+H]^+$, indicating the presence of one bromine atom in **21**. Its molecular formula was thus established as $C_{13}H_{16}N_3O_4Br$, by HRESIMS in conjugation with the NMR data. Its IR spectrum showed absoption bands at 3420, 1682, and 1624 cm^{-1}, ascribable to hydroxy, carboxy, and imine functional groups, respectively. The ^1H and ^{13}C NMR (Table 4.1, Figures 4.4 and 4.5) and HMQC spectroscopic data of **21** revealed signals for two heteroaromatic methine protons at δ_H 7.24 (H-2) and 6.79 (H-4), and an ester carbonyl carbon at δ_C 158.8 (C-6), two heteroaromatic methine carbons at δ_C 124.7 (C-2) and 116.4 (C-4), an sp^2 quaternary carbon at δ_C 121.9 (C-5), and a brominated heteroaromatic quaternary carbon at δ_C 96.1 (C-3), characteristic of those of a 4-bromopyrrole-2-carboxylic acid ester.[100,101] The remaining ^1H NMR spectroscopic data revealed signals for two methines at δ_H 7.99 (H-13) and 3.67 (H-11), an oxymethylene at δ_H 4.39 (H-8a) and 4.24 (H-8b), an *N*-methyl group at δ_H 3.13 (H_3-17), a methylene at δ_H 2.52 (H-10a) and 1.63 (H-10b), a tertiary methyl group at δ_H 1.38 (H_3-15), and a secondary amino proton at δ_H 12.51 (H-1). Analyses of the ^{13}C NMR and HMQC spectra revealed the existence of a carbonyl carbon at δ_C 168.1 (C-16), an imine methine carbon at δ_C 151.9 (C-13), an oxymethylene carbon at δ_C 66.4 (C-8), a quaternary carbon at δ_C 56.3 (C-9), a methine carbon at δ_C 50.4 (C-11), a methylene carbon at δ_C 33.9 (C-10), an *N*-methyl carbon at δ_C 35.6 (C-17), and a tertiary methyl carbon at δ_C 20.7 (C-15). The presence of an *N*-methyl tetrahydropyrimidinium ring with the carboxylate moiety at C-11 was suggested by the $^1H-^1H$ COSY correlations of

H_2-10/H-11, and the HMBC correlations from H_2-8 to C-9/C-10, H_2-10 to C-9/C-11, H_3-17 to C-9/C-13, H-13 to C-9/C-11/C-17, H_3-15 to C-8/C-9/C-10, and H-10b/H-11 to C-16 (Figure 4.6a). In addition, the connectivity of the 4-bromopyrrole-2-carboxylic acid and the *N*-methyl tetrahydropyrimidinium ring through C-8-O-C-6 was supported from the HMBC correlation of H_2-8 to C-6. The ^{1}H and ^{13}C NMR spectroscopic data of **21** were very similar to those of the known compound, *N*-methylmanzacidin C, isolated from the marine sponge *Axinella brevistyla*.[102] The relative configuration of **21** was determined from the coupling constants and the NOESY data (Figure 4.6b). The axial/*pseudo*-axial relationship between H-10a and H-11 (5.2 Hz) and the equatorial/*pseudo*-equatorial relationship between H-10a and the carboxylate moiety at C-11 were confirm from the coupling constants between H-10b and H-11 (12.0 Hz). The NOESY correlations of H-10b/H-11 and of H-10a/H_3-15, as well as the lack of a NOESY correlation of H-11/H_3-15, suggested that the C-15 methyl group is equatorially oriented and adopts a β-configuration with that of the carboxylate moiety at C-16, while the methylene group at C-8 was assumed to adopt the α-configuration.

The previously reported steroselective total synthesis of manzacidin C unambiguously confirmed its 9*S*,11*S* configuration.[103] Furthermore, absolute configurations of *N*-methylmanzacidin C were assigned as 9*S* and 11*S* by comparison of its optical rotation ($[\alpha]_D^{23}$ +36.4°) with that of the synthesized manzacidin C ($[\alpha]_D^{22}$ +37°).[102] However, **21** exhibited a negative optical rotation value. Therefore, both C-9 and C-11 of **21** were assumed to be *R* configurations. Furthermore, this assignment was also supported by comparison of the experimental and calculated ECD spectra analysis (Figure 4.7), Thus, the structure of **21** was assigned as an enantiomer of *N*-methylmanzacidin C, and named clathrirole A.

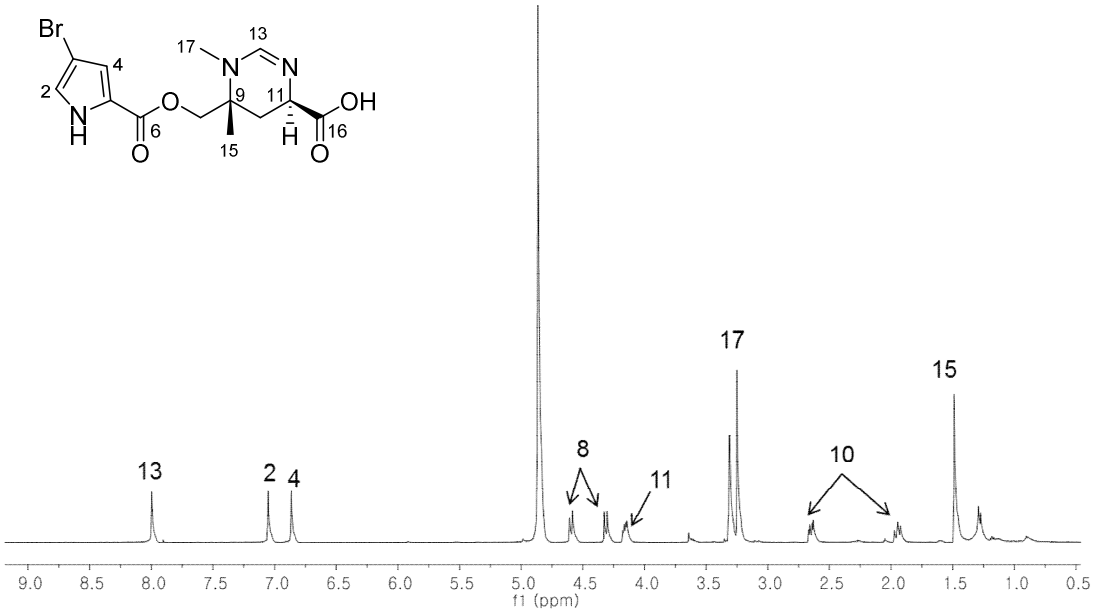


Figure 4.4 ^{1}H NMR spectrum (500 MHz) of **21** in CD_3OD

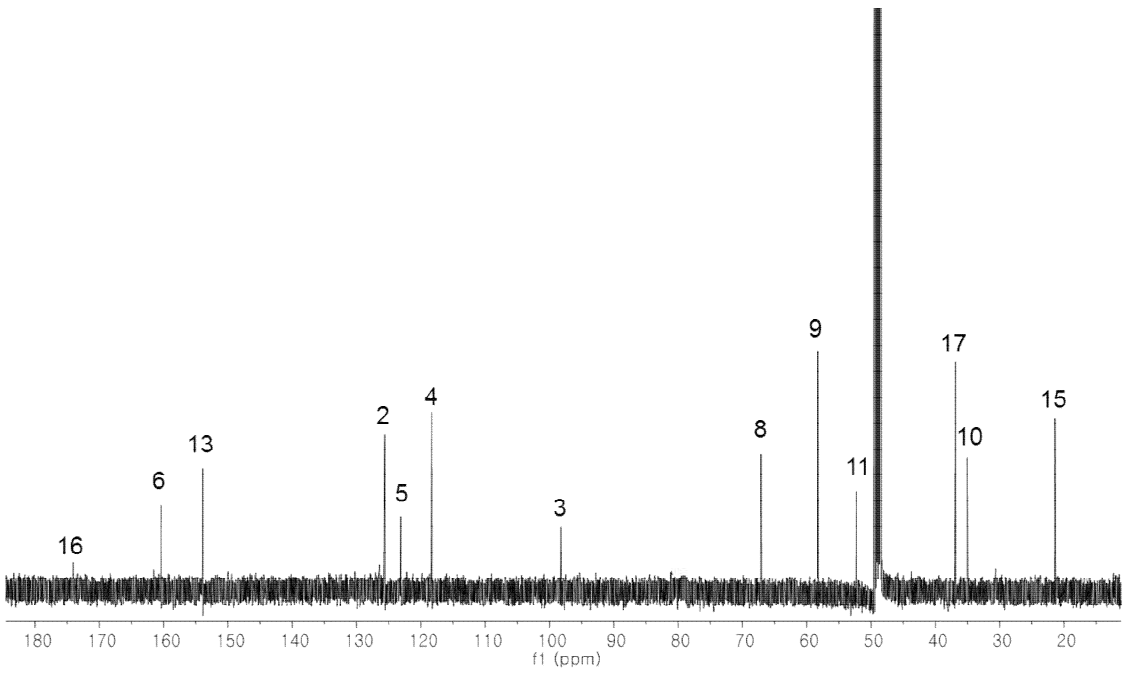


Figure 4.5 ^{13}C NMR spectrum (125 MHz) of **21** in CD_3OD

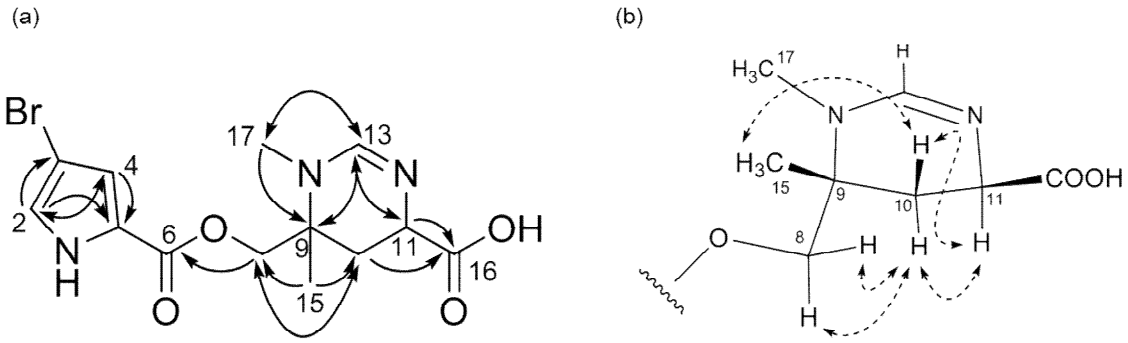


Figure 4.6 ^{1}H-^{1}H COSY correlations (bold lines) and key HMBC correlations (arrows) (a) and key NOESY correlations (dashed arrows) of **21** (b)

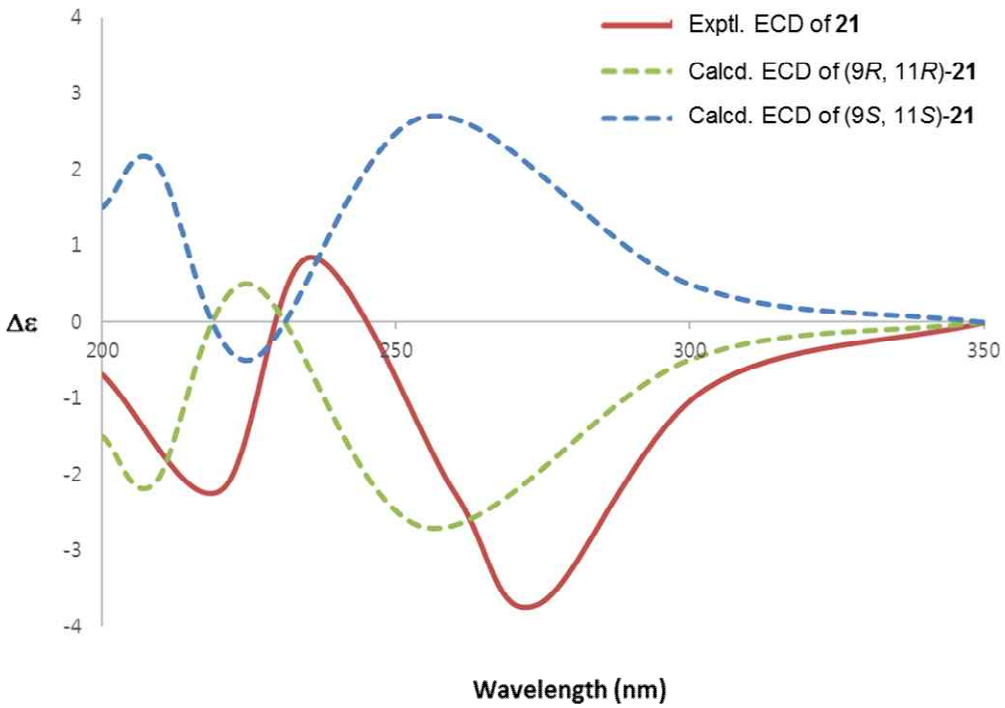


Figure 4.7 Experimental and calculated ECD spectra of **21**

Table 4.1 ^{1}H and ^{13}C NMR data for clathrirole A (**21**).

No.	**21**[a]		**21**[b]	
	δ_C	δ_H (mult., *J* in Hz)	δ_C	δ_H (mult., *J* in Hz)
1		12.51(s)		
2	124.7	7.24 (d, 1.2)	125.8	7.04 (br, s)
3	96.1		98.4	
4	116.4	6.79 (d, 1.7)	118.5	6.86 (br, s)
5	121.9		123.3	
6	158.8		160.6	
8	66.4	4.39 (d, 11.6)	67.3	4.59 (d, 11.9)
		4.24 (d, 11.6)		4.31 (d, 11.9)
9	56.3		58.4	
10	33.9	2.52[c]	35.2	2.65 (dd, 5.2, 14.3)
		1.63 (dd, 12.0, 14.3)		1.96 (dd, 10.9, 14.3)
11	50.4	3.67 (dd, 5.2, 12.0)	52.4	4.15 (dd, 5.2, 10.9)
13	151.9	7.99 (s)	154.1	7.98 (s)
15	20.7	1.38 (3H, s)	21.6	1.49 (3H, s)
16	168.1		174.2	
17	35.6	3.13 (3H, s)	37.1	3.25 (3H, s)

[a] ^{1}H NMR at 500 MHz, ^{13}C NMR at 125 MHz, measured in DMSO-d_6

[b] ^{1}H NMR at 500 MHz, ^{13}C NMR at 125 MHz, measured in CD_3OD

[c] Overlapping resonance with solvent peak

4.3.2 Clathrirole B (22)

Compound **22** was obtained as a white amorphous solid with $[\alpha]_D^{25}$ –29.3° (*c* 0.1, $CHCl_3$), and was revealed to have the molecular formula $C_{13}H_{17}N_3O_4$ by HRESIMS (*m/z* 280.1292). The IR spectrum displayed the presence of the hydroxy (3424 cm^{-1}), carboxy (1683 cm^{-1}), and imine (1616 cm^{-1}) functional groups. The ^1H and ^{13}C NMR data of **22** (Table 4.2, Figures 4.8 and 4.9) were quite similar to those of **21** recorded in CD_3OD (Table 4.1, Figures 4.4 and 4.5). The significant difference between **22** and **21** was the presence of a heteroaromatic methine proton on the pyrrole ring at C-3 in **22**, instead of bromine in **21**. This was verified from the $^1H-^1H$ COSY correlations of H-2/H-3 and H-3/H-4, and the HMBC correlations from H-2 to C-3/C-4/C-5, from H-3 to C-4/C-5, and from H-4 to C-2/C-3/C-5 (Figure 4.10a). Furthermore, the NOESY experiment suggested that **22** has the same relative configuration as that of **21** (Figure 4.10b). The relative configuration of **22** was also confirmed by comparisons of the ^1H and ^{13}C NMR data with those of the structurally most similar known compound, manzacidin D, isolated from the marine sponge *Astrosclera willeyana*.[104] The significant differences between **22** and manzacidin D were sets of proton and carbon signals at C-10 (δ_H 2.66 and 1.95 and δ_C 35.3 in **22**; δ_H 2.37 and 2.30 and δ_C 33.5 in manzacidin D) and at C-11 (δ_H 4.19 and δ_C 52.4 in **22**; δ_H 4.11 and δ_C 51.4 in manzacidin D), as well as the carbon signal at C-16 (δ_C 174.2 in **22**; δ_C 181.4 in manzacidin D), suggesting that the relative configuration of the carboxylate moiety at C-11 in **22** was the β-orientation. Furthermore, the optical rotation of **22** showed negative as same as **21**, suggesting that absolute configurations of C-9 and C-11 of **22** were assumed to adopt *R*. Hence, the structure of **22** was determined as a diastereomer of manzacidin D at C-11, and was given the trivial name clathrirole B.

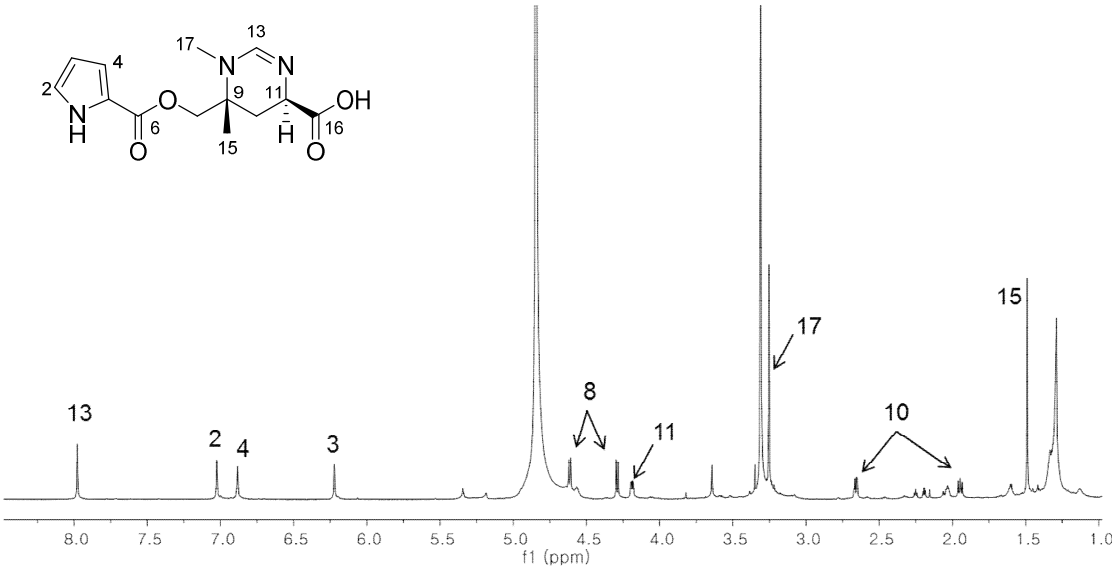


Figure 4.8 ^{1}H NMR spectrum (500 MHz) of **22** in CD_3OD

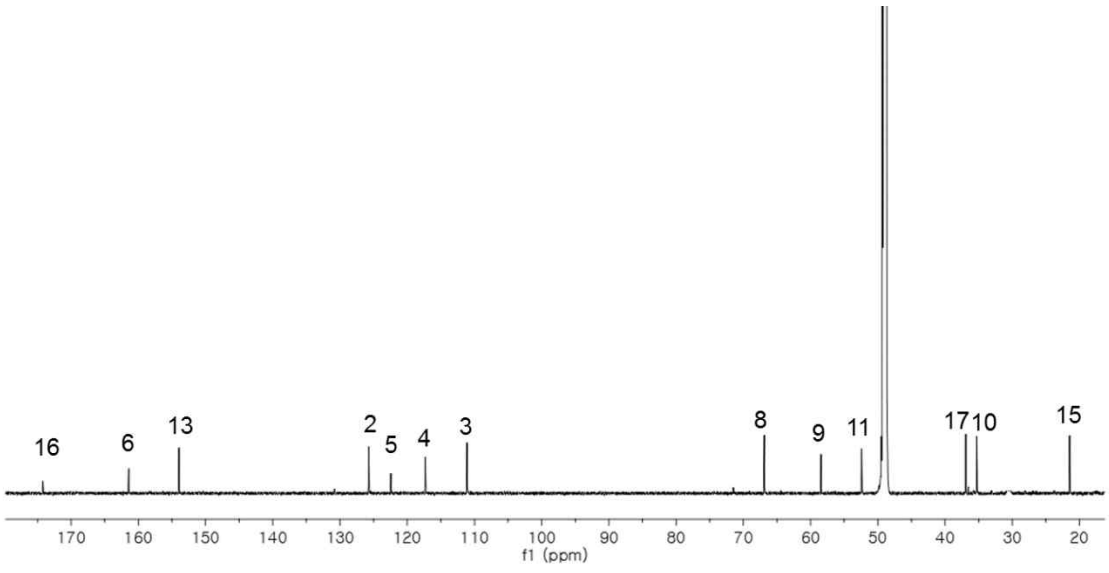


Figure 4.9 ^{13}C NMR spectrum (125 MHz) of **22** in CD_3OD

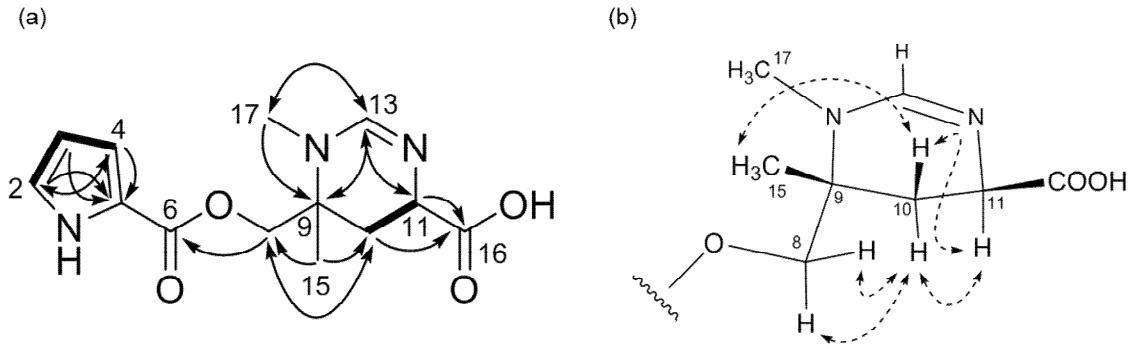


Figure 4.10 ^{1}H-^{1}H COSY correlations (bold lines) and key HMBC correlations (arrows) (a) and key NOESY correlations (dashed arrows) of **22** (b)

Table 4.2 ^{1}H and ^{13}C NMR data for clathrirole B (**22**).

No.	**22**[a]	
	δ_C	δ_H (mult., *J* in Hz)
2	125.7	7.03 (dd, 1.4, 2.2)
3	111.1	6.22 (dd, 2.2, 3.6)
4	117.3	6.88 (dd, 1.4, 3.6)
5	122.4	
6	161.4	
8	66.9	4.62 (d, 11.7)
		4.29 (d, 11.7)
9	58.5	
10	35.3	2.66 (dd, 5.4, 14.4)
		1.95 (dd, 10.8, 14.4)
11	52.4	4.19 (dd, 5.4, 10.8)
13	153.9	7.98 (s)
15	21.5	1.49 (3H, s)
16	174.2	
17	36.9	3.25 (3H, s)

[a] ^{1}H NMR at 900 MHz, ^{13}C NMR at 225 MHz, measured in CD_3OD

4.4 Anti-melanin deposition activities of clathrirole A (21) and clathrirole B (22)

I evaluated the effect of two new compounds (**21** and **22**) on anti-melanin deposition activities in a mouse melanoma cell line (B16-F10). However, both compounds did not show any anti-melanin deposition activites (Figure 4.7).

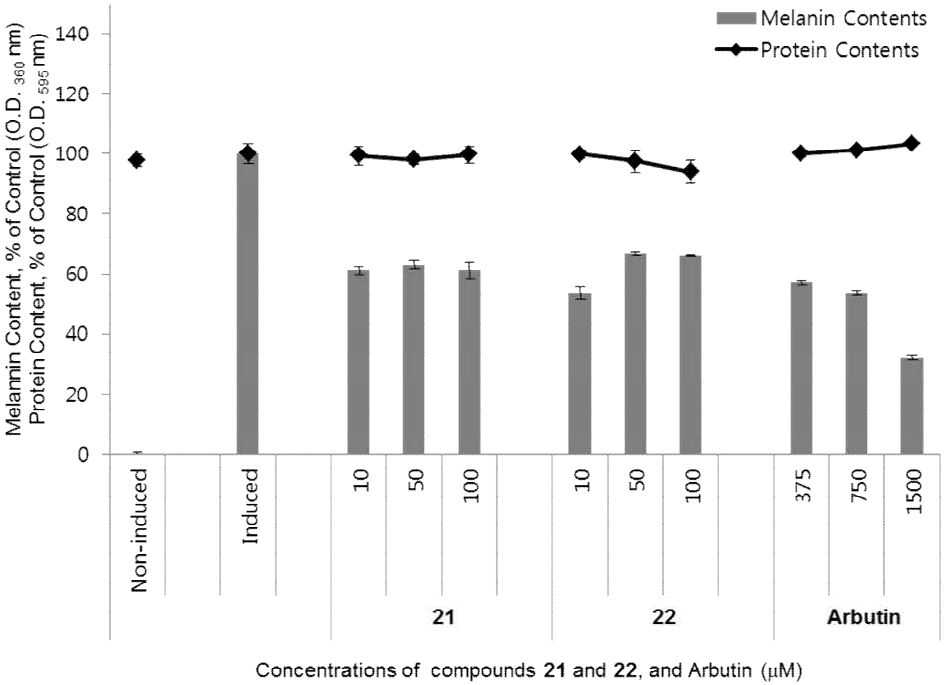


Figure 4.7 Anti-melanin deposition activities of compounds **21** and **22** against α-MSH and IBMX-induced melanogenesis, as well as protein contents in B16-F10 cell line
This assay procedure was performed as same as those of chapter 2.

4.5 Antifungal activities of compounds clathrirole A (21) and clathrirole B (22)

N-methylmanzacidin C, the enantiomer of **21**, reportedly possessed antifungal activity against *Saccharamyces cerevisiae* strain.[102] Based on this reason, antifungal activities of **21** and **22** were assessed with *S. cerevisiae*. Cyclohexamide was used as positive control. However, compounds **21** and **22** did not show any activity against *S. cerevisiae* at a concentration of 200 μM (Table 4.4). These observations would suggest that the absolute configurations (C-9 and C-11) are related in the antifungal activity of *N*-methylmanzacidin C.[99]

Table. 4.4 Antifungal activities of compounds **21** and **22** against *Saccharamyces cerevisiae* strain

Compounds	**Concentration (μM)**
Chlathrirole A (**21**)	> 200
Chlathrirole B (**22**)	> 200
Cyclohexamide [a]	< 3.16

[a] Positive control

4.6 Summary of chapter 4

Two new pyrrolo-2-aminoimidazoles, clathriroles A (**21**) and B (**22**), were isolated from the 50% MeOH fraction from the MeOH-acetone mixture (2:1) crude extract of *C. prolifera*. Compound **21** was an enantiomer of *N*-methylmanzacidin C with antifungal activity, whereas **22** was a diastereomer of manzacidin D. However, compounds **21** and **22** did not show anti-melanin deposition activity. Furthermore, unlike *N*-methylmanzacidin C, **21** and **22** did not show antifungal activity against *S. cerevisiae*. Thus, these observations may suggest that the absolute configurations play an important role for exhibiting the antifungal activity in this type of compounds.

To the best of our knowledge, pyrrolo-2-aminoimidazole compounds were isolated for the first time from *C. prolifera*. Furthermore, this is the first report for the chemical constituents from Myanmar marine sponges.

Conclusions

In this study, the chemical constituents of two plants, *P. serratifolia* and *J. multifida*, and one marine sponge *C. prolifera* collected in Myanmar were analyzed for their anti-melanin deposition activity against α-MSH and IBMX induced B16-F10. The chemical investigation of the plants' active extracts led to isolation of 20 compounds including five new lignoids **1**−**5** and 15 known compounds **6**−**20**. Compounds **4**, **11**, **15**, and **20** exhibited significant anti-melanin deposition activities with the IC_{50} values of 18.4, 11.2, 49.9, and 37.5 μM, respectively. Furthermore, **4** and **20** inhibited the expression of *Tyr* mRNA, while **11** inhibited the expression of *Mitf* mRNA. In contrast, **1**−**3**, **5**, and **7** showed melanogenesis enhancing activities. In addition, two new pyrrolo-2-aminoimidazoles **21** and **22** were isolated from *C. prolifera*. However, **21** and **22** did not show anti-melanin deposition activities. Taken together, our present study suggested that the less studied Myanmar natural resources are potential as new sources of secondary metabolites for anti-melanin deposition agents.

Experimental

I. General experimental procedures

General methods

Optical rotations were recorded on a Jasco P2100 polarimeter. UV spectra were measured on a Shimadzu UV-160A spectrophotometer. IR spectra were recorded with KBr pellets on a Jasco FT/IR-460 Plus spectrometer. CD spectra were obtained using a JASCO-J-805 spectropolarimeter. NMR spectra were recorded at 500 MHz (^{1}H NMR) and 125 MHz (^{13}C NMR) on a JEOL 500II spectrometer on a JEOL ECX-500 spectrometer, or at 600 MHz (^{1}H NMR) and 150 MHz (^{13}C NMR) on a Bruker AVANCE III HD 600 spectrometer with a QCI-F CryoProbe or BrukerAvance III 900 MHz NMR spectrometer, 900 MHz (^{1}H NMR) and 225 MHz (^{13}C NMR) at RIKEN Yokohama. Chemical shift values are expressed in δ (ppm) downfield from TMS as an internal standard. The high-resolution mass spectra were recorded on a JEOL MStation JMS-700 spectrometer. Medium Pressure Liquid Chromatography (MPLC) was performed using Büchi Sepacore system (Büchi Labortechnik AG, Flawil, Switzerland). HPLC was mainly performed with an Agilent Technologies 1260 quat pump with a JEOL detector. For HPLC column chromatography, COSMOSIL 5C_{18}-AR-II (10 × 250 mm) was used. Open column chromatography was performed with normal-phase silica gel (silica gel 60N, spherical, neutral, 40–50 μm, Kanto Chemical Co., Inc., Japan) and Cosmosil 75C18-OPN (Nacalai Tesque Inc., Kyoto, Japan). Analytical and preparative TLCs were performed on pre-coated silica gel 60F_{254} plates and RP-18F_{254} plates (0.25-mm thick for analytical TLC and 0.50-mm thick for preparative TLC (pTLC), Merck KGaA, Darmstadt, Germany).

Extraction and preparation of test solution

Five natural products were dried and used for making powder, which was macerated with $CHCl_3$ and MeOH to obtain $CHCl_3$ and MeOH crude extracts. After solvent was evaporated under reduced pressure, the crude extract was dissolved in DMSO and used for the anti-melanin deposition assay.

Cell culture and Anti-melanin Deposition Assay

B16-F10 mouse melanoma cells (RCB1158) were grown in Dulbecco's Modified Eagle Medium (DMEM), supplemented with 10% heat incubated FBS (Sigma-Aldrich) and 1% penicillin (10,000 U/mL)-streptomycin (10 mg/L) (Gibco). The B16-F10 cells were seeded in a 24-well plate at 5.0×10^4 cells/well and cultured in 500 μL of medium (DMEM at 37 °C, under a 5% CO_2 and 95% air atmosphere). After 24 h of culture, 500 μL of medium containing different doses of the tested samples (final conc. 10, 50, and 100 μM), α-MSH (final conc. 0.25 μM), and IBMX (final conc. 100 μM) was added to each well. After 48 h incubation, 500 μL of the medium was discarded, and 500 μL of medium containing different doses of the tested samples, α-MSH, and IBMX was added to each of the wells at the concentrations of the same as described above and further incubated for 48 h. The cells were then washed twice with PBS (200 μL) and lysed by incubation in 1 N NaOH (150 μL) at 95 °C for 15 min, and then the absorbance at 360 nm was measured with a microplate reader (SH-1200, Corona). The effect of the samples on the cell proliferation and viability was evaluated by measuring the absorbance of the total protein content at 595 nm with a Bio-Rad Protein Assay. Arbutin (Sigma) was used as positive controls for the anti-melanin deposition and melanogenesis enhancing activities, respectively, in the present study.

Tyrosinase inhibition activity

Tyrosinase assay was performed with 2.5 mM of L-DOPA as substrate and 80 units/mL of mushroom tyrosinase on 96-well plate (final concentration of **4**, **11**, **15** and **20** at 6.25, 12.5, 25, 50, 100, and 200 μM), and the assay mixture was allowed to proceed at 37 °C. The absorbance of DOPA quinone was measured at 492 nm intermittently for 30 min. Kojic acid (Tokyo Chemical Industry, Japan) was used as a positive control.

Reverse transcription-PCR

B16-F10 cells were seeded 6.0×10^5 cells/dish on 6-cm dish, and induced exposure to IBMX (100 μM) and α-MSH (0.25 μM) with/without **4**, **11**, **15** and **20** for 24 h. After the treatment, cells were washed with PBS and lysed in 500 μL of TRIsure reagent (Nippon Genetics, Tokyo). Reverse transcriptions were performed using the ReverTra Ace kit (Toyobo, Osaka). Polymerase chain reactions were carried out using the PCR kit from GeneRed. 2μg/μL of 1st strand cDNA was used for each PCR reaction with the synthesized forward and reverse primers listed below: *GAPDH* (forward: 5′-TCATCATCTCCGCCCCTTC-3′, reverse: 5′-TGCCTGCTTCACCACCTTCT-3′), *MITF* (forward: 5′-GTGCAGACCCACCTGGAAAAC-3′, reverse: 5′-AGTTAAGAGT GAGCATAGCCATAG-3′), *TYR* (forward: 5′-GATCAGAAGAGTATAATAGCCAT-3′, reverse: 5′-CAATATAAGGGCTGTAAAAGCCT-3′), *TRP-1* (5′-GATATGGCGAAGC GCACAAC-3′,reverse: 5′-GTGCCATGTGAGAAAAGCGG-3′), and *TRP-2* (5′-CCAA CTGCAGCGTGTATGACT-3′, reverse: 5′-GTCTGTGCACACGTCACACT-3′). All PCR products were separated by 2% agarose gel electrophoresis and visualized by ethidium bromide staining.

II. Experimental detail of chapter 2

Plant material

The dried powder of the *P. serratifolia* (4.8 kg) wood was collected from Myeik Township, Tanintharyi Region, Myanmar, in February 2018, and identified by an authorized botanist in the Department of Botany, University of Yangon. A voucher specimen (TMPW 27829) was deposited at the Museum of Materia Medica, Research Center for Ethnomedicines, Institute of Natural Medicine, University of Toyama, Japan.

DFT/TDDFT calculations

To generate the conformers subjected to the DFT/TDDFT calculations, Merck Molecular Force Field (MMFF) calculations were performed by using the Spartan '14 software package (Wavefunction Inc., Irvine, CA, USA), and 21, 68, and 12 low-energy conformers were generated from **2**, **3**, and **5**, respectively.

All DFT/TDDFT calculations were conducted using the Gaussian 09 software.[105] Initially, each low-energy conformer obtained by MMFF calculations was subjected to geometry optimization by the DFT method at the B3LYP/6-31G(d) level, with the Polarizable Continuum Model (PCM) in MeOH. Subsequently, to estimate the thermal free energy (ΔG) and check for the presence of imaginary frequencies, each optimized conformer was subjected to a frequency calculation at the B3LYP/6-31G(d) level with the PCM in MeOH. Based on the estimated thermal energy, the abundance ratio of each conformer was determined by the Boltzmann distribution, and finally, we selected 3 conformers from **2** (in total, occupying approximately 90%), 6 conformers from **3** (in total, occupying apporoximately 95%), and 5 conformers from **5** (in total,

occupying approximately 90%) for ECD calculations. Calculations of the ECD spectra of all conformers were performed by using the TDDFT method at the B3LYP/6-31G(d) level with PCM in MeOH, and the weighted-average spectra were compared with the experimental ECD spectra recorded in MeOH.

Extraction and isolation procedure

The dried powdered wood of *P. serratifolia* (4.8 kg) was sonicated in $CHCl_3$ (8 L, 90 min, ×4) at room temperature and the solvent was removed using an evaporator under reduced pressure to obtain the $CHCl_3$ extract (31.5 g). The $CHCl_3$ extract (31.5 g) was subjected to silica gel column chromatography using *n*-hexane–EtOAc (10:1, 8:2, 7:3, 5:5, 3:7, 2:8, 0:10, v/v) as a solvent system to give ten fractions (Fr. 1–10).

Fraction 7 (1.9 g) was rechromatographed on silica gel column chromatography with *n*-hexane–EtOAc (10:1, 7:3, 5:5, 3:7, 0:10, v/v) to obtain four subfractions (Fr. 7-1–7-4). A portion of subfraction 7-4 was further chromatographed on Cosmosil 75C18-OPN resin with a MeCN–MeOH–acetone–H_2O solvent system (1:1:1:2) to afford oleanonic acid (**10**, 4.2 mg).

Fraction 8 (1.0 g) was subjected into silica gel column, which was eluted with *n*-hexane–EtOAc (10:1, 7:3, 5:5, 3:7, 0:10, v/v) to afford four subfractions (Fr. 8-1–8-4). Subfraction 8-4 was further purified by reversed-phase HPLC, eluted with an 80% MeOH isocratic solvent system and monitored at the wavelength of 254 nm, to afford (-)-aptosimon (**7**, 2.0 mL/min, t_R = 9.2 min, 3.4 mg) and (-)-diasesamin-di-γ-lactone (**8**, 2.0 mL/min, t_R = 11.0 min, 17.1 mg).

Fraction 9 (1.5 g) was rechromatographed on silica gel column with *n*-hexane–EtOAc (10:1 to 0:10, v/v) to give five subfractions (Fr. 9-1–9-5). (2α,

3α)-Dihydroxyolean-12-en-28-oic acid (**11**, 3.3 mg) was obtained from the further purification of subfraction 9-2 on Cosmosil 75C18-OPN resin with MeOH–H_2O (4:1).

Fraction 10 (8.1 g) was subjected to silica gel column, using an *n*-hexane–CH_2Cl_2–EtOAc (2:2:1, v/v) solvent system, to give seven subfractions (Fr. 10-1–10-7). Subfraction 10-3 was subjected to chromatography on Cosmosil 75C18-OPN with MeOH–H_2O (4:1) to yield three subfractions (Fr. 10-3-1–10-3-3). Subfraction 10-3-2 was then purified by normal-phase pTLC, using *n*-hexane–CH_2Cl_2–EtOAc (2:2:1, v/v), to isolate premnan B (**2**, 1.6 mg). Subfraction 10-4 was purified by reversed phase open column chromatography eluted with MeCN–MeOH–H_2O (2:2:1, v/v) to give four subfractions (10-4-1–10-4-4), and subfraction 10-4-2 was further purified by reverse-phase pTLC with MeOH–H_2O (4:1, v/v), to yield taungtangyiol C (**3**, 3.0 mg), 7,9-dihidroxydolichanthin B (**4**, 8.1 mg), and premnan C (**5**, 2.1 mg). (3*R*,4*S*)-4-(1,3-Benzodioxol-5-ylcarbonyl)-3-[(*R*)-1-(1,3-benzodioxol-5-yl)-1-hydroxymethyl]tetrahydro-2-furanone (**6**, 1.6 mg) and (+)-epi-sesaminone (**9**, 4.0 mg) were obtained from the purification of a portion of subfraction 10-5-1 by reverse-phase pTLC with MeOH–H_2O (4:1, v/v). Premnan A (**1**, 1.7 mg) was obtained by reverse-phase pTLC with MeOH–H_2O (4:1, v/v) from subfraction 10-5-2.

Premnan A (1): pale yellow, amorphous solid; $[\alpha]^{25}_D$ +83.2° (*c* 0.1, MeOH); UV (MeOH) λ_{max} (log ε) 247 (3.95), 260 (3.99), 360 (3.80) nm; IR (KBr) ν_{max} 3463, 2923, 2854, 2369, 2343, 2071, 1656, 1640, 1592, 1503, 1485, 1442, 1370, 1286, 1231, 1167, 1138, 1097, 1039, 931 cm^{-1}; CD (MeOH) ($\Delta\varepsilon$) 215 (–13.35), 234 (+7.61), 258 (–10.40), 317 (–4.02), 348 (+6.77); ^1H and ^{13}C NMR data, see Table 2.1; HRESIMS *m/z*

375.0869 $[M+Na]^+$ (calcd. for $C_{20}H_{16}O_6Na$: 375.0839).

Premnan B (2): white, amorphous solid; $[\alpha]^{25}_D$ +1.6° (*c* 0.1, MeOH); UV (MeOH) λ_{max} (log ε) 245 (3.70), 288 (3.78) nm; IR (KBr) ν_{max} 3470, 2964, 2920, 2853, 2371, 1638, 1498, 1446, 1408, 1261, 1097, 1033, 933, 865, 803 cm^{-1}; CD (MeOH) ($\Delta\varepsilon$) 205 (–5.72), 216 (+6.46), 234 (+12.14), 258 (+4.94), 269 (+5.18); ^1H and ^{13}C NMR data, see Tables 2.2; HRESIMS *m/z* 409.0868 $[M+Na]^+$ (calcd. for $C_{20}H_{18}O_8Na$: 409.0894).

Taungtangyiol C (3): white, amorphous solid; $[\alpha]^{25}_D$ –55.5° (*c* 0.1, MeOH); UV (MeOH) λ_{max} (log ε) 247 (4.07), 285 (4.05) nm; IR (KBr) ν_{max} 3436, 2964, 2931, 2359, 2328, 1713, 1450, 1377, 1241 cm^{-1}; CD (MeOH) ($\Delta\varepsilon$) 203 (–4.18), 227 (+4.16), 269 (–0.74), 283 (–0.50); ^1H and ^{13}C NMR data, see Tables 2.3; HRESIMS *m/z* 395.1101 $[M+Na]^+$ (calcd. for $C_{20}H_{20}O_7Na$: 395.1101).

7,9-Dihydroxydolichanthin B (4): white amorphous solid; $[\alpha]_D^{25}$ +8.7° (*c* 0.1, MeOH); UV λ_{max} (MeOH) nm (log ε): 245 (3.67), 288 (3.82) nm; IR (KBr) ν_{max} 3405, 2896, 2361, 2255, 2066, 1849, 1646, 1490, 1443, 1377, 1245, 1098, 1030, 1000, 929, 816 cm^{-1}; ^1H and ^{13}C NMR: see Table 2.4; HRESIMS *m/z* $[M+Na]^+$ (calcd. for $C_{20}H_{20}O_8Na$: 411.1050; found: 411.1049).

Premnan C (5): pale yellow, amorphous solid; $[\alpha]^{25}_D$ +4.7° (*c* 0.1, MeOH); UV (MeOH) λ_{max} (log ε) 245 (3.67), 285 (3.74) nm; IR (KBr) ν_{max} 3458, 2924, 2860, 2373, 2342, 1634, 1491, 1444, 1382, 1249, 1219, 1165, 1106, 1073, 1038, 1038, 934, 802 cm^{-1}; CD (MeOH); ($\Delta\varepsilon$) 195 (–5.75), 199 (+10.11), 204 (–13.47), 210 (–15.21),

225 (+10.39), 232 (+8.22); ^{1}H and ^{13}C NMR data, see Table 2.5; HRESIMS *m/z* 451.1368 $[M+Na]^{+}$ (calcd. for $C_{23}H_{24}O_8Na$: 451.1363).

(3*R*,4*S*)-4-(1,3-Benzodioxol-5-ylcarbonyl)-3-[(*R*)-1-(1,3-benzodioxol-5-yl)-1-hydroxy methyl]tetrahydro-2-furanone (6): white amorphous solid; ^{1}H NMR (500 MHz, $CDCl_3$) δ: 3.56 (dd, J = 8.0, 3.4 Hz, 1H, H-1), 4.56 (dd, J = 8.6, 9.2 Hz, 1H, H-4a), 4.18 (dd, J = 8.0, 8.6 Hz, 1H, H-4b), 4.43 (dd, J = 8.0, 16.0 Hz, 1H, H-5), 6.74 (m, 1H, H-6), 7.10 (d, J = 1.7 Hz, 1H, H-2′), 6.74 (m, 1H, H-5′), 7.24 (dd, J = 1.7, 8.0 Hz, 1H, H-6′), 6.04 (s, 2H, H-7′), 6.78 (d, J = 8.0 Hz, 1H, H-2″), 6.74 (m, 1H, H-5″), 6.62 (d, J = 8.6 Hz, 1H, H-6″), 5.59 (brs, 1H, H-7″a), 5.85 (brs, 1H, H-7″b); ^{13}C NMR data (125 MHz, $CDCl_3$) δ: 52.5 (C-1), 176.3 (C-2), 69.1 (C-4), 41.9 (C-5), 106.0 (C-6), 195.0 (C-7), 130.1 (C-1′), 107.9 (C-2′), 148.3 (C-3′), 152.4 (C-4′), 106.0 (C-5′), 124.8 (C-6′), 102.1 (C-7′), 134.3 (C-1″), 107.9 (C-2″), 147.8 (C-3″), 147.1 (C-4″), 108.2 (C-5″), 118.6 (C-6″), 101.1 (C-7″); The above data are identical with those of (3*R*,4*S*)-4-(1,3-benzodioxol-5-ylcarbonyl)-3-[(*R*)-1-(1,3-benzodioxol-5-yl)-1-hydroxym ethyl]tetrahydro-2-furanone in the literature.[57]

(-)-Aptosimon (7): white amorphous solid; ^{1}H NMR (500 MHz, $CDCl_3$) δ: 3.21 (m, 1H, H-1), 5.30 (d, *J* = 4.0 Hz, 1H, H-2), 3.43 (dd, *J* = 9.2, 3.5 Hz, 1H, H-5), 5.32 (d, *J* = 4.0 Hz, 1H, H-6), 4.32 (dd, *J* = 9.2, 6.9 Hz, 1H, H-8a), 4.02 (dd, *J* = 9.2, 4.6 Hz, 1H, H-8b), 6.82 (brs, 1H, H-2′), 6.76 (m, 1H, H-5′), 6.80 (m, 1H, H-6′), 5.96 (s, 2H, H-7′), 6.87 (brs, 1H, H-2″), 6.77 (m, 1H, H-5″), 6.85 (m, 1H, H-6″), 5.99 (s, 2H, H-7″); ^{13}C NMR data (125 MHz, $CDCl_3$) δ: 50.5 (C-1), 83.3 (C-2), 176.6 (C-4), 53.3 (C-5), 84.4 (C-6), 72.6 (C-8), 133.0 (C-1′), 108.3 (C-2′), 148.0 (C-3′), 147.2 (C-4′, C-4″),

105.7 (C-5′), 118.7 (C-6′), 101.4 (C-7′), 134.3 (C-1″), 108.5 (C-2″), 148.3 (C-3″), 106.0 (C-5″), 119.0 (C-6″), 101.2 (C-7″); The above data are identical with those of (-)-aptosimon in the literature.[58]

(-)-Diasesamin-di-γ-lactone (8): colorless amorphous solid; ^{1}H NMR (500 MHz, $CDCl_3$) δ: 3.54 (brs, 2H, H-1, H-5), 5.82 (brs, 2H, H-2, H-6), 6.76 (d, J = 1.2 Hz, 2H, H-2′, H-2″), 6.82 (d, J = 8.2 Hz, 2H, H-5′, H-5″), 6.79 (dd, J = 8.2, 1.2 Hz, 2H, H-6′, H-6″), 5.99 (s, 4H, H-7′, H-7″); ^{13}C NMR data (125 MHz, $CDCl_3$) δ: 48.3 (C-1, C-5), 81.8 (C-2, C-6), 174.6 (C-4, C-8), 131.7 (C-1′, C-1″), 105.2 (C-2′, C-2″), 148.4 (C-3′, C-3″), 148.6 (C-4′, C-4″), 108.8 (C-5′, C-5″), 118.5 (C-6′, C-6″), 101.6 (C-7′, C-7″); The above data are identical with those of (-)-diasesamin-di-γ-lactone in the literature.[58]

(+)-Epi-sesaminone (9): colorless amorphous solid; white amorphous solid; ^{1}H NMR (500 MHz, $CDCl_3$) δ: 4.01 (m, 1H, H-1), 3.76 (m, 1H, H-4a), 3.65 (m, 1H, H-4b), 2.86 (m, 1H, H-5), 4.65 (d, J = 9.2 Hz, 1H, H-6), 4. 28 (m, 1H, H-8a), 4.10 (m, 1H, H-8b), 6.95 (d, J = 1.7 Hz, 1H, H-2′), 6.76 (d, J = 8.0 Hz, 1H, H-5′), 6.84 (dd, J = 8.0, 1.7 Hz, 1H, H-6′), 6.05 (s, 2H, H-7′), 7.45 (d, J = 1.7 Hz, 1H, H-2″), 6.86 (d, J = 8.1 Hz, 1H, H-5″), 7.56 (dd, J = 8.1, 1.7 Hz, 1H, H-6″), 5.94 (s, 2H, H-7″); ^{13}C NMR data (125 MHz, $CDCl_3$) δ: 49.9 (C-1), 197.3 (C-2), 61.3 (C-4), 52.2 (C-5), 83.7 (C-6), 70.8 (C-8), 134.4 (C-1′), 107.1 (C-2′), 147.4 (C-3′), 148.0 (C-4′), 108.3 (C-5′), 120.1 (C-6′), 102.0 (C-7′), 131.4 (C-1″), 108.1 (C-2″), 148.4 (C-3″), 152.2 (C-4″), 108.0 (C-5″), 124.9 (C-6″), 101.0 (C-7″); The above data are identical with those of (+)-epi-sesaminone in the literature.[59]

Oleanonic acid (10): white amorphous solid; ^{1}H NMR (500 MHz, $CDCl_3$) δ: 5.31 (m, 1H, H-12), 2.82 (dd, J = 14.3, 4.6 Hz,1H, H-18), 1.09 (s, 3H, H-23), 1.03 (s, 3H, H-24), 1.05 (s, 3H, H-25), 0.82 (s, 3H, H-26), 1.15 (s, 3H, H-27), 0.92 (s, 3H, H-29), 0.94 (s, 3H, H-30); ^{13}C NMR data (125 MHz, $CDCl_3$) δ: 39.1 (C-1), 34.1 (C-2), 217.7 (C-3), 47.4 (C-4), 55.3 (C-5), 19.5 (C-6), 32.2 (C-7), 39.2 (C-8), 46.9 (C-9), 36.8 (C-10), 23.5 (C-11), 122.4 (C-12), 143.6 (C-13), 41.7 (C-14), 27.7 (C-15), 22.9 (C-16), 45.8 (C-17), 41.0 (C-18), 46.5 (C-19), 30.7 (C-20), 33.8 (C-21), 33.1 (C-22), 26.4 (C-23), 21.4 (C-24), 15.0 (C-25), 17.0 (C-26), 25.8 (C-27), 183.9 (C-28), 32.4 (C-29), 23.6 (C-30); The above data are identical with those of oleanonic acid in the literature.[60]

(2α, 3α)-Dihydroxyolean-12-en-28-oic acid (11): white amorphous solid; ^{1}H NMR (500 MHz, $CDCl_3$) δ: 4.01 (dt, *J* = 10.8, 3.5 Hz 1H, H-2), 3.44 (d, *J* = 2.8 Hz,1H, H-3), 5.30 (brs, 1H, H-12), 2.83 (dd, *J* = 14.3, 4.2 Hz,1H, H-18), 1.14 (s, 3H, H-23), 0.96 (s, 3H, H-24), 0.91 (s, 3H, H-25), 0.85 (s, 3H, H-26), 1.02 (s, 3H, H-27), 0.81 (s, 3H, H-29), 0.93 (s, 3H, H-30); ^{13}C NMR data (125 MHz, $CDCl_3$) δ: 41.7 (C-1), 66.5 (C-2), 78.9 (C-3), 38.1 (C-4), 48.1 (C-5), 18.0 (C-6), 32.4 (C-7), 39.4 (C-8), 47.3 (C-9), 38.2 (C-10), 23.2 (C-11), 122.4 (C-12), 143.7 (C-13), 40.9 (C-14), 28.5 (C-15), 23.4 (C-16), 46.4 (C-17), 40.9 (C-18), 45.8 (C-19), 30.4 (C-20), 33.6 (C-21), 32.7 (C-22), 28.5 (C-23), 21.8 (C-24), 16.3 (C-25), 17.1 (C-26), 26.1 (C-27), 182.9 (C-28), 33.1 (C-29), 23.6 (C-30); The above data are identical with those of (2α, 3α)-dihydroxyolean -12-en-28-oic acid in the literature.[61]

Taungtangyiol A: white amorphous solid; ^{1}H NMR (500 MHz, $CDCl_3$) δ: 2.45 (m, 1H, H-1), 4.86 (d, *J* = 5.2 Hz, 1H, H-2), 3.55 (dd, *J* = 1.4, 12.7 Hz, 1H, H-4a), 3.46

(dd, J = 1.0, 12.7 Hz, 1H, H-4b), 4.38 (d, J = 9.0 Hz, 1H, H-6), 3.91 (m, 1H, H-7a), 3.79 (m, 1H, H-7b), 7.01 (m, 1H, H-2′), 6.76 (m, 1H, H-5′), 6.84 (dd, J = 2.2, 10.1 Hz, 1H, H-6′), 5.97 (m, 1H, H-7′), 7.01 (m, 1H, H-2″), 6.82 (m, 1H, H-5″), 6.76 (m, 1H, H-6″), 5.95 (m, 1H, H-7″); ^{13}C NMR data (125 MHz, $CDCl_3$) δ: 61.5 (C-1), 84.4 (C-2), 75.9 (C-3), 84.2 (C-4), 84.2 (C-5), 73.8 (C-6), 61.4 (C-7), 133.2 (C-1′), 108.3 (C-2′), 148.2 (C-3′), 147.9 (C-4′), 107.2 (C-5′), 121.1 (C-6′), 101.3 (C-7′), 135.2 (C-1″), 108.1 (C-2″), 148.0 (C-3″), 147.6 (C-4″), 108.0 (C-5″), 120.2 (C-6″), 101.2 (C-7″).

III. Experimental detail of chapter 3

Plant material

The stems of *J. multifida* were purchased from Sandhi Brothers Trading Co. Ltd (Yangon, Myanmar) in November 2015. A voucher specimen (TMPW 28729) was deposited at the Museum of Materia Medica, Analytical Research Center for Ethnomedicines, Institute of Natural Medicine, University of Toyama, Japan.

Extraction and isolation procedure

The dried powder of the *J. multifida* stems (4.8 kg) were extracted with $CHCl_3$ under sonication (8L, × 4) at room temperature. The extract was then evaporated under reduced pressure to yield crude extract (11.0 g) and subjected to silica gel column chromatography using gradient solvent system of $CHCl_3$–EtOAc (10:1 to 0:10, v/v) to give five fractions (Fr. 1–5).

Fraction 2 (517.5 mg) was subjected to normal phase pTLC with *n*-hexane-EtOAc (2:1) to give scoparone (**12**, 1.4 mg).

Fraction 3 (1.4 g) was rechromatographed on reversed phase MPLC (120 g; 36×160 mm), eluted with a gradient mobile phase (MeOH–MeCN–H_2O = 1:1:4 to 1:1:1) to obtain four sub fractions (Fr. 3-1–3-4). Subfraction 3-1 was purified by silica gel column chromatography using $CHCl_3$–EtOAc (4:1 to 1:1, v/v), to isolate scopoletin (**13**, 5.2 mg) and salicifoliol (**14**, 3.0 mg).

Fraction 4 (3.8 g) was rechromatographed on reversed phase MPLC (120 g; 36×160 mm), eluted with a gradient mobile phase (MeOH–MeCN–H_2O = 1:1:4 to 1:1:1) to afford four sub fractions (Fr. 4-1–4-4). Sub fraction 4-1 was subjected to silica

gel column chromatography with $CHCl_3$–EtOAc (2:1 to 1:4, v/v) to give glaberide I (**15**, 2.7 mg). Subfraction 4-3 was subjected to sephadex LH-20 with 100% MeOH, followed by normal phase pTLC with *n*-hexane–EtOAc (1:1), to give pinoresinol (**16**, 4.7 mg), medioresinol (**17**, 1.2 mg), and syringaresinol (**18**, 5.2 mg). Subfraction 4-3 was further purified by Cosmosil 75C18-OPN with MeOH–H_2O (1:2) to yield matairesinol (**19**, 6.3).

Fraction 5 (4.9 g) was rechromatographed on Cosmosil 75C18-OPN with MeOH–H_2O (1:3 to 3:1, v/v) to yield five subfractions (Fr. 5-1–5-5). Subfraction 5-1 was subjected to sephadex LH-20 using 100% MeOH, followed by silica gel column chromatography with only $CHCl_3$ to afford shonanin (**20**, 5.3 mg).

Scoparone (12): white amorphous solid; ^{1}H NMR (500 MHz, $CDCl_3$) δ: 6.30 (d, J = 9.3 Hz, 1H, H-3), 7.63 (d, J = 9.3 Hz, 1H, H-4), 6.86 (s, 1H, H-5), 6.85 (s, 1H, H-8), 3.96 (s, 6H, OMe-6, OMe-7); ^{13}C NMR data (125 MHz, $CDCl_3$) δ: 161.4 (C-2), 113.6 (C-3), 143.2 (C-4), 111.4 (C-4a), 108.0 (C-5), 146.4 (C-6), 152.9 (C-7), 100.0 (C-8), 150.0 (C-8a), 56.4 (OMe-6, OMe-7); The above data are identical with those of scoparone in the literature.[86]

Scopoletin (13): white amorphous solid; ^{1}H NMR (500 MHz, DMSO-d_6) δ: 6.21 (d, J = 9.5 Hz, 1H, H-3), 7.91 (d, J = 9.5 Hz, 1H, H-4), 7.21 (s, 1H, H-5), 6.77 (s, 1H, H-8), 3.81 (s, 3H, OMe-6); ^{13}C NMR data (125 MHz, DMSO-d_6) δ: 160.7 (C-2), 111.6 (C-3), 144.5 (C-4), 110.5 (C-4a), 109.6 (C-5), 145.3 (C-6), 151.3 (C-7), 102.8 (C-8), 149.5 (C-8a), 56.0 (OMe-6, OMe-7); The above data are identical with those of scopoletin in the literature.[87]

Salicifoliol (14): pale yellowish amorphous solid; ^{1}H NMR (500 MHz, DMSO-d_6) δ: 3.58 (m, 1H, H-1), 4.48 (d, J = 1.7, 9.5 Hz, 1H, H-4a), 4.48 (d, J = 6.9, 9.5 Hz, 1H, H-4b), 3.11 (m, 1H, H-5), 4.63 (d, J = 6.3 Hz, 1H, H-6), 3.92 (dd, J = 3.4, 8.6 Hz, 1H, H-8a), 4.17 (t, J = 8.6 Hz, 1H, H-8b), 6.77 (dd, J = 1.7, 8.0 Hz, 1H, H-2′), 6.77 (dd, J = 1.7, 8.0 Hz, 1H, H-3′), 6.77 (dd, J = 1.7, 8.0 Hz, 1H, H-6′), 3.75 (s, 3H, OMe-5′); ^{13}C NMR data (125 MHz, DMSO-d_6) δ: 46.4 (C-1), 179.3 (C-2), 70.7 (C-4), 48.0 (C-5), 86.1 (C-6), 69.9 (C-8), 131.3 (C-1′), 119.3 (C-2′), 115.7 (C-3′), 146.8 (C-4′), 148.1 (C-5′), 111.0 (C-6′), 56.1 (OMe-5′); The above data are identical with those of salicifoliol in the literature. [88]

Glaberide I (15): white amorphous solid; ^{1}H NMR (500 MHz, $CDCl_3$) δ: 3.57 (m, 1H, H-1), 4.35 (d, J = 2.1, 9.5 Hz, 1H, H-4a), 4.48 (d, J = 6.9, 9.5 Hz, 1H, H-4b), 3.12 (m, 1H, H-5), 4.63 (d, J = 6.5 Hz, 1H, H-6), 3.93 (dd, J = 3.4, 8.7 Hz, 1H, H-8a), 4.20 (t, J = 8.7 Hz, 1H, H-8b), 6.63 (s, 2H, H-2′, H-6′), 3.75 (s, 6H, OMe-3′, OMe-5′); ^{13}C NMR data (125 MHz, $CDCl_3$) δ: 45.9 (C-1), 178.8 (C-2), 70.3 (C-4), 47.7 (C-5), 85.8 (C-6), 69.6 (C-8), 130.1 (C-1′), 103.8 (C-2′, C-6′), 148.1 (C-3′), 135.3 (C-4′), 148.1 (C-5′), 56.2 (OMe-3′, OMe-5′); The above data are identical with those of glaberide I in the literature. [89]

Pinoresinol (16): white amorphous solid; ^{1}H NMR (500 MHz, DMSO-d_6) δ: 3.03 (m, 2H, H-1, H-5), 4.60 (d, J = 4.0 Hz, 2H, H-2, H-6), 3.72 (dd, J = 3.4, 9.2 Hz, 2H, H-4a, H-8a), 4.12 (dd, J = 6.9, 9.2 Hz, 2H, H-4b, H-8b), 6.89 (d, J = 1.7 Hz, 2H, H-2′, H-2″), 6.72 (d, J = 8.0 Hz, 2H, H-5′, H-5″), 6.74 (dd, J = 8.0, 1.7 Hz, 2H, H-6′, H-6″), 3.76 (s, 6H, OMe-3′, OMe-3″); ^{13}C NMR data (125 MHz, DMSO-d_6) δ: 53.4 (C-1, C-5),

85.0 (C-2, C-6), 70.7 (C-4, C-8), 132.0 (C-1′, C-1″), 110.2 (C-2′, C-2″), 147.3 (C-3′, C-3″), 145.8 (C-4′, C-4″), 115.0 (C-5′, C-5″), 118.5 (C-6′, C-6″), 55.4 (OMe-3′, OMe-3″); The above data are identical with those of pinoresinol in the literature. [89]

Medioresinol (17): white amorphous solid; ^{1}H NMR (500 MHz, DMSO-d_6) δ: 3.14 (m, 1H, H-1), 4.71 (m, 1H, H-2), 3.87 (m, 2H, H-4a, H-8a), 4.25 (m, 2H, H-4b, H-8b), 6.86 (d, J = 0.6 Hz, 2H, H-2′, H-6′), 6.82 (m, 1H, H-2″), 6.77 (d, J = 8.1 Hz, 1H, H-3″), 6.95 (d, J = 1.7 Hz, 1H, H-6″), 3.85 (s, 6H, OMe-3′, OMe-5′), 3.86 (s, 3H, OMe-4″); ^{13}C NMR data (125 MHz, DMSO-d_6) δ: 55.8 (C-1), 88.1 (C-2), 73.2 (C-4), 56.0 (C-5), 88.0 (C-6), 73.1 (C-8), 133.6 (C-1′), 105.0 (C-2′), 149.8 (C-3′), 136.7 (C-4′), 149.8 (C-5′), 105.0 (C-6′), 134.2 (C-1″), 120.5 (C-2″), 116.5 (C-3″), 147.8 (C-4″), 149.6 (C-5″), 111.4 (C-6″), 57.3 (OMe-3′, OMe-5′), 56.9 (OMe-4″); The above data are identical with those of pinoresinol in the literature. [89]

Syringaresinol (18): white amorphous solid; ^{1}H NMR (500 MHz, DMSO-d_6) δ: 3.05 (m, 2H, H-1, H-5), 4.71 (m, 2H, H-2, H-6), 3.75 (m, 2H, H-4a, H-8a), 4.16 (dd, J = 7.0, 9.1 Hz, 2H, H-4b, H-8b), 6.60 (s, 4H, H-2′, H-6′, H-2″, H-6″), 3.75 (s, 12H, OMe-3′, OMe-5′, OMe-3″, OMe-5″); ^{13}C NMR data (125 MHz, DMSO-d_6) δ: 53.6 (C-1, C-5), 85.3 (C-2, C-6), 73.1 (C-4, C-8), 131.4 (C-1′, C-1″), 103.6 (C-2′, C-6′, C-2″, C-6″), 147.9 (OMe-3′, OMe-5′, OMe-3″, OMe-5″), 134.8 (C-4′, C-4″), 56.0 (OMe-3′, OMe-5′, OMe-3″, OMe-5″); The above data are identical with those of syringaresinol in the literature.[90]

Matairesinol (19): white amorphous solid; ^{1}H NMR (500 MHz, DMSO-d_6) δ:

2.67 (m, 1H, H-1), 3.85 (t, J = 8.6 Hz, 1H, H-4a), 4.06 (dd, J = 7.1, 8.6 Hz, 1H, H-4b), 2.42 (m, 1H, H-5), 2.49 (overlapped 2H, H-6), 2.73 (dd, J = 6.9, 13.8 Hz, 1H, H-7a), 2.80 (dd, J = 5.5, 13.8 Hz, 1H, H-7b), 6.73 (d, J = 1.9 Hz, 1H, H-2′), 6.68 (d, J = 8.4 Hz, 1H, H-5′), 6.58 (dd, J = 8.5, 1.9 Hz, 1H, H-6′), 6.60 (d, J = 2.1 Hz, 1H, H-2″), 6.65 (d, J = 8.0 Hz, 1H, H-5″), 6.47 (dd, J = 8.0, 2.1 Hz, 1H, H-6″), 3.71 (s, 6H, OMe-3′, OMe-3″); ^{13}C NMR data (125 MHz, DMSO-d_6) δ: 45.6 (C-1), 178.4 (C-2), 70.7 (C-4), 40.9 (C-5), 36.9 (C-6), 33.7 (C-7), 129.0 (C-1′), 113.5 (C-2′), 147.4 (C-3′), 145.1 (C-4′), 115.3 (C-5′), 122.9 (C-6′), 129.5 (C-1″), 112.7 (C-2″), 147.5 (C-3″), 145.0 (C-4″), 115.4 (C-5″), 121.5 (C-6″), 55.5 (OMe-3′, OMe-3″); The above data are identical with those of matairesinol in the literature.[87]

Shonanin (20): white amorphous solid; ^{1}H NMR (500 MHz, CD_3OD) δ: 1.90 (m, 2H, H-1, H-5), 3.57 (dd, J = 5.2, 11.0 Hz, 2H, H-2a, H-4a), 3.60 (dd, J = 5.1, 11.0 Hz, 2H, H-2b, H-4b), 2.56 (dd, J = 7.8, 13.7 Hz, 2H, H-6a, H-7a), 2.66 (dd, J = 7.0, 13.9 Hz, 2H, H-6b, H-7b), 6.59 (d, J = 1.9 Hz, 2H, H-2′, H-2″), 6.67 (d, J = 8.0 Hz, 2H, H-5′, H-5″), 6.55 (dd, J = 8.0, 1.9 Hz, 2H, H-6′, H-6″), 3.74 (s, 6H, OMe-3′, OMe-3″); ^{13}C NMR data (125 MHz, CD_3OD) δ: 44.3 (C-1, C-5), 62.3 (C-2, C-4), 44.3 (C-6, C-7), 134.0 (C-1′, C-1″), 113.5 (C-2′, C-2″), 149.0 (C-3′, C-3″), 145.6 (C-4′, C-4″), 115.9 (C-5′, C-5″), 122.9 (C-6′, C-6″), 56.3 (OMe-3′, OMe-3″); The above data are identical with those of shonanin in the literature. [92]

IV. Experimental detail of chapter 4

Sponge material

C. prolifera was collected from Taung-pan-gyi Island, Kyun Su Township, Tanintharyi Region, Myanmar, in November, 2015. The sample was identified by assistant lecturer Aung Aung Aye (Department of Marine Sciences, University of Myeik). A voucher specimen (TS.10) was deposited at the Department of Marine Sciences, University of Myeik.

Extraction and isolation procedure

Dried pieces of *C. prolifera* (79.5 g) were extracted in a MeOH and acetone mixture (2:1) with sonication (600 mL, 90 min× 6) at room temperature, and the solvent was evaporated under reduced pressure to obtain the crude extract (80 g), which was partitioned between EtOAc and water (8 × 0.6 L), to obtain the water- (9.6 g) and EtOAc-soluble portions (1.8 g). The water-soluble portion (9.6 g) was fractionated on a DIAION HP-20 column, which was eluted stepwise with 2 L to afford 3 fractions, 100% H_2O (Fr. 1), 50% MeOH (Fr. 2), and 100% MeOH (Fr. 3).

Fr. 2 (1.0 g) was subjected to chromatography on a sephadex LH-20 column using CH_2Cl_2–MeOH (7:3) to obtain five subfractions (Frs. 2-1–2-5). Subfraction 2-2 was further purified by reversed phase pTLC with MeOH–MeCN–H_2O (1:1:2), to furnish clathrirole A (**21**, 1.0 mg) and clathrirole B (**22**, 2.3 mg).

Clathrirole A (**21**): White amorphous solid; $[\alpha]_D^{25}$ –27.7°(*c* 0.1, $CHCl_3$); UV (MeOH) λ_{max} (log ε) 211 (4.0), 214 (4.0), 219 (4.0), 229 (4.1), 273 (4.1) nm; IR (KBr)

ν_{max} 3420, 2925, 2361, 1682, 1624, 1456, 1384, 1321, 1188, 1128, 1028 cm^{-1}; CD (MeOH) ($\Delta\varepsilon$) 200 (–0.69), 220 (–2.21), 236 (+0.86), 274 (–3.70); ^{1}H NMR (500 MHz, CD_3OD) and ^{13}C NMR (125 MHz, CD_3OD) data (see Table 4.1); HRESIMS: *m*/*z* 358.0398 $[M+H]^+$, 360.0390 $[M+H+2]^+$ (calcd. for $C_{13}H_{17}N_3O_4Br$, 358.0397).

Clathrirole B (**22**): White amorphous solid; $[\alpha]_D^{25}$ –29.3° (*c* 0.1, $CHCl_3$); UV (MeOH) λ_{max} (log ε) 207 (3.2), 215 (3.3), 220 (3.4), 223 (3.4), 229 (3.4), 268 (3.6) nm; IR (KBr) ν_{max} 3424, 2925, 2341, 1683, 1616, 1385, 1321, 1125 cm^{-1}; ^{1}H NMR (900 MHz, CD_3OD) and ^{13}C NMR (225 MHz, CD_3OD) data (see Table 4.2); HRESIMS: *m*/*z* 280.1292 $[M+H]^+$ (calcd. for $C_{13}H_{18}N_3O_4$, 280.1292).

DFT/TDDFT calculations

DFT/TDDFT calculations were performed with the same procedure as those of chapter 2 except for generating low-energy conformations of **21**.

All DFT/TDDFT calculations were conducted using the Gaussian 09 software.[102] Initially, each low-energy conformer obtained by MMFF calculations was subjected to geometry optimization by the DFT method at the B3LYP/6-31G(d) level, with the Polarizable Continuum Model (PCM) in MeOH. Subsequently, to estimate the thermal free energy (ΔG) and check for the presence of imaginary frequencies, each optimized conformer was subjected to a frequency calculation at the B3LYP/6-31G(d) level with the PCM in MeOH. Based on the estimated thermal energy, the abundance ratio of each conformer was determined by the Boltzmann distribution. Calculations of the ECD spectra of all conformers were performed by using the TDDFT method at the B3LYP/6-31G(d) level with PCM in MeOH, and the weighted-average spectra were

compared with the experimental ECD spectra recorded in MeOH.

Antifungal assay

S. cerevisiae was used for this assay. 50 mM of stock solutions of the samples were prepared in DMSO, and further diluted to 200, 100, 50, 25, and 12.5 μM in 96-well plates containing *S. cerevisiae* cultured in YPD medium [2% polypeptone (Nihon Pharmaceutical, Japan), 1% yeast extract (Difco, USA), and 2% glucose (Wako, Japan)]. The plates were incubated at 37 °C overnight, and then the MIC values were evaluated. Cyclohexamide (Nacalai Tesque, Japan) and DMSO were used as positive and negative controls, respectively.

References

1. Brenner M, Hearing VJ (2008) Modifying skin pigmentation-approaches through intrinsic biochemistry and exogenous agents. *Drug Discov Today Dis Mech* 5:189–199.
2. Niu C, Aisa HA (2017) Upregulation of melanogenesis and trosinase activity: potential agents for vitiligo. *Molecules* 22:1–28.
3. Fisk WA, Agbai O, Lev-Tov HA, Sivamani RK (2014) The use of botanically derived agents for hyperpigmentation: a systemic review. *J Am Acad Dermatol* 70:352–365.
4. Setyawati A, Yamaguchi K, Mitsunaga T (2018) Potential of medicinal plants extractives as anti-melanogenesis ingredients. *Review Agric Sci* 6:46–60.
5. Kim K, Leutou AS, Jeong H, Kim D, Seong CN, Nam S-J, Lim K-M (2017) Anti-pigmentary effect of (-)-4-hydroxysattabacin from the marine-derived bacterium *Bacillus* sp. *Mar Drugs* 15:138.
6. Kim M, Shin S, Lee J-A, Park D, Lee J, Jung E (2015) Inhibition of melanogenesis by *Gaillardia aristata* flower extract. *BMC complementary Alter Med* 15:449.
7. Chatatikun M, Yamauchi T, Yamasaki K, Aiba S, Chiabchalard A (2018) Anti melanogenic effect of *Croton roxiburghii* and *Croton sublyratus* leaves in α-MSH stimulated B16-F10 cells. *J Tradit Complement Med* doi: 10.1016/j.jtcme.2017.12.002.
8. Lassalle MW, Igarashi S, Sasaki M, Wakamatsu K, Ito S, Horikoshi T (2003) Effects of melanogenesis-inducing nitric oxide and histamine on the production of eumelanin and pheomelanin in cultured human melanocytes. *Pigment Cell*

Res 16:1–8.

9. Choi YK, Rho YK, Yoo KH, Lim YY, Li K, Kim BJ, Seo SJ, Kim MN, Hong CK, Kim DS (2010) Effects of vitamin C vs. multivitamin on melanogenesis: comparative study *in vitro* and *in vivo*. *Pharmacol Ther* 49:218–226.

10. Iijima C, Wong CP, Nugroho AE, Sotozono Y, Someya S, Hirasawa Y, Kaneda T, Hadi AH, Morita H (2016) Anti-melanin deposition activity of ceramicines from *Chisocheton ceramicus*. *J Nat Med* 70:702–707.

11. Qiao Z, Koizumi Y, Zhang M, Natsui M, Flores MJ, Gao L, Yusa K, Koyota S, Sugiyama T (2012) Anti-melanogenesis effect of *Glechoma hederacea* L. extract on B16 murine melanoma cells. *Biosci Biotechnol Biochem* 76:1877–1883.

12. Choi M-H, Shin H-J (2016) Anti-melanogenesis effect of quercetin. *Cosmetics* 18:1–16.

13. Chan GKL, Wu KQ, Wong ZCF, Fung AHY, Lin X, Lou LJ, Dong TT, Tsim KWK (2016) A high throughput screening platform for skin tuning properties from natural products: identification of skin tanning compounds. *J Chem Dermatol Sci Appl* 6:199–209.

14. Pillaiyar T, Namassivayam V, Manickam M, Hung SH (2018) Inhibitos of melanogenesis: an update review. *J Med Chem* 61:7395–7418.

15. Najaran ZT, Akaberi M, Vatani M, Emami SA (2016) Evaluation of antioxidant and anti-melanogenic activities of different extracts from aerial parts of Nepeta binaludensis Jamazad in murine melanoma B16F10 cells. *Iran J Basic Med Sci* 19:6.

16. Chang T-S (2012) Natural melanogenesis inhibitors acting through the

down-regulation of tyrosinase activity. *Materials* 5:1661–1685.

17. D′Mello SND, Finlay GJ, Baguley BC, Askarian-amiri ME (2016) Signaling pathways in melanogenesis. *Int J Mol Sci* 17:1144.

18. National biodiversity strategy and action plan (2015-2020), IUCN (International Union for Conservation of Nature), 2015.

19. Hadas E, Shipigel M, Ilan M (2009) Pharmaculate organic matter as a food source for a coral reef sponge. *J Exp Biol* 212:3643–3650.

20. Anjum K, Abbas SQ, Shah SAA, Akhter N, Batool S, Hassan SS (2016) Marine spnges as a drug treasure. *Biomol Ther* 24:347–362.

21. Perdicaris S, Vlachoginni T, Valavanidis A (2013) Bioactive natural substances from marine sponges: new developments and propects for future pharmaceuticals. *Nat Prod Chem Res* 1:115.

22. Higa T, Tanak J, Kitamura A, Koyama T, Takahashi M, Uchida T (1994) Bioactive compounds from marine sponges. *Pure & Appl Chem* 66:2227–2230.

23. Haefner B (2003) Drugs from the deep: marine natural products as drug candidates. *Drug Discov Today* 8:536–544.

24. Belaebi el H, Conteras GA, Chisti Y, Garcia CF, Molina GE (2003) Producing drugs from marine sponges. *BiotechnoAdv* 21:585–598.

25. Sipkema D, Franssen MC, Osinga R, Tramper J, Wijiffels RH (2005) Marine sponges as pharmacy. *Mar Biotechnol* 7:142–162.

26. Alcaraz MJ, Paya M (2006) Marine sponge metabolites for the control of inflammatory diseasses. *Curr Opin Investing Drugs* 7:974–979.

27. Blunt JW, Copp BR, Munro MH, Northcote PT, Prinsep MR (2006) Marine natural products. *Nat Prod Rep* 23:26–78.

28. Turk T, Ambrozic AJ, Batista Y, Strugar G, Kosmina R, Civovic S, Janussen D, Kauferstein S, Mebs D, Sepcic K (2013) Biological activities of ethanolic extracts from deep-sea Antarctic marine sponges. *Mar Drugs* 11:1126–1139.

29. Faulkner DJ (1998) Marine natural products. *Nat Prod Rep* 15:113–158.

30. Munro HMG, Blunt JW, Dumdei EJ, Hickford SJH, Lill RE, Li S, Battershill C N, Duckworth AR (1999) The discovery and development of marine compounds with pharmaceutical potential. *J Biotechnol* 70:15–25.

31. Faulkner DJ (2000) Marine natural products. *Nat Prod Rep* 17:7–55.

32. Faulkner DJ (2001) Marine natural products. *Nat Prod Rep* 18:149.

33. Faulkner DJ (2002) Marine natural products. *Nat Prod Rep* 19:1–48.

34. Sipkema D, Franssen MCR, Osinga R, Tramper J, Wijffels RH (2005) Marine sponges as pharmacy. *Marine Biotechnol* 7:142–162.

35. Mayer AM, Rodriguez AD, Berlinck RG, Hamann MT (2009) Marine pharmacology in 2005–6: marine compounds with anthelmintic, antibacterial, anti-coagulant, antifungal, anti-inflammatory, antimalarial, antiprotozoal, antituberculosis, and antiviral activities; affecting the cardiovascular, immune and nervous systems, and other miscellaneous mechanisms of action. *Biochim Biophys Acta* 1790:283–308.

36. Marcel J, Donatella DP, Jeanette HA, Fernando R, Alexander DC, Adeianna I (2016) The marine biodiscovery pipeline and ocean medicines of tomorrow. *J Mar Bio Assoc UK* 96:151–158.

37. Bose LV, Varghese GK, Habtemariam S (2013) Identification of acetoside as the active antioxidant principle of *Premna serratifolia* root wood tissues. *Phytopharmacology* 4:228–236.

38. Mali PY (2015) *Premna integrifolia* L.: A review of its biodiversity, traditional uses and phytochemistry. *Anc Sci Life* 35:4–11.

39. Husain A, Virmani OP (1992) Dictionary of Indian Medicinal Plants. Central Institute of Medicinal and Aromatic Plants. Vendams Books Ltd New Delhi.

40. Nguyen TBH, Pham TK, Chau VM, Nguyen XC, Nguyen PT, Phan VK (2008) Study on the chemical constituents of *Premna integrifolia* L.. *Nat Prod Commun* 3:1449–1452.

41. Gopal RH, Purushothaman KK (1984) Effect of plant isolates on coagulation of blood: an *in vitro* study. *Bull Medico Ethno Botanical Research* 5:171–177.

42. Rathore RS, Prakash A, Singh PP (1977) *Premna integrifolia* Linn., preliminary study of anti-inflammatory and anti-arthritic activity. *Rheumatism* 12:130–134.

43. Dash GK, Patrolm CP, Maiti AKJA (2005) Study on the anti-hyperglycaemic effect of roots of *Premna corymbosa. Nat Remedies* 5:31–34.

44. Rajendran R, Basha NS (2010) Antimicrobial activity of crude extracts and fractions of *Premna serratifolia* Linn. root. *Medicinal Plants* 2:33–38.

45. Yadav D, Masood N, Luqman N, Brindha P, Gupta MM (2013) Antioxidant furofuran lignans from *Premna integrifolia*. *Ind Crops Prod* 41:397–402.

46. Biradi M, Hullatti K (2017) Bioactivity guided isolation of cytotoxic terpenoids and steroids from *Premna serratifolia, Pharm Biol* 55:1375–1379.

47. Habtemarian S, Varghese GK (2015) A novel diterpene skleton: Identification of a highly aromatic, cytotoxic and antioxidant 5-methyl-10-demethyl-abietane type diterpene from *Premna serratifolia*. *Phytother Res* 29:80–85.

48. Jothi ET, Suryalakshmi PKPV, Srinivasababu P (2010) Gastroprotective potential of *Premna serratifolia* Linn. leaves against aspirin included ulcer in

albino rats. *Pharmacologyonlin* 3:189–198.

49. Karthikeyan M, Deepa MK (2011) Anti-inflammatory activity of *Premna corymbosa* (Burm.f.) Rottl. & Wild. leaves extracts in Wistar albino rats. *Asian Pac J Trop Med* 4:510–513.

50. Karthikeyan M, Deepa MKJ (2010) Antinociceptive activity of *Premna corymbosa* (Burm.f.) Rottl. & Wild. *Basic Clin Physiol Pharmacol* 2:1347–356.

51. Win NN, Woo S-Y, Ngwe H, Prema, Wong CP, Ito T, Okamoto Y, Tanaka M, Imagawa H, Asakawa Y, Abe I, Morita H (2018) Tetrahydrofuran lignans: Melanogenesis inhibitors from *Premna integrifolia* wood collected in Myanmar. *Fitoterapia* 127:308–313.

52. Barik BR, Bhowmik T, Dey AK, Patra A, Chatterjee A, Joy S, Susan T, Alam M, Kundu AB (1992) Premnazole, an isoxazole alkaloid of Premna integrifolia and Gmrlina arborea with anti-inflammatory activity. *Fitoterapia* 63:295–299.

53. Prashant YM (2016) Pharmacological potential of Premna *integrifolia* L. *Anc Sci Life* 35:132–142.

54. Mahesh B and Kiranumar H (2017) Bioactivity guided isolation of cytotoxic terpenoids and steroids from *Premna serratifolia*. *Pharm Biol* 55:1375–1379.

55. Woo S-Y, Hoshino S, Wong CP, Win NN, Awouafack MD, Prema, Ngwe H, Zhang H, Hayashi F, Abe I, Morita H (2019) Lignans with melanogenesis effects from *Premna serratifolia* wood. *Fitoterapia* 133:35–42.

56. Woo S-Y, Wong CP, Win NN, Hoshino S, Prema, Ngwe H, Abe I, Morita H (2019) A new tetrahydrofuran type lignan from *Premna serratifolia* wood. *Nat Prod Commun* 14:113–116.

57. Endres D, Lausberg V, Signore GD, Berner OMA (2002) General Approach to

the Asymmetric Synthesis of Lignans: (–) MethylPiperitol, (–)-Sesamin, (–)-Aschantin, (+)-Yatein, (+) Dihydroclusin, (+)-Burseran, and (–)-Isostegane. *Synthesis* 4:515–522.

58. Lin R-W, Tsai I-L, Duh C-Y, Lee, K-H, Cehn I-S (2004) New lignans and cytotoxic constituents from *Wikstroemia lanceolata*. *Planta Med* 70:234–238.

59. Marchand PA, Kato MJ, Lewis NG (1997) (+)-Episesaminone, a *Sesamum indicum* furofuran lignan. Isolation and hemisynthesis. *J Nat Prod* 60:1189–1192.

60. Fatope MO, Salihu L, Asante SK, Takeda Y (2002) Lavicidal activity of extracts and triterpenoids from *Lantana camara*. *Pharm Biol* 40:564–567.

61. Woo KW, Han JY, Choi SU, Kim KH, Lee KR (2014) Triterpenes from *Perilla frutescens* var. *acuta* and their cytotoxic activity. *Nat Prod Sci* 20:71–75.

62. Hu P, Li D-H, Hu X, Li S-G, Sai C-M, Sun X-C, Su T, Bai J, Wang Z-H, Li Z-L, Hua H-M (2016) Lignans and triterpenoids from *Vitex negundo* var. *heterophylla* and their biological evaluation. *Fitoterapia* 111:147–153.

63. Zheng C-J, Huang B-K, Han T, Zhang Q-Y, Zhang H, Rahman K, Qin L-P (2009) Nitric oxide scavenging lignans from *Vitex negundo* seeds. *J Nat Prod* 72:1627–1630.

64. Chawla AS, Sharma AK, Handa SS, Dhar KL (1992) A lignan from *Vitex negundo* seeds. *Phytochemistry* 31:4378–4379.

65. Ragasa CY, Ng VAS, Agoo EMG, Shen CC (2015) Chemical constituents of *Cycas vespertilio*. *Rev Bras Farmacogn* 25:526–528.

66. Ma Q-Y, Chen Y-L, Huang S-Z, Kong F-D, Dai H-F, Hue Y, Zhao Y-X (2018) Two new lignans from *Wikstroemia dolichantha*. *Chem Nat Compd* 54:22–25.

67. Huang D, Ding Y, Li Y, Zhang W, Fang W, Chen X (2006) Anti-tumor activity of a 3-oxo derivative of oleanolic acid. *Cancer Lett* 233:289–296.

68. Tief K, Hahne M, Schmidt A, Beermann F (1996) Tysosinase, the key enzyme in melanin synthesis, is expressed in murine brain. *Eur J Biochem* 241:12–16.

69. Thomas S **(**2016) Pharmacognostic and phytochemical constituents of leaves of *Jatropha*

multifida Linn. and *Jatropha podagrica* Hook. *J Pharmacogn Phytochem* 5:243–246.

70. Nancy YHH, Leobigildo CT, Angélica RM, Jaime JR, Cavazos ML (2018) Traditional uses and seed chemical composition of *Jatropha spp*. (Euphorbiaceae) in Tehucán-Cuicatlán, México. *Rev Biol Trop* 66:266–279.

71. Padua LS, Bunyapraphatsara N, Lemmes RHMJ **(**1999) Medicinal and poisonous plant 1. *Plant Resources of South-East Asia* No 12 1: Leiden, Backhuys Publishers.

72. Nayak BS, Patal KN (2009) A marvel plant-Jatropha: an appraisal. *Int J Pharm Sci Res* 1:35–39.

73. Das B, Ravikanth B, Reddy KR, Thirupathi P, Raju TV, Sridhar B **(**2008) Diterpenoids from *Jatropha multifida*. *Phytochemistry*, 69:2639–2641.

74. Carvalho C, Mariano LV, Negrão VS, Gonçalves P, Marcucci C (2018) Phenols, flavonoids and antiocidant activity of *Jatropha multifida* L. collected in Pindamonhangaba, Sao Paulo State, Brazil. *J Anal Pharm Res* 7:581–584.

75. Falodum A, Igbe I, Erharuyi O (2013) Chemical characterization, anti-inflmmatory and analgesic properties of *Jatropha multifida* root bark. *J Appl Sci Envion Manage* 17:357–362.

76. Hirota BCK, Miyazaki CA, Mercali MC, Verdan MC, Kalegari M, Gemin C,

Lordello ALL, Miguel MD, Miguel OG (2012) C-glucosyl flavones and a comparative study of the antioxidant, hemolytic and toxic potential of *Jatropha mutifida* leaves and bark. *Int J Phytomed* 4:1–5.

77. Kosasi S, Vander shis WG, Labadie RP (1989) Multifidol and multifidol glucoside from the latex of *Jatropha multifida. Phytochemisty* 28:2439–2441.

78. Zhu J-Y, Zhang C-Y, Dai J-J, Rahman K, Zhang H (2017) Diterpenoids with thioredoxin reductase inhibitory activities from *Jatropha multifida*. *Nat Prod Res* 31:2753–2758.

79. Das B, Kashinatham A, Venkataiah B, Srinivas KVNS, Mahender G, Reddy MR (2003) Cleimiscosin A, a coumarino-lignoid from *Jatropha gossypifolia*. *Biochem Syst Ecol* 31:1189–1191.

80. Aiyelaagbe OO (2001) Antibacterial activity of *Jatropha multifida* roots. *Fitoterapia* 72:544–546.

81. Shoji M, Woo S-Y, Masuda A, Win NN, Ngwe H, Takahashi E, Kido H, Morita H, Ito T, Kuzuhara T (2017) Anti-influenza virus activity of extracts fromthe stems of *Jatropha multifida* Linn. collected in Myanmar. *BMC Complement Altern Med* 17:96.

82. Anani K, Adjarah Y, Ameyapoh Y, Karou SD, Agbonon A, de Souza C, Gbeassor M (2016) Antimicrobial, anti-inflammatory and antioxidant activities of *Jatropha multifida* L. (Euphorbiaceae). *Pharmacognosy Res* 8:142–146.

83. Das B, Reddy KR, Ravikanth B, Raju TV, Sridhar BM, Khan PU, Rao JV, (2009) Multifidone: A novel cytotoxic lathyrane-type diterpene having an unusual six-membered a ring from *Jatropha multifida*. *Bioorg Med Chem Lett* 19:77–79.

84. Adesola AT, Adetunji OO (2007) The efficacy of *Jatropha multifida* in the management of oral candidiasis: a preliminary study. *Intern J Altern Med* 4:1–5.

85. Falodun A, Imieje V, Erharuyi O, Joy A, Langer P, Jacob M, Khan S, Abaldry M, Hamann M (2014) Isolation of antileishmanial, antimalarial and antimicrobial metabolites from *Jatropha multifida*. *Asian Pac J Trop Biomed* 4:374–378.

86. Gao W, Li Q, Chen J, Wang Z, Hua C (2013) Total synthesis of six 3,4-unsubstituted coumarins. *Molecules* 18:15613–15623.

87. Lina OOA, Braz-Filho R (1997) Dibenzylbutyrolactone lignans and coumarins from *Ipomoea cairica*. *J Braz Chem Soc* 3:235–238.

88. Aguiar RM, Alves CQ, David JM, Lima LCRL, David JP, Queiroz LP (2012) Antioxidant activities of isolated compounds from stems of *Mimosa invisa* Mart. Excolla. *Quim Nova* 35:567–570.

89. Kinjo J, Higuchi H, Fukui K, Nohara T (1991) Lignoids from Albizziae Coretex. II. A biodegradation pathway of syringaresinol. *Chem Pharm Bull* 39:2952–2955.

90. Abe F, Yamaguchi T (1988) 9α-hydroxypinoresinol, 9α-hydroxymedioresinol and related lignans from *Allamanda nerifolia*. *Phytochemistry* 27:575–577.

91. Fang J-M, Hsu K-C, Cheng Y-S (1989) Lignans from leaves of *Calocedrus formosana*. *Phytochemistry* 28:3553–3555.

92. Issacs LT, Kan J, Nguyen L, Videau P, Anderson MA, Wright TL, Hill RT (2009) Comparison of the bacterial communities of wild and captive sponge *Clathria prolifera* from the Chesapeake bay. *Mar Biotechnol* 11:758–770.

93. Collin R, Diaz MC, Norenburg J, Rocha RM, Sanches JA, Schulze A, Schwartz M, Valdes A (2005) Photographic identification guide to some common marine invertebrates of Bocas Del Toro, Panama. *Caribb J Sci* 41:638–707.

94. Capon RJ, Miller M, Rooney F (2000) Clathrins A–C: metabolites from a southern Australian marine sponge, *Clathria* species. *J Nat Prod* 63:821–824.

95. Capon RJ, Miller M, Rooney F (2001) Mirabilin G: a new alkaloid from a southern Australian marine sponge, *Clathria* species. *J Nat Prod* 64:643–644.

96. Rudi A, Yosief T, Loya S, Hizi A, Schleyer M, Kashman Y (2001) Clathsterol, a novel anti-HIV-1 RT sulfated sterol from the sponge *Clathria* species. *J Nat Prod* 64:1451–1453.

97. Zuleta IA, Vitelli ML, Baggio R, Garland MT, Seldes AM, Palermo JA (2002) Novel pteridine alkaloids from the sponge *Clathria* sp. *Tetrahedron* 58:4481–4486.

98. Naggar ME, Conte M, Capon RJ (2010) Mirabilins revisited: polyketide alkaloids from a southern Australian marine sponge, *Clathria* sp. *Org Biomol Chem* 8:407–412.

99. Woo S-Y, Win NN, Wong CP, Ito T, Hoshino S, Ngwe H, Aye AA, Han NM, Zhang H, Hayashi F, Abe I, Morita H (2018) Two new pyrrolo-2-aminoimidazoles from a Myanmarese marine sponge, *Clathria prolifera*. *J Nat Med* 72:803–807.

100. Kobayashi J, Tsuda M, Murayama T, Nakamura H, Ohizumi Y, Ishibashi M, Iwamura M, Ohta T, Nozoe S (1990) Ageliferins, potent actomyosin Atpase activators from the Okinawan marine sponge *Agelas* sp. *Tetrahedron* 46:5579–5586.

101. Kobayashi J, Kanda F, Ishibashi M, Shigamori H (1991) Manzacidins A-C, Novel Tetrahydropyrimidine Alkaloids from the Okinawan marine sponge *Hymeniacidon* sp. *J Org Chem* 56:4574–4576.

102. Tsukamoto S, Tane K, Ohta T, Matsunaga S, Fusetani N, Soest RW (2001) Four new bioactive pyrrole-derived alkaloids from the marine sponge *Axinella brevistyla*. *J Nat Prod* 64:1576–1578.

103. Kosuke N, Tetsuro S, Toshiyuki T, Yasufumi O (2000) Total synthesis and absolute structure of manzacidin A and C. *J Am Chem Soc* 122:10708–10709.

104. Jahn T, König GM, Wright AD (1997) Manzacidin D: An unprecedented secondary metabolite from the "living fossil" sponge *Astrosclera willeyana*. *Tetrahedron Lett* 38:3883–3884.

105. Frisch MJ, Trucks GW, Schlegel HB, Scuseria GE, Robb MA, Cheeseman JR, Scalmani G, Barone V, Petersson GA, Nakatsuji H, Li X, Caricato M, Marenich A, Bloino J, Janesko BG, Gomperts R, Mennucci B, Hratchian HP, Ortiz JV, Izmaylov AF, Sonnenberg JL, Williams-Young D, Ding F, Lipparini F, Egidi F, Goings J, Peng B, Petrone A, Henderson T, Ranasinghe D, Zakrzewski VG, Gao J, Rega N, Zheng G, Liang W, Hada M, Ehara M, Toyota K, Fukuda R, Hasegawa J, Ishida M, Nakajima T, Honda Y, Kitao O, Nakai H, Vreven T, Throssell K, Montgomery JA, Jr Peralta JE, Ogliaro F, Bearpark M, Heyd JJ, Brothers E, Kudin KN, Staroverov VN, Keith T, Kobayashi R, Normand J, Raghavachari K, Rendell A, Burant JC, Iyengar SS, Tomasi J, Cossi M, Millam JM, Klene M, Adamo C, Cammi R, Ochterski JW, Martin RL, Morokuma K, Farkas O, Foresman JB, and Fox DJ (2016) Gaussian 09 Revision A. 02 Gaussian, Inc., Wallingford CT,.

List of publications

This doctoral thesis summarizes the full contents of the following publications.

1) Woo S-Y, Win NN, Wong CP, Ito T, Hoshino S, Ngwe H, Aye AA, Han NM, Zhang H, Hayashi F, Abe I, Morita H (2018) Two new pyrrolo-2-aminoimidazoles from a Myanmarese marine sponge, *Clathria prolifera*. ***J Nat Med*** 72:803–807.
2) Woo S-Y, Hoshino S, Wong CP, Win NN, Awouafack MD, Prema, Ngwe H, Zhang H, Hayashi F, Abe I, Morita H (2019) Lignans with melanogenesis effects from *Premna serratifolia* wood. ***Fitoterapia*** 133:35–42.
3) Woo S-Y, Wong CP, Win NN, Hoshino S, Prema, Ngwe H, Abe I, Morita H (2019) A new tetrahydrofuran type lignan from *Premna serratifolia* wood. ***Nat Prod Commun*** 14:113–116.

Acknowledgements

I would like to express my deepest and sincere gratitude to my supervisor Prof. Hiroyuki Morita, Division of Natural Products Chemistry, Institute of Natural Medicine, University of Toyama, Japan, for his valuable instruction, guidance, suggestion and encouragements on my research to achieve my PhD degree.

I am also greatly indebted to Assistant Prof. Chin Piow Wang, Division of Natural Products Chemistry, Institute of Natural Medicine, University of Toyama, Japan, for his valuable suggestions, support, and comments throughout this study.

I am highly grateful to former Associate Prof. Takuya Ito, Faculty of Pharmacy, Osaka Ohtani University, Japan, to and former Assistant Prof. Takashi Matsui for their guidance and kindness to my study.

I would like to express of my sincere gratitude to Prof. Kastuko Komatsu, Division of Pharmacognosy, Institute of Natural Medicine, University of Toyama, Japan, and associate Associate Prof. Suresh Awale, Division of Natural Drug Discovery, Institute of Natural Medicine, University of Toyama, Japan, for their comments, suggestions and evaluating my thesis.

I am also greatly indebted to Prof. Ikuro Abe and Mr. Shotaro Hoshino, Laboratory of Natural Products Chemistry, Graduate School of the Faculty of Pharmaceutical Sciences, The University of Tokyo, Japan, for the assistance in the analyses of NMR and CD calculation and thoughtful suggestions on discussion.

I would like to thanks to express my thanks to Dr. Huipin Zhang and Dr. Fumiki Hayashi, RIKEN Spring-8 Center, Japan, for the help to measure NMR.

I would like to thanks to Dr. Hla Ngwe (Prof., retired University of Yangon, Myanmar), Dr. Nang Mya Han (Prof., retired Myeik University, Myanmar) and Mr.

Aung Aung Aye, Department of Marine Sciences, Myeik University, Myanmar for sample collection.

I extend my heartfelt thanks to all members in Division of Natural Products Chemistry for the support and friendship during my study in the University of Toyama, Japan.

I would like to acknowledge my sincere thanks to Ostuka foundation for the scholarship grant and financial support.

Finally, I am greatly indebted to my family for their love, understanding, support, and encouragement throughout the whole of my life.

Soyeun Woo

Toyama, Japan

Supplementary data

List of Supporting Information

Figure S1. ^{1}H NMR spectrum (500 MHz) of **1** in $CDCl_3$

Figure S2. ^{13}C NMR spectrum (125 MHz) of **1** in $CDCl_3$

Figure S3. HMQC spectrum of **1** in $CDCl_3$

Figure S4. HMBC spectrum of **1** in $CDCl_3$

Figure S5. ^{1}H-^{1}H COSY spectrum of **1** in $CDCl_3$

Figure S6. NOESY spectrum of **1** in $CDCl_3$

Figure S7. Experimental ECD spectra of **1** and vitexdoin A

Figure S8. HRESIMS spectrum of **1**

Figure S9. IR spectrum of **1**

Figure S10. ^{1}H NMR spectrum (600 MHz) of **2** in $CDCl_3$

Figure S11. ^{13}C NMR spectrum (150 MHz) of **2** in $CDCl_3$

Figure S12. HMQC spectrum of **2** in $CDCl_3$

Figure S13. HMBC spectrum of **2** in $CDCl_3$

Figure S14. ^{1}H-^{1}H COSY spectrum of **2** in $CDCl_3$

Figure S15. NOESY spectrum of **2** in $CDCl_3$

Figure S16. ECD spectra of **2**

Figure S17. Low-energy conformers of **2** optimized by DFT method at B3LYP/6-31G(d) level with PCM in MeOH (**2A-2C**), and the calculated ECD spectrum of **2A-2C** by TDDFT method at B3LYP/6-31G(d) level with PCM in MeOH.

Figure S18. HRESIMS spectrum of **2**

Figure S19. IR spectrum of **2**

Figure S20. HMQC spectrum of **3** in $CDCl_3$

Figure S21. ^{1}H NMR spectrum (500 MHz) of **3** in $CDCl_3$

Figure S22. ^{13}C NMR spectrum (125 MHz) of **3** in $CDCl_3$

Figure S23. HMBC spectrum of **3** in $CDCl_3$

Figure S24. ^{1}H-^{1}H COSY spectrum of **3** in $CDCl_3$

Figure S25. NOESY spectrum of **3** in $CDCl_3$

Figure S26. Experimental and calculated ECD spectra of **3**

Figure S27. Low-energy conformers of **3** optimized by DFT method at B3LYP/6-31G(d) level with PCM in MeOH (**3A-3F**) and the calculated ECD spectrum of **3A-3F** by TDDFT method at B3LYP/6-31G(d) level with PCM in MeOH.

Figure S28. HRESIMS spectrum of **3**

Figure S29. IR spectrum of **3**

Figure S30. ^{1}H NMR spectrum (500 MHz) of **4** in DMSO-d_6

Figure S31. ^{13}C NMR spectrum (125 MHz) of **4** in DMSO-d_6

Figure S32. HMQC spectrum of **4** in DMSO-d_6

Figure S33. HMBC spectrum of **4** in DMSO-d_6

Figure S34. ^{1}H-^{1}H COSY spectrum of **4** in DMSO-d_6

Figure S35. NOESY spectrum of **4** in DMSO-d_6

Figure S36. HRESIMS spectrum of **4**

Figure S37. IR spectrum of **4**

Figure S38. ^{1}H NMR spectrum (500 MHz) of **5** in $CDCl_3$

Figure S39. ^{13}C NMR spectrum (125 MHz) of **5** in $CDCl_3$

Figure S40. HMQC spectrum of **5** in $CDCl_3$

Figure S41. HMBC spectrum of **5** in $CDCl_3$

Figure S42. ^{1}H-^{1}H COSY spectrum of **5** in $CDCl_3$

Figure S43. NOESY spectrum of **5** in $CDCl_3$

Figure S44. Experimental and calculated ECD spectra of **5**

Figure S45. Low-energy conformers of **5** optimized by DFT method at B3LYP/6-31G(d) level with PCM in MeOH (**5A-5D**) and the calculated ECD spectrum of **5A-5D** by TDDFT method at B3LYP/6-31G(d) level with PCM in MeOH.

Figure S46. HRESIMS spectrum of **5**

Figure S47. IR spectrum of **5**

Figure S48. ^{1}H NMR spectrum (500 MHz) of **21** in CD_3OD

Figure S49. ^{13}C NMR spectrum (125 MHz) of **21** in CD_3OD

Figure S50. HMQC spectrum of **21** in CD_3OD

Figure S51. HMBC spectrum of **21** in CD_3OD

Figure S52. ^{1}H-^{1}H COSY spectrum of **21** in CD_3OD

Figure S53. NOESY spectrum of **21** in CD_3OD

Figure S54. ^{1}H NMR spectrum (500 MHz) of **21** in DMSO-d_6

Figure S55. ^{13}C NMR spectrum (125 MHz) of **21** in DMSO-d_6

Figure S56. HMQC spectrum of **21** in DMSO-d_6

Figure S57. HMBC spectrum of **21** in DMSO-d_6

Figure S58. ^{1}H-^{1}H COSY spectrum of **21** in DMSO-d_6

Figure S59. NOESY spectrum of **21** in DMSO-d_6

Figure S60. Experimental and calculated ECD spectra of **21**

Figure S61. HRESIMS spectrum of **21**

Figure S62. IR spectrum of **21**

Figure S63. ^{1}H NMR spectrum (900 MHz) of **22** in CD_3OD

Figure S64. ^{13}C NMR spectrum (225 MHz) of **22** in CD_3O

Figure S65. HMQC spectrum of **22** in CD_3OD

Figure S66. HMBC spectrum of **22** in CD_3OD

Figure S67. ^{1}H-^{1}H COSY spectrum of **22** in CD_3OD

Figure S68. NOESY spectrum of **22** in CD_3OD

Figure S69. HRESIMS spectrum of **22**

Figure S70. IR spectrum of **22**

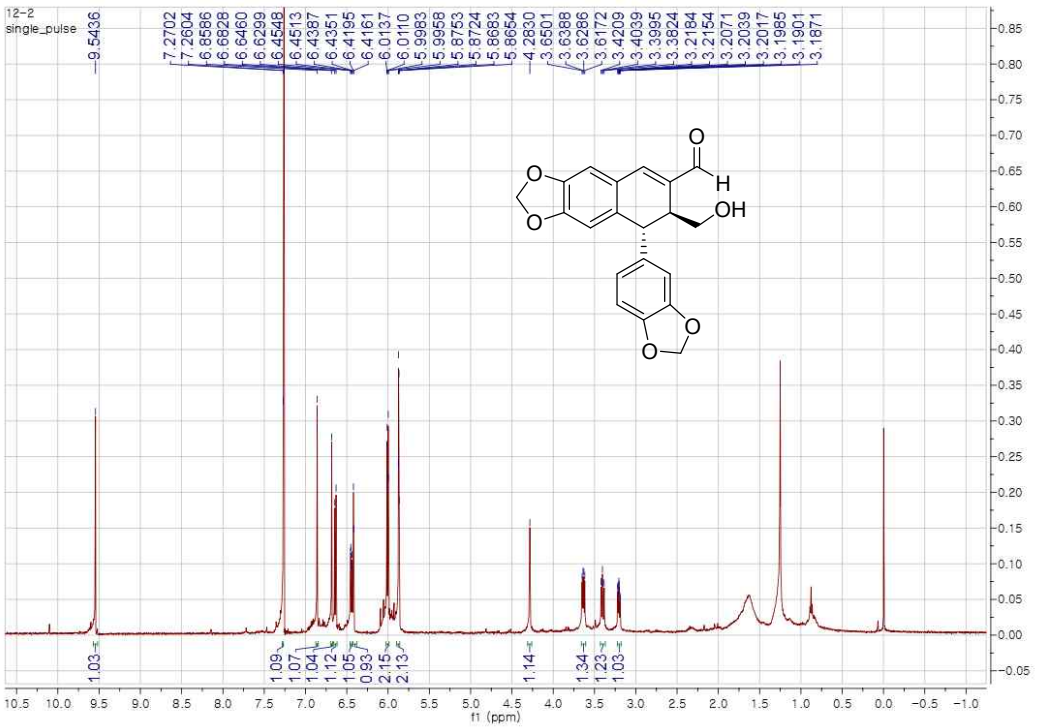


Figure S1. ^{1}H NMR spectrum (500 MHz) of **1** in $CDCl_3$

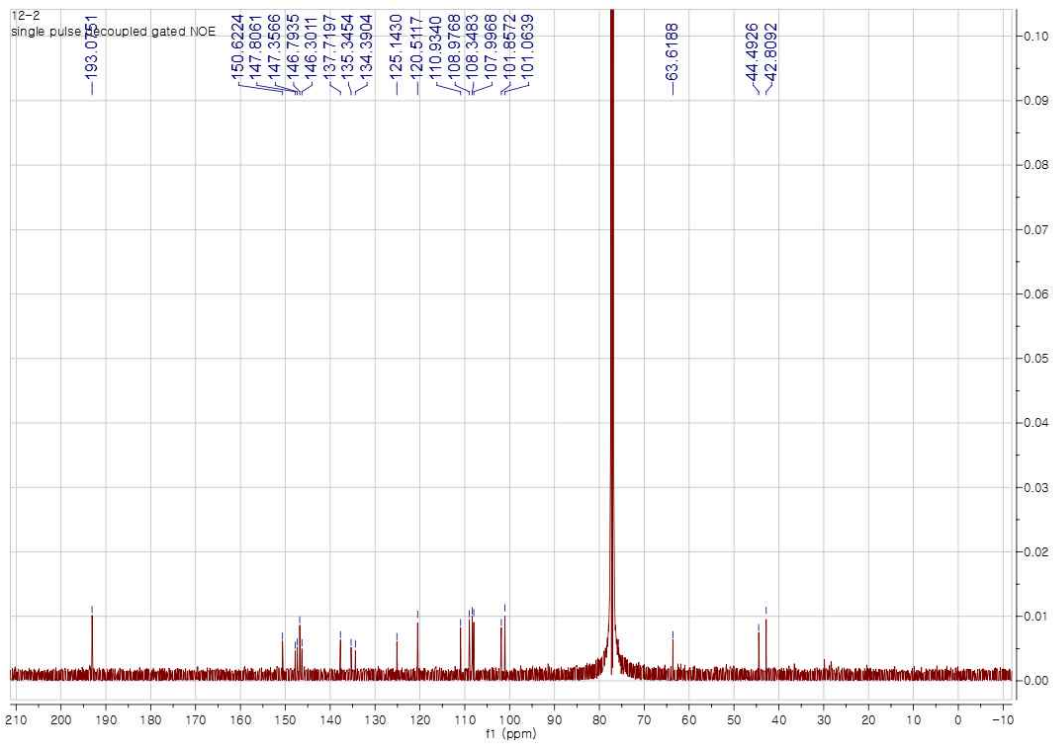


Figure S2. ^{13}C NMR spectrum (125 MHz) of **1** in $CDCl_3$

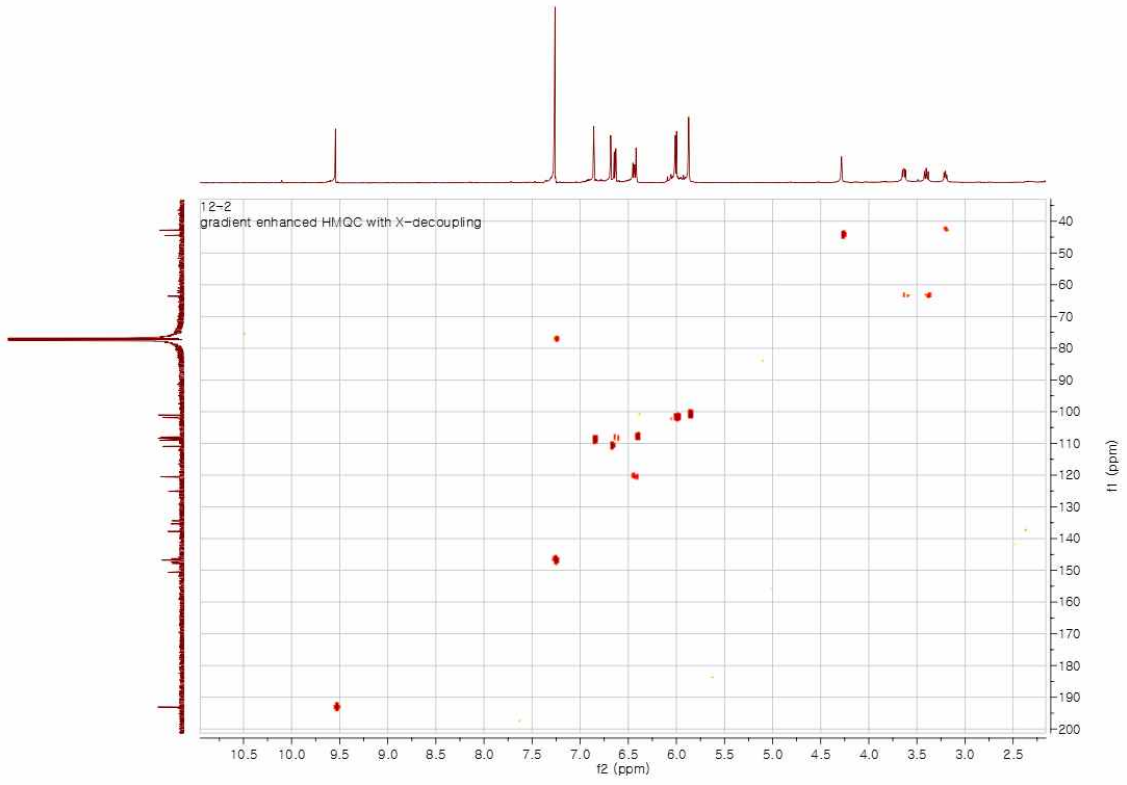


Figure S3. HMQC spectrum of **1** in $CDCl_3$

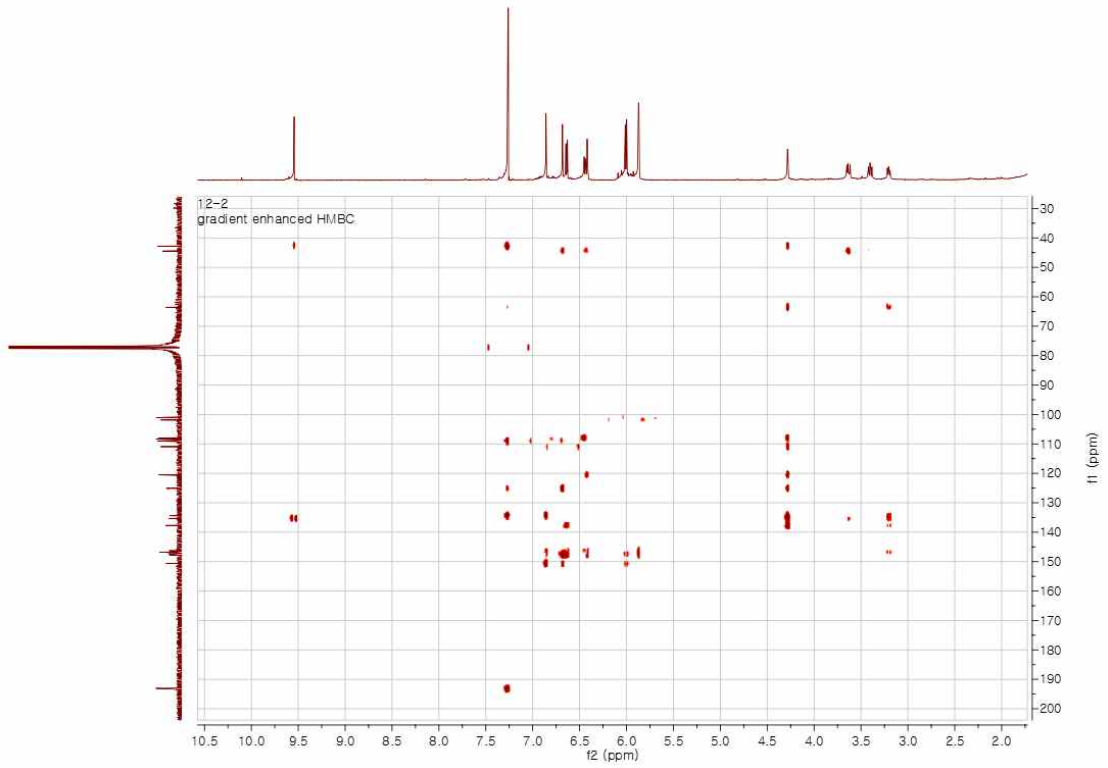


Figure S4. HMBC spectrum of **1** in $CDCl_3$

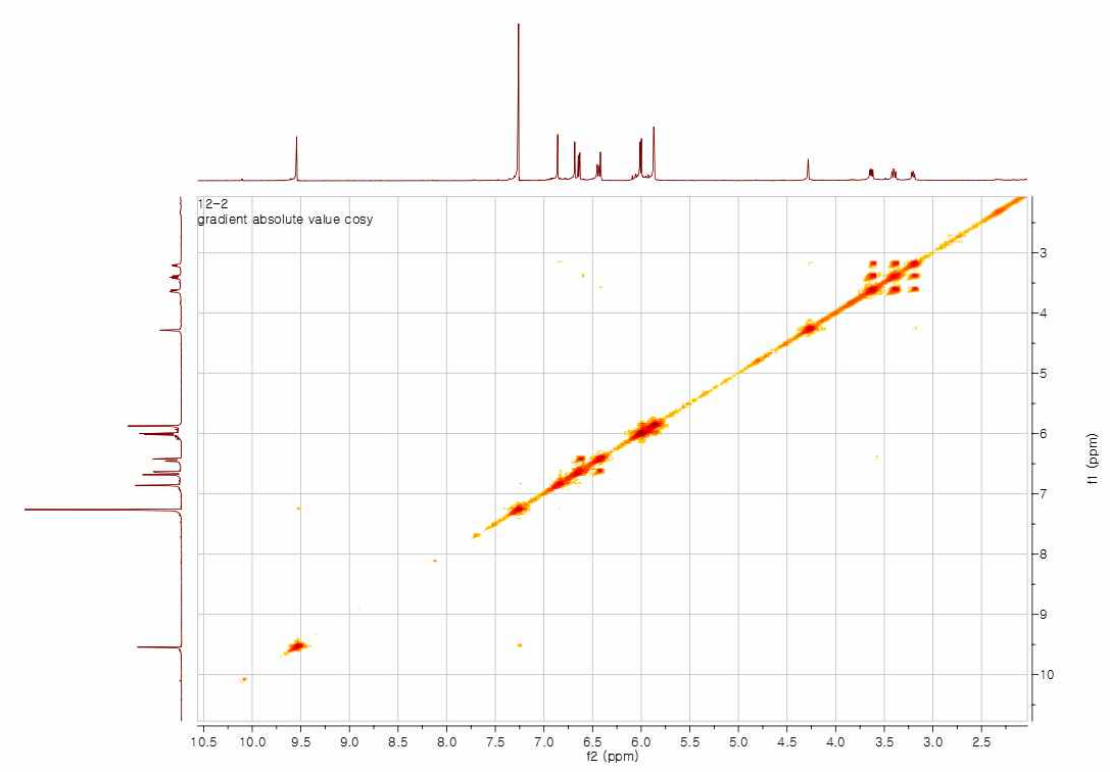


Figure S5. ^{1}H-^{1}H COSY spectrum of **1** in $CDCl_3$

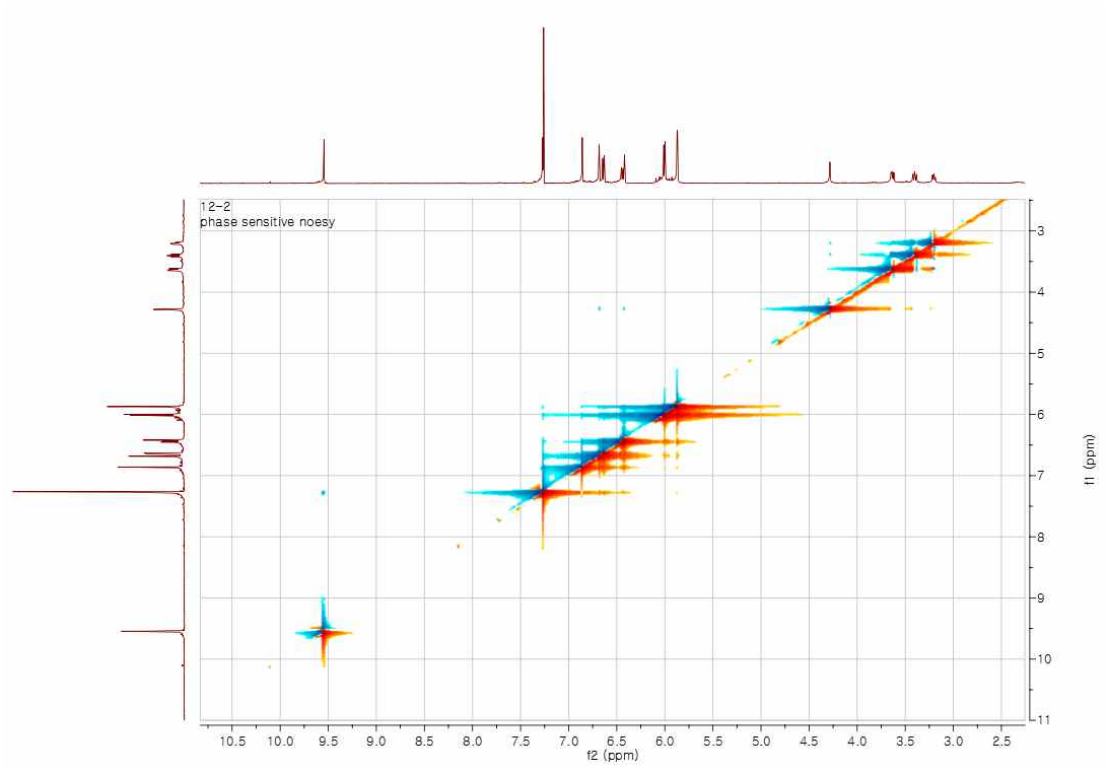


Figure S6. NOESY spectrum of **1** in $CDCl_3$

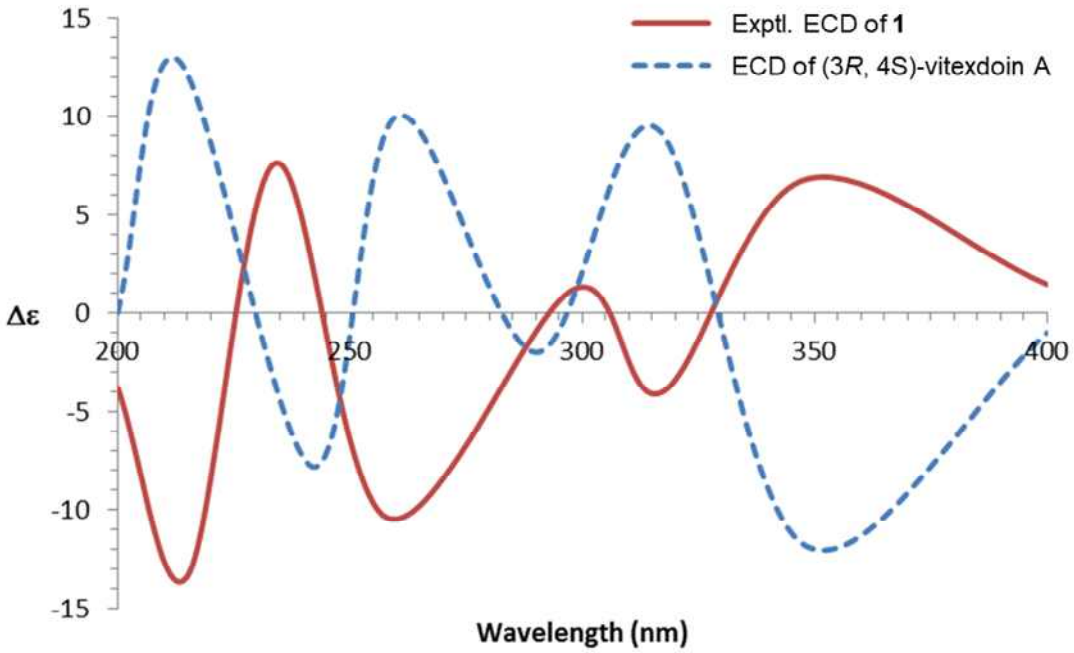
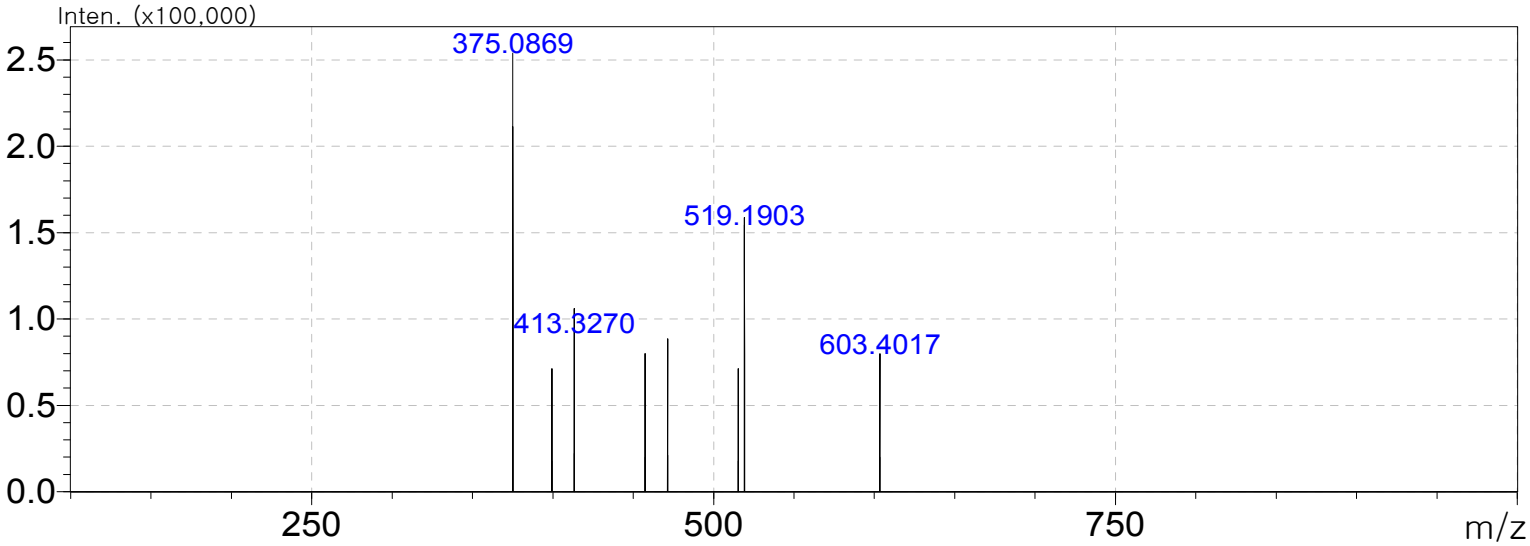
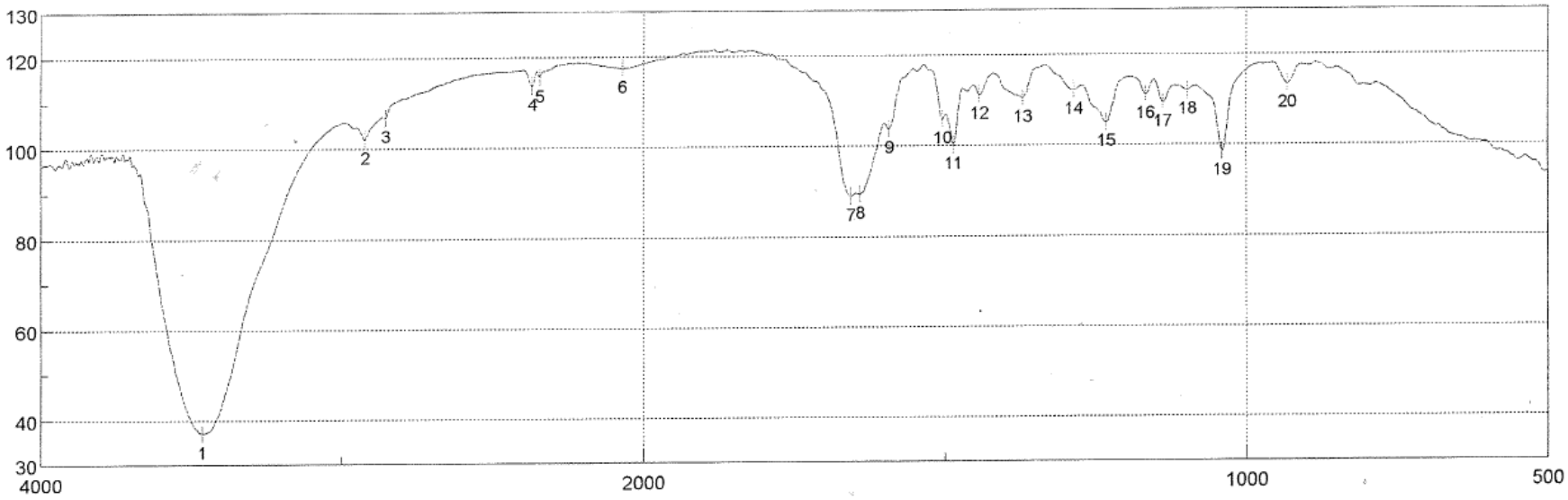


Figure S7. Experimental ECD spectra of **1** and vitexdoin A



#	Mass	Diff (mDa)	Formula	DBE
1	352.0947	3.0	C_{20} H_{16} O_6	13.0

Figure S8. HRESIMS spectrum of **1**



No.	cm-1	%T	No.	cm-1	%T	No.	cm-1	%T	No.	cm-1	%T	No.	cm-1	%T
1	3463	37.00	2	2923	102.03	3	2854	106.79	4	2369	113.78	5	2343	115.63
6	2071	117.51	7	1656	88.94	8	1640	89.38	9	1592	103.82	10	1503	105.85
11	1485	100.22	12	1442	111.36	13	1370	110.54	14	1286	112.24	15	1231	105.04
16	1167	111.20	17	1138	109.45	18	1097	112.20	19	1039	98.56	20	931	113.48

Figure S9. IR spectrum of **1**

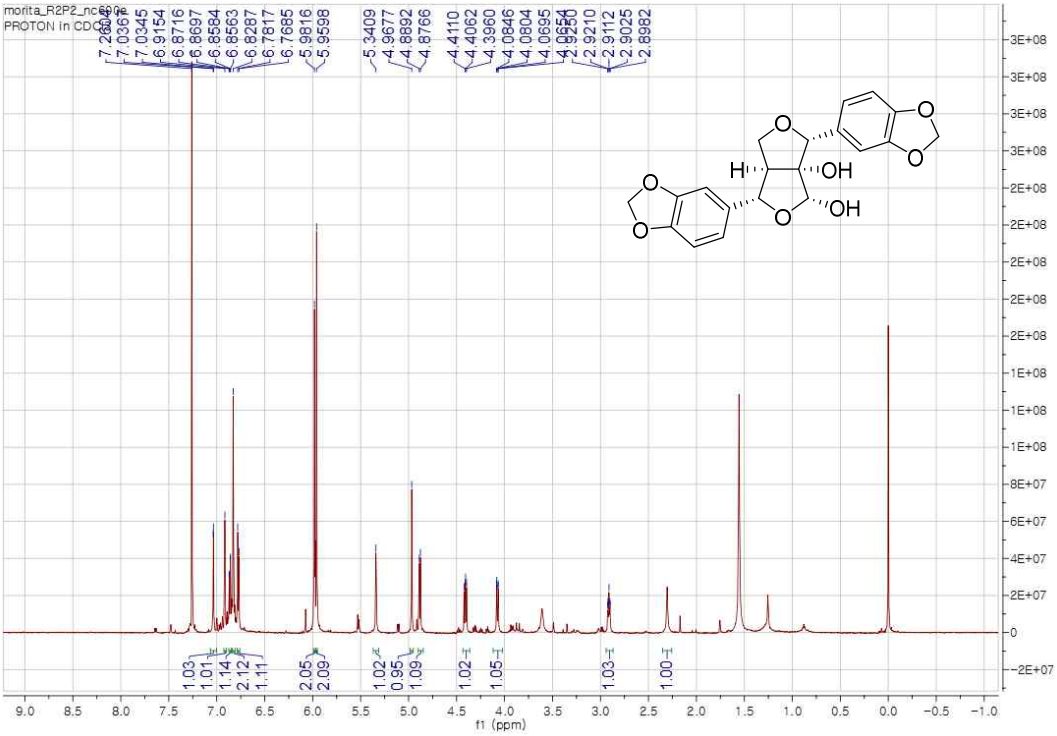


Figure S10. ^{1}H NMR spectrum (600 MHz) of **2** in $CDCl_3$

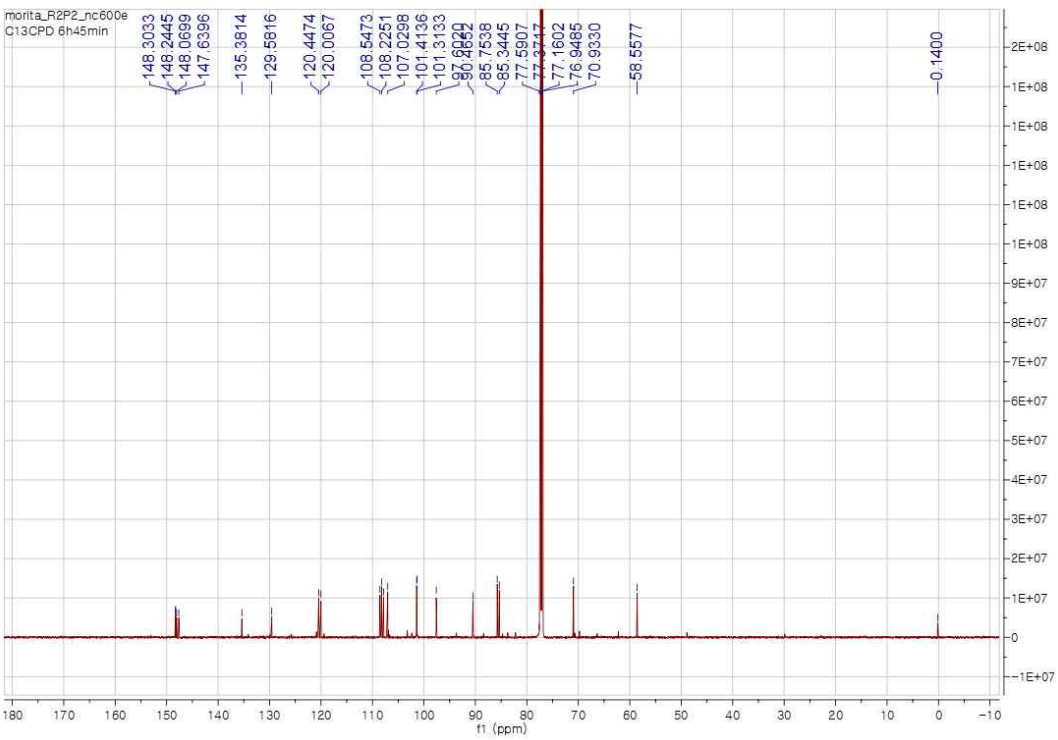


Figure S11. ^{13}C NMR spectrum (150 MHz) of **2** in $CDCl_3$

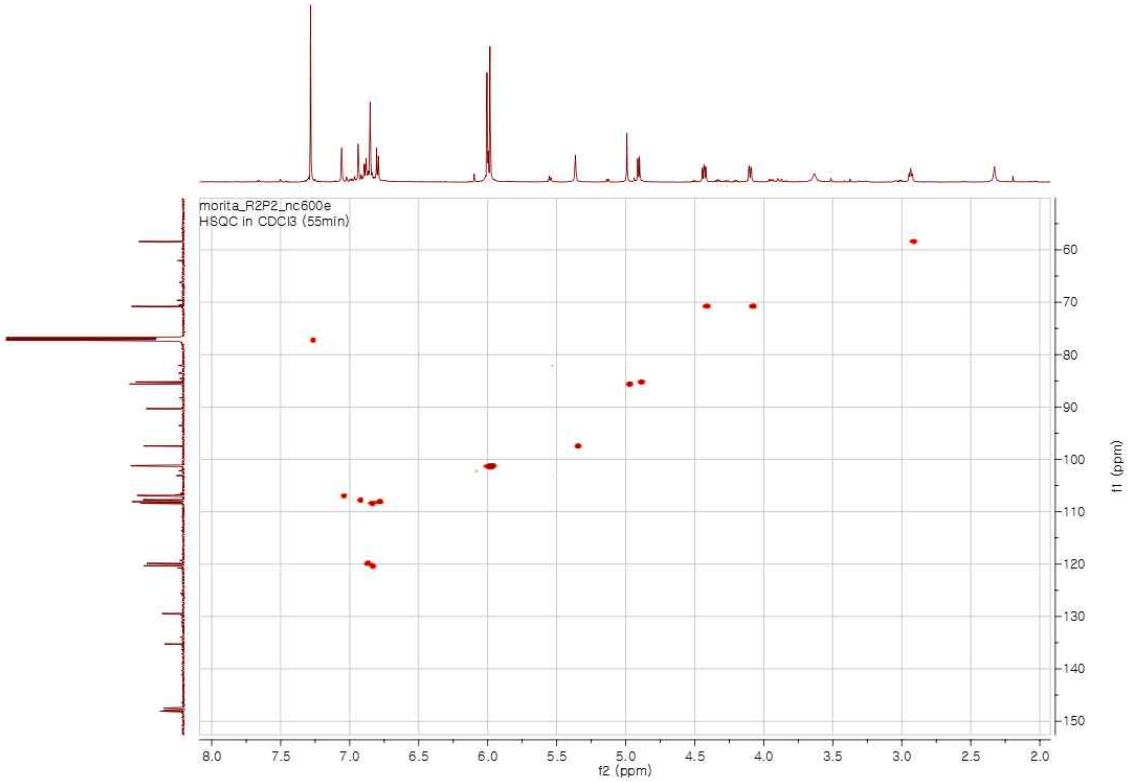


Figure S12. HMQC spectrum of **2** in $CDCl_3$

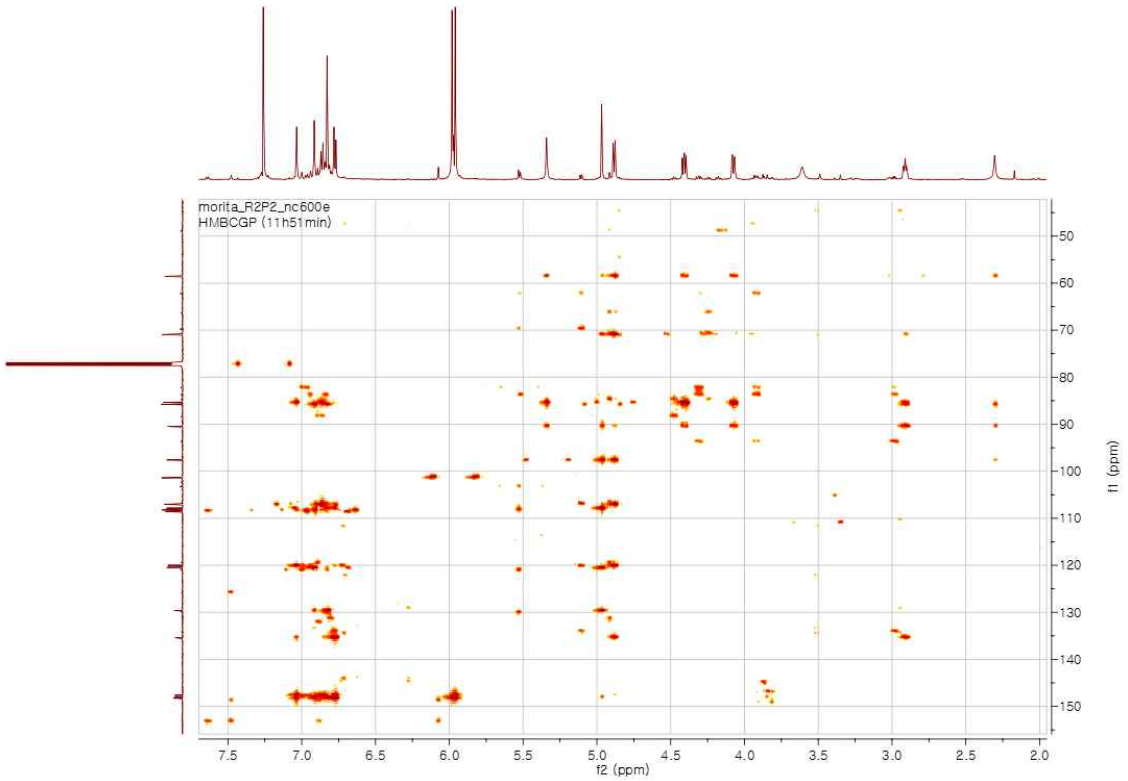


Figure S13. HMBC spectrum of **2** in $CDCl_3$

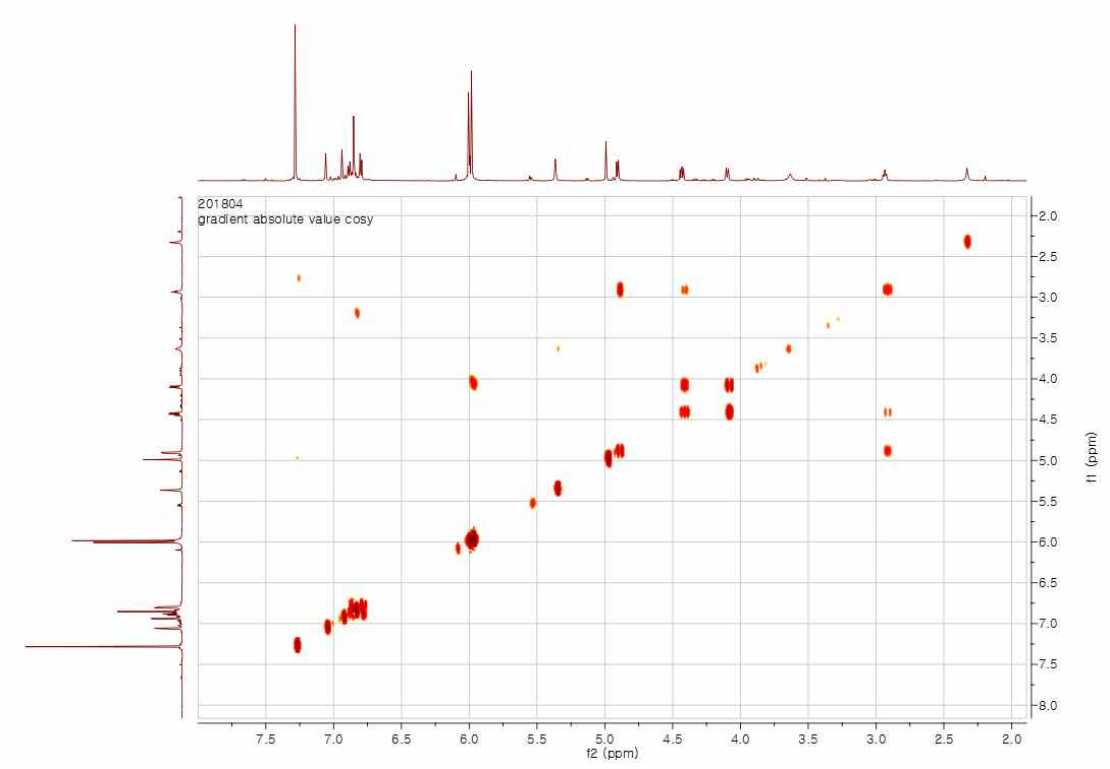


Figure S14. ^{1}H-^{1}H COSY spectrum of **2** in $CDCl_3$

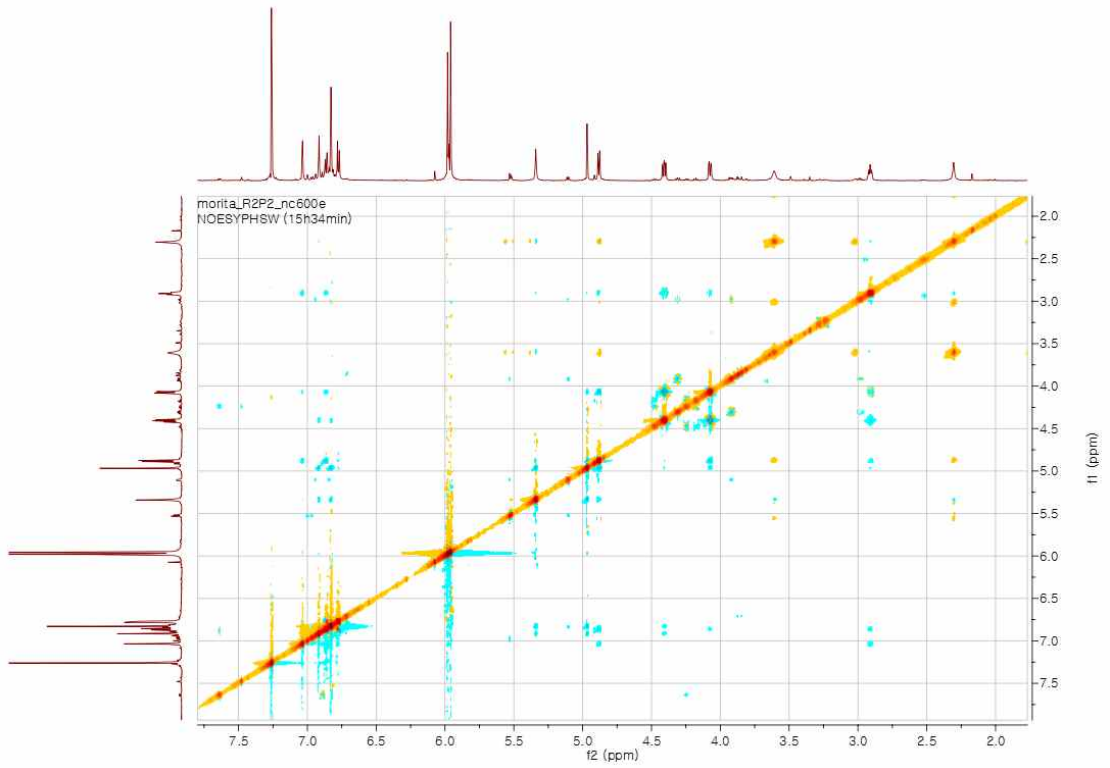


Figure S15. NOESY spectrum of **2** in $CDCl_3$

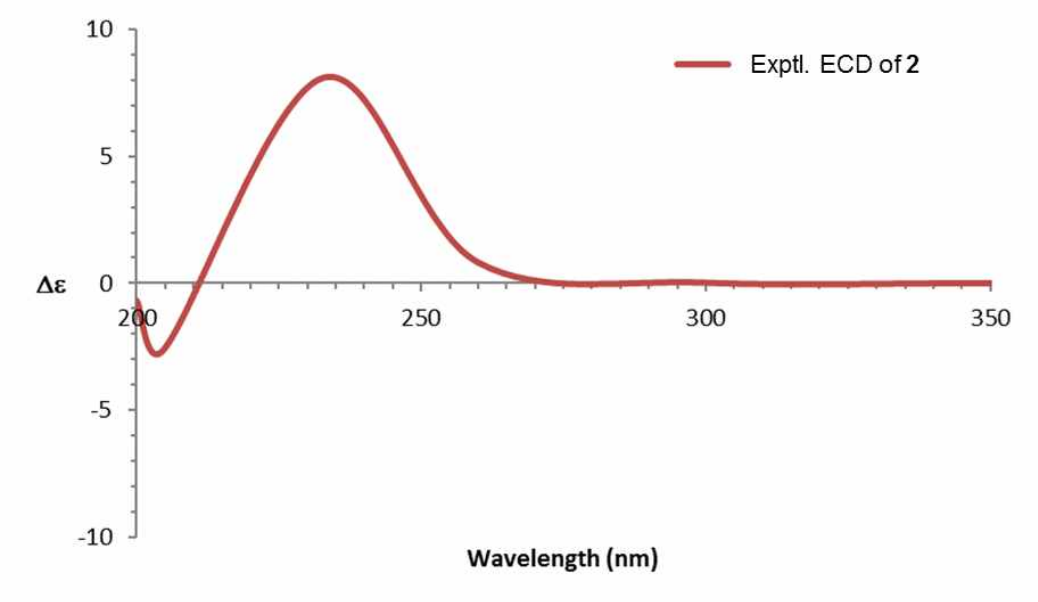
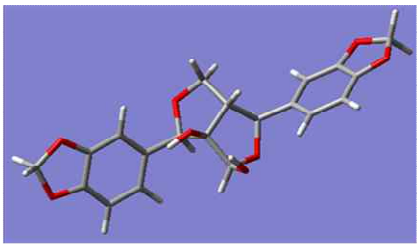
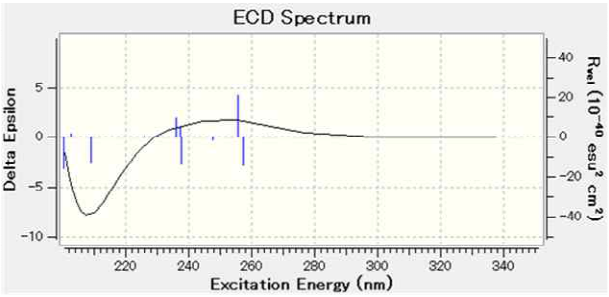
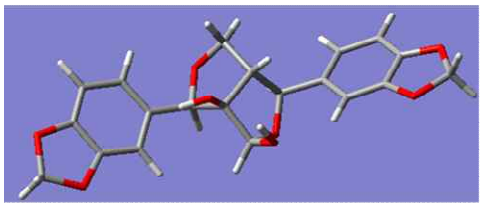


Figure S16. ECD spectra of **2**

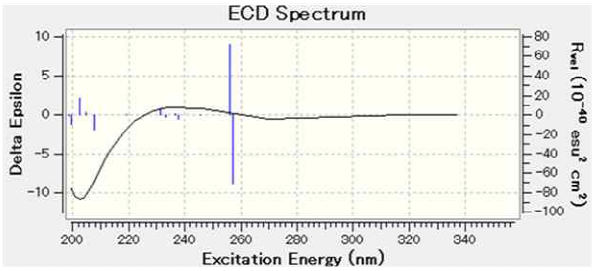


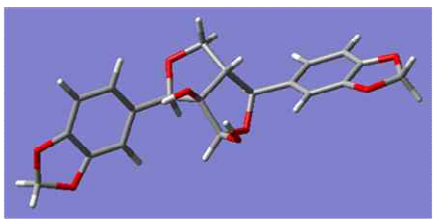
2-A (72.1%, ΔG = 0.00 kJ/mol)





2-B (7.7%, ΔG = 5.55 kJ/mol)





2-C (7.4%, ΔG = 5.63 kJ/mol)

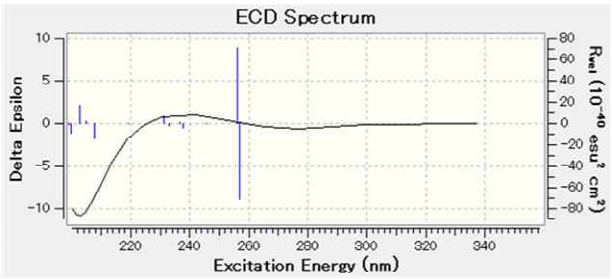
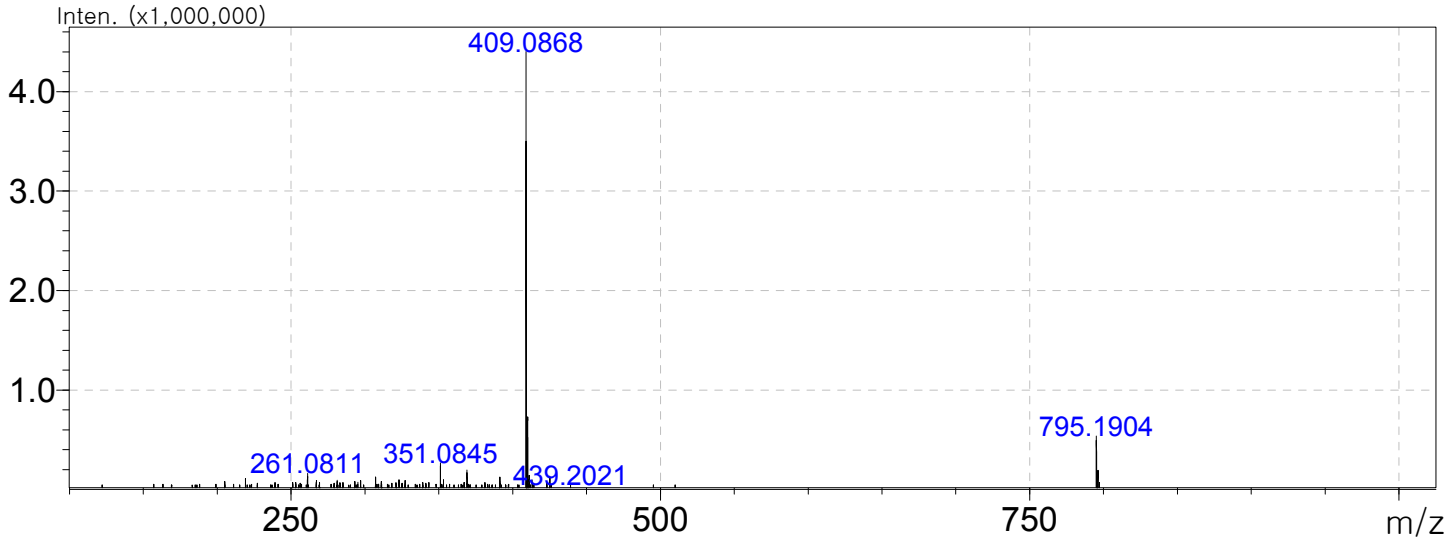
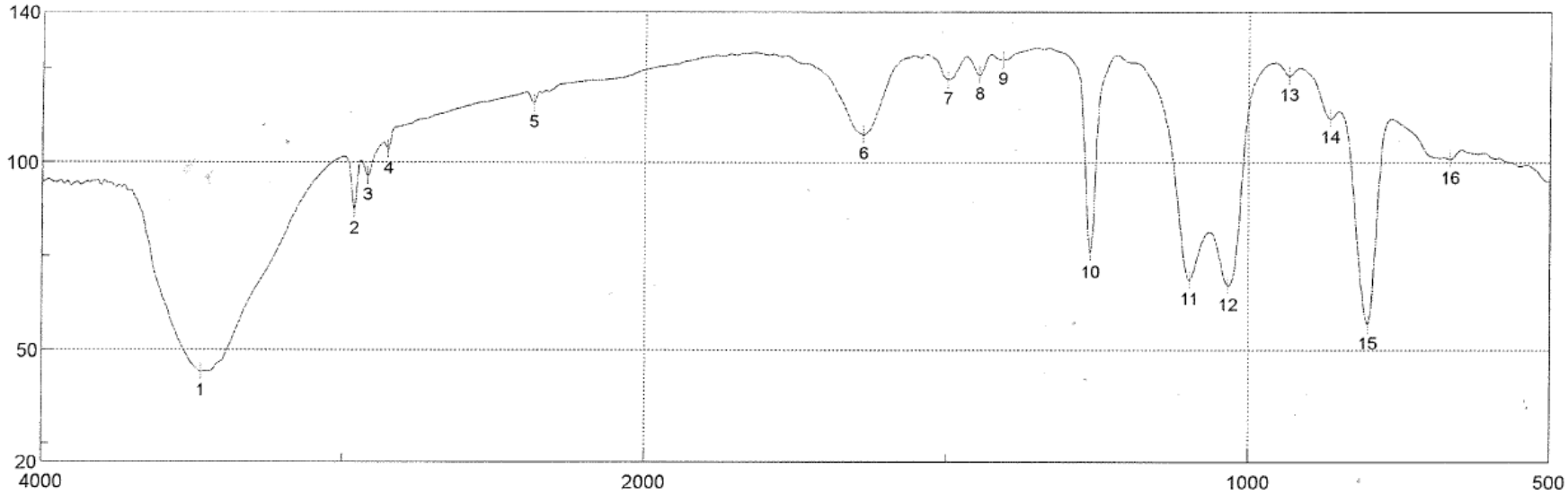


Figure S17. Low-energy conformers of **2** optimized by DFT method at B3LYP/6-31G(d) level with PCM in MeOH (**2A-2C**), and the calculated ECD spectrum of **2A-2C** by TDDFT method at B3LYP/6-31G(d) level with PCM in MeOH. The abundance ratio of each conformer was determined based on the thermal free energies obtained by the frequency calculation at the same level. In this figure, we only showed the result of one side of enantiomer (1*R*, 2*R*, 5*R*, 6*S*, 8*R*).



#	Mass	Diff (mDa)	Formula	DBE
1	386.1002	2.6	C_{20} H_{18} O_8	12.0

Figure S18. HRESIMS spectrum of **2**



No.	cm-1	%T	No.	cm-1	%T	No.	cm-1	%T	No.	cm-1	%T	No.	cm-1	%T
1	3470	44.19	2	2964	87.50	3	2920	96.43	4	2853	103.50	5	2371	115.88
6	1638	107.43	7	1498	122.14	8	1446	123.32	9	1408	127.43	10	1261	75.88
11	1097	68.78	12	1033	67.30	13	933	123.14	14	865	111.82	15	803	56.98
16	666	101.04												

Figure S19. IR spectrum of **2**

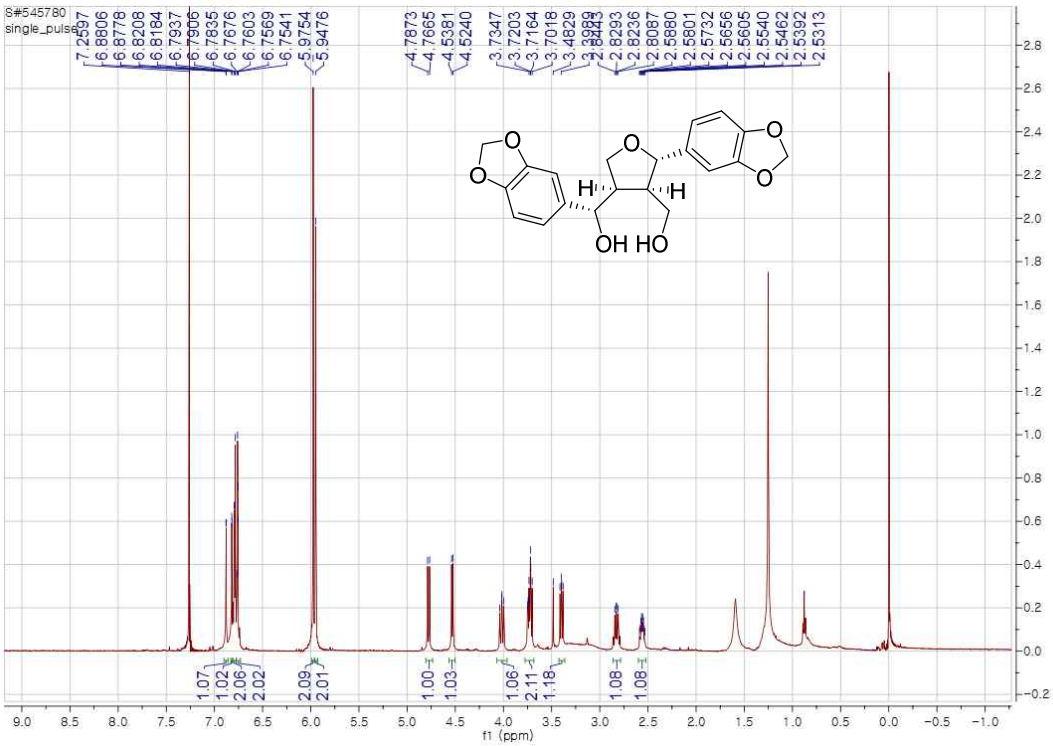


Figure S20. ^{1}H NMR spectrum (500 MHz) of **3** in $CDCl_3$

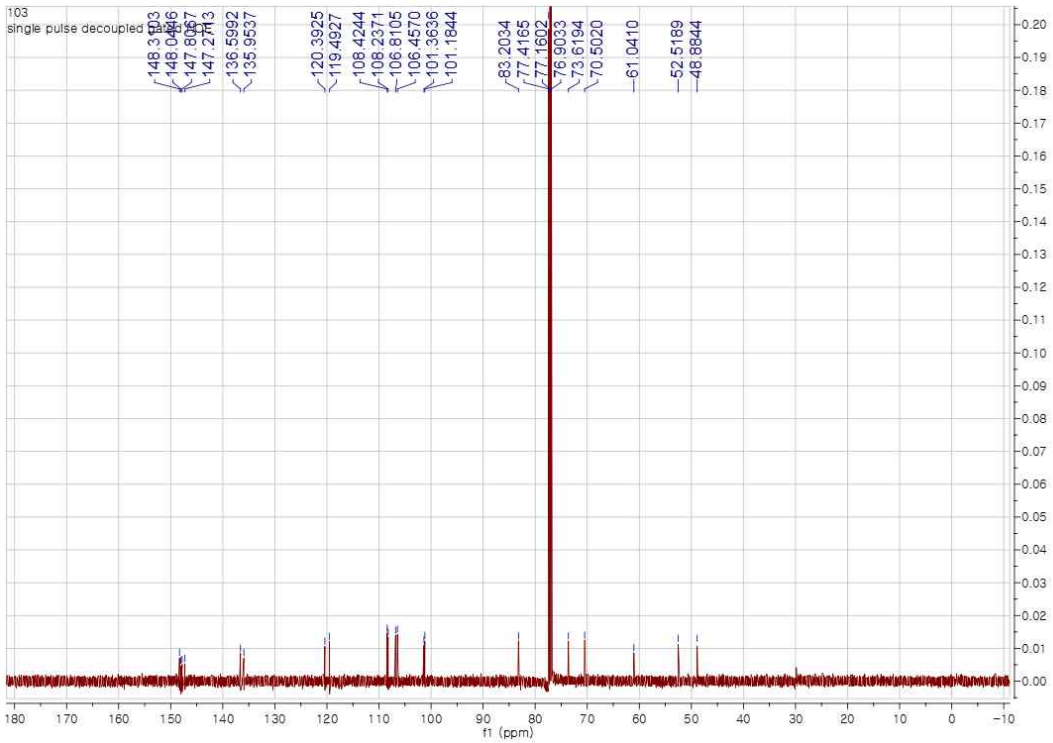


Figure S21. ^{13}C NMR spectrum (125 MHz) of **3** in $CDCl_3$

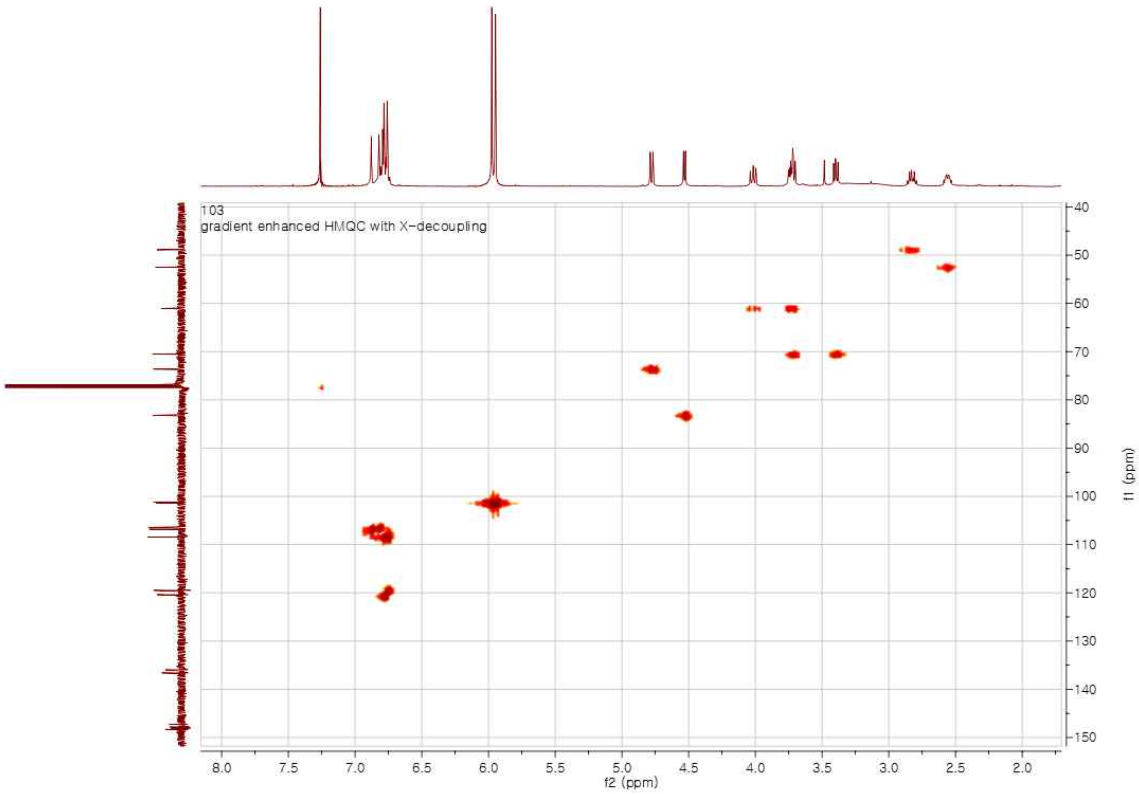


Figure S22. HMQC spectrum of **3** in $CDCl_3$

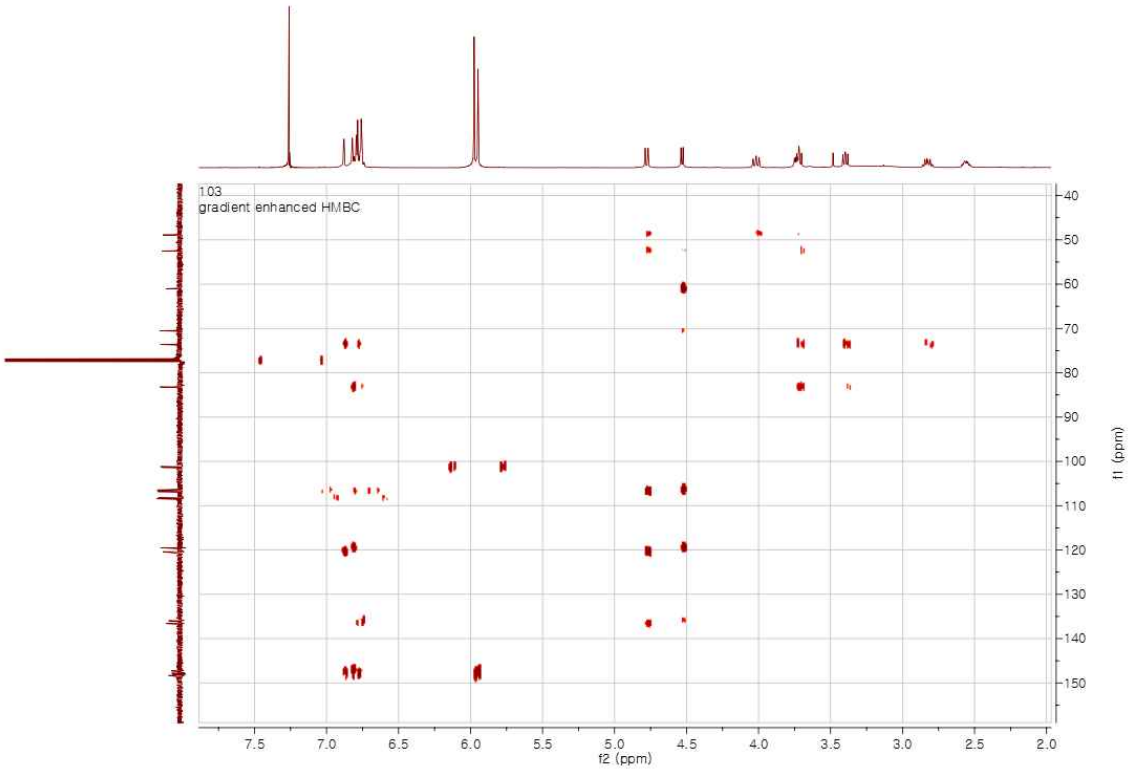


Figure S23. HMBC spectrum of **3** in $CDCl_3$

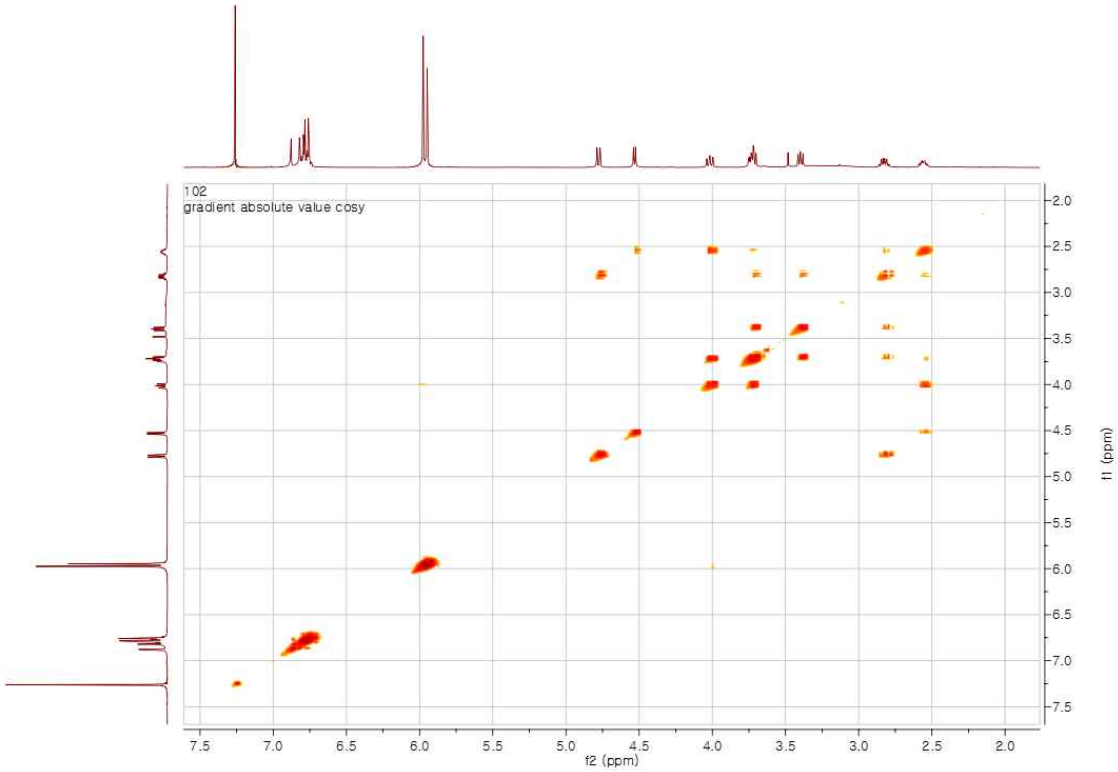


Figure S24. ^{1}H-^{1}H COSY spectrum of **3** in $CDCl_3$

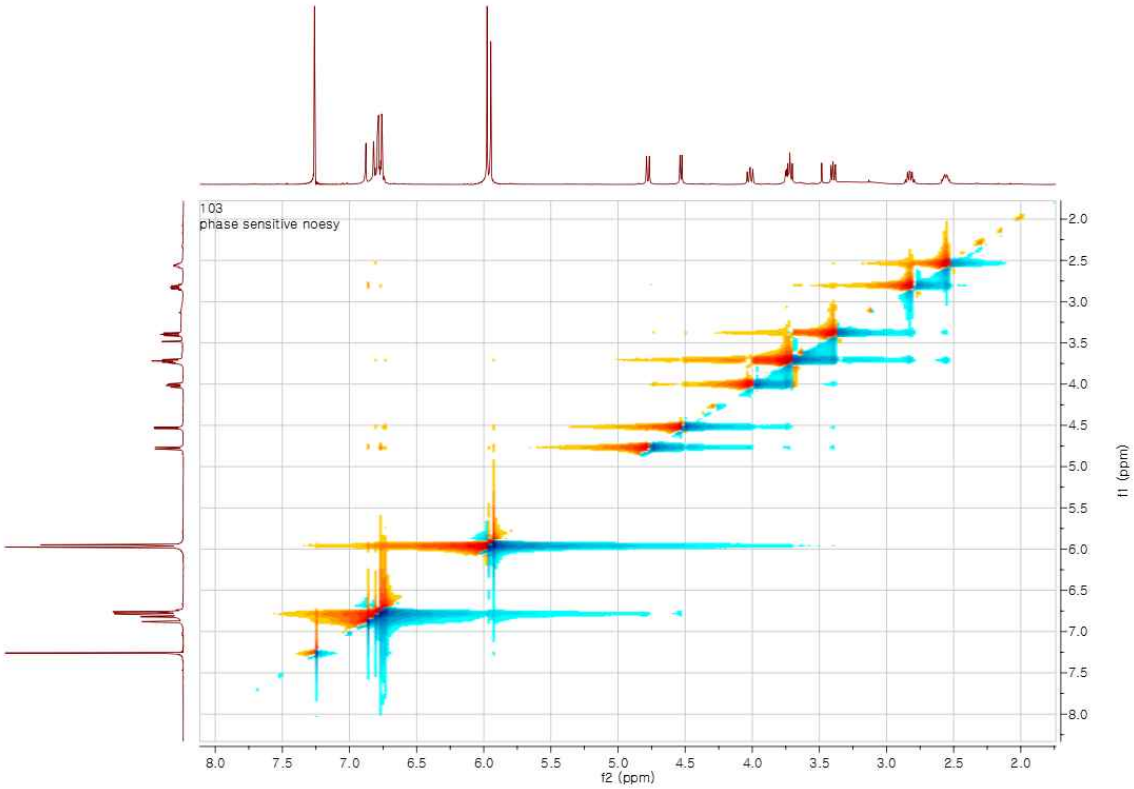


Figure S25. NOESY spectrum of **3** in $CDCl_3$

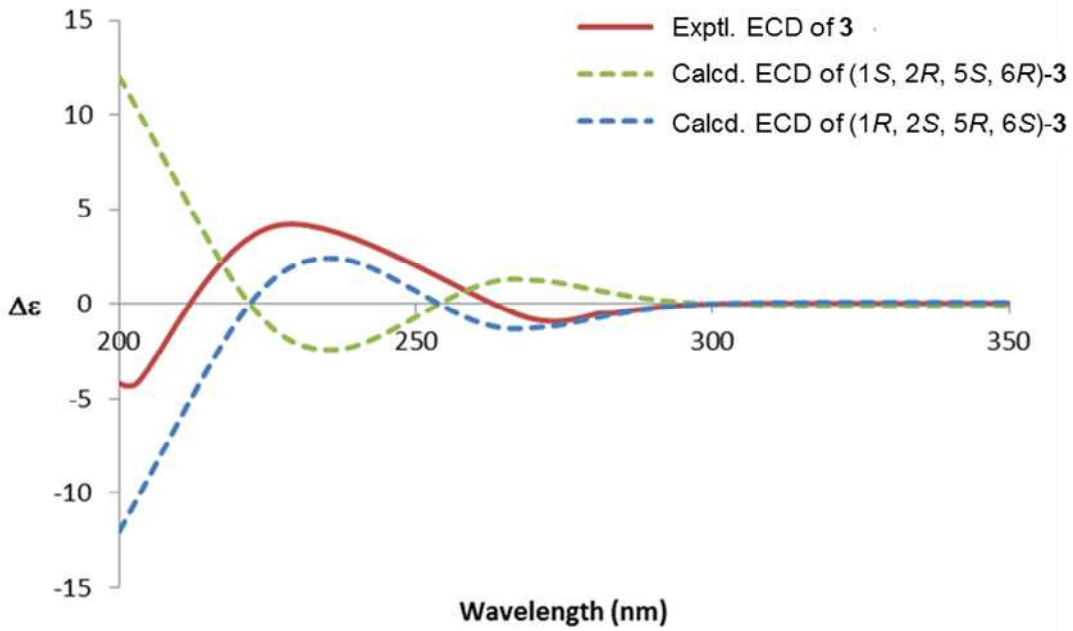


Figure S26. Experimental and calculated ECD spectra of **3**

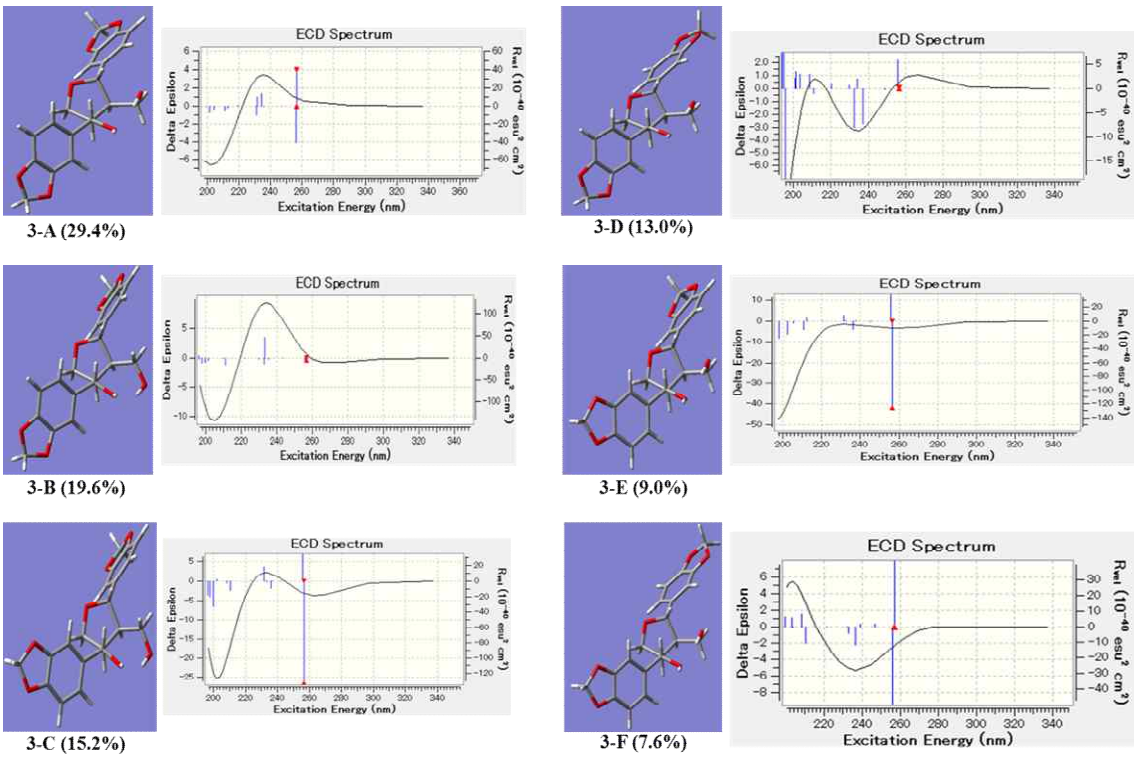
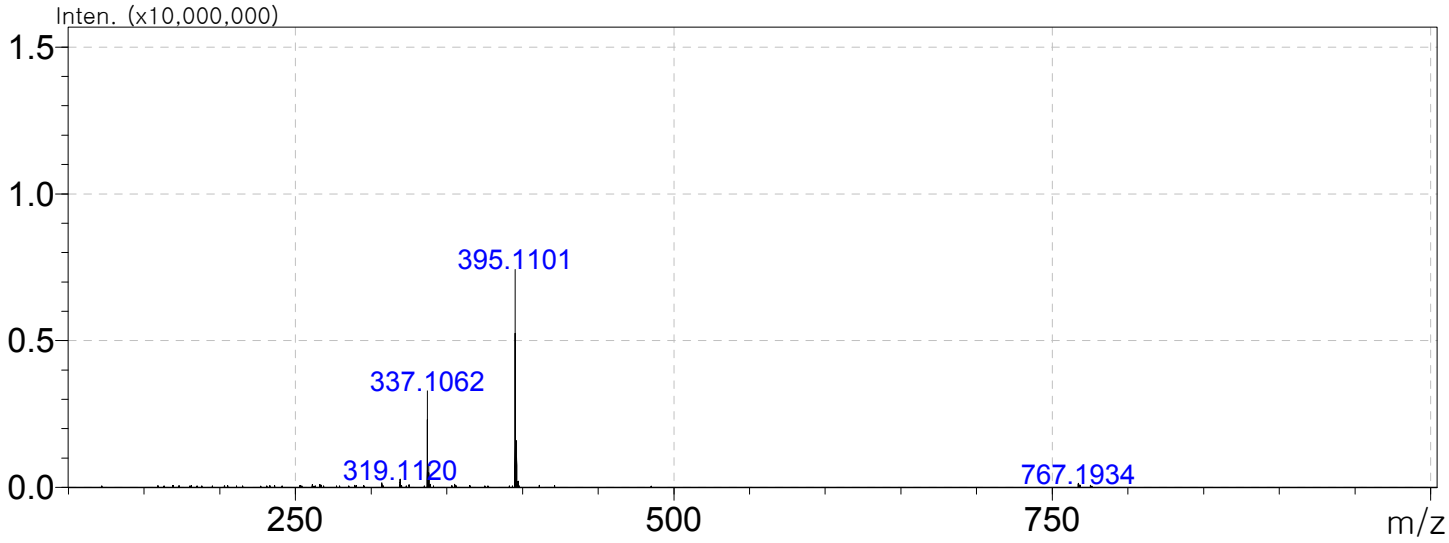
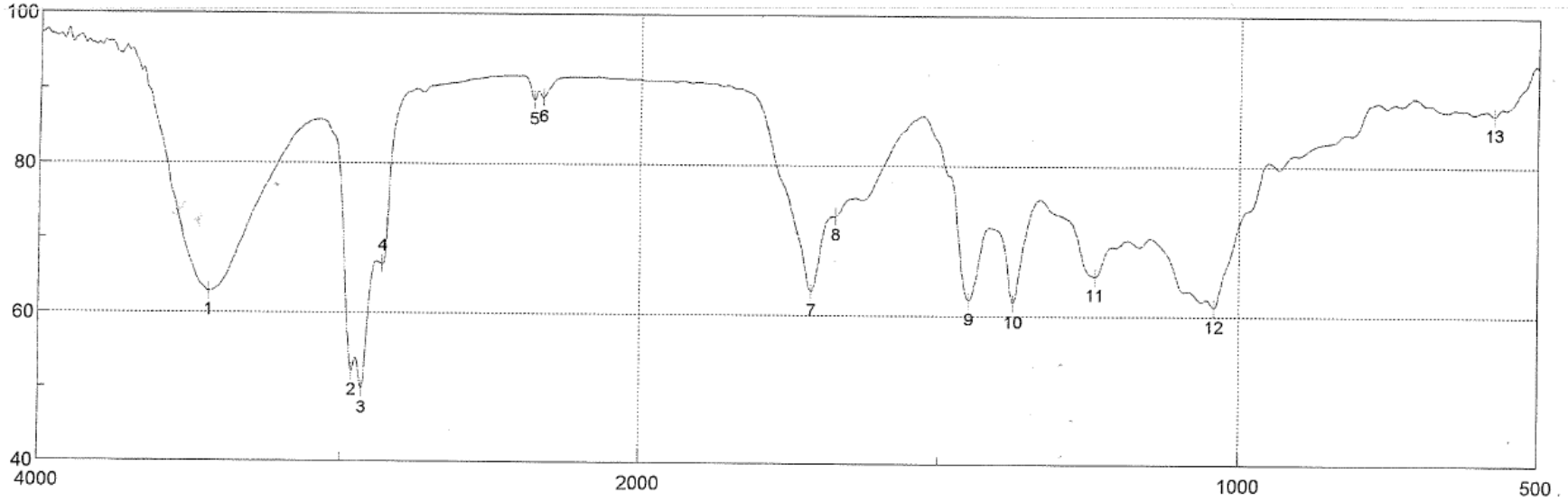


Figure S27. Low-energy conformers of **3** optimized by DFT method at B3LYP/6-31G(d) level with PCM in MeOH (**3A-3F**) and the calculated ECD spectrum of **3A-3F** by TDDFT method at B3LYP/6-31G(d) level with PCM in MeOH. The abundance ratio of each conformer was determined based on the thermal free energies obtained by the frequency calculation at the same level. In this figure, we only showed the result of one side of enantiomer (1*R*, 2*S*, 5*R*, 6*S*).



#	Mass	Diff (mDa)	Formula	DBE
1	372.1209	0.0	C_{20} H_{20} O_7	11.0

Figure S28. HRESIMS spectrum of **3**



No.	cm-1	%T	No.	cm-1	%T	No.	cm-1	%T	No.	cm-1	%T	No.	cm-1	%T
1	3436	62.81	2	2964	52.16	3	2931	49.74	4	2865	66.60	5	2359	88.52
6	2328	88.85	7	1713	63.14	8	1673	73.27	9	1450	62.07	10	1377	61.71
11	1241	65.33	12	1041	61.17	13	574	87.00						

Figure S29. IR spectrum of **3**

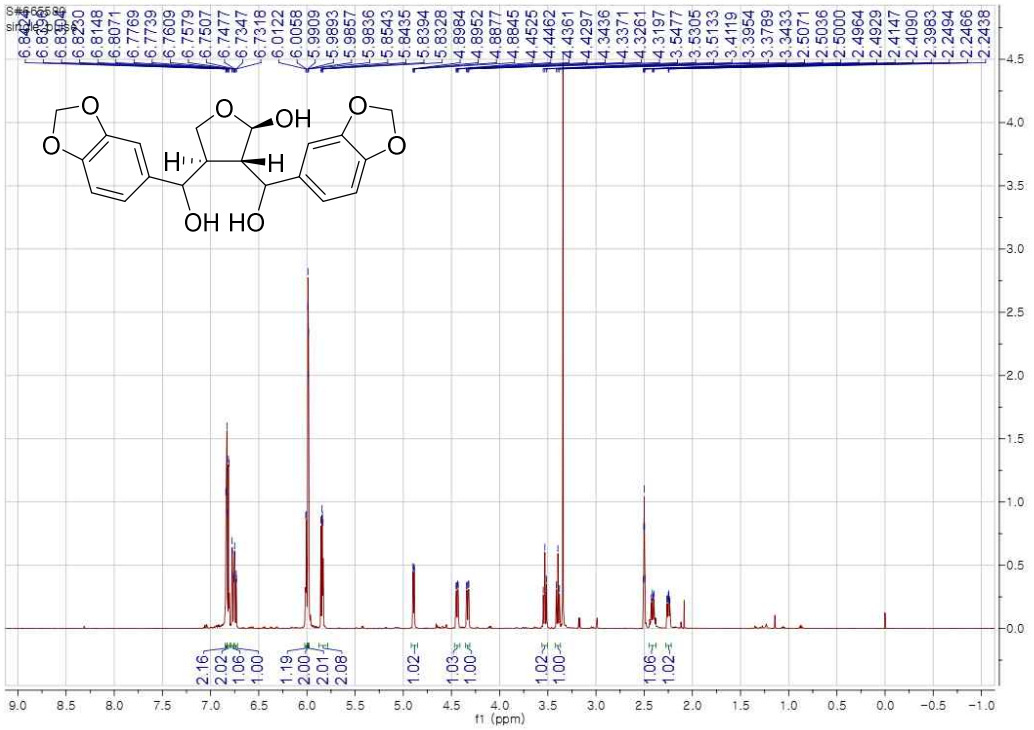


Figure S30. ^{1}H NMR spectrum (500 MHz) of **4** in DMSO-d_6.

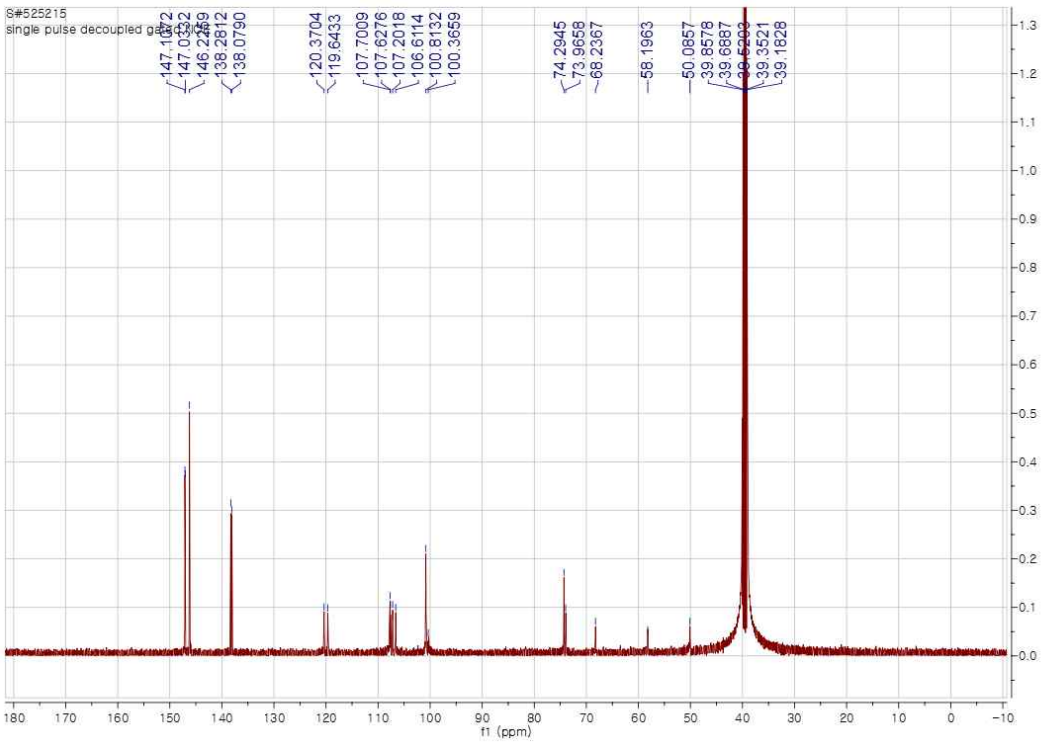


Figure S31. ^{13}C NMR spectrum (125 MHz) of **4** in DMSO-d_6.

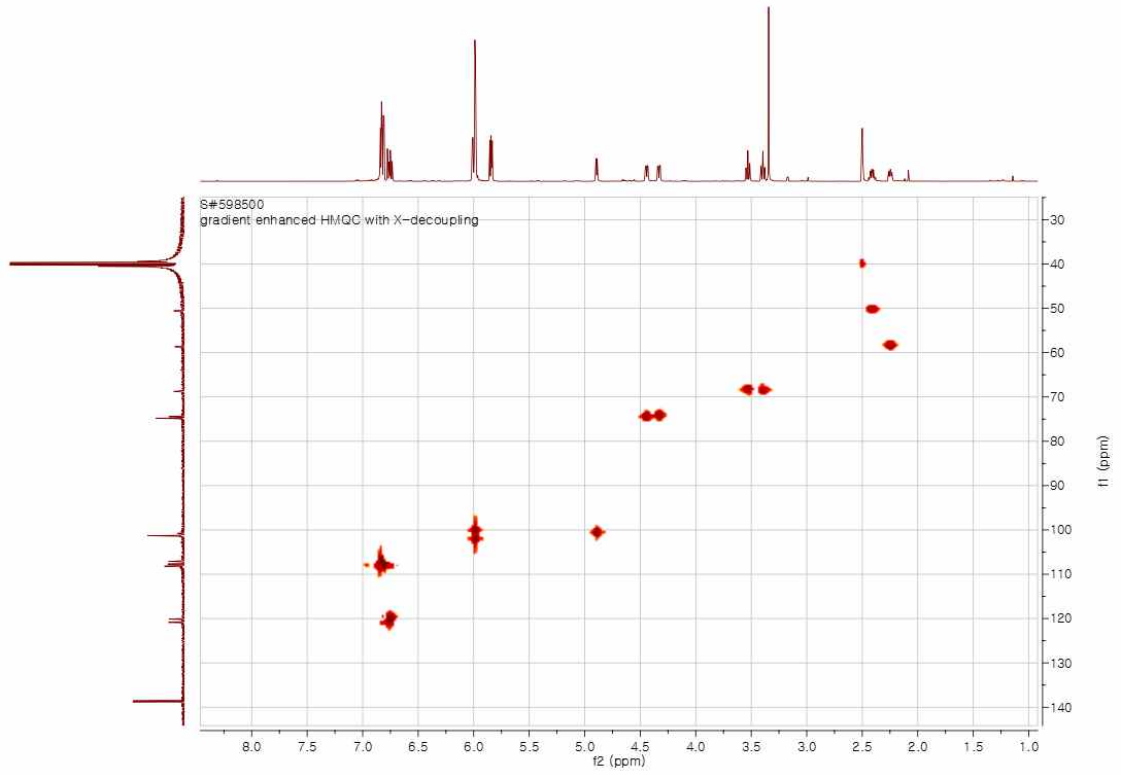


Figure S32. HMQC spectrum of **4** in DMSO-d_6

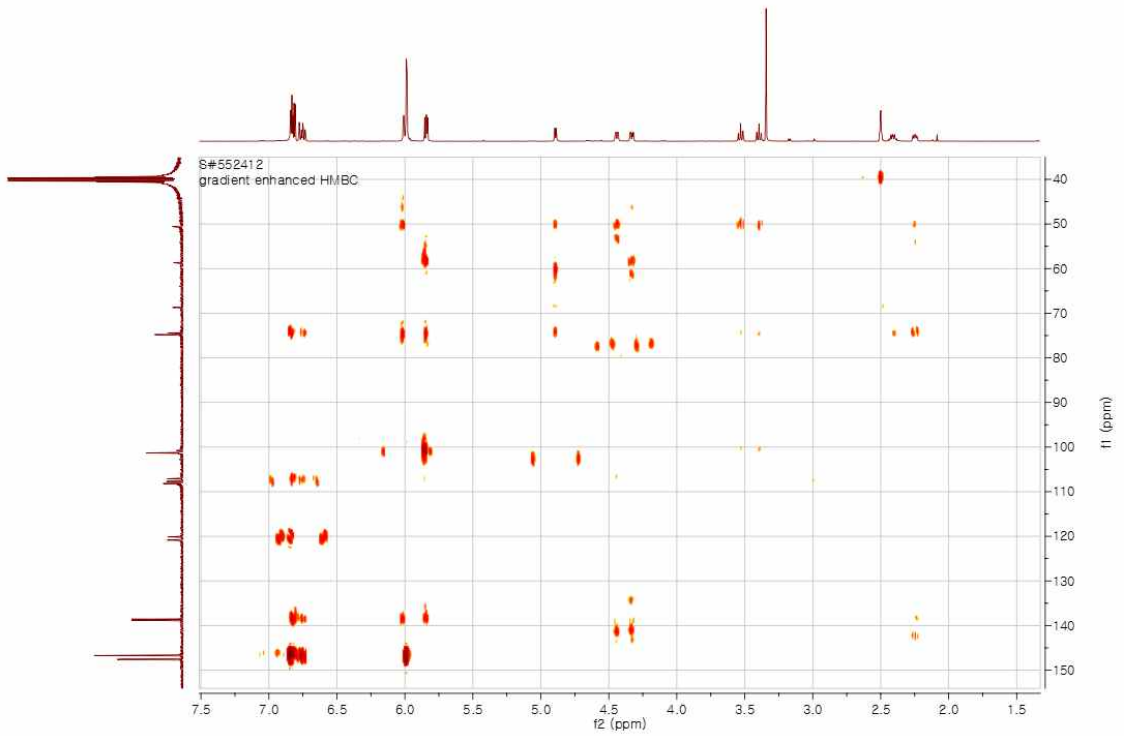


Figure S33. HMBC spectrum of **4** in DMSO-d_6

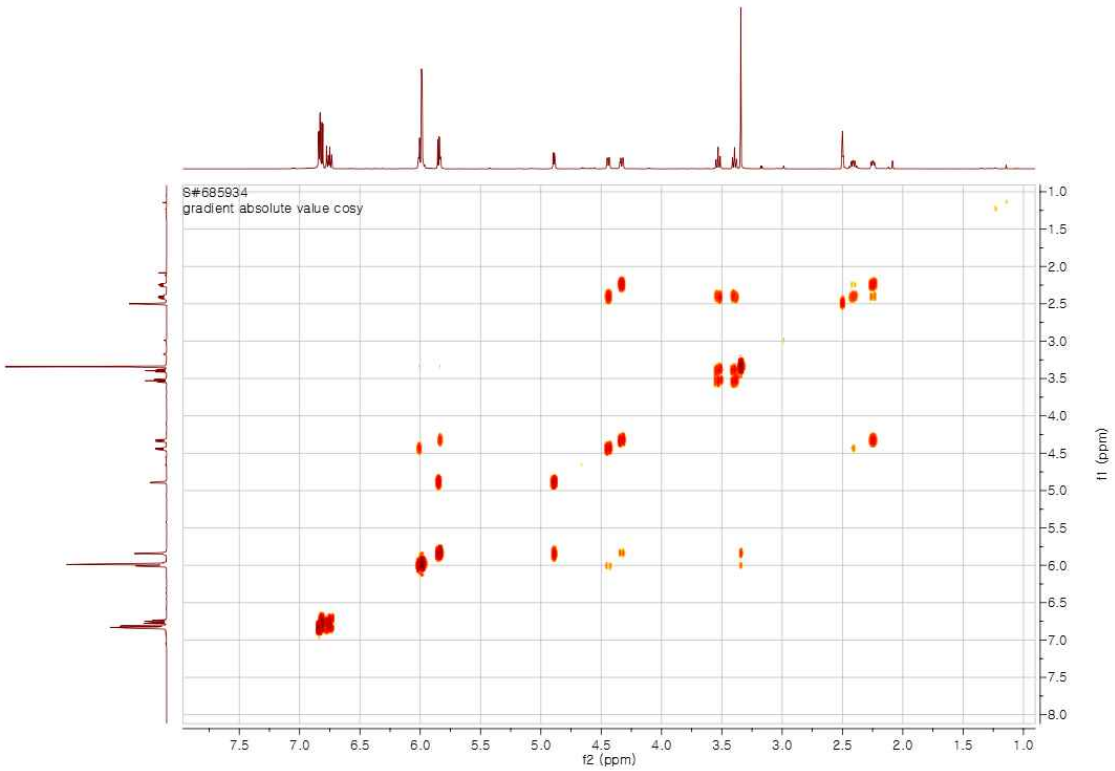


Figure S34. ^{1}H-^{1}H COSY spectrum of **4** in DMSO- d_6

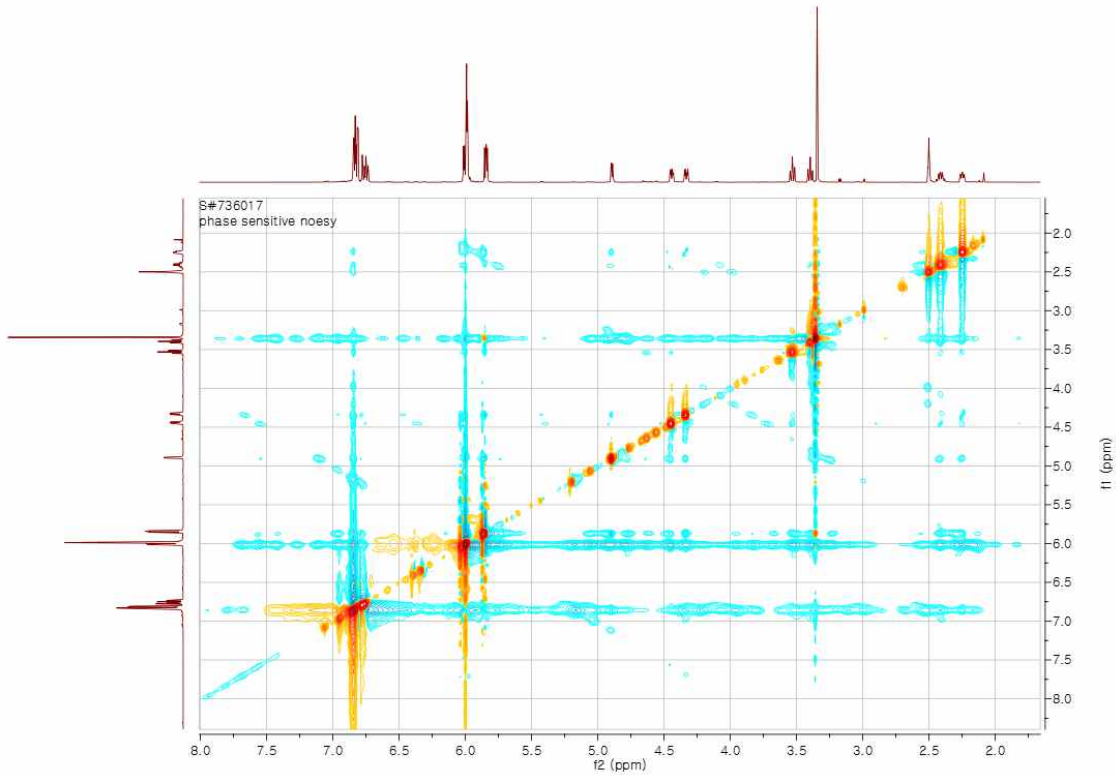
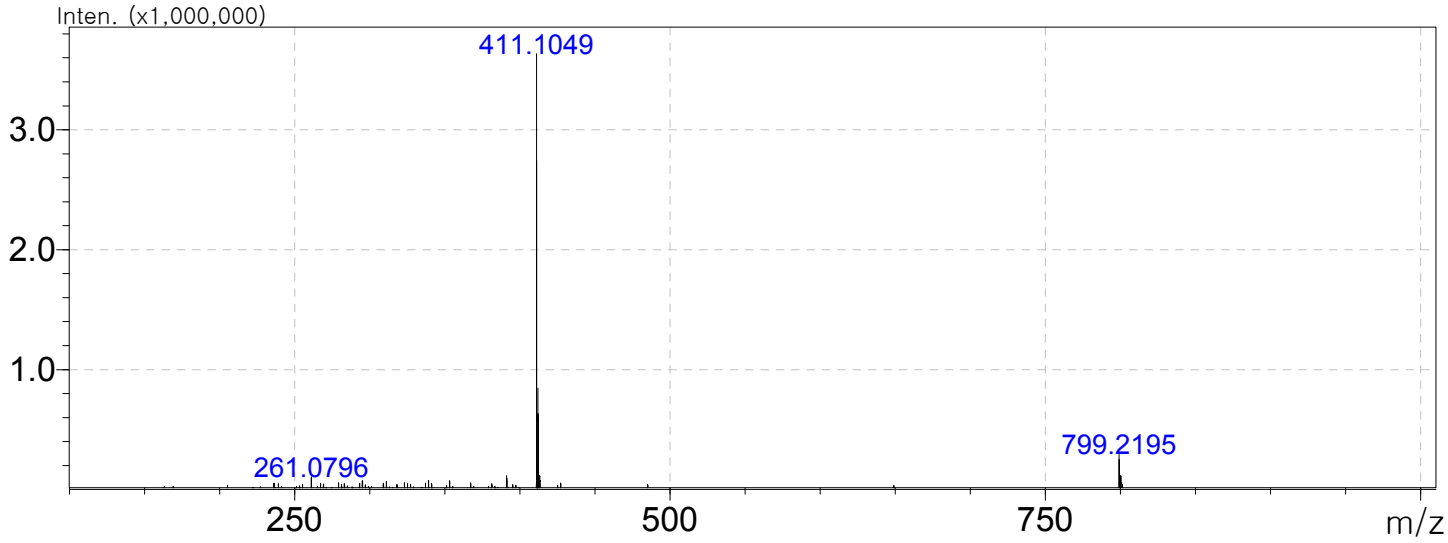
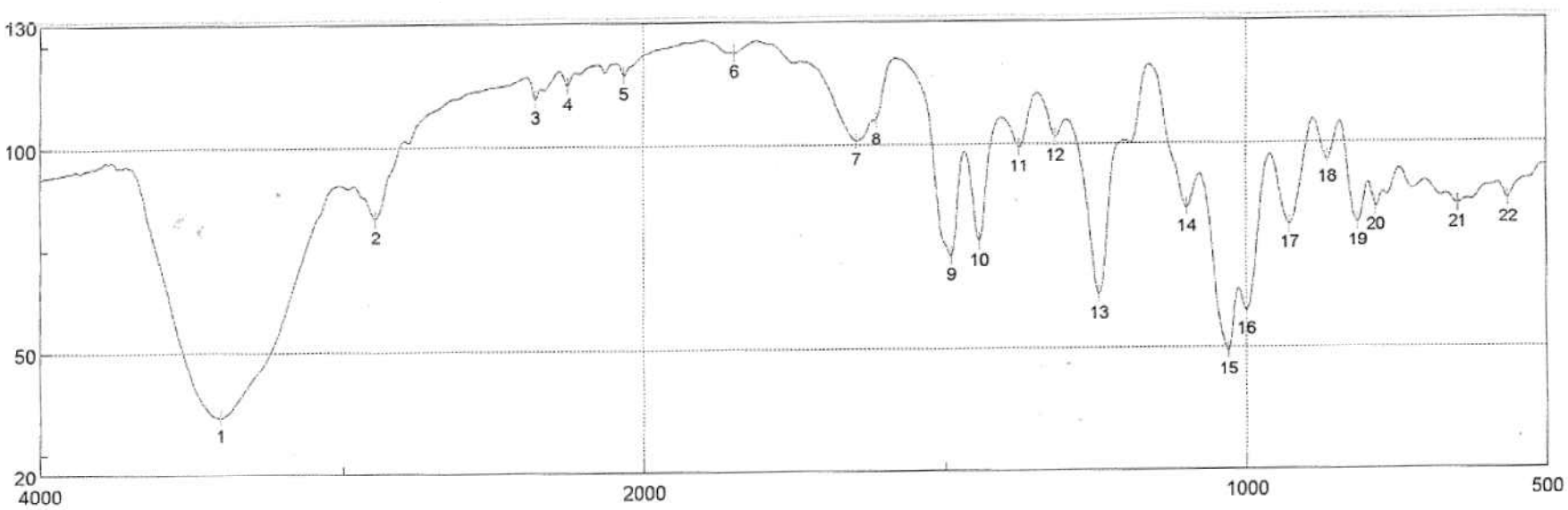


Figure S35. NOESY spectrum of **4** in DMSO-d_6



#	Mass	Diff (mDa)	Formula	DBE
1	388.1158	0.1	C_{20} H_{20} O_8	11.0

Figure S36. HRESIMS spectrum of **4**



No.	cm-1	%T	No.	cm-1	%T	No.	cm-1	%T	No.	cm-1	%T	No.	cm-1	%T
1	3405	34.16	2	2896	82.58	3	2361	111.64	4	2255	114.91	5	2066	117.27
6	1849	122.60	7	1646	101.02	8	1613	106.01	9	1490	72.71	10	1443	76.20
11	1377	99.18	12	1317	101.81	13	1245	63.17	14	1098	84.18	15	1030	49.10
16	1000	58.97	17	929	79.98	18	865	95.94	19	816	80.43	20	786	84.20
21	649	84.74	22	564	85.90									

Figure S37. IR spectrum of **4**

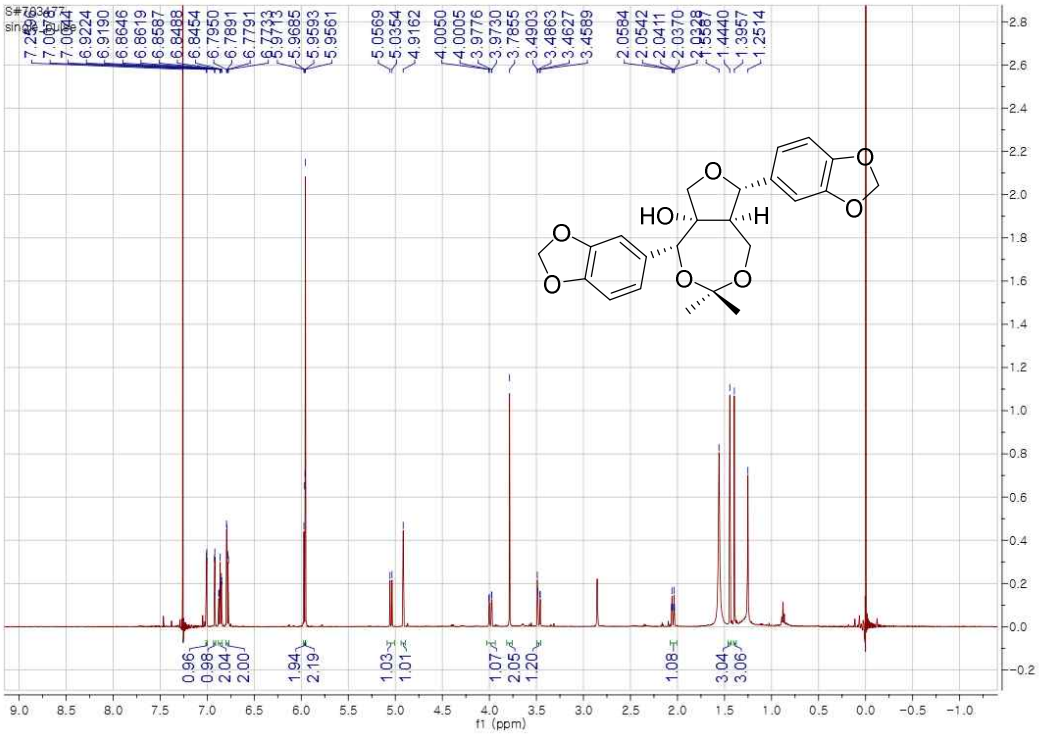


Figure S38. ^{1}H NMR spectrum (500 MHz) of **5** in $CDCl_3$

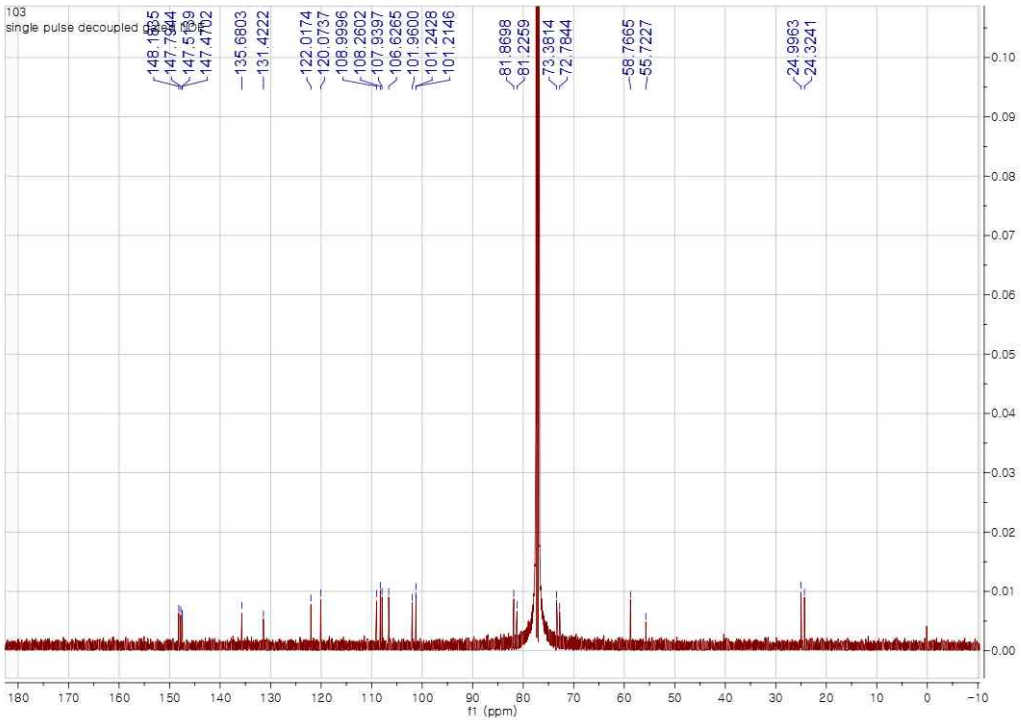


Figure S39. ^{13}C NMR spectrum (125 MHz) of **5** in $CDCl_3$

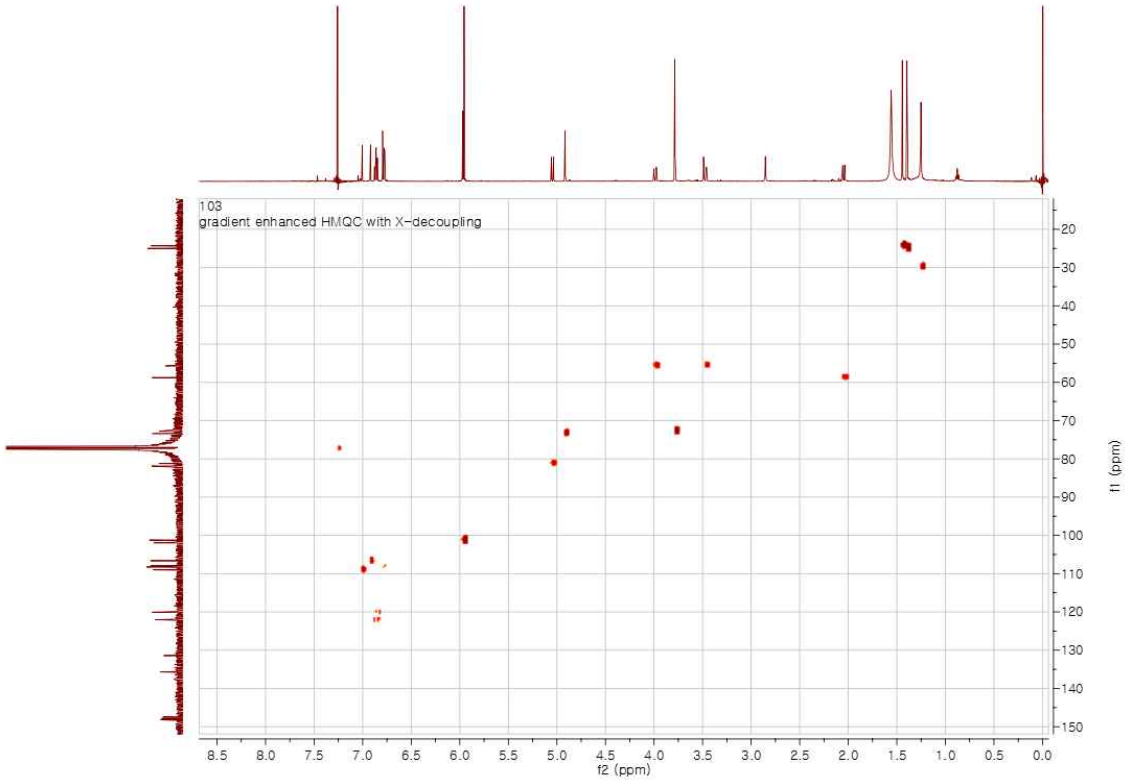


Figure S40. HMQC spectrum of **5** in $CDCl_3$

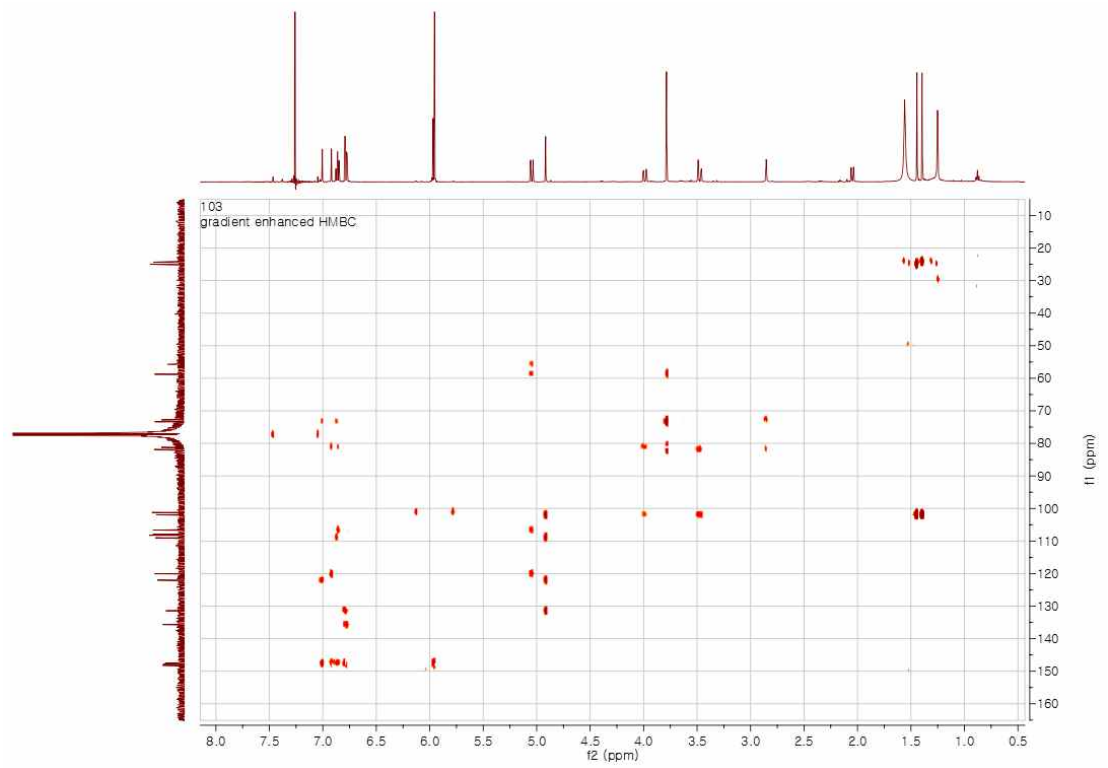


Figure S41. HMBC spectrum of **5** in $CDCl_3$

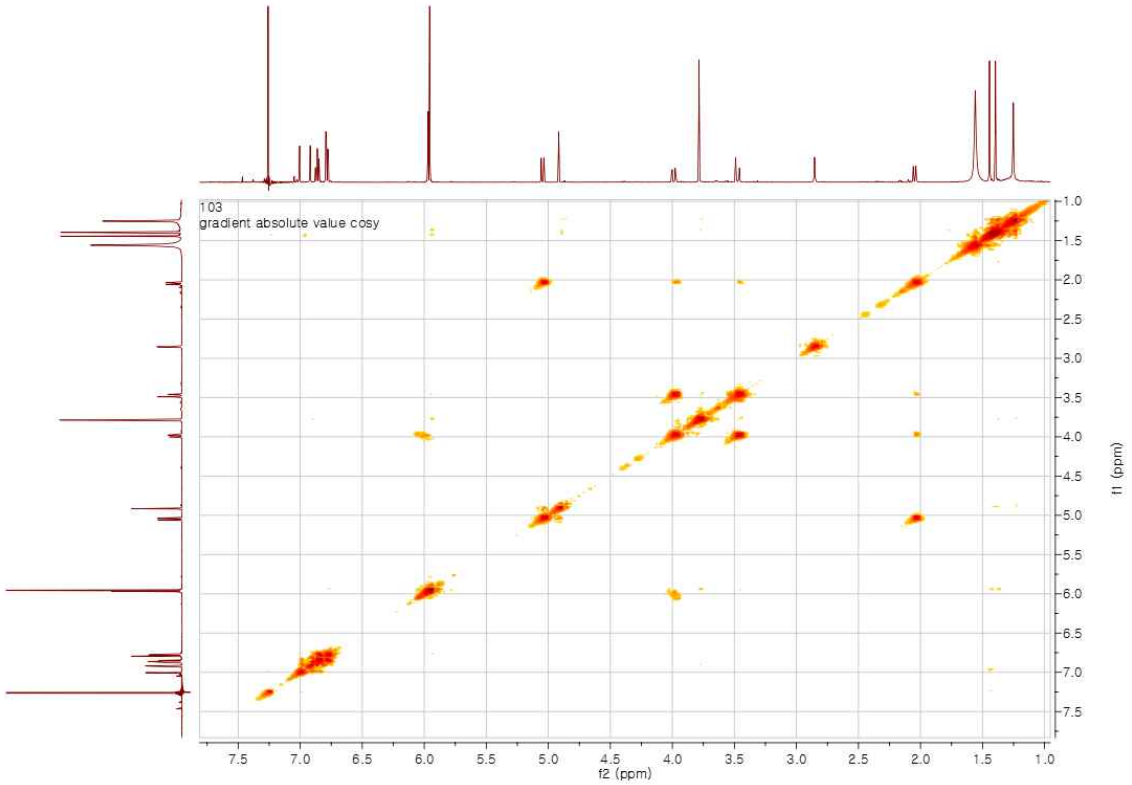


Figure S42. ^{1}H-^{1}H COSY spectrum of **5** in $CDCl_3$

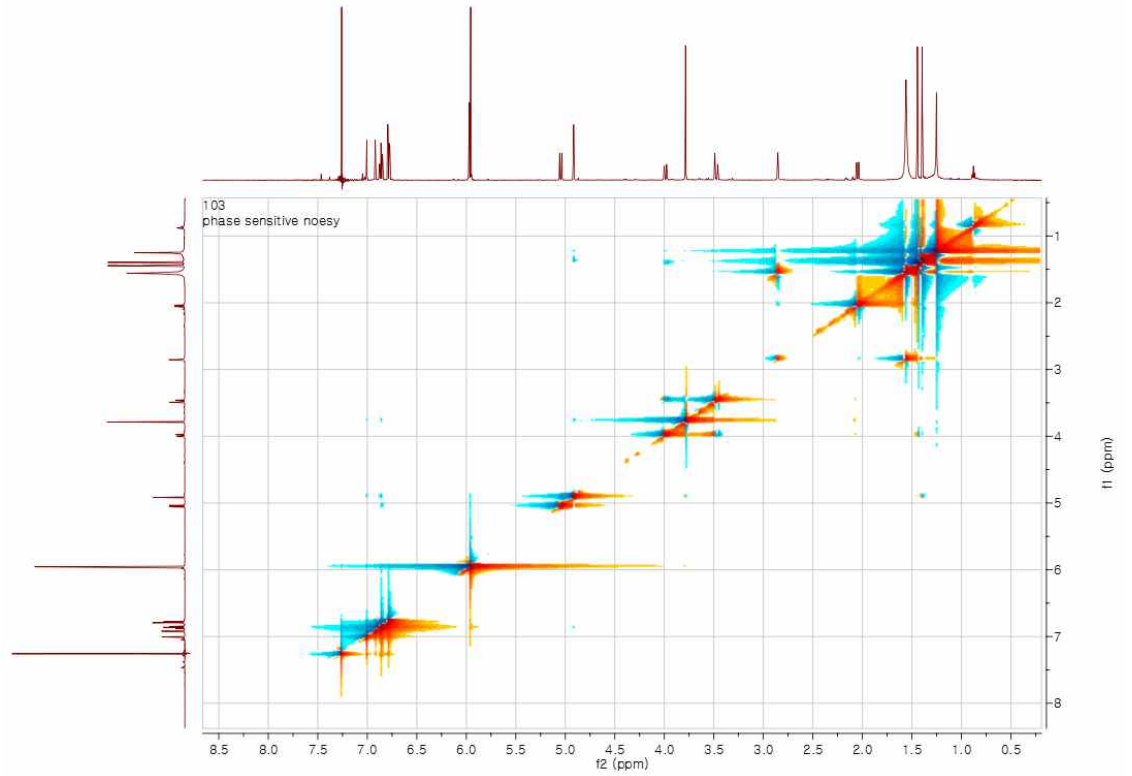


Figure S43. NOESY spectrum of **5** in $CDCl_3$

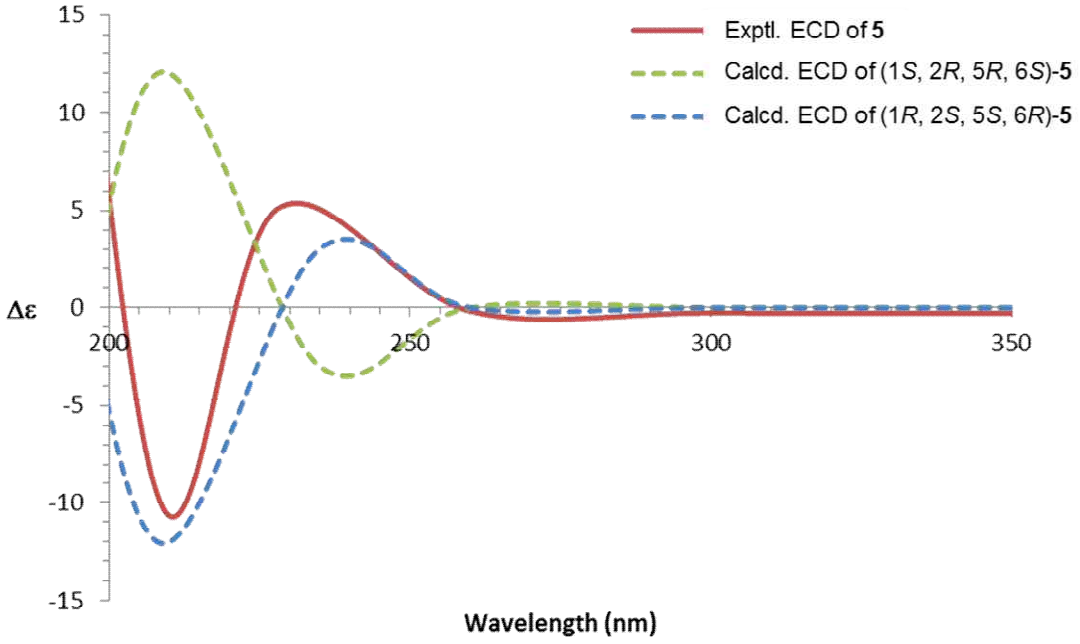


Figure S44. Experimental and calculated ECD spectra of **5**

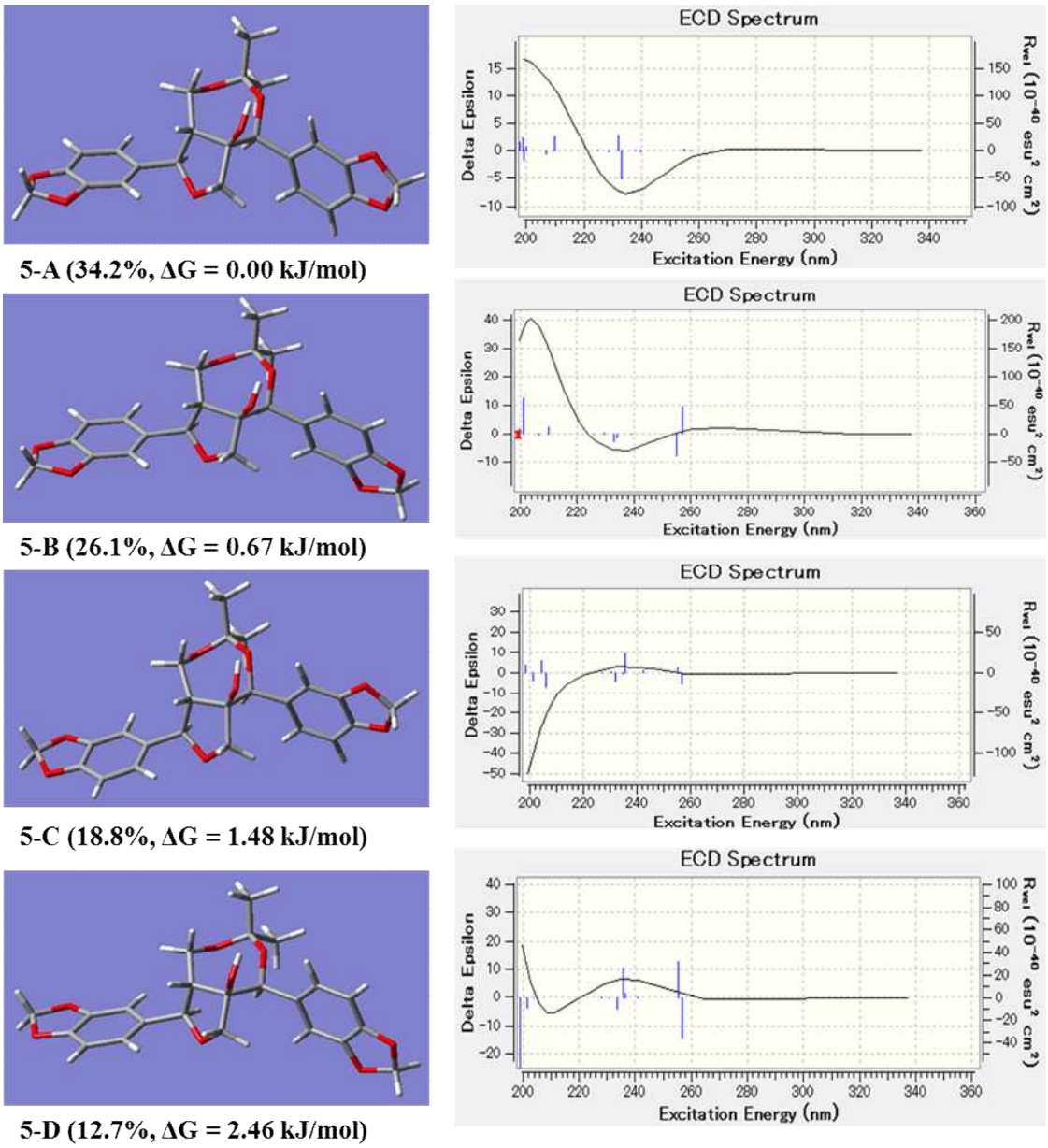
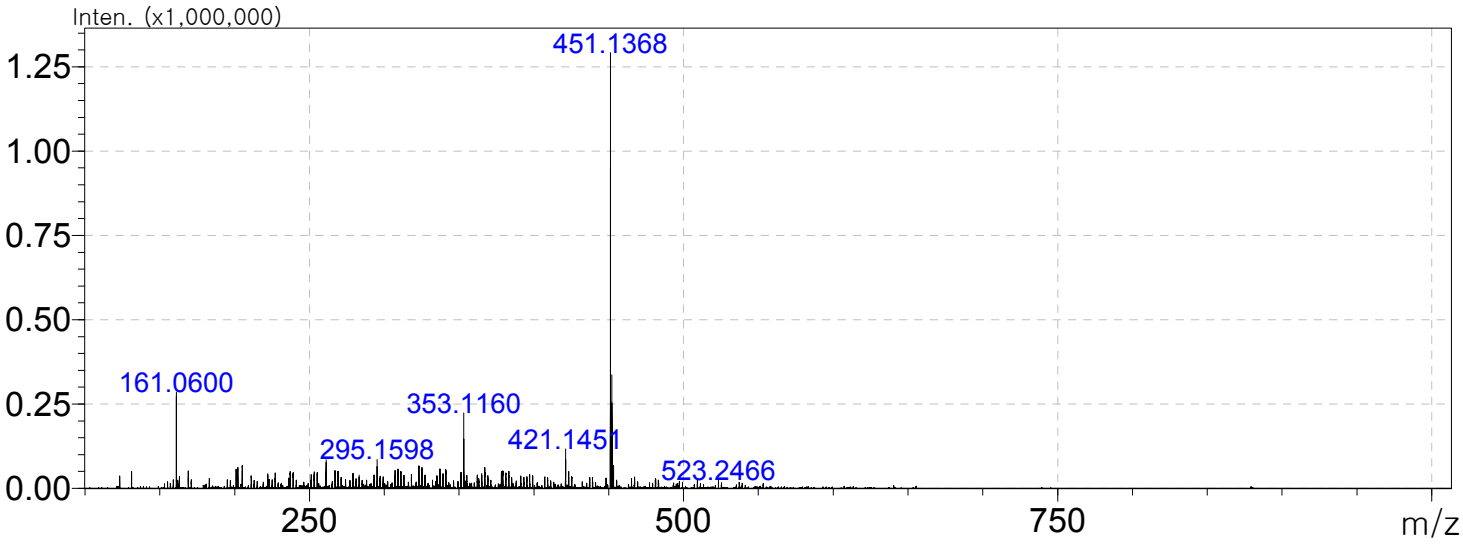
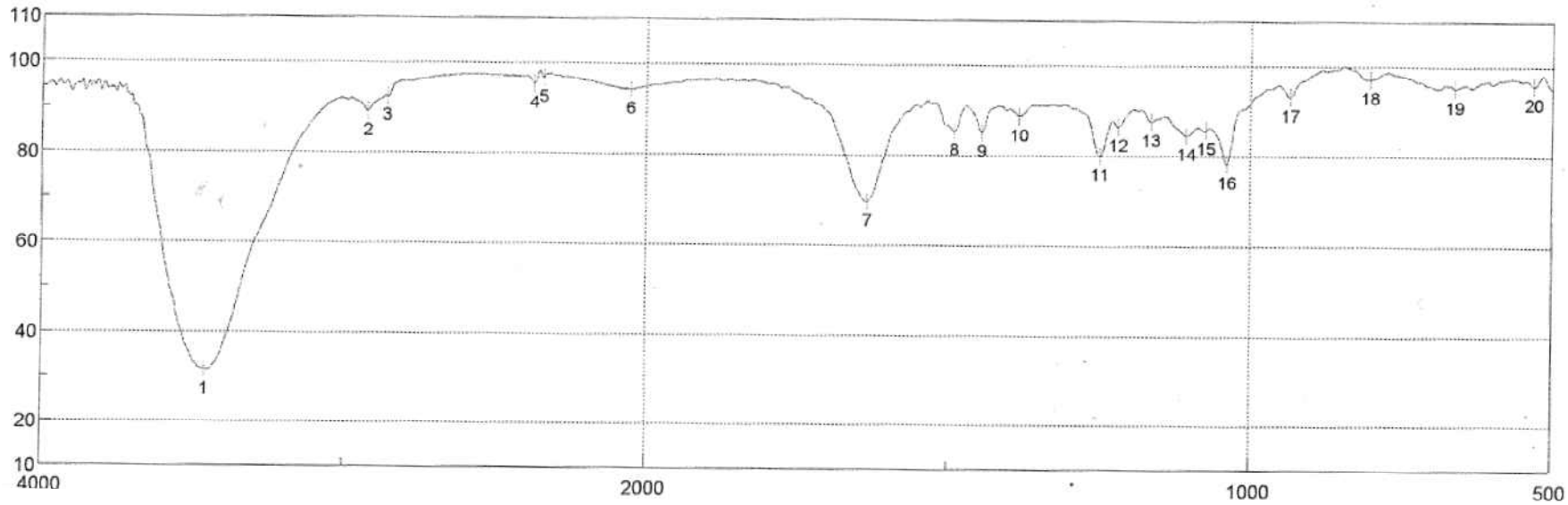


Figure S45. Low-energy conformers of **5** optimized by DFT method at B3LYP/6-31G(d) level with PCM in MeOH (**5A-5D**) and the calculated ECD spectrum of **5A-5D** by TDDFT method at B3LYP/6-31G(d) level with PCM in MeOH. The abundance ratio of each conformer was determined based on the thermal free energies obtained by the frequency calculation at the same level. In this figure, we only showed the result of one side of enantiomer (1*R*, 2*S*, 5*S*, 6*R*).



#	Mass	Diff (mDa)	Formula	DBE
1	428.1471	0.5	C_{23} H_{24} O_8	12.0

Figure S46. HRESIMS spectrum of **5**



No.	cm-1	%T	No.	cm-1	%T	No.	cm-1	%T	No.	cm-1	%T	No.	cm-1	%T
1	3458	31.37	2	2924	89.18	3	2860	92.47	4	2373	95.49	5	2342	96.70
6	2053	94.26	7	1634	69.64	8	1491	85.41	9	1444	85.20	10	1382	88.77
11	1249	79.93	12	1219	86.59	13	1165	87.68	14	1106	84.63	15	1073	85.83
16	1038	78.14	17	934	93.15	18	802	97.23	19	662	95.13	20	531	95.79

Figure S47. IR spectrum of **5**

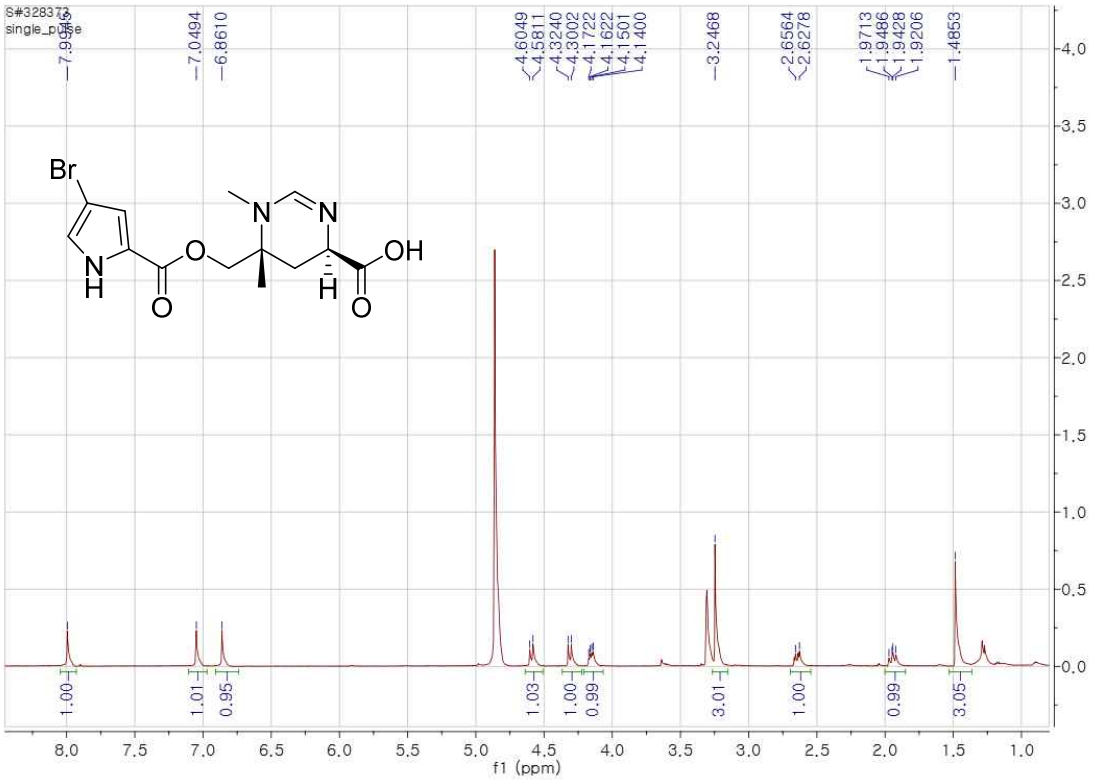


Figure S48. ^{1}H NMR spectrum (500 MHz) of **21** in CD_3OD

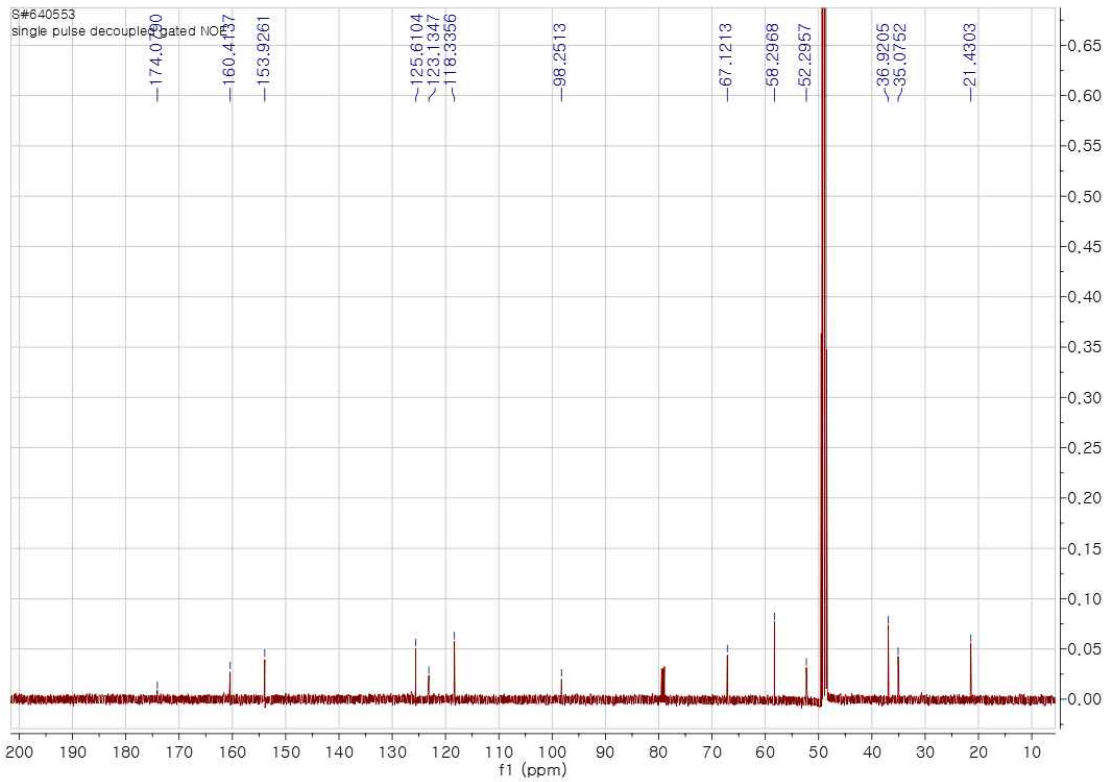


Figure S49. ^{13}C NMR spectrum (125 MHz) of **21** in CD_3OD

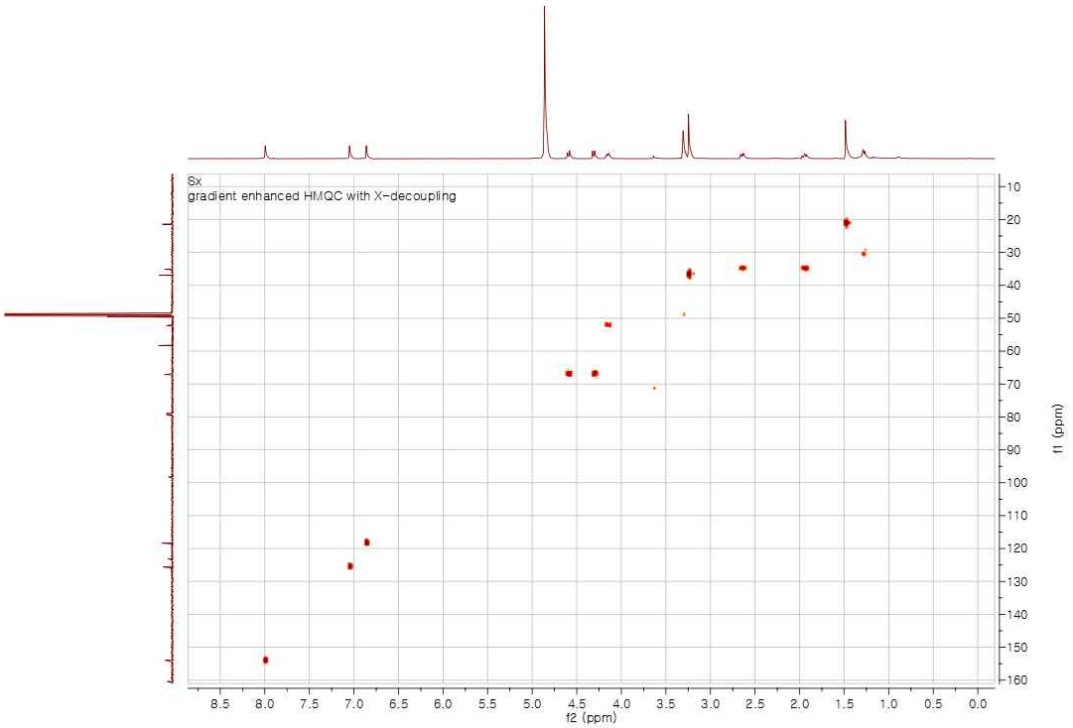


Figure S50. HMQC spectrum of **21** in CD_3OD

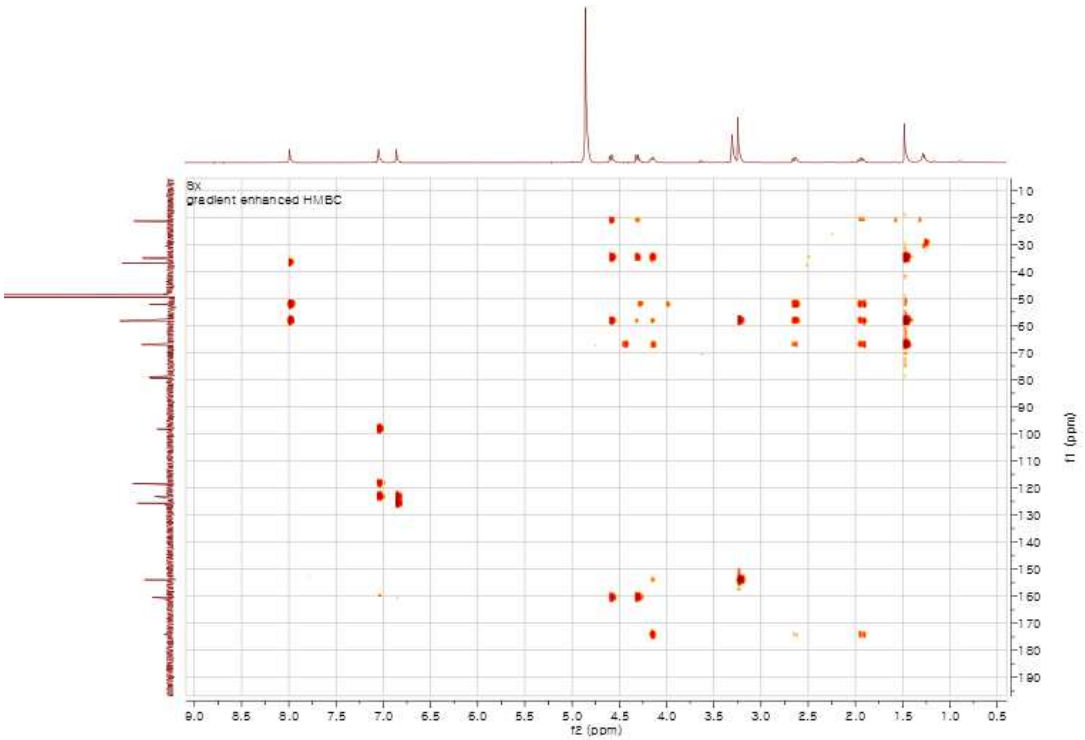


Figure S51. HMBC spectrum of **21** in CD_3OD

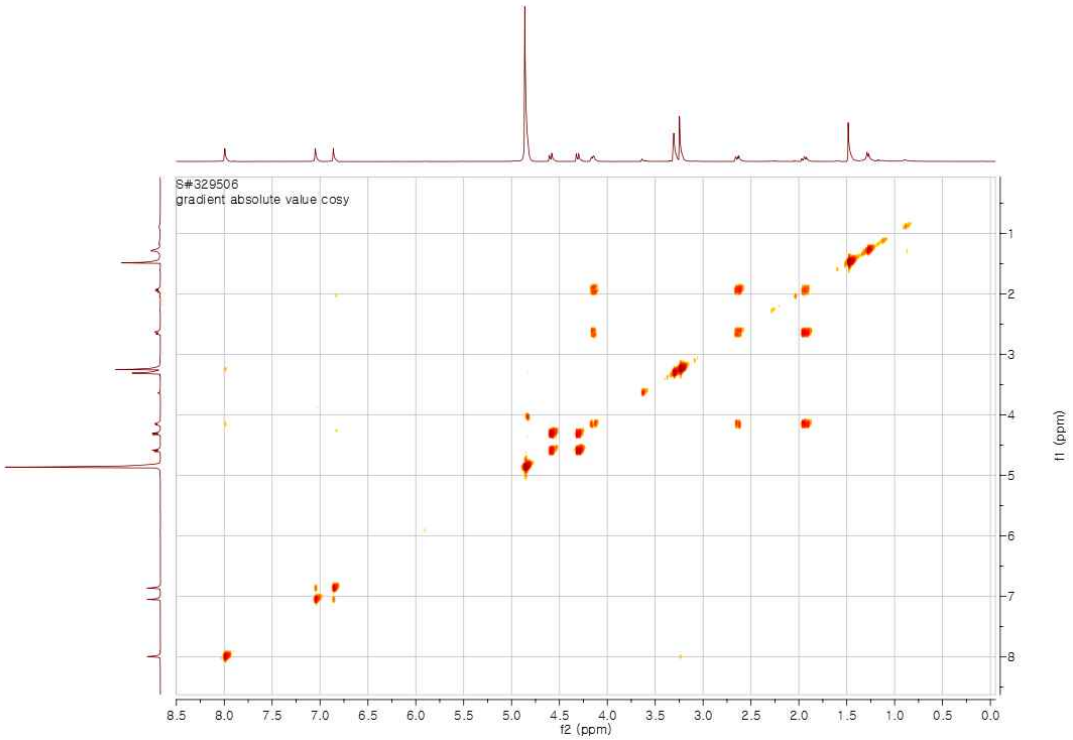


Figure S52. ^{1}H-^{1}H COSY spectrum of **21** in CD_3OD

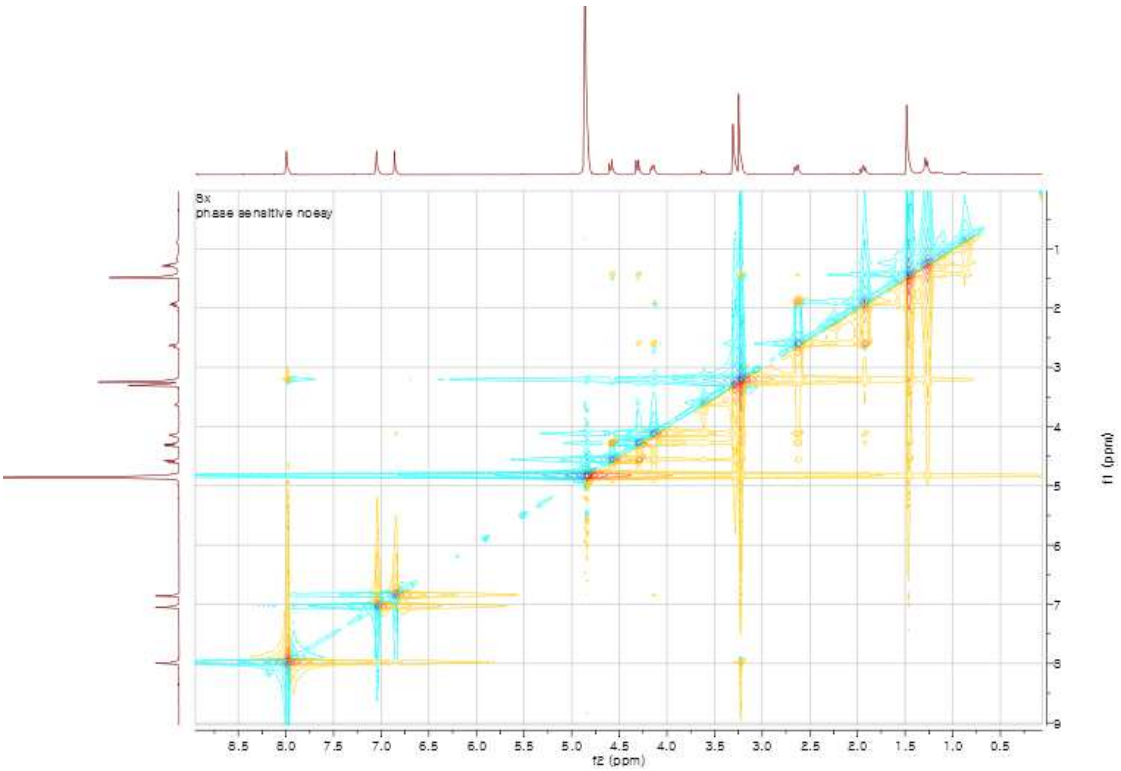


Figure S53. NOESY spectrum of **21** in CD_3OD

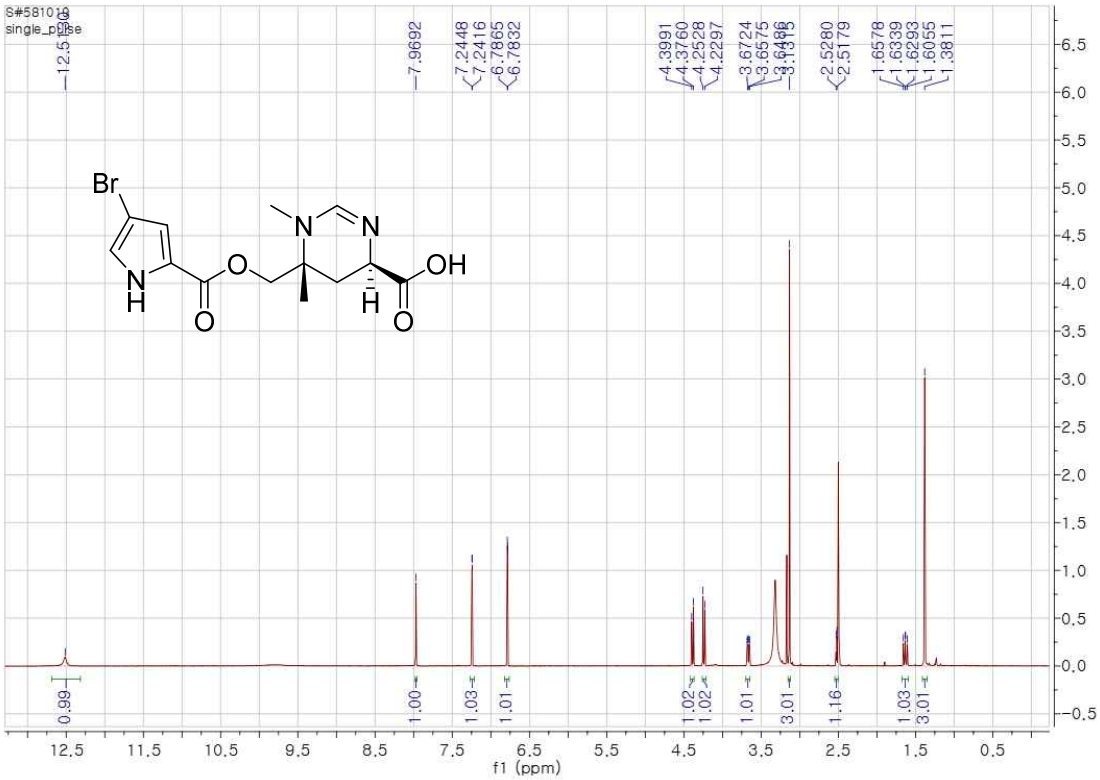


Figure S54. ^{1}H NMR spectrum (500 MHz) of **21** in DMSO-d_6

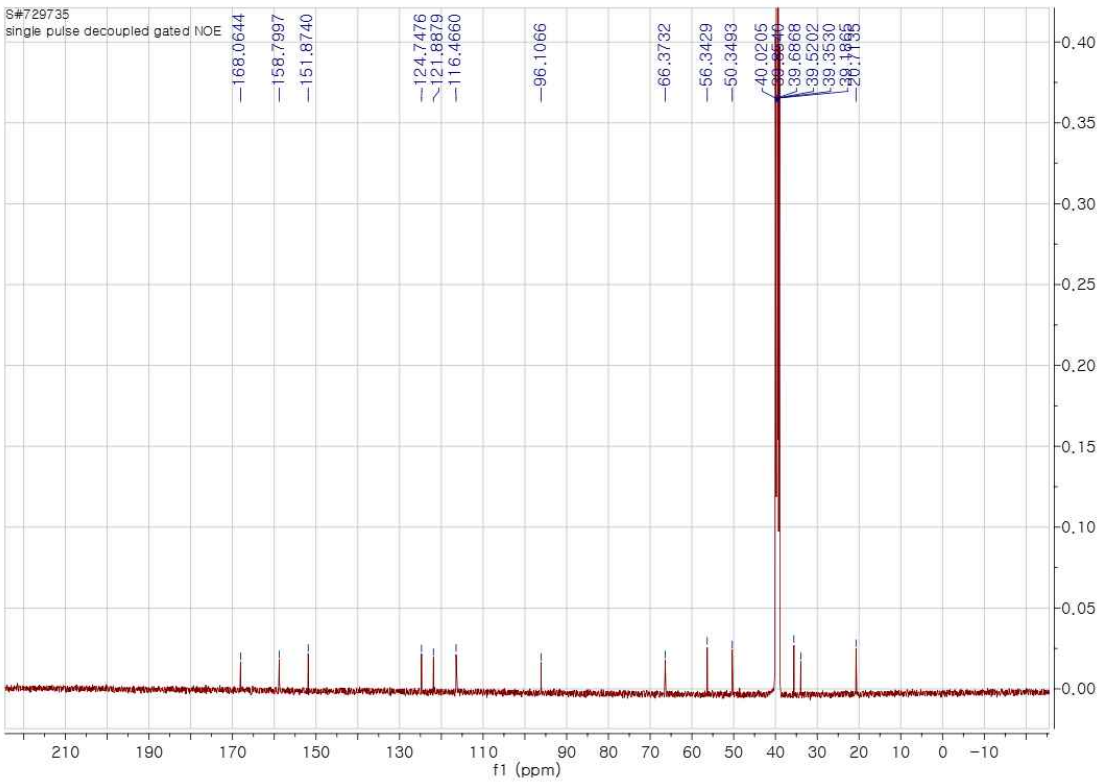


Figure S55. ^{13}C NMR spectrum (125 MHz) of **21** in DMSO-d_6

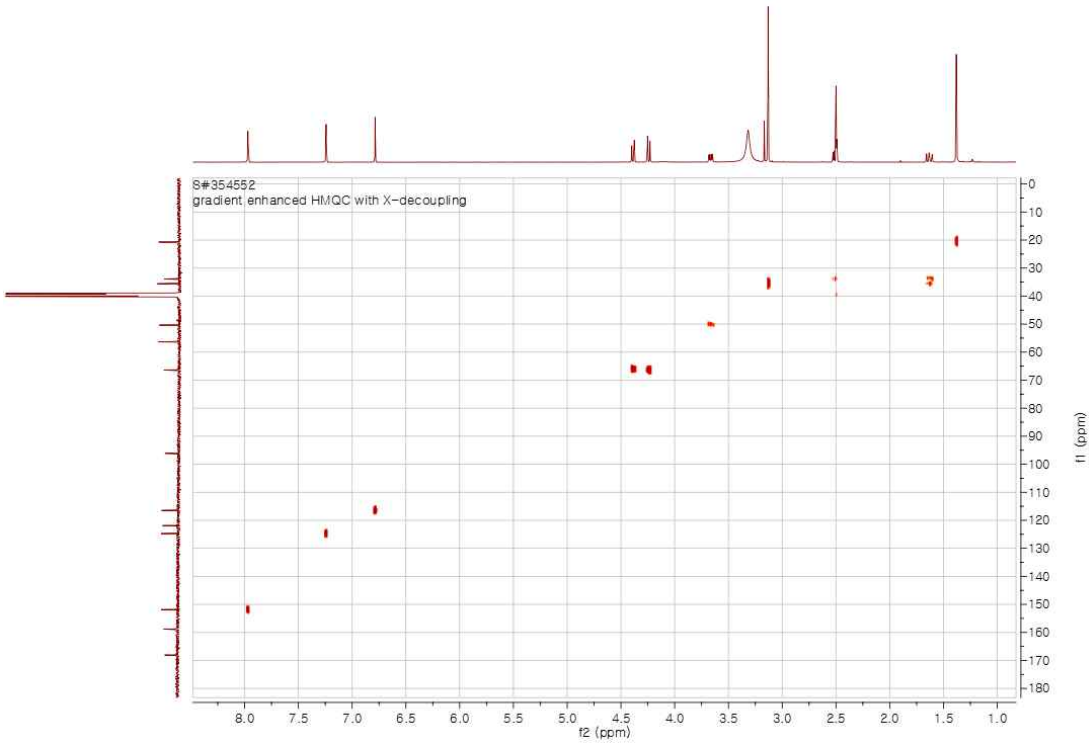


Figure S56. HMQC spectrum of **21** in DMSO-d_6

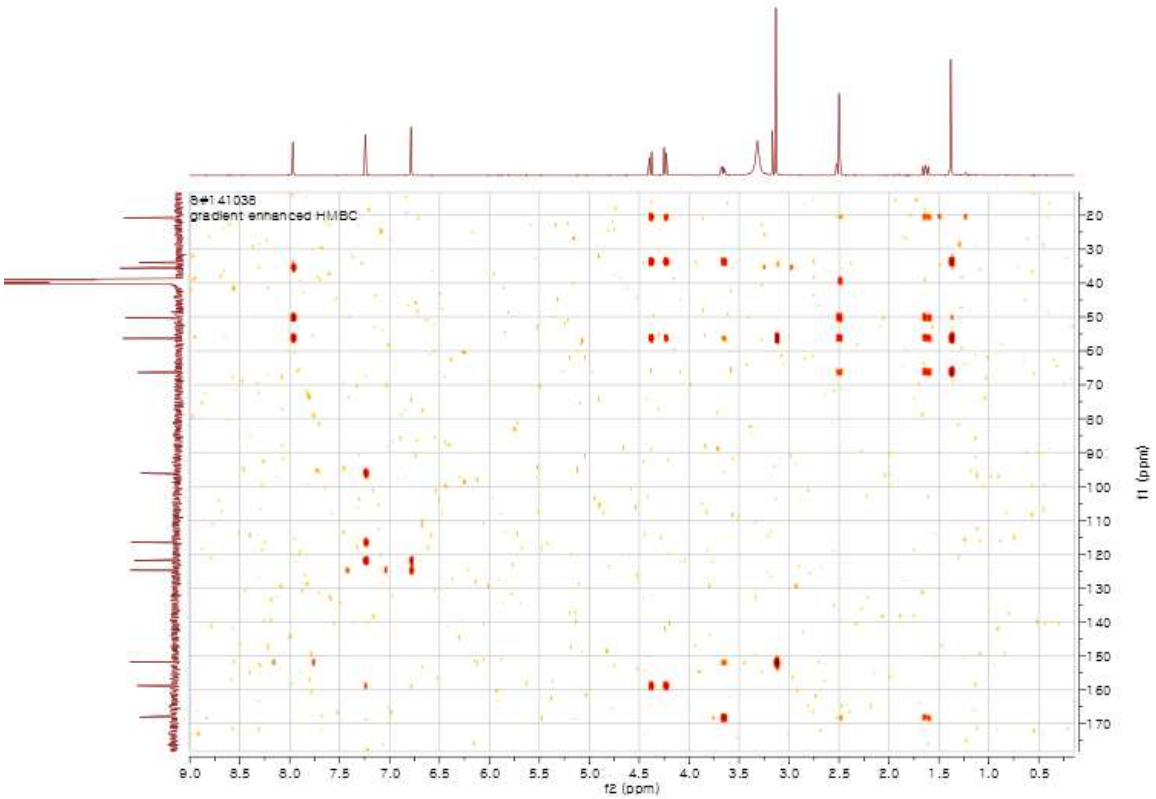


Figure S57. HMBC spectrum of **21** in DMSO-d_6

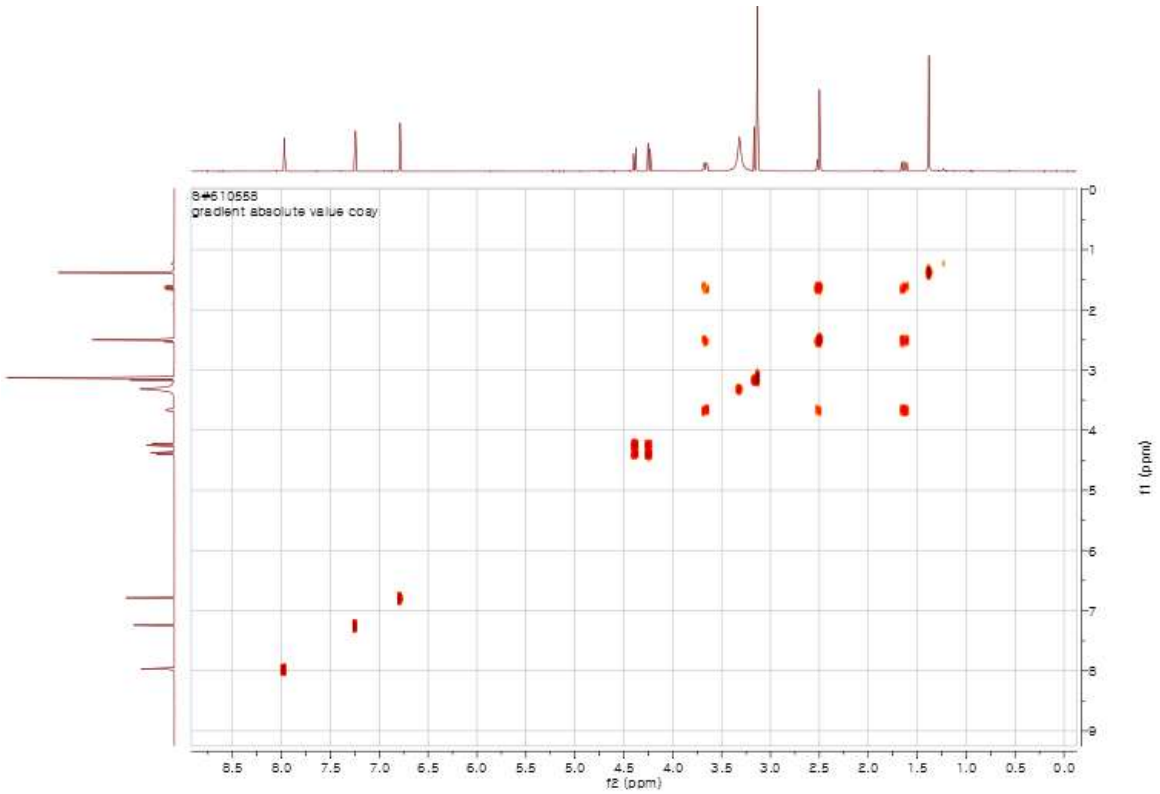


Figure S58. ^{1}H-^{1}H COSY spectrum of **21** in DMSO-d_6

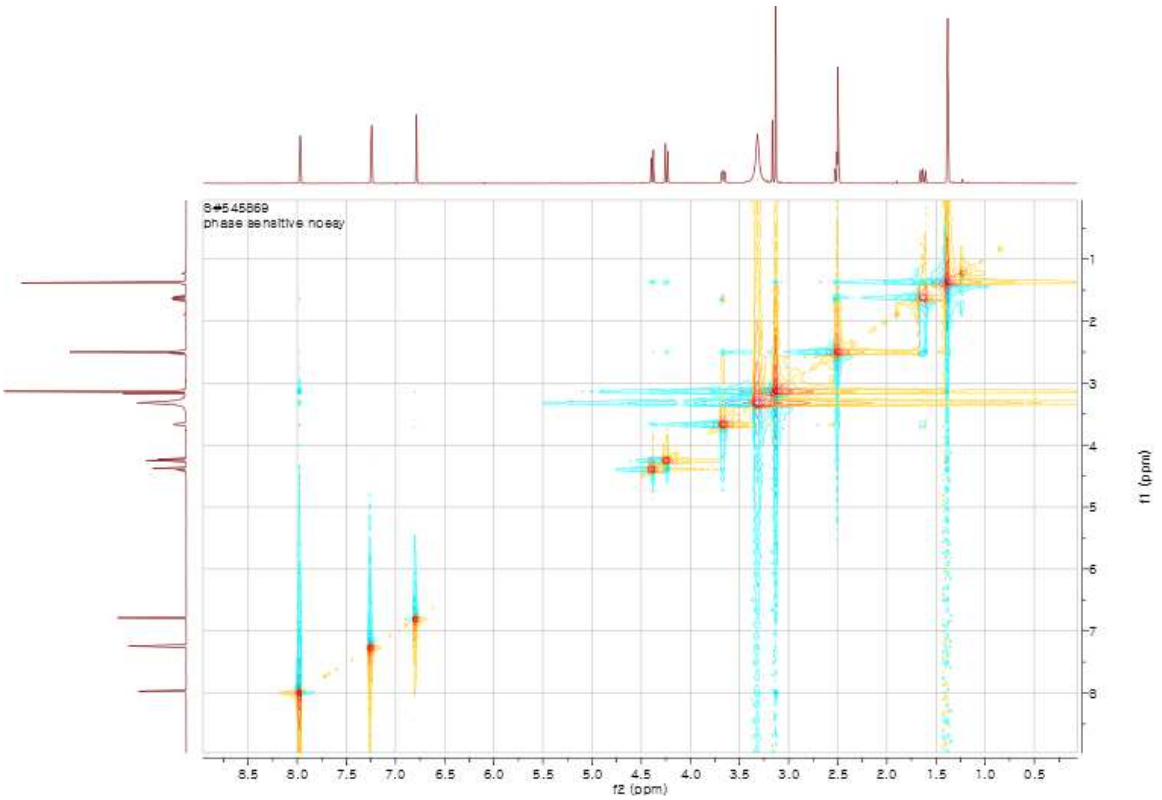


Figure S59. NOESY spectrum of **21** in DMSO-d_6

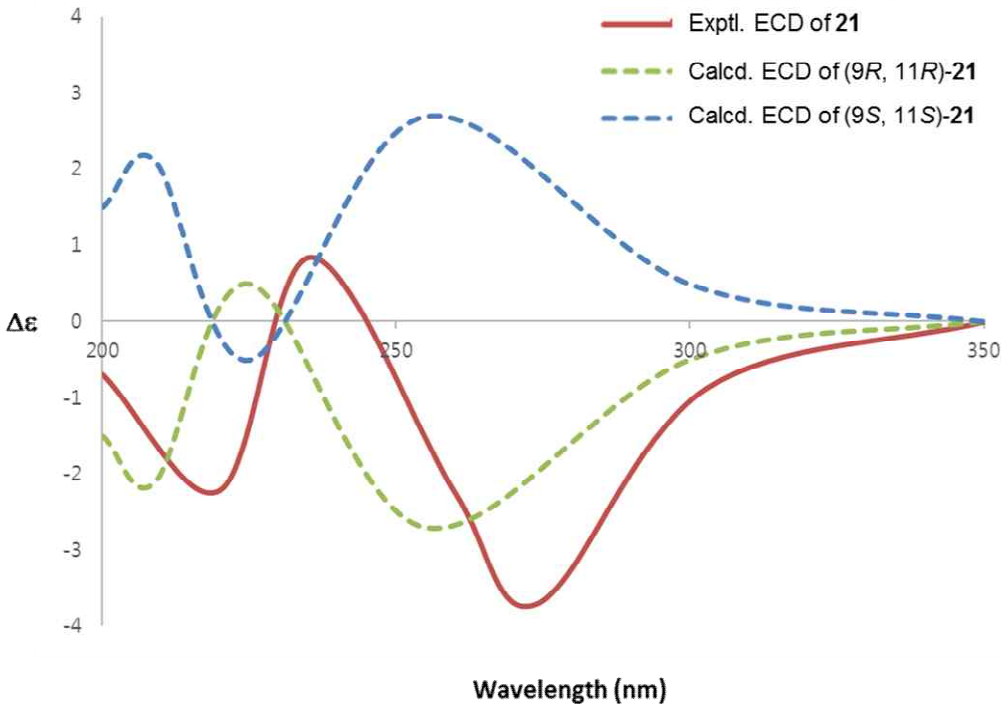
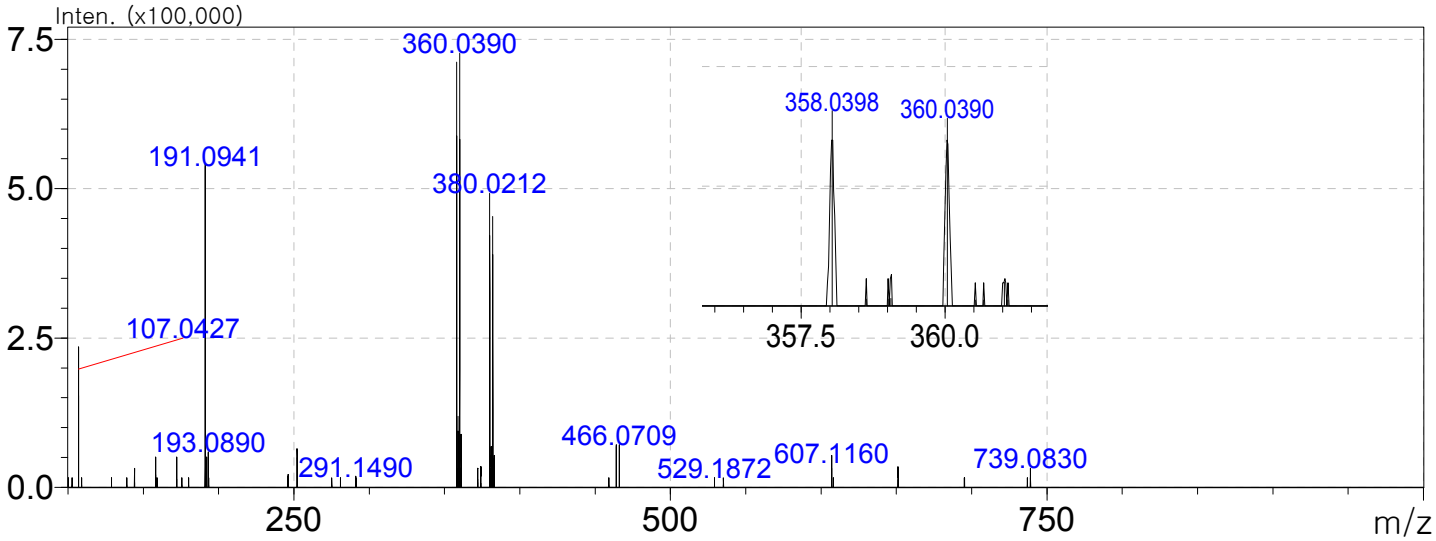
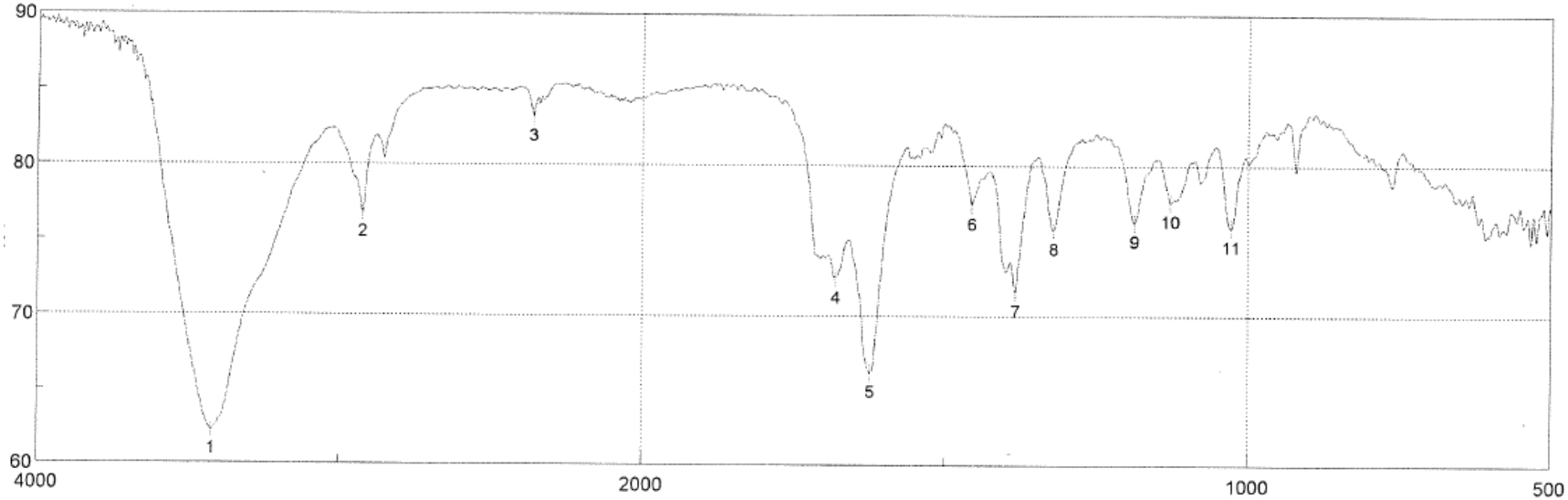


Figure S60. Experimental and calculated ECD spectra of **21**



#	Mass	Diff (mDa)	Formula	DBE
1	357.0324	0.1	$C_{13}H_{16}N_3O_4Br$	7.0

Figure S61. HRESIMS spectrum of **21**



No.	cm-1	%T	No.	cm-1	%T	No.	cm-1	%T	No.	cm-1	%T	No.	cm-1	%T
1	3420	62.23	2	2925	76.79	3	2361	83.16	4	1682	72.47	5	1624	66.17
6	1456	77.37	7	1384	71.57	8	1321	75.74	9	1188	76.23	10	1128	77.59
11	1028	75.88												

Figure S62. IR spectrum of **21**

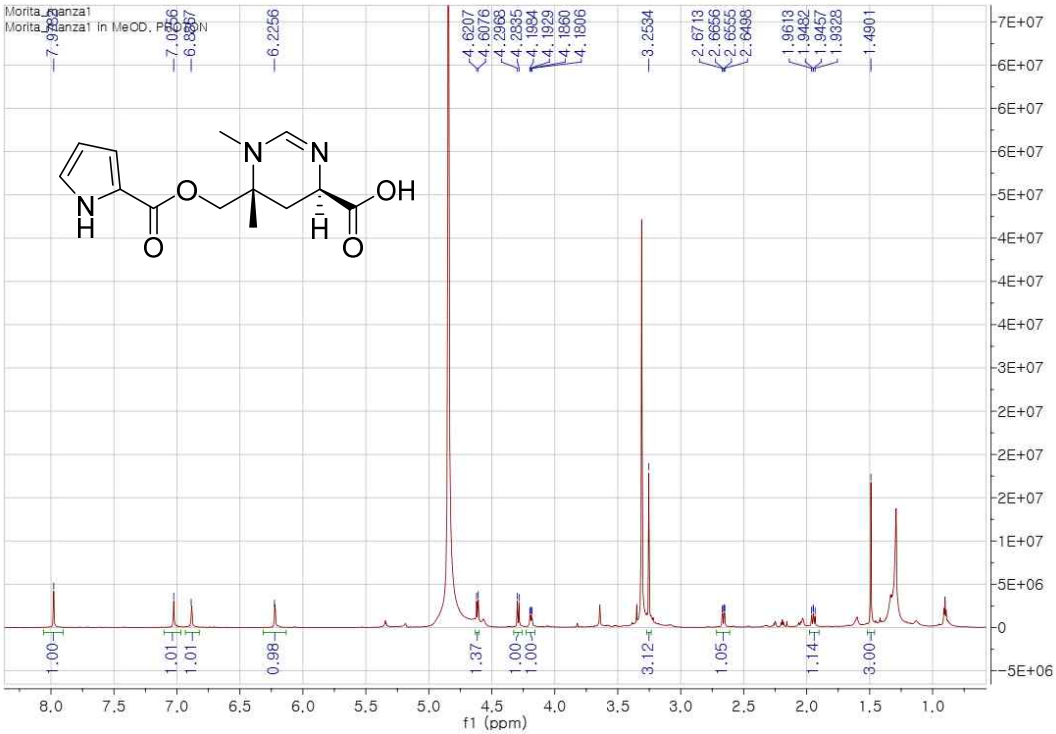


Figure S63. ^{1}H NMR spectrum (900 MHz) of **22** in CD_3OD

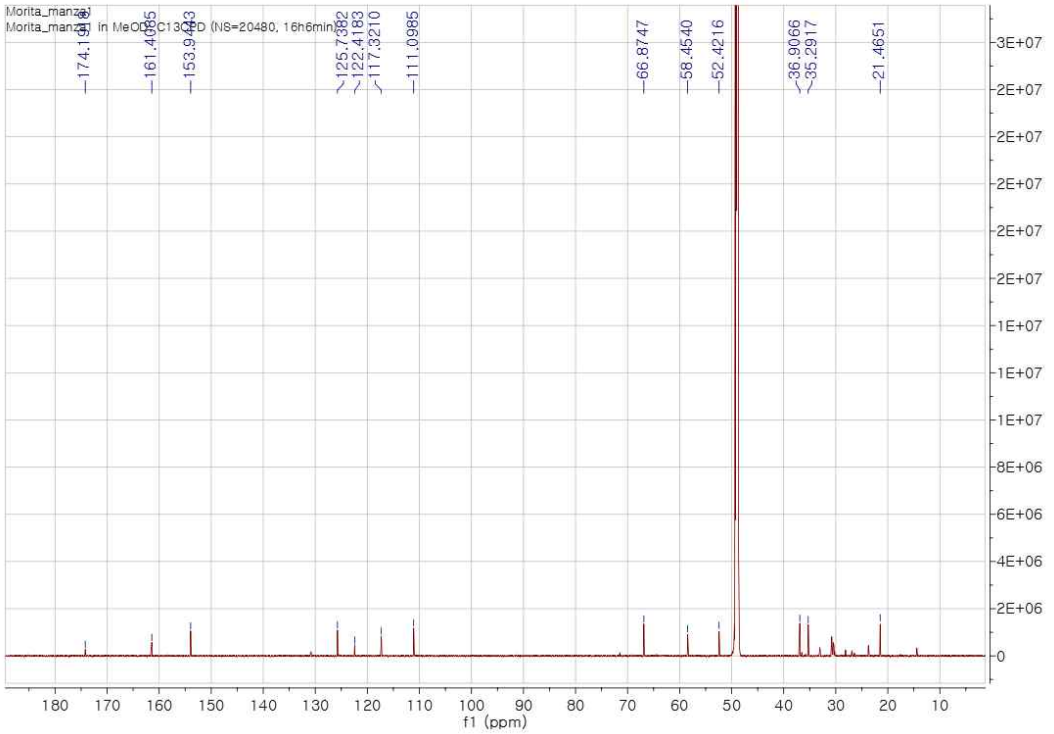


Figure S64. ^{13}C NMR spectrum (225 MHz) of **22** in CD_3OD

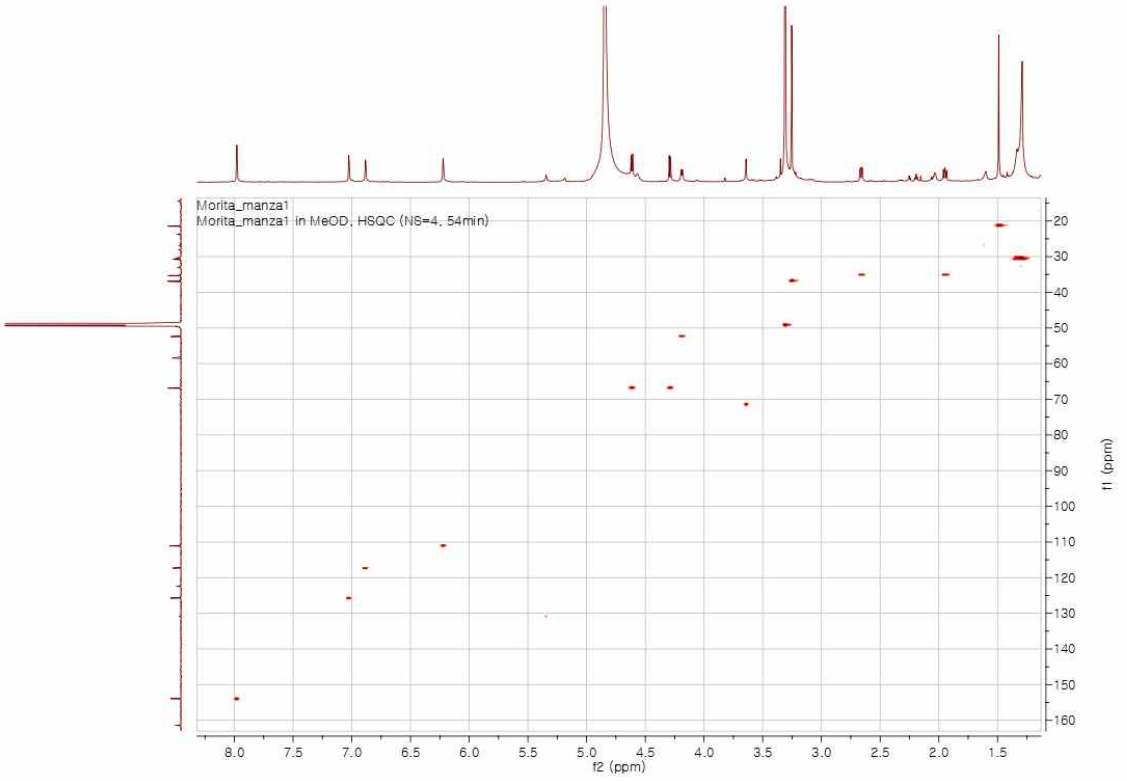


Figure S65. HMQC spectrum of **22** in CD_3OD

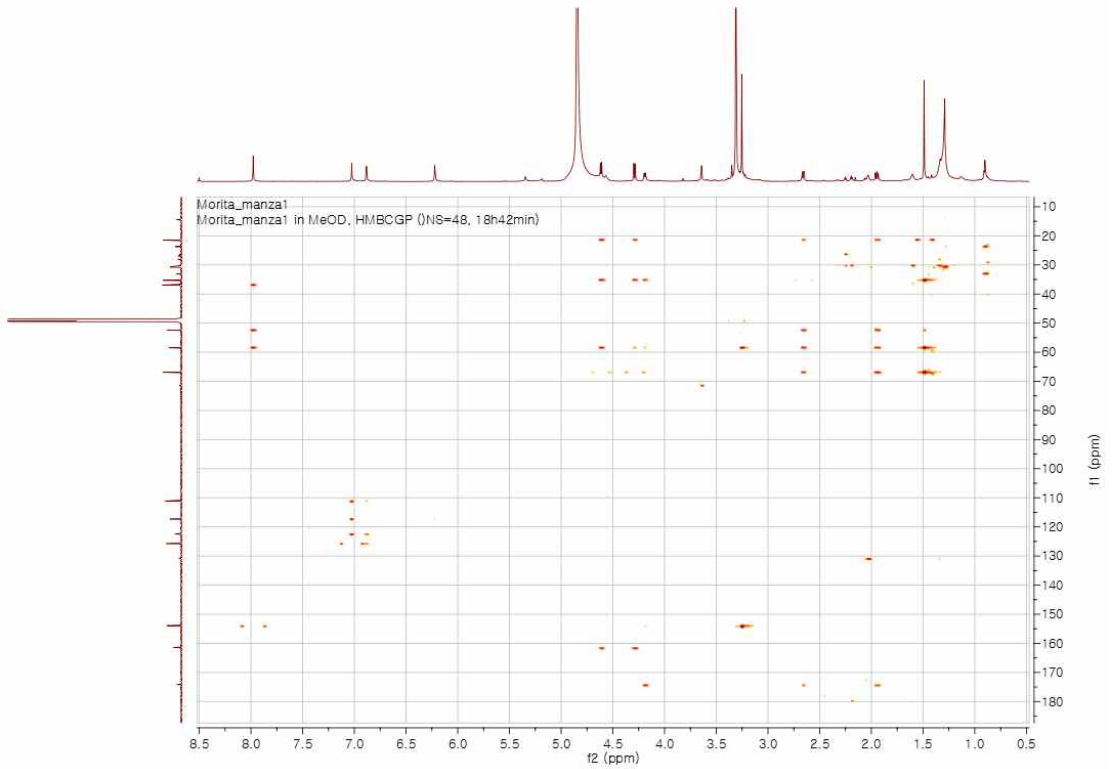


Figure S66. HMBC spectrum of **22** in CD_3OD

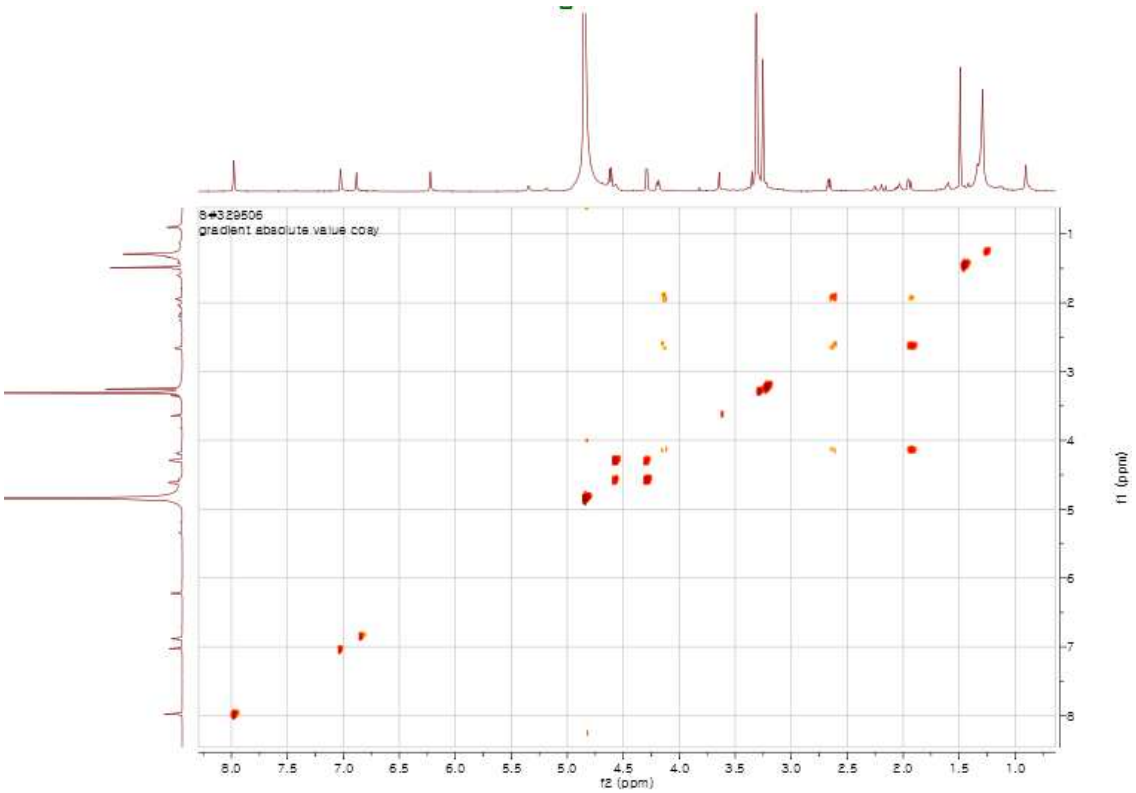


Figure S67. ^{1}H-^{1}H COSY spectrum of **22** in CD_3OD

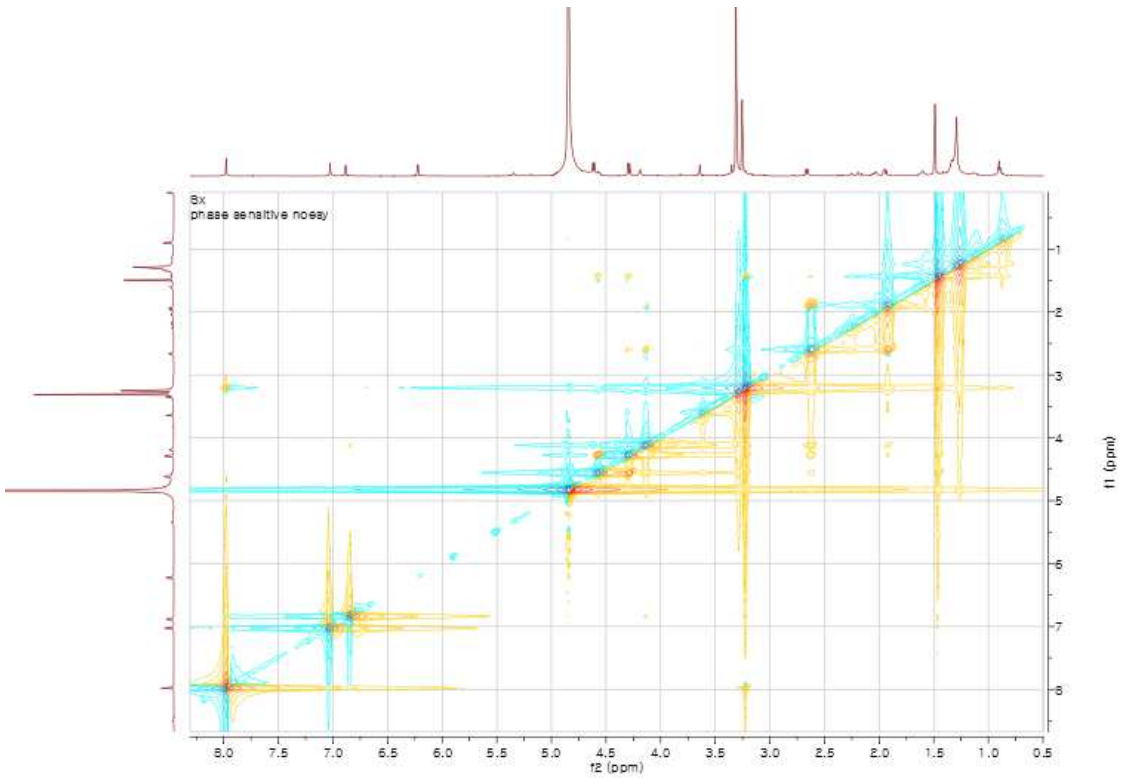
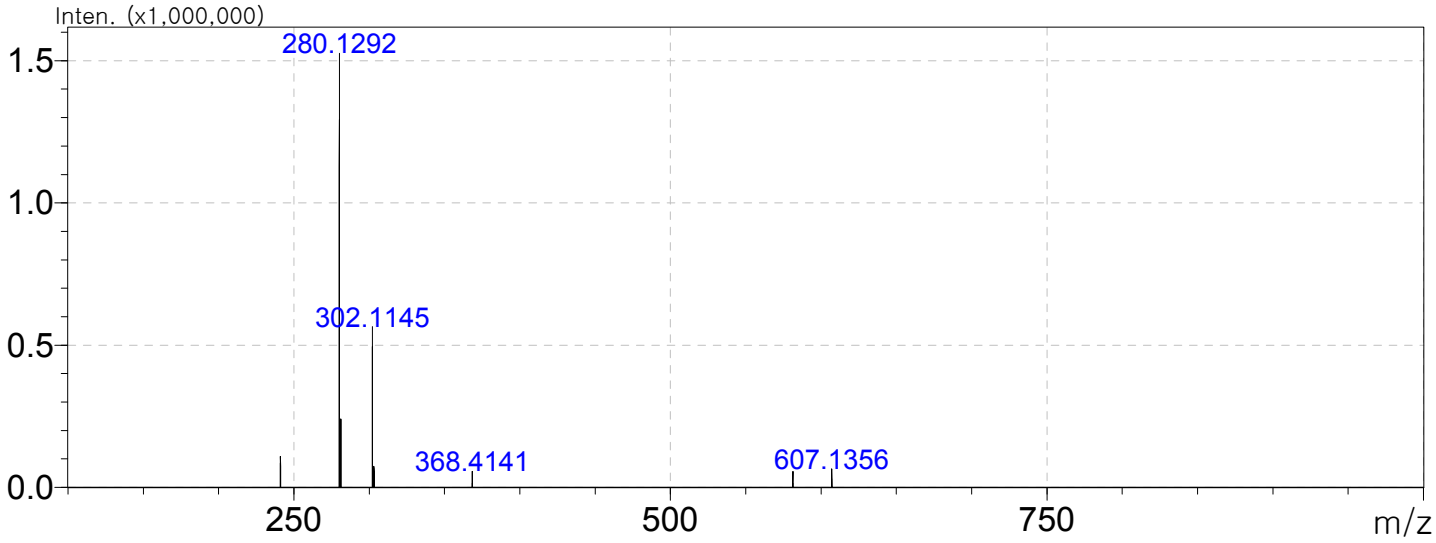
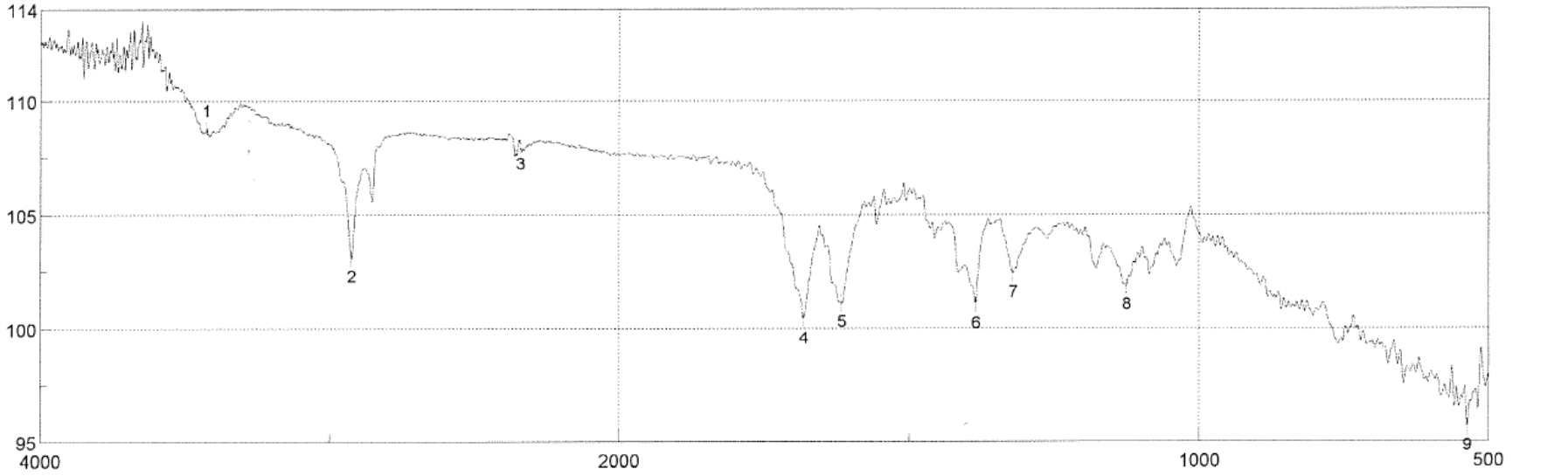


Figure S68. NOESY spectrum of **22** in CD_3OD



#	Mass	Diff (mDa)	Formula	DBE
1	279.1219	0.0	C_{13} H_{17} N_3O_4	7.0

Figure S69. HRESIMS spectrum of **22**



No.	cm-1	%T	No.	cm-1	%T	No.	cm-1	%T	No.	cm-1	%T	No.	cm-1	%T
1	3424	108.79	2	2925	103.09	3	2341	108.01	4	1683	100.37	5	1616	101.09
6	1385	101.03	7	1321	102.40	8	1125	101.84	9	537	95.62			

Figure S70. IR spectrum of **22**